Environmental Science and Engineering

Zuoyu Sun
Prodip K. Das *Editors*

Proceedings of the 10th International Conference on Energy Engineering and Environmental Engineering

Springer

Environmental Science and Engineering

The ultimate goal of this series is to contribute to the protection of our environment, which calls for both profound research and the ongoing development of solutions and measurements by experts in the field. Accordingly, the series promotes not only a deeper understanding of environmental processes and the evaluation of management strategies, but also design and technology aimed at improving environmental quality. Books focusing on the former are published in the subseries Environmental Science, those focusing on the latter in the subseries Environmental Engineering.

Zuoyu Sun · Prodip K. Das
Editors

Proceedings of the 10th International Conference on Energy Engineering and Environmental Engineering

Springer

Editors
Zuoyu Sun
Department of Energy and Power Engineering
Beijing Jiaotong University
Beijing, China

Prodip K. Das
University of Edinburgh
Edinburgh, UK

ISSN 1863-5520 ISSN 1863-5539 (electronic)
Environmental Science and Engineering
ISBN 978-3-031-48203-8 ISBN 978-3-031-48204-5 (eBook)
https://doi.org/10.1007/978-3-031-48204-5

This Springer imprint is published by the registered company Springer Nature Switzerland AG
The registered company address is: Gewerbestrasse 11, 6330 Cham, Switzerland

Paper in this product is recyclable.

Organizing Committees

Conference Chair

Assoc. Prof. Yusong Yu, Beijing Jiaotong University, China

Program Committee Chair

Assoc. Prof. Zuoyu Sun, Beijing Jiaotong University, China

Technical Program Chairs

Assoc. Prof. Xueqian Fu, China Agricultural University, China
Assoc. Prof. Wong Ling Tim, Hong Kong Polytechnic University, Hong Kong, China

Publicity Chair

Assoc. Prof. Yang Wang, Harbin Engineering University, China

Technical Program Committees

Prof. Ayşegül Aşkın, Eskişehir Osmangazi University, Turkey
Prof. Bachir Achour, University of Biskra, Algeria
Prof. Ahmad Zuhairi Abdullah, Universiti Sains Malaysia, Malaysia

Prof. Jose Francisco Armendariz-Lopez, Universidad Autónoma de Baja California, México
Dr. Hamed H. Aly, Dalhousie University, Canada
Prof. Zhe Chen, Aalborg Universitet, Denmark
Dr. Daniele Contini, Istituto di Scienze dell'Atmosfera e del Clima, Italy
Dr. Cheng Siong Chin, Newcastle University in Singapore, Singapore
Assoc. Prof. Maciej Dzikuć, University of Zielona Gora, Poland
Dr. Radu Godina, NOVA University Lisbon, Portugal
Prof. Gordon Huang, University of Regina, Canada
Assoc. Prof. Andrés Honrubia-Escribano, Universidad de Castilla-La Mancha, Spain
Asst. Prof. Svenja Hanson, University of Nottingham Ningbo, China
Prof. Teik-Thye Lim, Nanyang Technological University, Singapore
Prof. Solomon Leung, Idaho State University, USA
Assoc. Prof. Yaolin Lin, University of Shanghai for Science and Technology, China
Dr. Chong Ng, Offshore Renewable Energy Catapult, UK
Assoc. Prof. Melih Onay, Van Yuzuncu Yil University, Turkey
Dr. Parthiba Karthikeyan Obulisamy, Purdue University, IN, USA
Prof. Siti N. B. Rahmat, Universiti Tun Hussein Onn Malaysia, Malaysia
Prof. Farhad Shahnia, Murdoch University, Australia
Assoc. Prof. Marcello Ruberti, University of Salento, Italy
Assoc. Prof. Hongwei Wu, University of Hertfordshire, UK
Asst. Prof. Yao Yu, North Dakota State University, USA
Prof. Jian-Ping Zheng, University at Buffalo, The State University of New York, USA
Asst. Prof. Xiaolei Zhang, Shenzhen Graduate School of Harbin Institute of Technology, China

Publication Chairs

Assoc. Prof. Zuoyu Sun, Beijing Jiaotong University, China
Assoc. Prof. Prodip Das, Newcastle University, UK

Preface

The 10th International Conference on Energy Engineering and Environmental Engineering (ICEEEE2023) was held on August 6–8, 2023, in Singapore. ICEEEE2023 provided both online and onsite contributions, and we are delighted to present this proceedings to showcase the latest advancements in energy and environmental engineering.

ICEEEE is an open forum for discussion, learning, and professional growth and development. We discussed the transformation of innovation and creativity in energy, environment, and sustainable development. We featured world-class speakers, editors, and participants from China (mainland), Hong Kong, Taiwan, Singapore, Philippine, Russia, South Africa, Nigeria, Japan, and South Korea. ICEEEE2023 received about 60 submissions (full papers and abstracts) and final include 22 full papers in the proceedings.

We would like to express our sincere gratitude to all the individuals who contributed to ICEEEE2023. A special thanks to all chairs and program committee members for organizing all sessions and reviewing all the submissions. This is to ensure the quality of presented research which is vital to the success of the conferences.

Last but not least, we extend gratitude to the Environmental Science and Engineering staff for coordinating, supporting, and running this smooth publication process.

We hope ICEEEE benefits all of you and look forward to meeting you all at ICEEEE2024!

The Organizing Committee of ICEEEE2023

Zuoyu Sun
Beijing Jiaotong University
Beijing, China

Prodip K. Das
University of Edinburgh
Edinburgh, UK

Contents

Chapter 1
Experimental Evaluation of a Diesel Engine Performance and Emission Characteristics Powered by Hybrid Biodiesel and Butanol Blends

Shumani Ramuhaheli and Christopher Enweremadu

Abstract The increased demand of fossil fuels used in a diesel engine might be taken as one of the important aspects which inspire researchers to look for alternative fuels. This current study evaluates the performance and exhaust gases of hybrid biodiesel from waste vegetable oil and soybean oil with the addition of n-butanol (butanol) blends. The different percentages of butanol such as 5, 10, and 15 with hybrid biodiesel were experimentally compared to hybrid biodiesel (BM100) and standard diesel (D100). The parameters of the diesel engine comprise the brake power, brake specific fuel consumption, and brake thermal efficiency, whereas the emissions comprise hydrocarbons and Bosch smoke number. It was found that the hybrid biodiesel-butanol blends (BMBT5, BMBT10, and BMBT15) decreased the brake power by 12.0, 13.0, and 14.4% compared to hybrid biodiesel. For brake specific fuel consumption, hybrid biodiesel-butanol blends (BMBT5, BMBT10, and BMBT15) increased by 13.6, 14.9, and 16.8% whereas brake thermal efficiency increased by 1.5, 1.6, and 1.8% compared to hybrid biodiesel at the maximum speed. For exhaust gas emissions, hybrid biodiesel (BM100) and its butanol blends (BMBT5, BMBT10, and BMBT15) decreased hydrocarbons by 4, 5.6, 8, and 28.8% compared to diesel whereas Bosch smoke emissions decreased by 21.1, 31.6, 31.0, and 29.9% compared to diesel at the maximum speed. It can be concluded that hybrid biodiesel and butanol blends appear as a superior alternative fuel for neat diesel in a diesel engine.

Keywords Hybrid biodiesel · Butanol · Diesel engine · Performance · Emission characteristics

S. Ramuhaheli (✉) · C. Enweremadu
University of South Africa, Science Campus, Florida 1709, Johannesburg, South Africa
e-mail: ramuhs@unisa.ac.za

C. Enweremadu
e-mail: enweercc@unisa.ac.za

Z. Sun and P. K. Das (eds.), *Proceedings of the 10th International Conference on Energy Engineering and Environmental Engineering*, Environmental Science and Engineering, https://doi.org/10.1007/978-3-031-48204-5_1

1.1 Introduction

The increase of energy demand and worried about harmful effects to the atmosphere and its natural systems have driven researchers to look for alternative energy to substitute fossil fuels. During the last decade, non-renewable fuels turned out to be the leading energy provider to the automotive industries and power generation. This has heavily affected the environment through its harmful emissions namely NO_x, CO_2, CO, HC, and smoke (Chow et al. 2021). The fear of the reduction of nonrenewable fuels has driven scientists to come up with the idea for cleaner and renewable energy. However, biodiesel fuel might be used as an alternative energy for nonrenewable energy to run diesel engines and power generation. Biodiesel has gained recognition due to its renewable nature, non-harmful, and lower exhaust gas emissions compared to neat diesel (Mirhashemi and Sadrnia 2020). The existence of oxygenated content of biodiesel enhanced engine combustion hence exhaust gas emissions decreased compared to neat diesel. Moreover, biodiesel shows excellent lubricity to enhance the performance of a diesel engine. These improvements has encouraged researchers to increase biodiesel production from multiple feedstocks for long term (Pinheiro Pires et al. 2019). So far, biodiesel from sunflower oil, soybean, waste cooking oil, and rapeseed oil are the core sources for biodiesel production worldwide (Dabi and Saha 2019).

Nevertheless, ahead from the advantages of biodiesel, numerous deficiencies have been noticed in diesel engines powered by biodiesel. The density, viscosity, HC, smoke, and NO_x of biodiesel are generally superior compared to neat diesel. A wide report stated by Noor et al. (2018) found that the fuel efficiency and NO_x emissions of used oil biodiesel increased compared to neat diesel for a marine engine. Furthermore, (Rochelle and Najafi 2019) suggested that the fuel efficiency of biodiesel is higher whereas the brake power decreased compared to neat diesel in a gas turbine engine. Fuel stability and feedstock costs are the major restrictions for the production of biodiesel. However, the tactics of blending fuel might be good to improve biodiesel properties. The properties, performance and exhaust gas emissions of biodiesel might be enhanced by blending with alcohol fuel.

Butanol is a transparent sustainable energy obtained in propylene (C_3H_6) and has a greater stability performance and its heating value is higher. Currently, butanol is regarded as a fractional replacement for diesel mixtures because its oxygen content and cetane number (CN) are higher, but butanol's latent heat of evaporation is lower than ethanol (Devarajan et al. 2022). A few studies have been conducted to evaluate the engine characteristics and emitted gases fueled with the addition of butanol-biodiesel and equated to standard diesel and biodiesel.

Reference (Zhang and Balasubramanian 2016) investigated the impacts of butanol addition to biodiesel to evaluate the engine parameters and emitted gas. The findings indicated that butanol blends increased brake BSFC and BTE equated to pure biodiesel at low load and medium load conditions. Furthermore, increasing the fraction volume of butanol blends leads to the reduction of particle emissions in all tested circumstances.

Reference (Patil and Patil 2018) evaluated the engine characteristics and emitted gas of a diesel engine powered by biodiesel from fresh vegetable oil and butanol mixtures. Different fractions of butanol (5, 10, 15, and 20%) were compared to biodiesel from fresh vegetable oil and standard diesel. The authors indicated that the increase of butanol percentage leading to an increase of BSFC and NO_x whereas BTE decreased compared to pure biodiesel and standard diesel at different speeds. Carbon monoxide for pure biodiesel and neat diesel attained minimum values equated to butanol mixtures.

Reference (Wei et al. 2018) evaluated and compared the impacts of butanol fractions to pure biodiesel on engine parameters and emitted gases using different load conditions and constant speeds. The authors indicated that the fuel consumption for biodiesel and its n-butanol mixtures attain higher values equated to pure biodiesel. The BTE of biodiesel-butanol blends and neat biodiesel indicated that no significant difference was observed due to the maximum burning cylinder temperature that decrease the cooling impact of alcohol. The CO emitted with biodiesel-butanol mixtures obtain the maximum values equated to pure biodiesel and standard diesel at all load conditions. However, the NO_x emissions of biodiesel-butanol blends decreased compared to pure biodiesel fuel.

Reference (Yilmaz and Davis 2016) evaluates the engine characteristics and emitted gas of a diesel generator powered by neat diesel, waste vegetable biodiesel, 10, 20, and 40 vol% of butanol mixtures at various loads. The outcomes of the investigation indicated that BSFC of neat diesel and pure biodiesel attain lower values compared to all biodiesel-butanol blends. Compared to standard diesel and pure biodiesel, the biodiesel-butanol blends increased CO and hydrocarbon emissions for all load conditions, whereas NO_x emission decreased at full load conditions.

It is important to specify that numerous scientists have investigated the addition of butanol fractions into biodiesel and biodiesel-diesel to evaluate the parameters of the diesel engine. However, they did not further study the addition of butanol fractions into hybrid biodiesel. Therefore, the objective of this investigation is to experimentally evaluate the effect of hybrid biodiesel added with 5, 10, and 15% n-butanol percentage volume to assess the engine performance and emitted gases, using standard diesel as a reference fuel for comparison. The engine characteristics to be evaluated are BP, BSFC, and BTE. The emission characteristics are hydrocarbon and Bosch smoke number.

1.2 Materials and Procedures

1.2.1 Production of Biodiesel and Preparation

Biodiesel fuel was produced using waste vegetable oil and soybean oil through the transesterification method where methanol was applied as alcohol and sodium hydroxide as catalyst. Biodiesel preparations are neat diesel (D100), hybrid biodiesel

Table 1.1 Fuel properties

Properties	D100	BM100	BMBT5	BMBT10	BMBT15
Density (kg/m^3)	0.8263	0.886	0.882	0.878	0.872
Viscosity (mm^2/s)	2.66	4.411	4.068	3.633	3.259
Heating value (MJ/kg)	42.5	41.5	37.3	37	36.5

of waste vegetable oil and soybean oil (BM100), and hybrid biodiesel mixed with 5% (BMBT5), 10% (BMBT10), and 15% (BMBT15) of butanol blends. The properties of fuels such as D100, BM100, BMBT5, BMBT10, and BMBT15 are exhibited in Table 1.1 according to ASTM standards.

1.2.2 Experimental Procedures

This experimental investigation used a Yanmar diesel engine with 70 mm of stroke, 57 mm of bore diameter, and 3.5 kW of maximum power output to test the fuel samples as indicated in Fig. 1.1. The technical details of the Yanmar diesel engine are exhibited in Table 1.2. The emitted gases were assessed using a Bosch exhaust gas analyzer. The diesel engine remained at a full load condition and a constant compression ratio. The uncertainty test was performed at various apparatus to evaluate the uncertainties of the various measured parameters. The accuracy of different types of apparatus is exhibited in Table 1.3. Before the fuel samples experiment, the diesel engine was fueled with neat diesel for 20 min to warm up and gain steady conditions. The exhaust gas analyzer was placed on the exhaust tailpipe to assess HC and smoke emissions.

1.3 Results and Discussions

1.3.1 Brake Power

Figure 1.2 exhibits the variation of brake power for standard diesel, hybrid biodiesel, and hybrid biodiesel-butanol blends at full load conditions. The figure exhibited that when the speed of the engine increased, the brake power increased. This was caused by the improvement of engine performance during the test (Al-Dawody et al. 2022). At the maximum speed, diesel fuel attained the maximum value compared to all green fuels. The decrease of brake power for green fuel was possibly caused by lower heating value with the increase of the BSFC of the engine.

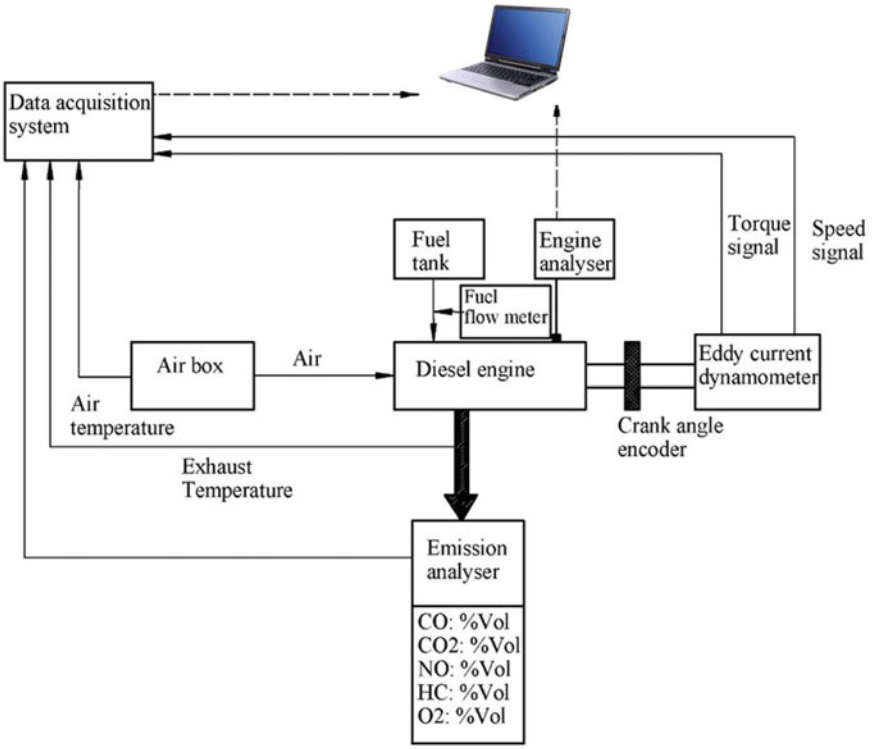

Fig. 1.1 Layout of the experimental setup

Table 1.2 Technical descriptions of Yanmar diesel engine

Specifications	Descriptions
Model	L48N6CF1T1AA
Type	4 stroke, single cylinder, air cooled, diesel engine
Rated power	3.5 kW at 3600 rpm
Bore × stroke	57 × 70 mm
Injection system	Direct injection

Table 1.3 Uncertainties of the parameters

Instrument	Range	Accuracy (ppm)	Uncertainty (ppm)
NO	0–5000 ppm	± 1	± 1
HC	0–9999 ppm	± 1	± 1
Smoke	0–100 vol%	± 1	± 1

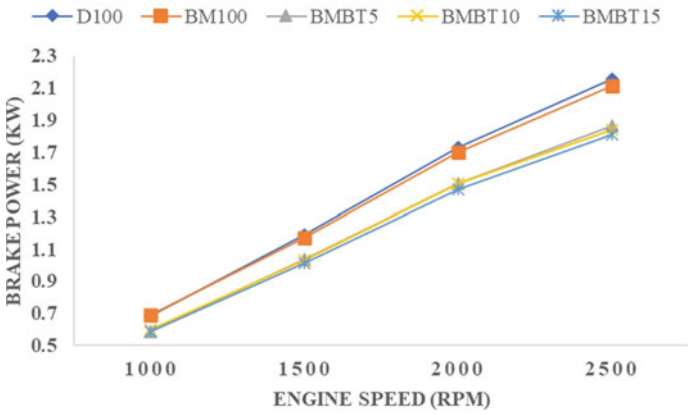

Fig. 1.2 Variation of brake power with different speeds

1.3.2 Brake Specific Fuel Consumption

The BSFC for neat diesel, hybrid biodiesel, and butanol blends is exhibited in Fig. 1.3. The results from the graph exhibited that all hybrid biodiesel-butanol blends increased equated to neat diesel and pure hybrid biodiesel. This increase of biodiesel mixture-butanol blends was influenced by the decrease of the heating value of butanol in comparison to D100 and BM100 which decrease the quantity of energy released during the combustion processes hence increasing the BSFC (Devarajan et al. 2022). The diesel engine used a large capacity of green fuels to produce a marginally similar power output to standard diesel fuel (Sachuthananthan et al. 2023). The maximum BSFC for B100, BM100, BMBT5, BMBT10, and BMBT15 was 271.1 g/kWh, 276.5 g/kWh, 314.1 g/kWh, 317.8 g/kWh and 322.9 g/kWh respectively.

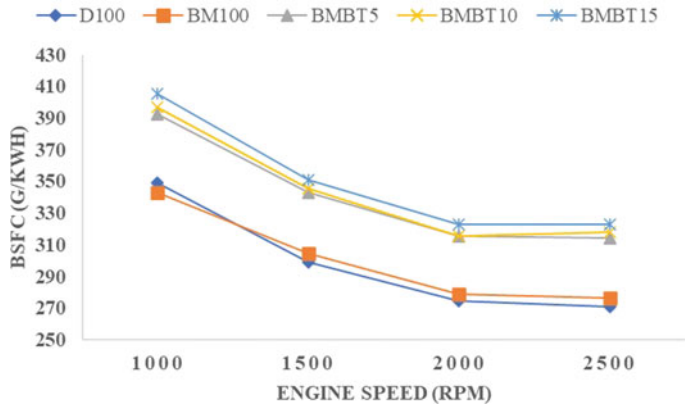

Fig. 1.3 Variation of brake specific fuel consumption with different speeds

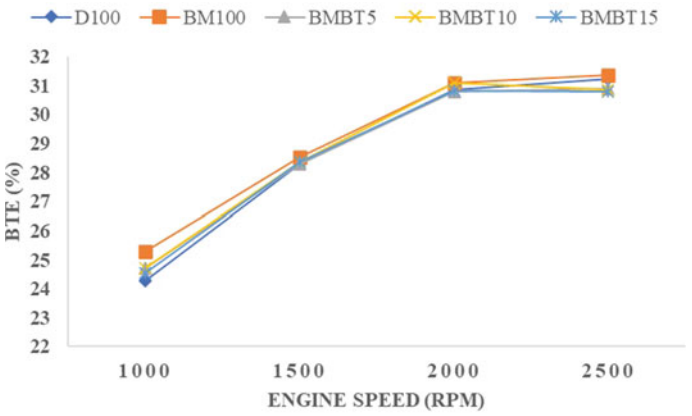

Fig. 1.4 Variation of brake thermal efficiency with different speeds

1.3.3 Brake Thermal Efficiency

Figure 1.4 exhibits the BTE for neat diesel, hybrid biodiesel, and its n-butanol blends percentage. The data indicated that the BTE for all n-butanol mixtures decreased compared to standard diesel and hybrid biodiesel at the maximum speed. The BTE of BMBT15 attained the lowest value compared to all fuels tested due to the result of higher latent heat of evaporation that affects the BTE of the engine (Chen et al. 2014). The D100, BM100, BMBT5, BMBT10, and BMBT15 was found to be 31.245%, 31.373%, 30.893%, 30.866%, and 30.798% respectively. It can be noted from the graph that when brake thermal efficiency increased, the butanol fraction increased up to 10%. This was caused by the possibility of high oxidation for hybrid biodiesel that enhance the quality of combustion hence the BTE of the diesel engine increase (Sachuthananthan et al. 2021).

1.3.4 Hydrocarbon Emissions

Figure 1.5 exhibits the deviation of HC gases for D100, BM100, BMBT5, BMBT10, and BMBT15 at various speeds. The results indicated that BM100, BMBT5, BMBT10, and BMBT15 decrease the hydrocarbon emissions compared to standard diesel. This reduction was due to effective combustion and a lower ignition delay period for hybrid biodiesel (Devarajan et al. 2022). The high content of oxygen for butanol blends further decreased the emitted gas at all engine speeds (Asha et al. 2022). At 2500 rpm, the hydrocarbon emissions for D100, BM100, BMBT5, BMBT10, and BMBT15 were 125 ppm, 120 ppm, 118 ppm, 115 ppm, and 89 ppm respectively. The higher oxygen content of n-butanol leads to a decrease in hydrocarbon discharge.

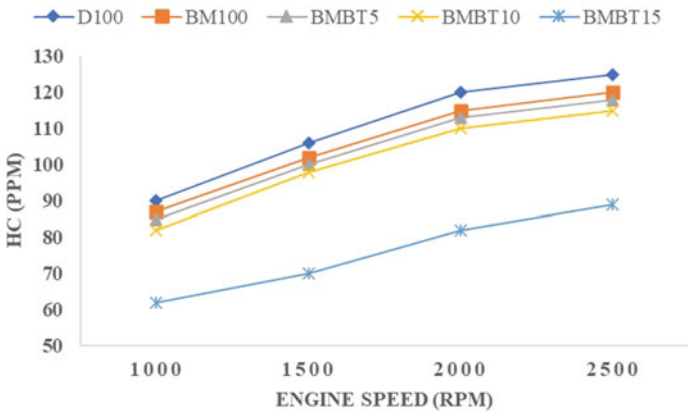

Fig. 1.5 Variation of hydrocarbon with different speeds

1.3.5 Smoke Emissions

Figure 1.6 exhibits the Bosch smoke number for D100, BM100, BMBT5, BMBT10, and BMBT15 with different speeds. The findings from the graph discovered that all n-butanol blends attain the lowest smoke emitted than standard diesel and hybrid biodiesel. This decrease was caused by lower heating value and higher latent heat of butanol compared to standard diesel fuel. It was observed from the graph that BM100, BMBT5, BMBT10, and BMBT15 decreased by 21.1, 31.6, 31.0, and 29.9% in comparison to standard diesel fuel at the highest speed. Similar kind of this results has been reported by Kandasamy et al. (2019).

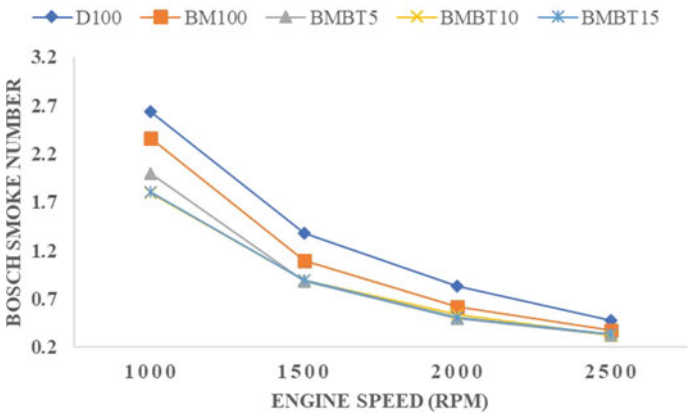

Fig. 1.6 Variation of Bosch smoke number with different speeds

1.4 Conclusions

This investigation summarizes the effect of D100, BM100, BMBT5, BMBT10, and BMBT15 to assess the performance and emitted gas of diesel engine. At maximum speed, the blending of butanol fractions increased BSFC due to lower heating value. The BSFC of BM100, BMBT5, BMBT10, and BMBT15 increased by 2.0, 15.9, 17.2, and 19.1% compared to neat diesel. The BTE of all butanol mixtures decreased compared to hybrid biodiesel. In terms of emission characteristics, the hybrid biodiesel-butanol blends decrease hydrocarbon and Bosch smoke number compared to standard diesel, which is primarily related to higher oxygen content, which enables the reduction of emissions.

References

Al-Dawody MF, Rajak U, Jazie AA, Al-Farhany K, Saini G, Verma TN, Nashine P (2022) Production and performance of biodiesel from cladophora and fucus green diesel. Sustain Energy Technol Assessments 53:102761

Asha P, Natrayan L, Geetha B, Beulah JR, Sumathy R, Varalakshmi G, Neelakandan S (2022) IoT enabled environmental toxicology for air pollution monitoring using AI techniques. Environ Res 205:112574

Chen Z, Wu Z, Liu J, Lee C (2014) Combustion and emissions characteristics of high n-butanol/diesel ratio blend in a heavy-duty diesel engine and EGR impact. Energy Convers Manage 78:787–795

Chow MR, Ooi JB, Chee KM, Pun CH, Tran MV, Leong JCK, Lim S (2021) Effects of ethanol on the evaporation and burning characteristics of palm-oil based biodiesel droplet. J Energy Inst 98:35–43

Dabi M, Saha UK (2019) Application potential of vegetable oils as alternative to diesel fuels in compression ignition engines. J Energy Inst 92(6):1710–1726

Devarajan Y, Munuswamy DB, Nalla BT, Choubey G, Mishra R, Vellaiyan S (2022) Experimental analysis of *Sterculia foetida* biodiesel and butanol blends as a renewable and eco-friendly fuel. Ind Crops Prod 178:114612

Kandasamy SK, Selvaraj AS, Rajagopal TKR (2019) Experimental investigations of ethanol blended biodiesel fuel on automotive diesel engine performance, emission and durability characteristics. Renew Energy 141:411–419

Mirhashemi FS, Sadrnia H (2020) NO_x emissions of compression ignition engines fueled with various biodiesel blends: a review. J Energy Inst 93(1):129–151

Noor CM, Noor M, Mamat MR (2018) Biodiesel as alternative fuel for marine diesel engine applications. Renew Sustain Energy Rev 94:127–142

Patil VV, Patil RS (2018) Investigations on partial addition of n-butanol in sunflower oil methyl ester powered diesel engine. J Energy Resour Technol 140

Pinheiro Pires AP, Arauzo J, Fonts I, Domine ME, Fernández Arroyo A, Garcia-Perez ME, Montoya J, Chejne F, Pfromm P, Garcia-Perez M (2019) Challenges and opportunities for bio-oil refining: a review. Energy Fuels 33(6):4683–4720

Rochelle D, Najafi H (2019) A review of the effect of biodiesel on gas turbine emissions and performance. Renew Sustain Energy Rev 105:129–137

Sachuthananthan B, Vinoth R, Reddy DR, Bandari V, Anusha P (2021) Environmental impact on the use of diesel waste plastic oil nano-additive blends in a DI diesel engine. Int J Nanotechnol 18(11–12):990–1006

Sachuthananthan B, Vinoth R, Reddy PL, Naik G, Sandeep B (2023) Behaviour assessment of diesel engine operated using butanol-methyl ester of water hyacinth blends. Mater Today Proc 72:1785–1791

Wei L, Cheung C, Ning Z (2018) Effects of biodiesel-ethanol and biodiesel-butanol blends on the combustion, performance and emissions of a diesel engine. Energy 155:957–970

Yilmaz N, Davis SM (2016) Polycyclic aromatic hydrocarbon (PAH) formation in a diesel engine fueled with diesel, biodiesel and biodiesel/n-butanol blends. Fuel 181:729–740

Zhang ZH, Balasubramanian R (2016) Investigation of particulate emission characteristics of a diesel engine fueled with higher alcohols/biodiesel blends. Appl Energy 163:71–80

Chapter 2
Greenhouse Gas Treatment in the New Normal

Parin Somani

Abstract Events occurring during the coronavirus (covid-19) pandemic including implementation of social distancing regulations, resulted in a vast reduction in the number of transport vehicles being used. This created an impact upon the amount of greenhouse gas emissions being emitted, particularly highlighting a reduction in the levels of carbon dioxide. This study aims to understand the effects of greenhouse gases on the environment due to the covid-19 pandemic. There is an objective to recommend a recovery plan towards facilitating new energy production, storage, and transmission of greenhouse gases, thereby contributing to a sustainable environment in the new normal. A review of published and grey literature sources has been conducted through electronic and manual sources. Results have revealed that carbon dioxide and methane are deemed as two most important greenhouse gases, while nitrate particles and nitrogen oxides are dominant two air pollutants. Emissions appear to have returned to levels pre-pandemic, hence there is urgent need to ensure a transition to technology that emits low carbon levels. If this is not implemented swiftly, severe environmental threats like global warming and climate change will be accelerated. Recommendations like turning carbon dioxide into methanol, in addition to storing renewable energy forms like solar energy and wind energy are discussed. There is a need to work together to recover from the covid-19 pandemic implementing a novel and more greener transition process, to produce and consume greenhouse gases. It is necessary to facilitate the increase in economical transformations around the world to help sustain global environments.

Keywords Greenhouse gas · Emissions · New energy · New normal · Storage · Transmission

P. Somani (✉)
London Organisation of Skills Development, London, United Kingdom
e-mail: drparinsomani@gmail.com

Z. Sun and P. K. Das (eds.), *Proceedings of the 10th International Conference on Energy Engineering and Environmental Engineering*, Environmental Science and Engineering, https://doi.org/10.1007/978-3-031-48204-5_2

2.1 Introduction

Events occurring during the coronavirus (covid-19) pandemic including implementation of social distancing regulations, resulted in a vast reduction in the number of transport vehicles being used. This created an impact upon the amount of greenhouse gas emissions being emitted, particularly highlighting a reduction in the levels of carbon dioxide. The covid-19 pandemic has affected social, economic and environmental factors (Somani 2021a). Nations across the world rely on fossil fuels to generate energy in order to meet the demands of energy required to sustain the needs of human beings. The intentional burning of fossil fuels result in the release of greenhouse gases including carbon dioxide, methane and nitrogen dioxide. They have an adverse effect on the climate and on human health (Somani 2021b). According to the United Nations, the fossil fuels gas, coal and oil are the major contributors of global climate change. This is because it is responsible for more than 75% of global greenhouse emissions and approximately 90% of carbon dioxide emissions (UN 2023a). The earth is covered with greenhouse gas emissions like a blanket, consequently trapping heat from the sun resulting in climate change and global warming. It is evident that the world has been gradually getting warmer than in previous years as temperatures rise, however there is a disruption in nature's balance. Consequently, all life forms on earth including human beings are at risk (UN 2023a).

From research carried out by our world in data within 2016, from studies conducted by the World Resources Institute and Climate Watch, results indicate that there has been an increase in global growth and resource consumption as 49.5 billion tonnes of carbon dioxide emissions were emitted into the world (Ghosh 2020). This was emitted through human actions in a variety of sectors. Figure 2.1 illustrates the sectors that contribute of greenhouse gas emissions. It is evident that energy use contributes to approximately three-quarters of emissions. Agriculture and land use, contribute to approximately one-fifth of the emissions which is heightened when including the who food system. This can include food processing, packaging, transport and retail, while waste and industry comprise of the eight per-cent remaining. According to the IPCC's fifth Assessment Report AR5, brief descriptions have been included for each category.

As highlighted in Fig. 2.1, there are four dominant categories that contribute towards global greenhouse emissions including energy, agriculture, waste and industry. Albeit energy consumption contributes to approximately three-quarters of energy consumption (Table 2.1).

Within each sector there are micro-elements that contribute to the overall percentage contribution illustrated in Fig. 2.1.

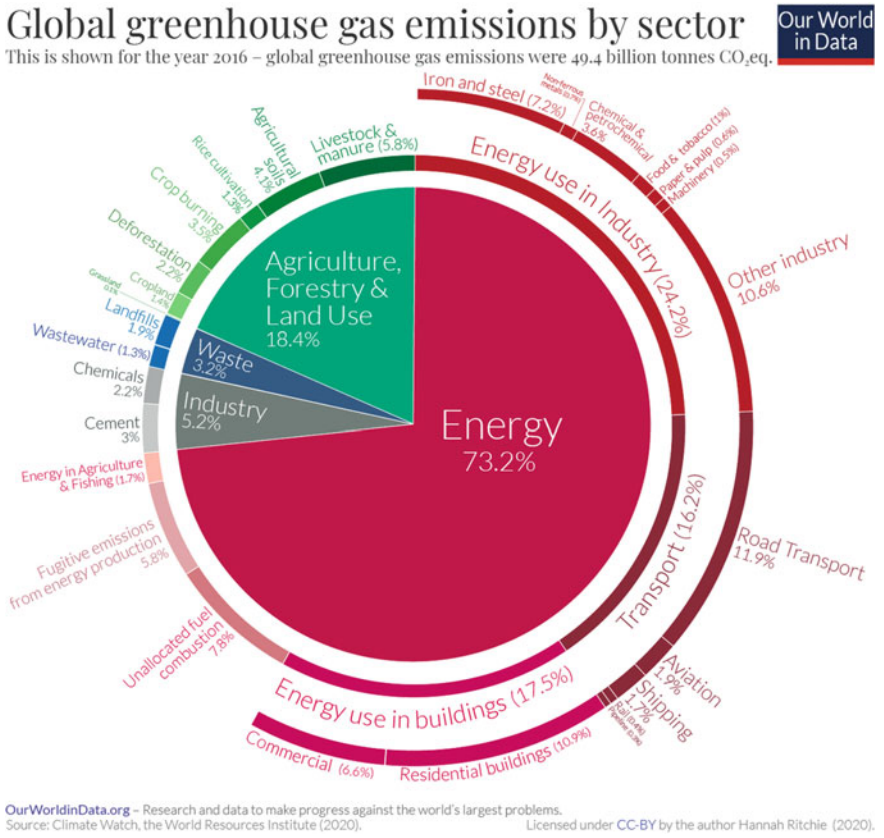

Fig. 2.1 Illustrates global greenhouse gas emissions segregated into sectors (Ritchie 2020)

Table 2.1 Highlights the percentage of global greenhouse emissions (Our World in Data 2021)

Sector contributing to emissions	Percentage contribution (%)
Energy	73.2
Agriculture, forestry and land use	18.4
Industrial processes	5.2
Waste	3.2

2.1.1 Objectives

This study aims to understand the effects of greenhouse gases on the environment due to the covid-19 pandemic. There is an objective to recommend a recovery plan towards facilitating new energy production, storage, and transmission of greenhouse gases, thereby contributing to a sustainable environment in the new normal. A review

of published and grey literature sources has been conducted through electronic and manual sources.

2.2 Results and Discussion

Results have revealed that carbon dioxide and methane are deemed as two most important greenhouse gases, while nitrate particles and nitrogen oxides are dominant two air pollutants. Emissions appear to have returned to levels pre-pandemic, hence there is urgent need to ensure a transition to technology that emits low carbon levels. If this is not implemented swiftly, severe environmental threats like global warming and climate change will be accelerated.

Carbon Dioxide

Globally within societies, there are billions of individuals that are completely reliant upon their vehicles to transport them between destinations. Dominantly there is a use of fossil fuels including petrol and diesel to power their vehicles, hence constituting towards a 12% global emission level. During the covid-19 pandemic there was a reduction in the number of cars on the road and aviation vehicles. Although vehicles were still used for the transportation of goods, according to NASA during the pandemic, there was a massive decrease in greenhouse gas emissions and air pollution. In 2020 there was a decrease of 5.4% in carbon dioxide emissions, however the atmospheric carbon dioxide proceeded to increase at the same rate as previous years. This was expected due to results recorded in carbon dioxide levels from historical events like the 1973 oil shortage. It is based on research carried out by NASA, which revealed that natural processes contributed towards steady atmospheric concentrations deemed to be within normal range. Hence, although the 5.4% decrease of greenhouse gas emissions was viewed as significant, the current levels have reached to those near pre-pandemic. This could be due to a reduction in carbon dioxide pressure at the surface of the ocean within the air (Yuen 2023). They also found a link between air quality and the climate that requires further research.

2.2.1 Methane, Air Pollutants and Transmission

An ozone layer can be created through mixing nitrogen oxides with other compounds within the atmosphere in sunlight. This can result in dangerous impacts upon the health of not only human beings, but also plants and animals. The ozone layer was reduced globally due to nitrogen oxide mixed with covid-19 related drops. NASA has utilised a satellite to measure various pollutants, revealing "that pollutant reacts to form a short-lived molecule called the hydroxyl radical, which plays an important role in breaking down long-lived gases in the atmosphere" (Rasmussen 2021). Although

the reduction of nitrogen oxide during the covid-19 pandemic was perceived as beneficial, cleansing methane from the atmosphere became limited. It has been proven that in comparison to carbon dioxide, methane is more effective as it traps heat in the atmosphere. Therefore, even a ten percent reduction in methane levels influenced global societies. Nevertheless, decreased methane levels did not impinge upon atmospheric methane concentration, and an increase of 0.3% within the past year has contributed towards an increased rate in comparison to the previous ten years. This could be because of a reduction in the hydroxyl radical, resulting from decreased nitrogen oxides in the atmosphere, contributing to methane's presence in the atmosphere for a longer period of time.

In the short-term Fig. 2.2 highlights how the covid-19 pandemic has created an impact upon global greenhouse gas emissions. It is evident that the covid-19 has created an impact upon carbon dioxide emissions, it has impacted the economy and energy, a recovery plan and sustainability is required. Electricity and heat have 25% contributing factors to Global greenhouse gas emission, while agriculture and land is 24%, industries are 21%, transit is 14%, other energy is 10%, food waste is 7% and buildings are 6%.

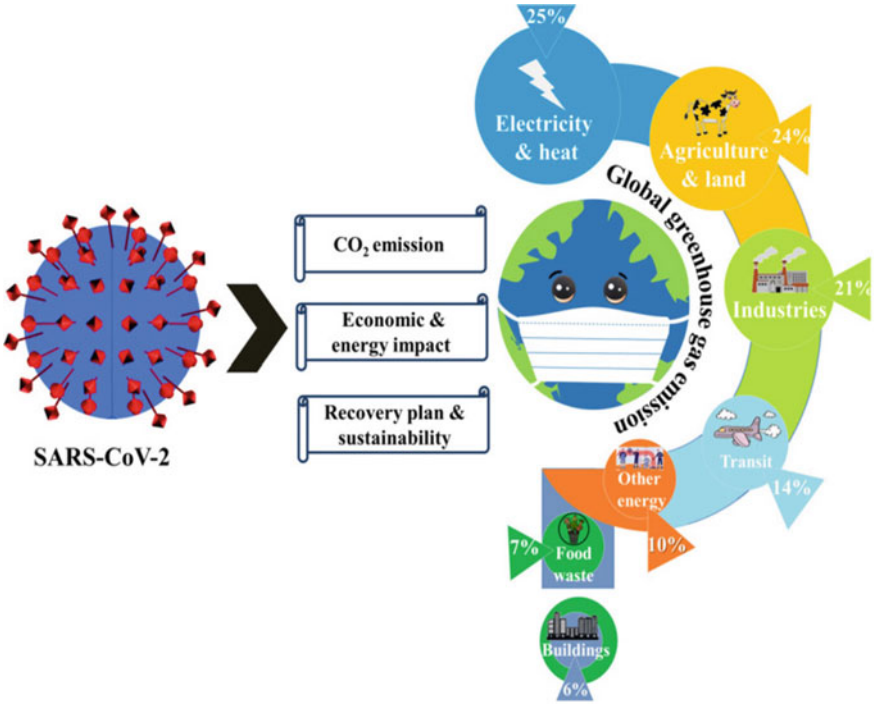

Fig. 2.2 Kumar et al. (2022) illustrates covid-19 impacts on global greenhouse gas emissions

2.2.2 New Energy Production

As fossil fuels are the greatest contributors to global climate change, they contribute to more than 75% of the global greenhouse emissions, and approximately 90% of carbon dioxide emissions. Due to this, it is imperative that there needs to be a 50% reduction in carbon dioxide emission by the year 2030, if the 2050 goal on net-zero is going to be achieved. For this to occur, it is vital to source alternative energy sources and stop relying on fossil fuels. Energy needs to be reliable, sustainable, affordable, and clean (UN 2023b). Renewable energy sources are available within countries globally, and provide a means through which nations can create more diverse economies and provide protection from depending on the rise in price of fossil fuels, creating new employment positions, cultivating a better quality of life through alleviating poverty and facilitating economic growth. One of the largest financial barriers around the world challenging the shift to renewable energy are fossil fuel subsidies. Particularly as in 2020, 5.9 trillion US Dollars were spent on subsidising the fossil fuel industry (IMF 2022). However, they are deemed as inequitable and inefficient because within developing countries the consumption of fossil fuels is a benefit to 20% of the most affluent population. Thus, when subsides from fossil fuels are transitions to renewable energy it facilitates a decrease in emissions and an increase in employment positions impacting economic growth. There is also an impact on increased public health and equality, and it can progress communities that are vulnerable particularly those from lower socio-economic backgrounds. According to the UN, energy is "at the heart of climate challenge" (UN 2023b) but it has also been noted as being a key to the solution. Nature can replenish renewable energy sources like solar power and wind power, and they emit very little or no greenhouse gasses and associate pollutants in the air, in addition they are more cost-effective. Therefore, global societies should try to focus on progressing new energy production from renewable energy sources.

2.2.3 Storage

Carbon dioxide capture and storage is a low carbon technology that can be utilised to help facilitate nations to achieve zero emissions. Large energy sources can use the carbon dioxide capture and storage, they include power stations, cement factories, or oil refineries. By storing more carbon dioxide than its production can contribute towards the negative emission and help to achieve the target of net-zero. Carbon dioxide can be captured at the source, then transported and stored in geological formations deep underneath the ground. There are attempts to make carbon dioxide storage, permanent, cost effective and useful part of the energy transition process. However, it is important to consider the following:

- The character and capacity of potential storage strata
- How stored carbon dioxide might interact with the rocks they are surrounded by
- Technologies demonstrating the permanent storage of carbon dioxide

- Operation in the long-term and site closure
- Community concerns
- Social attitudes (BGS 2023).

Storing and capturing carbon dioxide can facilitate societies endeavour to reach zero-emissions. This is a key component of energy transition. When fossil fuels are burnt at power plants, carbon dioxide can be removed via post-combustion, pre-combustion and oxyfuel combustion. Hydrogen production is another medium through which carbon dioxide emission can be reduced, particularly when electrical power using batteries are not suitable. This can include heavy good vehicles, trains and domestic heating appliances. Converting this energy into hydrogen will be beneficial, however the financial implication to execute this process is higher, particularly through electrolysis of water utilising renewable power. A more cost-effect way to convert to hydrogen is using natural gas to produce hydrogen through methane reformation. Nevertheless, carbon dioxide can be captured directly from the open atmosphere, however this methos requires more research and has greater financial implications.

2.3 Conclusion

Multiple sectors and associated processes have an impact upon global emissions. Thus, it is inadequate to concentrate on one sector to find a solution to climate change. Just focusing on food processes, transport, deforestation, or electricity on its own it not sufficient. Although the covid-19 pandemic revealed decreased levels of greenhouse gas emissions, they have nearly returned to levels pre-pandemic within the new normal. This is despite a reduction in economical activities and many individuals adopting the work from home culture. Individuals are still emitting greenhouse gases to maintain their economic stability within contemporary life. Thus, there is a requirement to implement sustainable strategies within different sectors with low-carbon emitting technology that can be incorporated within daily practice for long-term use. A commitment and accountability are required from financial systems like banks and other private and public financial organisations from around the world, as they should aim to focus their lending to progress the transition to renewable energy. It is evident that we can only achieve real energy security, financial stability pertaining to power and employment opportunities that are sustainable through a transition to renewable energy.

2.3.1 Recommendations

There is a need to work together to recover from the covid-19 pandemic, implementing a novel and more greener transition process, to produce and consume

greenhouse gases. It is necessary to facilitate the increase in economical transformations around the world to help sustain global environments. Human beings need to minimise the amount of greenhouse gases that are being released into the atmosphere. We must aim to replace high energy fossil fuels with low energy sources, contributing to a reduction in the overall attempt to zero emissions. It is low carbon technologies that contribute to the success of low energy emission adoption globally.

As three-quarters of emissions are attached to the energy sector, it is impossible to eliminate its use completely without having a detrimental impact on societies without successful contingency plans in place. The complete decarbonisation of electrical supplies would have a grave impact on heating to keep us warm, but also on road transportation hence a gradual shift to utilising electric vehicles would be advantageous. However, low-carbon technologies are not available to cope with the shipping and aviation transport, hence solutions to reduce emissions from these is necessary to find through further research. Although utilising electrical vehicles can facilitate a decrease in the world using fossil fuels, there are still challenges that need to be overcome.

Governmental and non-governmental initiatives should be promoted within societies to educate and encourage individuals to use renewable energy sources and implement initiatives to facilitate a reduction in global greenhouse gases. For example, 'Share the Road Program' which encourages individuals to cycle and walk opposed to using vehicles on the road. In addition, bike-sharing schemes to encourage individuals to leave their cars and contribute to a reduction in air pollution. Successful campaigns from nations around the world should be shared and implemented to help humanity.

References

BGS (2023) Understanding carbon capture and storage. British Geological Survey Natural Environmental Research Council, UK

Ghosh I (2020) A Global breakdown of greenhouse gas emissions by sector, 06 Nov 2020 [online]. Available https://www.visualcapitalist.com/a-global-breakdown-of-greenhouse-gas-emissions-by-sector/

IMF (2022) Climate change fossil fuel subsides. International Monetary Fund

Kumar A, Singh P, Raizada P, Hussain CM (2022) Impact of COVID-19 on greenhouse gases emissions: a critical review. Sci Total Environ: 806

Our World in Data (2021) A global breakdown of greenhouse gas emissions by sector. Retrieved from Visualcapitalist: https://www.visualcapitalist.com/cp/a-global-breakdown-of-greenhouse-gas-emissions-by-sector/

Rasmussen C (2021) Emission reductions from pandemic had unexpected effects on atmosphere, 09 Nov 2021 [online]. Available https://www.jpl.nasa.gov/news/emission-reductions-from-pandemic-had-unexpected-effects-on-atmosphere

Ritchie H (2020) Sector by sector: where do global greenhouse gas emissions come from? 28 Sept 2020 [online]. Available https://ourworldindata.org/ghg-emissions-by-sector

Somani P (2021) Progressing organisational behaviour towards a new normal. J Econ Fin Manage Stud: 1628–1633

Somani P (2021) Impact of climate change and covid-19 on health. J Hunan Univ Nat Sci: 184–193

UN (2023a) Causes and effects of climate change. United Nations, Geneva
UN (2023b) Climate action. United Nations, Geneva
Yuen K (2023) Orbiting carbon observatory-2. NASA Jet Propulsion Laboratory, California

Chapter 3
Discussion on Radiation Intensity of UVC-LED Different Arrangement Types

Ming-Jui Hung, Cheng-Han Li, Yan-Cheng Wang, and Po-Jung Wang

Abstract Ultraviolet germicidal irradiation (UVGI), due to its characteristics such as mature technology, fast sterilization rate and no secondary pollution for dry disinfection, after the COVID-19 epidemic has been gradually applied to the purification of air conditioning systems such as medical institutions, food hygiene and office buildings and other fields. However, in response to the signing of the "Minamata Convention" for the international ban on mercury in 2013, and UVC-LED has the advantages of no preheating, power saving, small size, long life, non-toxicity, and single band, it has been gradually replaced trend for traditional UV lamps. In view of this, this research uses UV illuminance meter, light source test box, spectrum analyzer and other equipment, a series of experiments were conducted on the radiation intensity of different layout types of UVC-LEDs, the light attenuation with distance, and the characteristics of medium penetration, in order to serve as a reference for the application of environmental disinfection and sterilization on site.

Keywords UVGI · UVC-LED · Disinfection

3.1 Introduction

The COVID-19 epidemic has swept the world so far, not only affecting normal human social activities (Social activities) and various industrial behaviors, but also causing major losses in human economy, life and property. Among them, the spread of SARS-CoV-2 strains through airborne transmission is the main way to cause cluster infection in indoor or closed spaces. Therefore, various space protection measures

M.-J. Hung · C.-H. Li (✉) · Y.-C. Wang · P.-J. Wang
Department of Safety, Health and Environmental Engineering, Ming Chi University of Technology, Taipei, Taiwan
e-mail: hanhan870924@gmail.com

M.-J. Hung
e-mail: mingjui@mail.mcut.edu.tw

Z. Sun and P. K. Das (eds.), *Proceedings of the 10th International Conference on Energy Engineering and Environmental Engineering*, Environmental Science and Engineering, https://doi.org/10.1007/978-3-031-48204-5_3

and immune building technologies against COVID-19, such as wet-type disinfection (WTD), fumigation-type disinfection (FTD), dry-type disinfection (DTD), and self-type disinfection (STD), have sprung up and developed vigorously in response to COVID-19. Among them, UVC-LED is more widely used in COVID-19 epidemic protection due to its advantages of no preheating, power saving, small size, long life and non-toxicity.

3.2 Materials and Methods

The materials and equipment used in this research mainly include: UVC-LED, UV illuminance meter, lens and reflective medium, etc., which are introduced as follows:

(1) **UVC-LED**

The emission wavelength is 280 nm, and its appearance is shown in Figs. 3.1, 3.2 and 3.3.

(2) **UV Illuminance Meter**

The UV illuminance meter used in this experiment is shown in Fig. 3.4, and the sensing wavelength range is 220–320 (nm), Intensity measurement range 0–100 mW/cm^2 and working temperature: 0 to + 50 °C, etc. Generally, it can be calibrated once every 3–5 years.

(3) **Lens**

The lenses used in this experiment are shown in Fig. 3.5, including plano lenses, plano-convex lenses, convex-planar lenses, biconvex lenses, plano-concave lenses, concave-plano lenses, and bi-concave lenses.

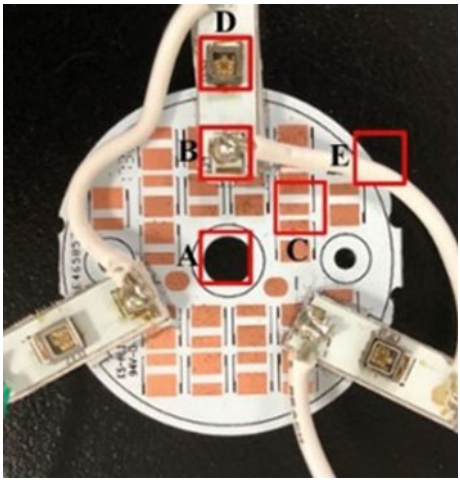

Fig. 3.1 3 UVC-LEDs

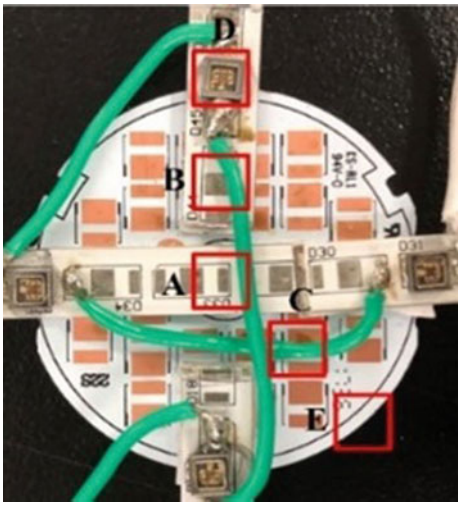

Fig. 3.2 4 UVC-LEDs

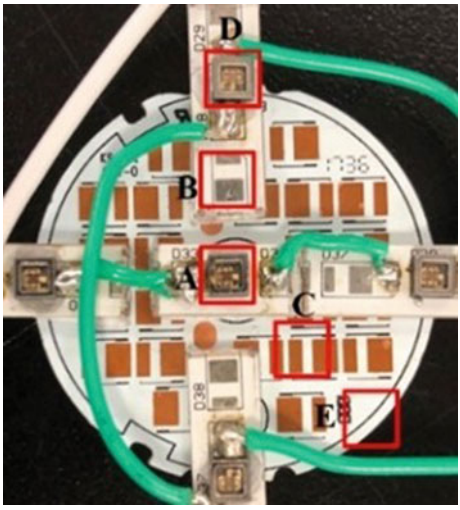

Fig. 3.3 5 UVC-LEDs

(4) **Reflective Medium**

The reflective medium used in this experiment is shown in Fig. 3.6, including aluminum, stainless steel, zinc, iron, and teflon.

In this research, the "basic performance measurement" of UVC-LED is carried out in the laboratory, including: the measurement and distribution of the radiation intensity of UVC-LED, the penetration and reflection characteristics of the medium, and the penetration characteristics of the lens. This study will conduct two sets of tests, the first set measures the radiation intensity of UVC-LEDs with three different layout methods by using a UV illuminance meter, and divides the surface into five

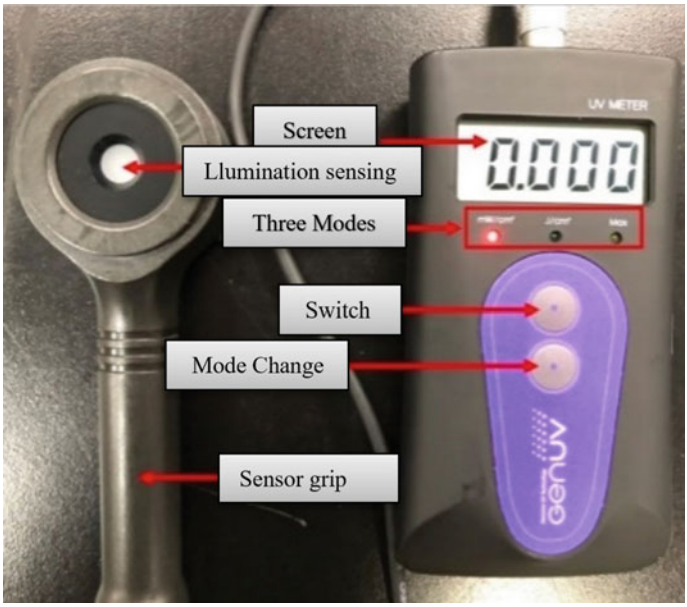

Fig. 3.4 UV illuminance meter

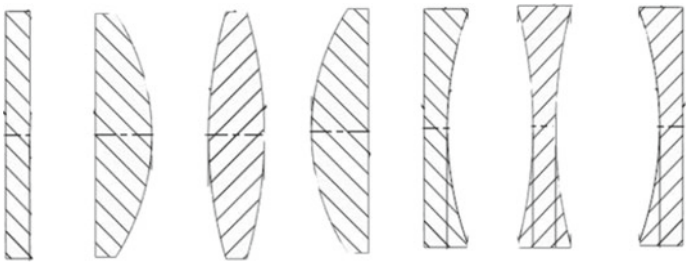

Fig. 3.5 Different types of lenses

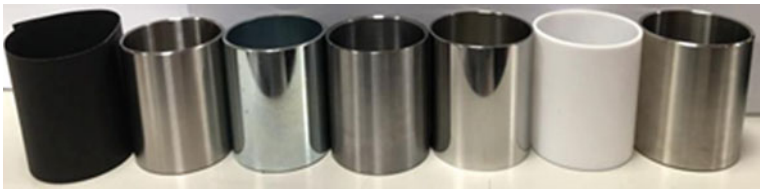

Fig. 3.6 Different types of reflective media

areas: A, B, C, D, and E, with the increase of distance test the strength of five areas. The other group sets the penetrating and reflecting medium and lens between the UVC-LED and the UV illuminance meter, and then measures the radiation intensity by using the UV illuminance meter. In order to ensure the safety of the measurement, a black cloth must be laid inside the test box, gloves and long sleeves must be worn during the test to prevent direct contact between ultraviolet rays and the human body.

3.3 Results and Discussion

Due to space limitations, only the test results of 5 UVC-LEDs are shown in Fig. 3.7. Strong radiation intensity can be measured in A and D areas at 0 cm, and the radiation intensity of D area drops a lot at 1 cm, the radiation intensity is stronger in the C area, and the radiation intensity in the E area has always been weaker. The radiation intensity of the 5 UVC-LEDs decreases with the distance until 16 cm is 0 $\mu W/cm^2$.

Table 3.1 shows the medium that UVC-LED radiation cannot penetrate. PET is most commonly used in the manufacture of plastic bottles, it is the only plastic material that cannot penetrate in this test. Common A4 paper, microscope cover glass and laboratory commonly used gloves are likewise an impenetrable medium for the radiation of UVC-LEDs. Table 3.2 shows the medium through which UVC-LED radiation can penetrate. The PVC used in this test is a plastic wrap with a penetration rate of 85%. Although it is thinner than PE and PP, its penetration rate is similar. In other words, if the thickness is the same, the penetration rate of PVC will be poor. PE is a zipper bag commonly used in general life, and PP is a commonly used packaging material, and the penetration rates of the two are similar. PS and PLA are thicker because they come from plastic boxes. The thickness of PLA is 4 times that of PE and PP, but the penetration rate is still 67%.

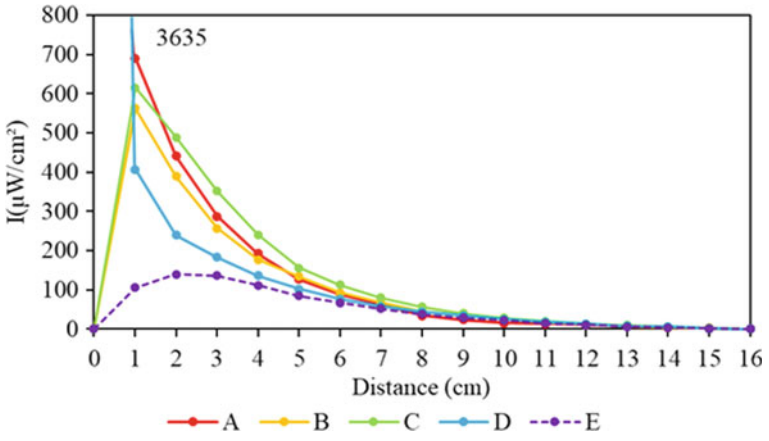

Fig. 3.7 Radiation intensity attenuation of 5 UVC-LEDs with distance

Table 3.1 Media that UVC-LEDs cannot penetrate

Medium	Thickness (mm)	Penetration rate (%)
PET	0.33	0
A4 paper	0.10	0
Cover slip	0.15	0
Latex gloves	0.10	0

Table 3.2 Mediums that allow UVC-LEDs to penetrate

Medium	Thickness (mm)	Penetration rate (%)
PVC	0.01	85
PE	0.04	86
PP	0.04	84
PS	0.16	39
PLA	0.16	67

As shown in Fig. 3.8, even though the thicknesses of all plastic materials are different, PE and PP have the same thickness, so the attenuation curves are more consistent, almost overlapping with the radiation intensity attenuation curves of the control group, PS and PLA have the same thickness, but The transmittance of PLA is better than that of PS, while PET cannot measure the radiation intensity, which is a medium that UVC-LED cannot penetrate.

Figure 3.9 shows the changes in radiation intensity after being reflected by different media. The control group is the radiation intensity measured without placing the reflective medium. After placing the black paper, no increase in the radiation

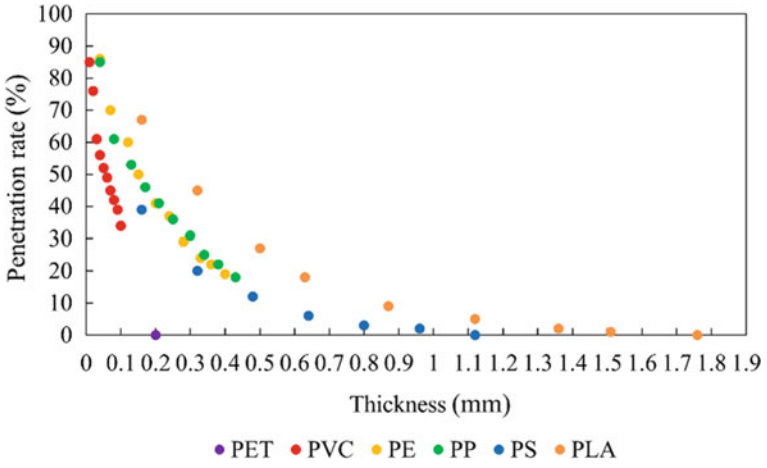

Fig. 3.8 The attenuation of the transmittance of the UVC-LED transparent medium after increasing the thickness

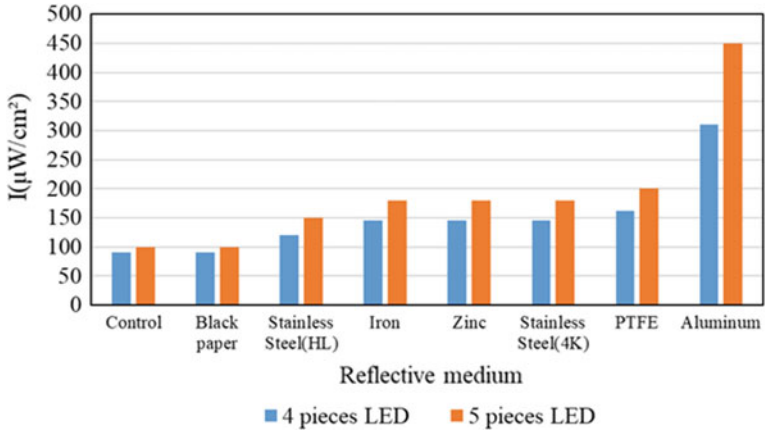

Fig. 3.9 Radiation intensity of UVC-LED after reflection by different media

intensity was found, and the radiation intensity was observed to increase when other reflective media were placed. Compared with the control group, aluminum has a higher increase factor, and the enhancement factors of 4 and 5 UVC-LEDs are 3.5 times and 4.5 times respectively. Teflon (PTFE) is the only reflective medium in this test that is more For non-metallic materials with better performance, the enhancement factors of 4 and 5 UVC-LEDs are 1.8 times and 2 times respectively, and the order of reflection effect is aluminum > PTFE > stainless steel 4 K = zinc = iron > stainless steel HL. Figure 3.10 shows the changes in the radiation intensity of UVC-LEDs through different types of lenses. The control group is the radiation intensity measured without placing the lens. After passing through the convex lens, the light will be focused to reduce the irradiation range, and the radiation intensity will increase. After passing through the concave lens, it will be It will make the light diverge and increase the irradiation range but the radiation intensity will decrease. The order of focusing effect is: plano-convex lens > biconvex lens > convex-plano lens > plano lens > plano-concave lens > concave-plano lens > bi-concave lens.

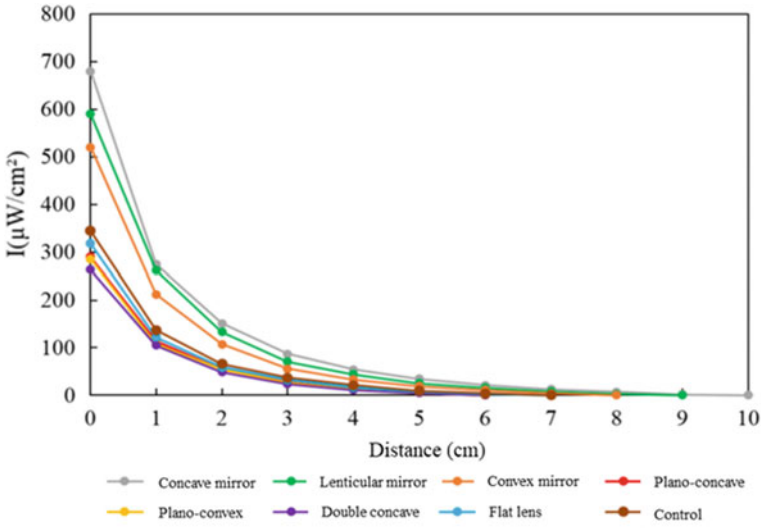

Fig. 3.10 Variation of radiation intensity of UVC-LED passing through different types of lenses

3.4 Conclusion

The test results show that the closer to the surface of the UVC-LED, the stronger the radiation intensity, and the 3 UVC-LEDs have no radiation intensity at a distance of 7 cm, and 4 UVC-LEDs and 5 UVC-LEDs will have no radiation intensity at a distance of 16 cm. Comparing the three types of modules, the radiation intensity of the five UVC-LEDs is higher except at a distance of 0 cm. The result of the radiation intensity distribution is that the three UVC-LEDs are all stronger in the D area except at a distance of 3 cm. In most cases, 4 UVC-LEDs have stronger radiation intensity in the B area, and 5 UVC-LEDs have stronger radiation intensity in the C area in most cases. At present, the only plastic material tested is PET, which cannot be penetrated by LED-UVC. The attenuation of the penetration rate of PVC is more obvious after the thickness is increased. The plastic material with better penetration effect is PLA, and the medium with better reflection is aluminum.

Bibliography

Ha JW, Back KH, Kim YH, Kang DH (2016) Efficacy of UV-C irradiation for inactivation of food-borne pathogens on sliced cheese packaged with different types and thicknesses of plastic films. Food Microbiol 57:172–177

Lindsley WG, McClelland TL, Neu DT, Martin Jr SB, Mead KR, Thewlis RE, Noti JD (2018) Ambulance disinfection using ultraviolet germicidal irradiation (UVGI): effects of fixture location and surface reflectivity. J Occup Environ Hygiene 15(1):1–12

Chapter 4
Hydrogen Leakage and Diffusion Simulation and Ventination Scheme Optimization in Confined Spaces for Electrolyser and Fuel Cell System

Guodong Li, Min Liu, Bo Zhao, Qiliang Wu, Tianqi Yang, Qingxin Ba, Xuefang Li, and Jinsheng Xiao

Abstract For the demonstrated application of an integrated system that includes electrolysis hydrogen production, compression hydrogen storage and fuel cells, this study conducts a numerical simulation of hydrogen leakage and diffusion in confined spaces with electrolyzers and fuel cells. Hydrogen is extremely flammable and explosive and can accumulate inside confined spaces so hydrogen leakage may lead to explosions in confined spaces like the electrolysis workshop and fuel cell room. Therefore, high-pressure hydrogen releases in confined spaces should be studied to provide a scientific basis for designing risk mitigation measures. The present work modeled hydrogen releases in the hydrogen production room and fuel cell room using the CFD method. The distribution of hydrogen gas in space at different moments was analyzed. Hydrogen concentrations were monitored at various locations, and the sensitivity of each monitoring point to hydrogen leakage was analyzed to investigate the optimal location of hydrogen detectors in the two confined spaces. The leaks were then simulated under different ventilation conditions to find a better ventilation solution. The results show that mechanical ventilation accelerates the diffusion of hydrogen to the outside. The space above the equipment is the best location for the hydrogen detector. The results of this study can inform the spatial layout of equipment and sensors in an integrated hydrogen system.

G. Li · T. Yang (✉) · J. Xiao
Hubei Research Center for New Energy and Intelligent Connected Vehicle, School of Automotive Engineering, Wuhan University of Technology, Wuhan 430070, China
e-mail: tqyang@whut.edu.cn

M. Liu (✉) · B. Zhao · Q. Wu
Research Institute of State Grid Zhejiang Electric Power Co., Ltd., Hangzhou 310006, China
e-mail: liumhb@126.com

Q. Ba · X. Li · J. Xiao
Institute of Thermal Science and Technology, Shandong University, Jinan 250061, China

Z. Sun and P. K. Das (eds.), *Proceedings of the 10th International Conference on Energy Engineering and Environmental Engineering*, Environmental Science and Engineering, https://doi.org/10.1007/978-3-031-48204-5_4

Keywords Hydrogen safety · Hydrogen leakage diffusion · CFD simulation · Confined space

4.1 Introduction

With the development of the world economy, the consumption of fossil fuels is increasing. There is an urgent need to find cleaner energy to replace fossil fuels to reduce the dependence on fossil fuels and reduce the pressure on environmental pollution. As a kind of clean energy without pollution, hydrogen energy has been widely concerned. Hydrogen is an ideal energy source because it reacts with oxygen to produce heat and water during combustion without polluting the environment (Najjar 2013). To better use hydrogen energy, fuel cell vehicle technology comes into being. In order to supplement energy for fuel cell vehicles, hydrogenation stations similar to petrol filling stations for fuel cars are also rapidly developed. However, hydrogen is very easy to diffuse in the air and is flammable and explosive, hydrogen can burn at a volume fraction of 4–75%, especially in some closed spaces like hydrogen refueling stations, if the leakage of hydrogen, the consequences are very terrible. Therefore, to ensure the safety of the enclosed space of the hydrogenation station and avoid economic losses, it is essential to study the hydrogen leakage in the confined space of the hydrogenation station.

At present, many scholars have conducted experiments studies on hydrogen leakage. Lacome et al. (2011) conducted experimental research on hydrogen dispersion under different leakage flows and diameters. It provides the basis for the validation of the CFD method. Stefano et al. (2019) conducted an experimental study on hydrogen leakage in an enclosed space, which designed a 1/15 nuclear facility room with a size of 0.47 × 0.33 × 0.20 m. Nine combinations of leakage flow and leakage locations were studied in the experiment, and the results can help better predict hydrogen dispersion in a confined space. Shu et al. (2021) proposed a simplified prediction model to predict the diffusion of hydrogen leakage and conducted a series of helium leakage experiments in an environmental chamber with helium instead of hydrogen to verify the accuracy of the prediction model. Tamura et al. (2014) conducted an experimental study of hydrogen leakage from a moving car and showed that a forced wind of 10 m/s can keep the vehicle in a safe condition.

In addition, there are many numerical simulation studies on hydrogen leakage and diffusion. Lin et al. (2023) used CFD methods to investigate the behaviour of hydrogen leakage and flaring from an offshore hydrogen production platform under different operating conditions. Li et al. (2023) developed a numerical model of a mobile hydrogen refueling station and carried out a numerical simulation study of hydrogen leakage and dispersion in this mobile hydrogen refueling station. Jia et al. (2023) considered the interaction between methane and hydrogen, established a gas mixture diffusion model, and studied the influence of gas pressure, leak hole diameter, and other factors on the diffusion range of methane and hydrogen mixture. Hou et al. (2023) developed a CFD model of a hydrogen fuel cell vehicle and investigated

the effect of obstacles on hydrogen diffusion under different ventilation conditions. Guan et al. (2023) used FLACS software to investigate hydrogen diffusion behaviour and concentration distribution in a hydrogen fuel cell chamber. The study found that smaller hydrogen pipe diameters help to reduce the possibility of hydrogen explosions. Su et al. (2022) studied the diffusion characteristics of leakage of hydrogen-containing natural gas in kitchens using Fluent software and analyzed the effects of factors such as hydrogen content ratio and ventilation conditions on their diffusion characteristics. Zhang et al. (2022) used the Large-Eddy Simulation model to investigate the effect of different shapes of leak openings on hydrogen leakage in confined spaces. The diffusion behaviour of hydrogen in naturally ventilated spaces in different directions was investigated by Zhang et al. (2021). Li et al. (2018) conducted a simulation study of hydrogen leakage in passenger cabins using a passenger ship. The simulation results identified walls and corners as the best locations for sensor placement.

4.2 Methods

CFD models of the hydrogen production room and fuel cell room in the hydrogenation station were established using Fluent software, and then the hydrogen leakage in these two confined spaces was numerically simulated.

4.2.1 Control Equations

The process of leakage and diffusion conforms to the basic equations of fluid control, namely, the equation of mass conservation, momentum conservation, and energy conservation.

Mass conservation equation:

$$\frac{\partial p}{\partial t} + \nabla \cdot (\rho \boldsymbol{u}) = 0 \tag{4.1}$$

where ρ is the density, t is time, and $\boldsymbol{u}$ is the velocity vector in the x, y, and z directions.

Momentum conservation equation:

$$\frac{\partial (\rho \boldsymbol{u})}{\partial t} + \nabla \cdot (\rho u \boldsymbol{u}) = -\nabla p + \nabla \cdot \overline{\tau} + \boldsymbol{F} \tag{4.2}$$

where p is the pressure, $\overline{\tau}$ is the viscous stress and $\boldsymbol{F}$ is the volume force.

Energy conservation equation:

$$\frac{\partial\left(\rho c_p T\right)}{\partial t}+\nabla\cdot\left(\rho c_p \boldsymbol{u} T\right)=\frac{\partial}{\partial x}\left(k\frac{\partial T}{\partial x}\right)+\frac{\partial}{\partial y}\left(k\frac{\partial T}{\partial y}\right)+\frac{\partial}{\partial z}\left(k\frac{\partial T}{\partial z}\right)+\emptyset+S_h \tag{4.3}$$

where c_p is the specific heat capacity, T is the temperature, k is the heat transfer coefficient, $\emptyset$ is the dissipation function, S_h is the internal heat source in a fluid.

All gases in this study obey the gas equation of state:

$$PV=mRT \tag{4.4}$$

In this study, hydrogen is mixed with air after leakage and there is component transport, the component transport equation is as follows:

$$\begin{aligned}\frac{\partial(\rho c_i)}{\partial t}+\nabla\cdot(\rho c_i \boldsymbol{u})&=\frac{\partial}{\partial x}\left(D_i\frac{\partial(\rho c_i)}{\partial x}\right)\\&+\frac{\partial}{\partial y}\left(D_i\frac{\partial(\rho c_i)}{\partial y}\right)+\frac{\partial}{\partial z}\left(D_i\frac{\partial(\rho c_i)}{\partial z}\right)\end{aligned} \tag{4.5}$$

where c_i represents the bulk density of component i and D_i is the diffusion coefficient i.

In this study, the standard $k-\varepsilon$ model was chosen to study the effects of turbulence.

Turbulent kinetic energy transport equation:

$$\frac{\partial(\rho K)}{\partial t}+\frac{\partial(\rho\overline{u}_i K)}{\partial x_i}=\frac{\partial}{\partial x_j}\left[\left(\mu+\frac{\mu_t}{Pr_K}\right)\frac{\partial K}{\partial x_j}\right]+G_K+G_b-\rho\varepsilon-Y_M+S_K \tag{4.6}$$

Standard model turbulence dissipation rate transport equation:

$$\frac{\partial(\rho\varepsilon)}{\partial t}+\frac{\partial(\rho\overline{u}_i\varepsilon)}{\partial x_i}=\frac{\partial}{\partial x_j}\left[\left(\mu+\frac{\mu_t}{Pr_\varepsilon}\right)\frac{\partial\varepsilon}{\partial x_j}\right]+C_{\varepsilon1}\frac{\varepsilon}{K}(G_K+C_{\varepsilon3}G_b)-C_{\varepsilon2}\rho\frac{\varepsilon^2}{K}+S_\varepsilon \tag{4.7}$$

where G_K is the turbulent kinetic energy due to variable speed, G_b is the turbulent kinetic energy due to buoyancy, Y_M is the fluctuation due to diffusion, Pr_K and Pr_ε are the turbulent Prandtl number of turbulent kinetic energy and dissipation rate, in that order.

The calculation formula for turbulent viscosity:

$$\mu_t=C_\mu\rho\frac{K^2}{\varepsilon} \tag{4.8}$$

The parameters of $k-\varepsilon$ model are shown in Table 4.1.

Table 4.1 Values of some parameters in the standard $k-\varepsilon$ model

Parameter	C_μ	σ_K	σ_ε	$C_{1\varepsilon}$	$C_{2\varepsilon}$	$C_{3\varepsilon}$
Value	0.09	1.0	1.3	1.44	1.92	1.0

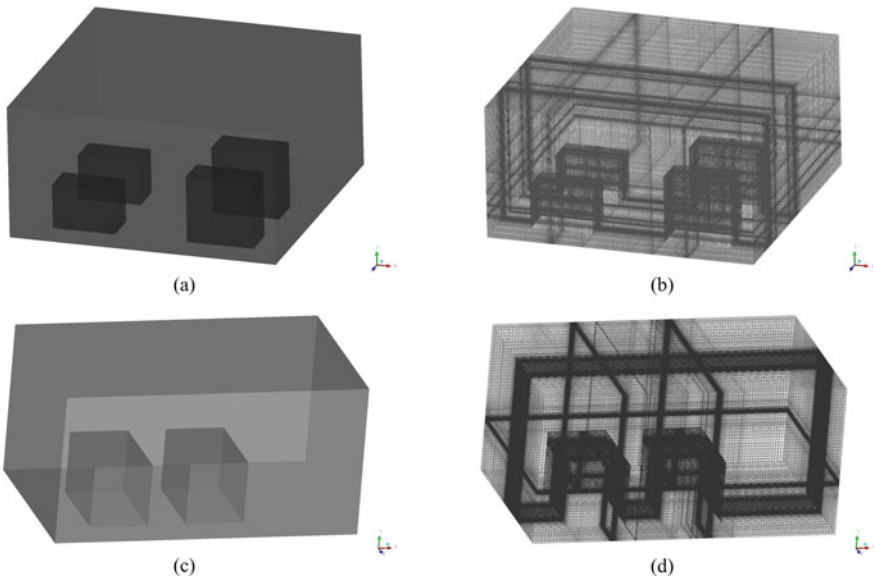

Fig. 4.1 Geometric models (**a**, **c**) and computational grids (**b**, **d**) of hydrogen production room (**a**, **b**) and fuel cell system room (**c**, **d**)

4.2.2 Model and Mesh Generation

In order to improve the accuracy of the numerical simulation, a hexahedral structural mesh was chosen for this study. Geometric models and computational grids are shown in Fig. 4.1. The grid is locally encrypted near the leak port, the closer to the leak port, the denser the grid, and the further away from the leak port, the sparser the grid. 96.7% of the grid quality is above 0.7, and 99.8% of the grid aspect ratio is less than 15, which has met the requirements of the numerical simulation in this study.

4.2.3 Model Parameters

An isometric model has been developed based on the actual dimensions of the hydrogen production room and the fuel cell room in the hydrogen refuelling station. The dimensions of the hydrogen production room are 12, 12 and 6 m in the X, Y and Z directions. And the fuel cell room dimensions are 12, 7.5 and 6 m in the X, Y

Table 4.2 Boundary conditions for individual parts in fluent

Object	Boundary condition types	Description
Leakage hole	Mass flow inlet	Set the mass flow rate, direction, composition of incoming material, etc.
Door	Pressure outlet	Set the ambient pressure at the outlet
Window	Pressure outlet	Set the ambient pressure at the outlet
Walls, floors, roofs, etc.	Wall	Stationary wall with no slip
Water electrolysis equipment and purification equipment	Wall	Stationary wall with no slip
Hydrogen production room	Fluid domain	An area where hydrogen leaks diffuse and mix with air

and Z directions. The boundary conditions of the model are shown in Table 4.2. This study chose a pressure-based solver to perform the transient calculations. Depending on the actual situation of the model, the negative direction of the Y-axis is chosen as the direction of gravity, and the acceleration of gravity is 9.81 m/s. Hydrogen leaks mixed with air and diffused in this study, and there are multiple substances transported, so the component transport model was chosen. In addition, the transport of components is accompanied by the transport of energy, and the energy model is also used in this work.

4.3 Results and Discussion

4.3.1 Contours of Hydrogen Molar Fraction at Different Times

Figure 4.2 shows hydrogen gas distribution at different times in the YZ section where the leak point is located. The hydrogen has not yet reached the ceiling at the start of the leak at 0.05 s. At 0.2 s, the hydrogen jets to the ceiling and begin to spread to the sides of the cross-section. At this moment, the leaking hydrogen still collects on the ceiling, forming a diffuse hydrogen cloud, as hydrogen is less dense than air. Within 0.2–2 s, the hydrogen cloud spreads from its position above the leakage point to the sides of the room. As the walls block the continued horizontal diffusion of the hydrogen cloud, the hydrogen gradually accumulates at the wall location, and as the volume fraction of hydrogen increases here, the hydrogen cloud gradually thickens and the hydrogen gradually spreads down the walls. At 5 s, the hydrogen near the walls has diffused to the general height of the room, while the hydrogen in the middle of the ceiling is diffusing downwards at a slower rate. As the hydrogen continues to

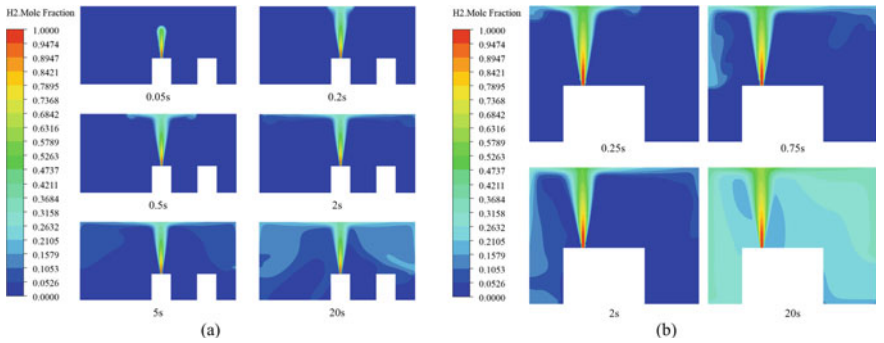

Fig. 4.2 Variation of hydrogen molar fraction with time in leakage port cross-sections in hydrogen production room (**a**) and fuel cell room (**b**)

leak, the room becomes more and more filled with hydrogen. At 20 s, the overall hydrogen volume fraction in the room increases, and hydrogen diffuses through most of the room, with higher volume fractions in the leak jet path and near the walls. The space for the fuel cell room is smaller and the risk of hydrogen leakage is greater. 0.25 s later, hydrogen has been ejected to the top of the ceiling and spreads in all directions. The hydrogen from the top of the ceiling reaches the left wall first and continues to diffuse downwards as the leak is closer to the left wall. After 0.75 s, the hydrogen from the ceiling diffuses to the right wall, which is less time than it would take in a hydrogen production room. The hydrogen on the left wall spreads downwards and reaches the floor by 2 s. Due to the smaller space in the fuel cell chamber, the concentration of hydrogen in the chamber is greater at the same time as the hydrogen leak.

4.3.2 Monitoring Point

When hydrogen leakage occurs in a closed space, timely detection of the leak will help reduce the harm caused by hydrogen leakage. Therefore, in this study, six monitoring points were set at different positions in the CFD model of the two rooms to explore the optimal installation position of the detector when hydrogen leakage occurs. Leakage centers in the hydrogen production and fuel cell rooms are (− 3.15, 2, 0.25) and (6.97, 2.5, 5.1), respectively.

Figure 4.3 shows the simulation results of the monitoring points in the two rooms, respectively. As shown in Fig. 4.3a, the P6 monitoring point in the hydrogen production room has the fastest reaction speed because it is directly above and closest to the leakage port. In contrast, monitoring points P1, P2 and P3, further away from the leak, have slower response rates and lower hydrogen concentrations. Figure 4.3b shows the simulation results of monitoring points between fuel cells. Similar to the

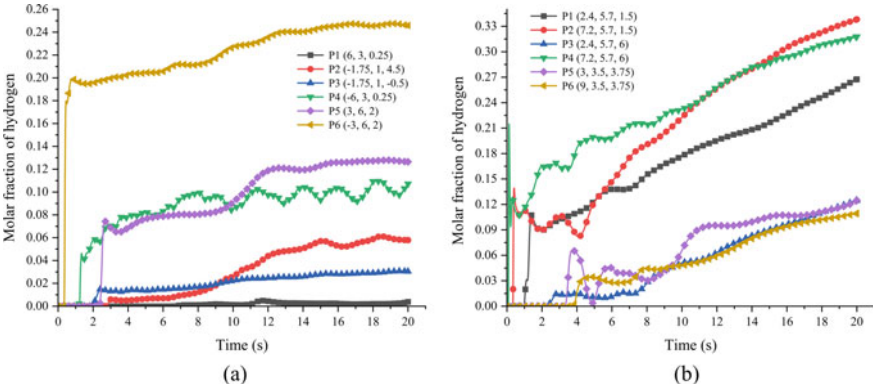

Fig. 4.3 Changes in the molar fraction of hydrogen at monitoring points in hydrogen production room (**a**) and fuel cell room (**b**)

law of hydrogen production, the closer the monitoring point is to the leakage center, the faster the reaction rate is.

4.3.3 Molar Fraction of Hydrogen on Lines at Different Times

As shown in Fig. 4.4a, this section examines the distribution of hydrogen concentrations along a specific straight line by selecting data at specified locations in the hydrogen production room model. The hydrogen molar fraction data are available at different times at the ceiling directly above the leak point and along the side walls. L1 is a straight line along the z-axis at a height of y = 6 m and a cross-section of x = − 3.15 m. L2 is a straight line along the y-axis at a z = 6 m height and a cross-section of x = − 3.15 m.

In the data plot for L1, no hydrogen reaches the position of the L1 straight line at 0.1 s, the area at the top of the leak port is reached by hydrogen in the straight line position until 0.2 s. The curves for 0.5 and 1 s show that the hydrogen gradually diffuses to both sides of the straight line over time, but the hydrogen concentration decreases as the diffusion proceeds. Comparing the curves for 10 and 20 s shows that the hydrogen has completely diffused to the positions on both sides of the straight line and that the molar fraction of hydrogen at the straight line position is gradually increasing as the leakage continues. The hydrogen concentration at the center is always higher than at the surrounding locations, as the hydrogen diffuses from the center to the surroundings. In the data plot for L2, the hydrogen is detected first at the high position in the straight line L2, as it gradually diffuses from the ceiling to the walls. The hydrogen at the top of the room slowly diffuses downwards, and the molar fraction of hydrogen decreases with decreasing altitude.

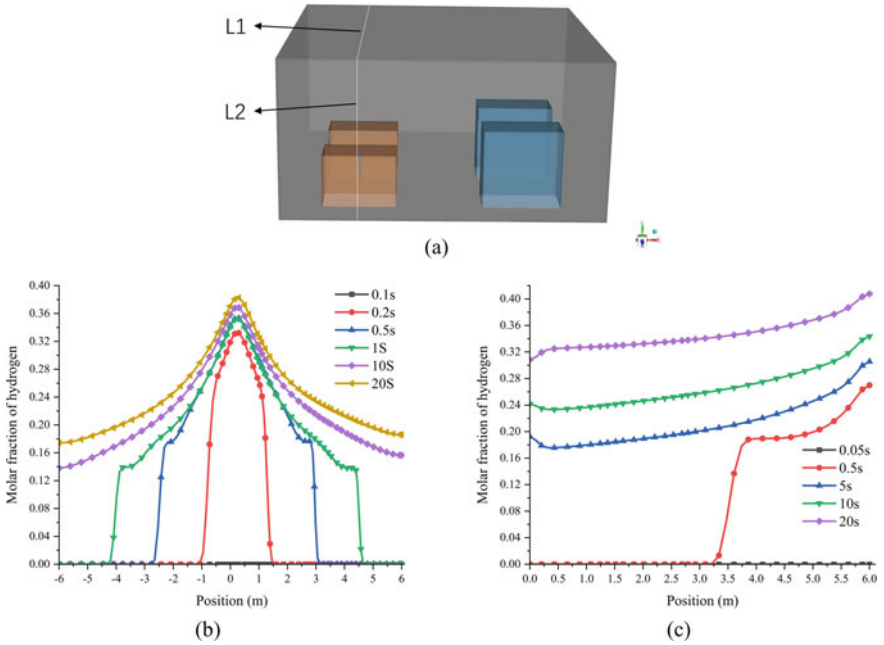

Fig. 4.4 Position of the lines in the hydrogen production room (**a**) and the distribution of the molar fraction of hydrogen on L 1 (**b**), L2 (**c**) at different times

4.3.4 The Effect of Ventilation

In order to study the effect of active ventilation on hydrogen leakage in confined spaces, several active vents were set up in the model and two ventilation scenarios were designed by opening different vents to study the effect of active ventilation on hydrogen leakage in comparison with natural ventilation. The vent arrangement is shown in Fig. 4.5a. The red outline shows the natural ventilation openings, including the doors in the front and rear walls and the window in the middle of the ceiling. The blue outline shows the active vents with a spacing of 3 m between them. Three schemes were chosen to simulate the hydrogen leakage under different ventilation conditions in Table 4.3.

Figure 4.5b shows the change in average molar fraction over 20 s for different ventilation conditions. The graph shows that adding active ventilation to natural ventilation helps to reduce the hydrogen concentration in the room. In comparison, the ventilation at the ceiling is more effective than at the side walls.

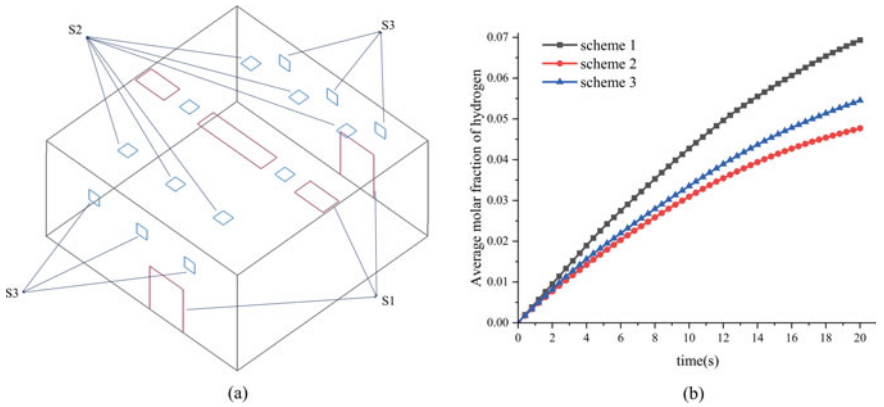

Fig. 4.5 Three ventilation schemes for the hydrogen production room (**a**) and the variation of the average hydrogen molar fraction for different ventilation schemes (**b**)

Table 4.3 Three ventilation schemes for the hydrogen production room

Operating conditions	Ventilation	Vent size (m)	Ventilation rate (m/s)
S1	Natural ventilation only		
S2	Natural ventilation and eight vents at the top	0.64 × 0.64	5
S3	Natural ventilation, six side vents and two central ceiling vents	0.64 × 0.64	5

4.4 Conclusion

In this study, numerical simulations were used to investigate the hydrogen leakage and diffusion behaviour in the water electrolysis hydrogen production room and the fuel cell room, as well as the effect of different ventilation conditions on hydrogen leakage and diffusion. Firstly, CFD models of the two confined spaces were developed based on the actual hydrogen refuelling station layout, and transient simulations of the hydrogen leakage and diffusion processes in the two rooms were carried out using ANSYS Fluent software to derive the hydrogen concentration distribution in each area of the rooms. Subsequently, transient simulations of hydrogen leakage and dispersion in the two rooms were carried out under different ventilation arrangements to compare and analyze the ventilation arrangement that is more conducive to reducing the hydrogen concentration in the rooms. The main results are as follows:

1. the hydrogen leak is very fast, reaching the ceiling in 0.2 s, starting to spread in all directions with the ceiling blocking it, covering the whole ceiling in about 5 s and then being blocked by the side walls, thus continuing to spread down the walls. Around 20 s, the hydrogen covers most of the room. The areas of high

hydrogen concentration are mainly in the path of the hydrogen jet and in the corners of the walls.

2. Among the six monitoring points set up in this paper, monitoring point P6 is located directly above the direction of the leak and is the first to detect the hydrogen leak, while the rest of the monitoring points detect the hydrogen leak after 1 s. There is also a large part of the water electrolysis room that is not equipped with a monitoring point and there may be a better location for a detector.
3. Adding different forced ventilation to the natural ventilation of the room helps to speed up the exit of hydrogen gas to the outside. In this paper, two forced ventilation solutions are provided, and after comparison, it is clear that the addition of forced ventilation to the ceiling of the room in case 2 is more effective for the escape of hydrogen gas.

Acknowledgements This research was funded by the Technology Project of the State Grid Zhejiang Electric Power Company, Ltd., "Research on risk identification and safety protection technology of electric-hydrogen coupling system" (No. B311DS221001).

References

De Stefano M, Rocourt X, Sochet I, Daudey N (2019) Hydrogen dispersion in a closed environment. Int J Hydrogen Energy 44(17):9031–9040

Guan W, Chen J, Chen L, Cao J, Fan H (2023) Safe design of a hydrogen-powered ship: CFD simulation on hydrogen leakage in the fuel cell room. J Marine Sci Eng 11(3)

Hou X, Lan H, Zhao Z, Li J, Hu C, Li Y (2023) Effect of obstacle location on hydrogen dispersion in a hydrogen fuel cell bus with natural and mechanical ventilation. Process Saf Environ Prot 171:995–1008

Jia W, Ren Q, Zhang H, Yang M, Wu X, and Li C (2023) Multicomponent leakage and diffusion simulation of natural gas/hydrogen mixtures in compressor plants. Safety Sci 157

Lacome JM, Jamois D, Perrette L, Proust CH (2011) Large-scale hydrogen release in an isothermal confined area. Int J Hydrogen Energy 36(3):2302–2312

Li F, Yuan Y, Yan X, Malekian R, Li Z (2018) A study on a numerical simulation of the leakage and diffusion of hydrogen in a fuel cell ship. Renew Sustain Energy Rev 97:177–185

Li Y, Wang Z, Shi X, Fan R (2023) Numerical investigation of the dispersion features of hydrogen gas under various leakage source conditions in a mobile hydrogen refueling station. Int J Hydrogen Energy 48(25):9498–9511

Lin H et al (2023) Numerical simulation and consequence analysis of accidental hydrogen fires in a conceptual offshore hydrogen production platform. Int J Hydrogen Energy 48(27):10250–10263

Najjar YSH (2013) Hydrogen safety: the road toward green technology. Int J Hydrogen Energy 38(25):10716–10728

Shu Z et al (2021) Dispersion characteristics of hydrogen leakage: Comparing the prediction model with the experiment. Energy 236

Su Y, Li J, Yu B, Zhao Y (2022) Numerical investigation on the leakage and diffusion characteristics of hydrogen-blended natural gas in a domestic kitchen. Renew Energy 189:899–916

Tamura Y, Takeuchi M, Sato K (2014) Effectiveness of a blower in reducing the hazard of hydrogen leaking from a hydrogen-fueled vehicle. Int J Hydrogen Energy 39(35):20339–20349
Zhang T et al (2022) Numerical study on the flow characteristics of pressurized hydrogen leaking into the confined space through different shaped orifices. Int J Hydrogen Energy 47(83):35527–35539
Zhang X et al (2021) Numerical analysis of the hydrogen dispersion behavior in different directions in a naturally ventilated space. Appl Sci 11(2)

Chapter 5
Hydrogen Purification Characteristics Comparison Between Zeolite Adsorbents 13X and LiX

Chenglong Li, Chunyan Song, Shuo Ma, Bo Zhang, Ziyu Yang, Shicheng Li, Tianqi Yang, Richard Chahine, and Jinsheng Xiao

Abstract Zeolite is a commonly used material for hydrogen purification by pressure swing adsorption (PSA) technology to remove weak components such as N_2 and CO, so the selection of zeolite material is critical to the influence of hydrogen purification performance. In this study, the adsorption capacity of CO_2/CO/N_2/H_2/Ar in zeolite 13X and zeolite LiX was fitted by temperature-dependent Dual-site Langmuir (TD DSL) isotherm model, and the adsorption selectivity, working capacity and isosteric heat adsorption of the two adsorbents were compared and analyzed. The findings demonstrated that zeolite 13X had a higher CO_2 adsorption capacity than zeolite LiX. However, zeolite 13X had a lower CO and N_2 adsorption capacity than zeolite LiX. The selectivity of α-CO/H_2 and α-N_2/H_2 in zeolite LiX is higher than that of zeolite 13X. The working capacity of CO at 13X is slightly higher than that of LiX, while the working capacity of N_2 at LiX is slightly higher than that of 13X. Therefore, zeolite LiX is more suitable for removing N_2 and CO gas than 13X. The selectivity of Ar/H_2 in zeolite LiX is lower than that in zeolite 13X, and the working capacity of Ar in the two adsorbents is almost the same. Therefore, zeolite 13X is more suitable for removing Ar than LiX. The TD DSL model can accurately predict

C. Li · S. Li
Automobile Technology and Service College, Wuhan City Polytechnic, Hubei 430064, China

C. Song · B. Zhang
Shandong Electric Power Engineering Consulting Institute Co., Ltd., Shangdong 250013, China

C. Li · Z. Yang · T. Yang (✉) · J. Xiao
Hubei Research Center for New Energy and Intelligent Connected Vehicle, School of Automotive Engineering, Wuhan University of Technology, Hubei 430070, China
e-mail: tqyang@whut.edu.cn

S. Ma
Intelligent Manufacturing and Automobile School, Chongqing College of Electronic Engineering, Chongqing 401331, China

R. Chahine · J. Xiao
Hydrogen Research Institute, Université du Québec À Trois-Rivières, Trois-Rivières, QC G8Z 4M3, Canada

Z. Sun and P. K. Das (eds.), *Proceedings of the 10th International Conference on Energy Engineering and Environmental Engineering*, Environmental Science and Engineering, https://doi.org/10.1007/978-3-031-48204-5_5

the static single adsorption behavior and dynamic breakthrough behavior of multi-component on the two adsorbents. The breakthrough behavior of multi-component shows that the weakest component gas (N_2 or Ar) as the major impurity is the first component to breakthrough.

Keywords Zeolite · Adsorbent characteristics · Hydrogen purification · TD DSL isotherm · Breakthrough curve

5.1 Introduction

As a kind of secondary energy with abundant sources, green and low carbon, hydrogen energy is an essential direction of the global energy technology revolution. Pressure swing adsorption (PSA) technology is an appropriate way to achieve high-purity hydrogen at low operating costs and high efficiency. PSA technology is developed based on the principle that the adsorbent material has a stronger selective adsorption performance for impurity gas than hydrogen (Moon et al. 2016; Park et al. 2021). The selection of adsorbent materials in the PSA process is a key factor determining the overall performance of the PSA hydrogen purification process (Kim et al. 2022). When selecting suitable adsorption materials for PSA systems, adsorbent characteristics such as adsorption selectivity, working capacity, and adsorption thermodynamic characteristics should be considered (Yulia et al. 2021).

Various adsorbents have different adsorption selectivity for impurity gas (Zhou et al. 2015), so the layered bed composed of activated carbon and zeolite is commonly used to remove impurity gas (Xiao et al. 2020). For a layered bed, activated carbon is used to adsorb selectively CO_2 and light hydrocarbons such as CH_4. The zeolite is used as the second layer to remove carbon monoxide and nitrogen. It is crucial to investigate a PSA process by using zeolite since the zeolite plays a significant role in the primary part of the adsorption bed (Xiang et al. 2020). Lee et al. used activated carbon (AC), zeolite 13X and zeolite LiX as adsorbents to compare the adsorption capacity of six component gases at different temperatures (293 K, 308 K and 323 K). Different adsorption isotherm models were used to fit the experimental data to study the adsorption equilibrium and kinetics of gas in different adsorbents (Park et al. 2016, 2014; Hong et al. 2022).

In this work, the adsorption equilibria of CO_2, CO, N_2, Ar and H_2 on zeolite 13X and zeolite LiX were compared and analyzed. By comparing the working capacity, isosteric adsorption heat and adsorption selectivity, the separation characteristics of two adsorbents was comprehensively evaluated. In addition, the dynamic breakthrough curves of the hydrogen mixture in the two adsorbents were compared.

5.2 Mathematical Modeling of Adsorbent Characteristics

In our previous study, experimental adsorption amounts of CO_2, CO, N_2, CH_4 and H_2 on pelletized zeolite 13X were correlated with common-used isotherm models and temperature-dependent (TD) isotherm models (Li et al. 2023). This study mainly uses the TD dual-site Langmuir (DSL) model to calculate and compare the adsorption characteristics of zeolite 13X and zeolite LiX.

5.2.1 Pure Component and Multi-Component Isotherms

Based on the Langmuir model, the DSL model assumes dual-site adsorption sites and can be applied to the heterogeneous surface of adsorbents (Hong et al. 2022):

$$q = q_{m,\mathrm{DSL1}} \frac{B_{\mathrm{DSL1}} p}{1 + B_{\mathrm{DSL1}} p} + q_{m,\mathrm{DSL2}} \frac{B_{\mathrm{DSL2}} p}{1 + B_{\mathrm{DSL2}} p} \tag{5.1}$$

where q is the adsorption amount, p is the pressure, $q_{m,\mathrm{DSL}}$ and B_{DSL} are the saturation capacity and the affinity for the two sites, respectively.

The variables B_{DSL1} and B_{DSL2} in the DSL model can be expressed in the temperature-dependent form:

$$q_{m,\mathrm{DSL1}} = K_{\mathrm{DSL1}} \tag{5.2}$$

$$B_{\mathrm{DSL1}} = K_{\mathrm{DSL2}} \exp(K_{\mathrm{DSL3}}/T) \tag{5.3}$$

$$q_{m,\mathrm{DSL2}} = K_{\mathrm{DSL4}} \tag{5.4}$$

$$B_{\mathrm{DSL2}} = K_{\mathrm{DSL5}} \exp(K_{\mathrm{DSL6}}/T) \tag{5.5}$$

So temperature-dependent dual-site Langmuir (TD DSL) is given as (Hong et al. 2022):

$$q = K_{\mathrm{DSL1}} \frac{K_{\mathrm{DSL2}} \exp(K_{\mathrm{DSL3}}/T) p}{1 + K_{\mathrm{DSL2}} \exp(K_{\mathrm{DSL3}}/T) p} + K_{\mathrm{DSL4}} \frac{K_{\mathrm{DSL5}} \exp(K_{\mathrm{DSL6}}/T) p}{1 + K_{\mathrm{DSL5}} \exp(K_{\mathrm{DSL6}}/T) p} \tag{5.6}$$

The extended TD DSL model is usually used for the adsorption of multi-component gas (Moon et al. 2016; Park et al. 2021):

$$q_j = K_{\mathrm{DSL1},j}\frac{K_{\mathrm{DSL2},j}\exp\left(K_{\mathrm{DSL3},j}/T\right)p_j}{1+\sum_{j=1}^{n}K_{\mathrm{DSL2},j}\exp\left(K_{\mathrm{DSL3},j}/T\right)p_j} + K_{\mathrm{DSL4},j}\frac{K_{\mathrm{DSL5},j}\exp\left(K_{\mathrm{DSL6},j}/T\right)p_j}{1+\sum_{j=1}^{n}K_{\mathrm{DSL5},j}\exp\left(K_{\mathrm{DSL6},j}/T\right)p_j} \tag{5.7}$$

where j is the gas component.

The fitting parameters of the TD DSL model on zeolite LiX and 13X for pure components are shown in Table 5.1. The fitting results of TD DSL to each component are shown in Fig. 5.1a–e. The TD DSL fitting results agree with the experimental data (Park et al. 2016, 2014). By comparison, zeolite 13X had a higher CO_2 adsorption amount than zeolite LiX. However, zeolite 13X had a lower adsorption amount of CO, N_2, Ar and H_2 than LiX. The adsorption isotherm data shows that the adsorption capacity of zeolite adsorbent to CO_2 gas at low pressure is also very high, which will cause difficulty in CO_2 desorption. Therefore, CO_2 will be avoided from entering the zeolite layer when designing the layered bed. From the perspective of the adsorption amount of CO_2, zeolite LiX is more suitable. For removing CO and N_2, zeolite LiX is also more suitable than zeolite 13X. However, the zeolite LiX has higher H_2 adsorption amount than 13X, so the two adsorbents cannot be judged not only from the adsorption capacity but also from the other adsorbent characteristic indicators.

TD DSL model: K_{DSL1}, mol/kg; K_{DSL2}, 1/kPa; K_{DSL3}, K; K_{DSL4}, mol/kg; K_{DSL5}, 1/kPa; K_{DSL6}, K.

Table 5.1 Isotherm parameters of TD DSL models on zeolite LiX and 13X (Li et al. 2023)

Component	Adsorbent	TD DSL model					
		K_{DSL1}	$K_{\mathrm{DSL2}}*10^6$	K_{DSL3}	K_{DSL4}	$K_{\mathrm{DSL5}}*10^9$	K_{DSL6}
CO_2	LiX	3.077	2052	2013	2.78	4.097E-5	7755
	13X	3.395	17.96	2964	2.305	6.304	4291
CO	LiX	1.214	0.6224	3514	2.465	312.1	2577
	13X	2.708	0.266	2502	1.165	392.1	3006
N_2	LiX	0.8707	0.1115	3488	2.361	468.2	2284
	13X	2.761	1.177	1955	0.547	73.29	3064
H_2	LiX	5.309	4.352	707.3	0.03141	0.4728E9	2238
	13X	3.101	0.6638	1294	1.118	38,190	52.41
Ar	LiX	5.618	2.165	1359	0.10733	1957	1396
	13X	3.597	2.57	1373	2.171	12.23	2407

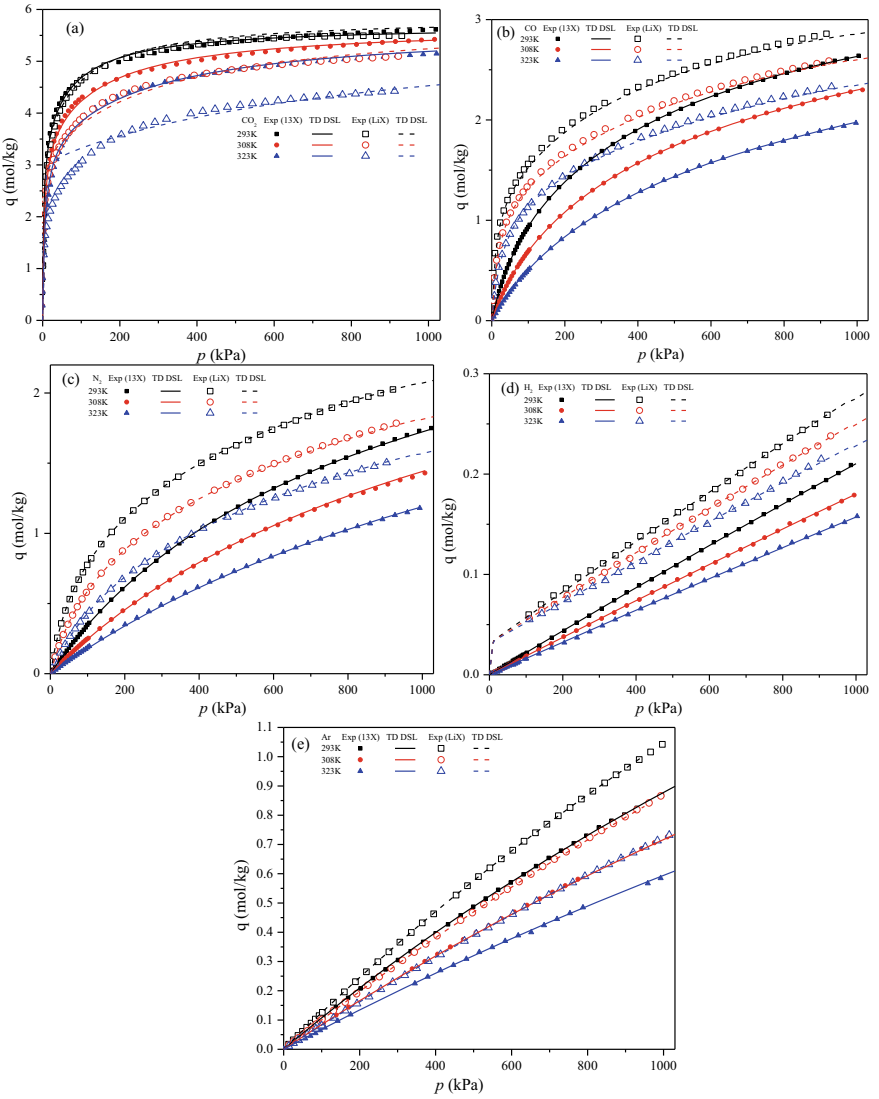

Fig. 5.1 Adsorption isotherms of **a** CO_2, **b** CO, **c** N_2, **d** H_2 and **e** Ar (solid symbol: experimental data of 13X from Ref. (Park et al. 2016); hollow symbol: experimental data of LiX from Ref. (Park et al. 2014), solid line: TD DSL for zeolite 13X, dash line: TD DSL for zeolite LiX)

5.2.2 Ideal Adsorbed Solution Theory Model

The selectivity of an adsorbent is an important indicator for evaluating the purification performance, which determines the adsorption and separation efficiency of the adsorbent towards the adsorbate (Xiang et al. 2020). The commonly used method for

solving selectivity is the ideal adsorbed solution theory (IAST) (Chang et al. 2022) (Oschatz and Antonietti 2018). From the IAST, the spreading pressure π is given by (Zhou et al. 2015),

$$\pi_i^0\left(p_i^0\right) = \frac{RT}{A}\int_0^{p_i^0} q d\ln p \tag{5.8}$$

where p_i^0 is the gas pressure of component i that corresponds to the spreading pressure π. A is the specific surface area of the adsorbent, R is the molar gas constant.

For binary adsorption of components 1 and 2, the IAST requires

$$y_1 p_t = x_1 p_1^0, (1 - y_1) p_t = (1 - x_1) p_2^0 \tag{5.9}$$

where y_i and x_i are the molar fractions of component i in gas phase and adsorbed phase, respectively, and p_t is the total gas pressure. Combining Eq. (5.8) and (5.9), x_i can be obtained. In a binary mixture, adsorption selectivity is defined as:

$$\alpha_{12} = x_1 y_2 / x_2 y_1 \tag{5.10}$$

Another important adsorbent characteristic parameter is the working capacity (WC). The higher the WC, the higher the product productivity. The working capacity is defined as:

$$\mathrm{WC} = q(p_h, T_h) - q(p_l, T_l) \tag{5.11}$$

where $q(p_h, T_h)$ is the gas adsorption amount under adsorption conditions, and $q(p_l, T_l)$ is the gas adsorption amount under regeneration conditions (Elfving et al. 2017). The pressure for regeneration in this article is set to 1 bar.

5.2.3 Clausius–Clapeyron Equation

The isosteric heat of adsorption, Q_{st}, is the heat released when the adsorbate binds to the solid surface of the adsorbent. Generally, the Clausius–Clapeyron equation is utilized to solve the heat of adsorption from different adsorption isotherm models:

$$Q_{st} = RT^2(\partial \ln p / \partial T)_q \tag{5.12}$$

5.3 Results and Discussion

5.3.1 Comparison of Selectivity and Working Capacity Calculated by IAST Between Zeolite 13X and LiX

The characteristics of a suitable adsorbent have high working capacity, high adsorption selectivity, and low adsorption heat (Edens et al. 2023). As shown in Fig. 5.2, for zeolite LiX and zeolite 13X, the selectivity order is α-$CO_2/H_2 > \alpha$-$CO/H_2 > \alpha$-$N_2/H_2 > \alpha$-Ar/H_2. The adsorption selectivity order of each impurity gas over H_2 is the same as the order of the adsorption capacity. The working capacity of each impurity gas also follows a similar pattern. Because zeolite LiX and 13X have a high adsorption affinity for CO_2 at both low and high pressure, the working capacity of zeolite LiX and 13X for CO_2 is not very high. For CO and N_2 gases, the selectivity of α-CO/H_2 and α-N_2/H_2 on zeolite LiX is higher than that on 13X. The working capacity of CO at 13X is slightly higher than that of LiX, while the working capacity of N_2 at LiX is slightly higher than that of 13X. Therefore, zeolite LiX is more suitable for removing N_2 and CO gases than 13X. The selectivity of Ar/H_2 in zeolite LiX is lower than that in zeolite 13X, and the working capacity of Ar in the two adsorbents is not significantly different. Therefore, zeolite 13X is more suitable for removing Ar than LiX.

5.3.2 Comparison of Isosteric Heat of Adsorption Between Zeolite 13X and LiX

Isosteric heat of adsorption is often used to evaluate the affinity between gas molecules and adsorbent materials. The isosteric heats of adsorption for zeolite 13X and LiX were calculated by the Clausius–Clapeyron equation along with the temperature dependence (TD) Sips isotherm model. The parameters of the TD Sips model are from Ref. (Park et al. 2016, 2014). As shown in Fig. 5.3, for the two zeolites, the sequence of heat of adsorption was $CO_2 > CO > N_2 > Ar > H_2$. which is the same as the order of adsorption capacity. The adsorption heat of each gas on zeolite LiX and zeolite 13X changes with the adsorption amount, thereby indicating the surface energy heterogeneity in each gas adsorption. By comparison, except for H_2 and Ar, the adsorption heat of CO_2, CO and N_2 on zeolite LiX is higher than that on zeolite 13X.

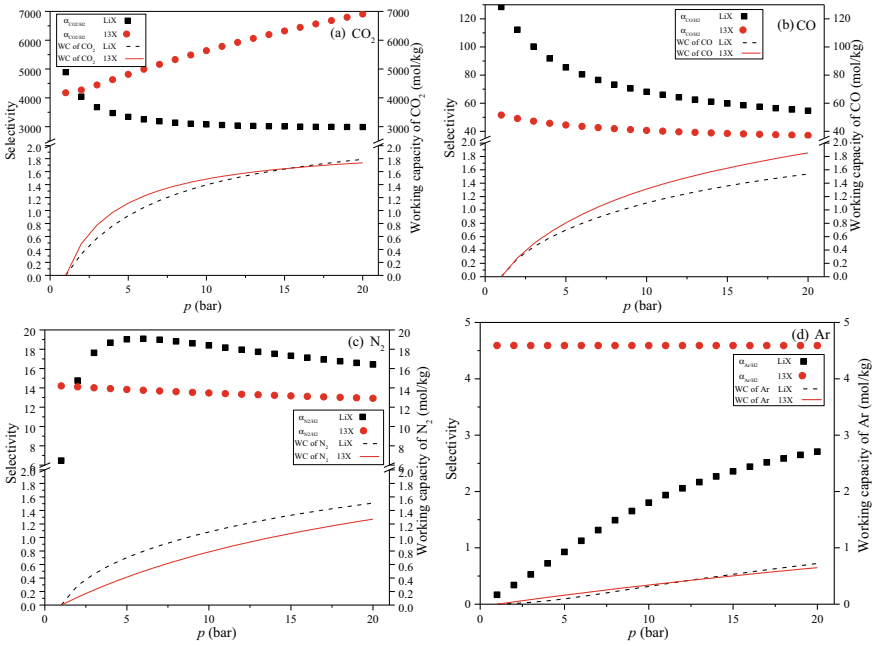

Fig. 5.2 Estimation of selectivity (symbol) and working capacity (line) using IAST for zeolite LiX (black) and zeolite 13X (red) at 308 K up to 20 bar for the (50/50 vol.%) binary mixture of **a** CO_2/H_2, **b** CO/H_2, **c** N_2/H_2, **d** Ar/H_2

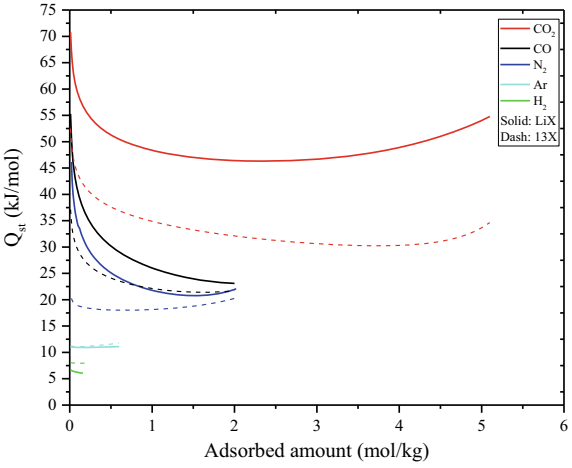

Fig. 5.3 Isosteric heat of adsorption on adsorbents as a function of adsorbed amount (Dash line: Zeolite 13X; Solid line: Zeolite LiX)

5.3.3 *Comparison of Breakthrough Curves Between Zeolite 13X and LiX*

The breakthrough curve dynamically reflects the adsorption capacity of the adsorbent to the adsorbate. Figure 5.4 shows the simulation of the breakthrough curves by the extended TD DSL for a mixture ($N_2/CO_2/H_2/CO$ = 44.6%/35.4%/19.9%/0.1%) at 10 bar and 3 LSTP/min feed flow rate in (a) the zeolite 13X bed and a mixture (H_2/ N_2/CO/CO_2/Ar = 88%/6%/3%/2%/1%) at 35 bar and 5 LSTP/min in (b) the zeolite LiX bed. The characteristics of the adsorption bed are the same, the reader can refer to Refs. (Moon et al. 2016; Park et al. 2021), the mathematical equations used in the Aspen Adsorption software for breakthrough curve simulation can refer to Ref. (Li et al. 2023). The breakthrough curve simulated by the extended TD DSL is in good agreement with the experimental values, indicating that TD DSL can effectively reflect the competitive adsorption behavior of multi-component gases in the adsorption bed.

By comparing the breakthrough behavior of four-component and five-component systems on zeolite 13X and LiX, the gas breakthrough order is same as the order of adsorption capacity. N_2 on zeolite 13X or Ar on zeolite LiX are the weakest component gases on four-component systems and five-component systems and they are the first component to breakthrough. CO_2, as a strong component gas, is the latest component to breakthrough. Therefore, to obtain high-purity hydrogen, the removal of weakest component gases is crucial.

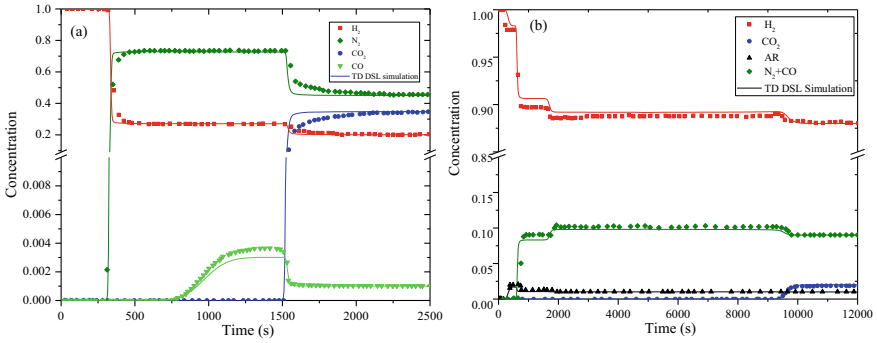

Fig. 5.4 Breakthrough curves in **a** the zeolite 13X bed at 10 bar and 3 LSTP/min feed flow rate [experimental data in symbols from Ref. (Park et al. 2021), simulation data in line by Aspen Adsorption software (Li et al. 2023)], **b** the zeolite LiX bed at 35 bar and 5 LSTP/min feed flow rate [experimental data in symbols from Ref. (Moon et al. 2016)]

5.4 Conclusion

Adsorption isotherm models can be used to evaluate and calculate the adsorbent characteristics. The ideal adsorbent usually has a high selectivity and working capacity, but a low adsorption heat. By comparing the selectivity and adsorption capacity, zeolite LiX is more suitable for removing N_2 and CO gas than 13X, and zeolite 13X is more suitable for removing Ar than LiX. By comparing the isosteric heat of adsorption, the adsorption heat of CO_2, CO and N_2 on zeolite LiX is higher than that on zeolite 13X. Therefore, the selection of the zeolite will involve a trade-off between two or more of the adsorbent characteristics. In future work, a comprehensive adsorption performance indicator will be considered to compare the two zeolite materials. The TD DSL model can accurately describe the static adsorption behavior and dynamic breakthrough behavior of multi-component gas on zeolites. From the breakthrough behavior of multi-component, the weakest component gases are the first gases to breakthrough. The research can provide guidance for selecting PSA materials for hydrogen purification, helping to customize and optimize separation for each specific PSA system.

Acknowledgements This research was funded by the Research Project of the Shandong Electric Power Engineering Consulting Institute Co., Ltd. (042300007948), the Shuguang Project of Knowledge Innovation Program from the Wuhan Science and Technology Bureau (2022010801020432, 2023010201020479), the National Natural Science Foundation of China (52176191), the Science and Technology Research Project of Education Department of Hubei Province (B2022607), the 111 Project of China (B17034), and the Innovative Research Team Development Program of the Ministry of Education of China (IRT_17R83).

References

Chang M, Wang F, Wei Y, Yang Q, Wang JX, Liu D et al (2022) Separation of CH_4/ N_2 by an ultra-stable metal–organic framework with the highest breakthrough selectivity. AlChE J 68

Edens SJ, McGrath MJ, Guo S, Du Z, Zhou H, Zhong L et al (2023) An upper bound visualization of design trade-offs in adsorbent materials for gas separations: CO_2, N_2, CH_4, H_2, O_2, Xe, Kr, and Ar adsorbents. Adv Sci e2206437

Elfving J, Bajamundi C, Kauppinen J, Sainio T (2017) Modelling of equilibrium working capacity of PSA, TSA and TVSA processes for CO_2 adsorption under direct air capture conditions. J CO_2 Utilization 22:270–277

Hong S-H, Chung K, Bang G, Kim K-M, Lee C-H (2022) Adsorption equilibria and kinetics of CO_2, CH_4, CO, N_2, and H_2 on KOH-treated activated carbon pellets up to 1000 kPa. Chem Eng J 431

Kim SH, Landa HOR, Ravutla S, Realff MJ, Boukouvala F (2022) Data-driven simultaneous process optimization and adsorbent selection for vacuum pressure swing adsorption. Chem Eng Res Des 188:1013–1028

Li C, Ye F, Chahine R, Yang T, Xiao J (2023) Genetic algorithm optimized artificial neural network models of single- and multi-component gas adsorption isotherms for hydrogen purification. Int J Hydrogen Energy. https://doi.org/10.1016/j.ijhydene.2023.04.352

Moon D-K, Lee D-G, Lee C-H (2016) H_2 pressure swing adsorption for high pressure syngas from an integrated gasification combined cycle with a carbon capture process. Appl Energy 183:760–774

Oschatz M, Antonietti M (2018) A search for selectivity to enable CO_2 capture with porous adsorbents. Energy Environ Sci 11:57–70

Park Y, Moon D-K, Kim Y-H, Ahn H, Lee C-H (2014) Adsorption isotherms of CO_2, CO, N_2, CH_4, Ar and H_2 on activated carbon and zeolite LiX up to 1.0 MPa. Adsorption 20:631–47

Park Y, Ju Y, Park D, Lee C-H (2016) Adsorption equilibria and kinetics of six pure gases on pelletized zeolite 13X up to 1.0 MPa: CO_2 , CO, N_2 , CH_4 , Ar and H_2. Chem Eng J. 292:348–65

Park Y, Kang J-H, Moon D-K, Jo YS, Lee C-H (2021) Parallel and series multi-bed pressure swing adsorption processes for H_2 recovery from a lean hydrogen mixture. Chem Eng J 408

Xiang H, Fan X, Siperstein FR (2020) Understanding ethane/ethylene adsorption selectivity in ethane-selective microporous materials. Sep Purif Technol 241

Xiao J, Li C, Fang L, Böwer P, Wark M, Bénard P et al (2020) Machine learning–based optimization for hydrogen purification performance of layered bed pressure swing adsorption. Int J Energy Res 44:4475–4492

Yulia F, Chairina I, Zulys A, Nasruddin (2021) Multi-objective genetic algorithm optimization with an artificial neural network for CO_2/CH_4 adsorption prediction in metal–organic framework. Therm Sci Eng Prog 25

Zhou X, Huang W, Miao J, Xia Q, Zhang Z, Wang H et al (2015) Enhanced separation performance of a novel composite material GrO@MIL-101 for CO_2/CH_4 binary mixture. Chem Eng J 266:339–344

Chapter 6
Numerical Simulation and Risk Assessment of Hydrogen Leakage from Fuel Cell System Room in Skid-Mounted Hydrogen Refueling Station

Xianglin Yan, Min Liu, Bo Zhao, Qiliang Wu, Tianqi Yang, Qingxin Ba, Xuefang Li, and Jinsheng Xiao

Abstract With the increasing use of hydrogen in countries around the world, the number of hydrogen refueling stations has grown. However, due to the characteristics of hydrogen, it is prone to serious consequences in case of leakage, and safety issues have been limiting the development of hydrogen energy. In this study, a fuel cell system room model of actual size was established, and the hydrogen leakage accident was simulated. The diffusion law of hydrogen leakage and the variation law of the volume and mass of flammable hydrogen at different leakage rates were analyzed. And it was found that the leakage rate has a small effect on the volume and a more significant effect on mass for the current room size. Then, the effect of ventilation wind speed on the volume and mass of the flammable hydrogen was investigated, and the results show that the volume decreases slowly and the mass decreases more rapidly with increasing wind speed. Finally, the TNT equivalent method was used to assess the extent of the effects of a flammable hydrogen explosion.

Keywords Skid-mounted hydrogen refueling station · CFD simulation · Hydrogen leakage · TNT equivalent method

X. Yan · T. Yang (✉) · J. Xiao
Hubei Research Center for New Energy and Intelligent Connected Vehicle, School of Automotive Engineering, Wuhan University of Technology, Wuhan 430070, China
e-mail: tqyang@whut.edu.cn

M. Liu (✉) · B. Zhao · Q. Wu
Research Institute of State Grid Zhejiang Electric Power Co., Ltd, Hangzhou 310006, China
e-mail: liumhb@126.com

Q. Ba · X. Li · J. Xiao
Institute of Thermal Science and Technology, Shandong University, Jinan 250061, China

Z. Sun and P. K. Das (eds.), *Proceedings of the 10th International Conference on Energy Engineering and Environmental Engineering*, Environmental Science and Engineering, https://doi.org/10.1007/978-3-031-48204-5_6

6.1 Introduction

With the growing concern about carbon emissions and climate change in countries around the world, hydrogen is increasingly being used as a clean secondary energy source in various countries. Meanwhile, electrolytic hydrogen production is one of the methods to effectively mitigate the indirectness of renewable energy sources (Yang et al. 2021). As the number of fuel cell vehicles and renewable energy generation systems has increased in recent years, more matching hydrogen refueling station facilities are needed. However, due to the nature of hydrogen, it is easy to cause accidents such as fires and explosions in case of leakage, so the diffusion law of hydrogen leakage and the hazards need to be analyzed.

In order to analyze the consequences of hydrogen leakage accidents, many scholars have conducted experimental and numerical simulation studies. Denisenko et al. (2009) summarized experimentally the diffusion mechanism of hydrogen gas. The results show that at hydrogen leak velocities below 150 m/s, the hydrogen diffusion pattern is a "Filling box", and the hydrogen diffusion pattern is a "Fading up box" at higher leak rates. Pitts et al. (2012). carried out a hydrogen leak explosion experiment in a residential depot. The findings showed that when there is no vehicle, the hydrogen fills from top to bottom; hydrogen gas collects around the vehicle as it is released underneath it. Choi et al. (2013) investigated the diffusion of hydrogen gas in an underground garage after leakage from a car and analyzed the effect of leakage flow and ventilators on hydrogen accumulation. Liang et al. (2019) analyzed the effects of leak direction, wind direction and speed on the outcome of a spill accident for the first renewable energy hydrogen refueling station in China. Goswami and Sun (2022) simulated the diffusion characteristics of a flammable cloud in a storage tank leakage accident at a hydrogen refueling stations and investigated the potential overpressure effects of vapor cloud explosions. Some other scholars have studied the dispersion of hydrogen leakage in small confined spaces (e.g., private garages (Venetsanos et al. 2010), ship cabins (Li et al. 2018), etc.) through simulations and found significant concentration stratification of flammable hydrogen clouds in confined spaces.

In addition, to investigate the fire accidents generated by hydrogen leaks, Scheferr et al. (2006) found through experiments that the size of a high-pressure hydrogen vertical jet flame is related to the storage pressure, leak diameter and mass flow rate. Brennan et al. (2009) performed a fundamental study of the flame length and width of hydrogen under-expansion jet fires based on a large vortex simulation method. Cirrone et al. (2019) used a vortex dissipative combustion model and a DO thermal radiation model to analyze the thermal radiation hazards of hydrogen under-expansion jet fires.

In summary, many scholars have conducted simulation studies and risk assessments of hydrogen leakage. It can be seen that these parameters, such as leak location, ambient wind speed, etc., have an impact on the outcome of a leak accident, especially in a relatively closed situation. However, skid-mounted hydrogen refueling stations (SHRS) and hydrogen refueling stations coupled with renewable energy

systems have been less studied. Therefore, in this paper, numerical simulations are conducted to evaluate the explosion hazard effects of flammable clouds in the event of hydrogen leakage from fuel cell vessels in SHRS.

6.2 Model Introduction and Validation

6.2.1 Fundamental Governing Equation

This paper uses Fluent software to simulate the hydrogen leak diffusion. The equations involved include the continuity equation, the energy conservation equation, and several others. The continuity equation is shown below:

$$\frac{\partial \rho}{\partial t} + \nabla \cdot (\rho \boldsymbol{u}) = 0 \tag{6.1}$$

where ρ is the density of hydrogen, kg/m^3; t is the time, s; $\boldsymbol{u}$ is the velocity vector in x, y, z directions, m/s.

The momentum equation can be expressed as:

$$\frac{\partial (\rho \boldsymbol{u})}{\partial t} + \nabla \cdot (\rho \boldsymbol{u}\boldsymbol{u}) = -\nabla p + \nabla \cdot \overline{\tau} + \boldsymbol{F} \tag{6.2}$$

where p is pressure, Pa; $\overline{\tau}$ is stress tensor, Pa, $\boldsymbol{F}$ is the body force, N.

The conservation of energy equation can be expressed as:

$$\begin{aligned} \frac{\partial \left(\rho c_p T\right)}{\partial t} + \nabla \cdot \left(\rho c_p \boldsymbol{u} T\right) &= \frac{\partial}{\partial x}\left(k \frac{\partial T}{\partial x}\right) \\ &+ \frac{\partial}{\partial y}\left(k \frac{\partial T}{\partial y}\right) + \frac{\partial}{\partial z}\left(k \frac{\partial T}{\partial z}\right) + \emptyset + S_h \end{aligned} \tag{6.3}$$

where c_p is the specific heat capacity at constant pressure, J/(kg K); T is temperature, K; k is thermal conductivity, W/(m·K); $\emptyset$ is dissipation function; S_h is the internal heat source in fluid, W/m^3.

The Species transport equation can be expressed as:

$$\begin{aligned} \frac{\partial (\rho c_i)}{\partial t} + \nabla \cdot (\rho c_i \boldsymbol{u}) &= \frac{\partial}{\partial x}\left(D_i \frac{\partial (\rho c_i)}{\partial x}\right) \\ &+ \frac{\partial}{\partial y}\left(D_i \frac{\partial (\rho c_i)}{\partial y}\right) + \frac{\partial}{\partial z}\left(D_i \frac{\partial (\rho c_i)}{\partial z}\right) \end{aligned} \tag{6.4}$$

where c_i is the volume fraction of component i; D_i is the diffusion coefficient of component i, m^2/s.

6.2.2 Model and Mesh Generation

The actual scene and dimensions of the fuel cell (FC) room of the proposed SHRS are modeled as shown in Fig. 6.1a. The FC system of this SHRS is centralized in a 5 m × 2.5 m × 3 m room, and the system includes two fuel cells. There are blinds and rolling doors on both sides of the room, where the size of the blinds is 4 m × 0.4 m, the rolling doors of the room are closed during the operation of the equipment, and there is an active ventilation window of size 0.6 × 0.6 m on the top of the room, and it is closed in non-emergency conditions. A hydrogen detection device is installed in the center of the ceiling (2.5 m, 2.99 m, 1.25 m) to detect hydrogen leaks. For calculation purposes, the equipment in the room was simplified, and only the FC system that could leak was retained, with the leak being the hydrogen inlet to the FC.

Figure 6.1b shows the meshing of the model, which is realized by ANSYS ICEM software. The main body of the room is divided by a hexahedral mesh, and the o-block mesh is used at the leakage location with local encryption. To verify the independence of the grids, four different numbers of grids were generated, with the four grids having a grid number of 1.3×10^5, 1.7×10^5, 2.1×10^5 and 2.5×10^5 respectively. The grid independence was verified by detecting the molar fraction of hydrogen gas located at the detection point of the ceiling position, as shown in Fig. 6.2. Based on the simulation results, considering the computational accuracy and time, a mesh number of 210,000 was finally selected for subsequent simulations.

Hydrogen leakage was simulated using Fluent software, and the turbulence model was chosen as the standard k-ε model for the calculations. The simulation process considers the effects of gravity and buoyancy. Consider the case of a severe pipe rupture leak. The notional nozzle method was used to simplify the leakage inlet. The simplified leakage port has a diameter of 64 mm and is set as a mass flow inlet at 0.22834 kg/s. The room door is closed and set as a closed wall. The louvers on both sides are set as pressure outlets and the active ventilation windows are set as velocity inlets or wall surface.

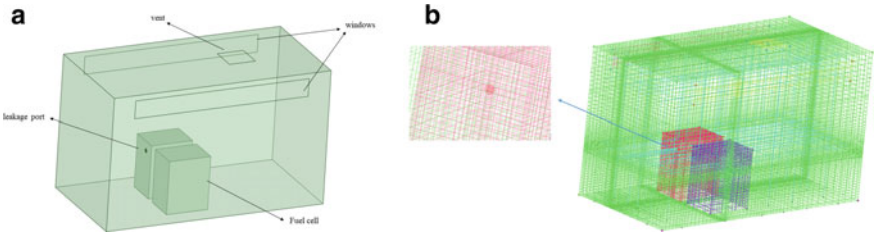

Fig. 6.1 Schematic diagram of 3D simplified model (**a**) and Grid division of fuel cell room (**b**)

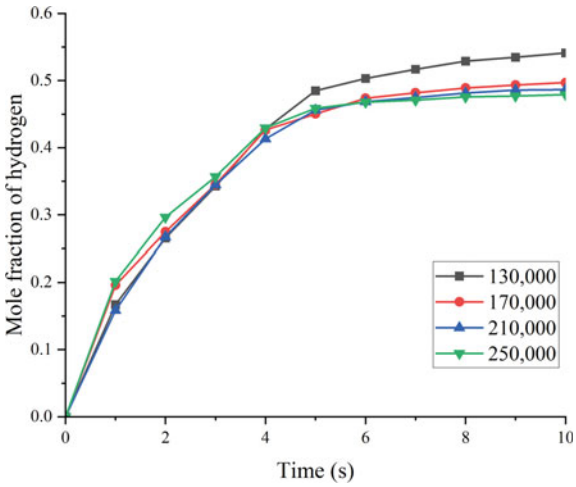

Fig. 6.2 Grid independence verification

6.3 Diffusion Characteristics of Flammable Hydrogen Clouds in Fuel Cell Room

6.3.1 Diffusion Characteristics Under Passive Ventilation

The hydrogen leakage simulation is performed with the boundary condition settings introduced in Sect. 2.2. The active ventilation window pass is not opened and set to closed wall. Figure 6.3 shows the variation of combustible hydrogen cloud in the FC room at different moments. From the figure, it can be seen that at a leak rate of 0.22834 kg/s, the hydrogen has spread to the wall in the direction of the leak opening in 0.1 s and started to spread in all directions. When the hydrogen gas leaked for 0.5 s, it spread to the surrounding walls and started to spread along the walls to the area with a low concentration of hydrogen in the room, and at the same time, the hydrogen gas that spread to the ground started to spread upward due to buoyancy. When 4 s elapsed, the room was already filled with a cloud of flammable hydrogen gas, and the concentration of hydrogen gas was high in the area close to the leak and relatively low in the area away from the leak. When leaking for 60 s, the concentration of flammable hydrogen increased further, with some areas approaching the upper limit of the flammable range, while near the window the hydrogen concentration at that location was at a lower value due to the release of hydrogen gas.

The variation of the flammable hydrogen cloud volume in the room with time is shown in Fig. 6.4a. The volume of the combustible hydrogen grows rapidly in 3 s time and finally the volume is stable and approximately equal to the volume of the room. This is due to the small space in the room of the SHRS and the high leakage rate when the high-pressure hydrogen from the FC system leaks, and the flammable hydrogen gas cloud cannot be released through the set windows. Figure 6.4b shows the variation of the mass of flammable hydrogen gas in the room with time. The mass

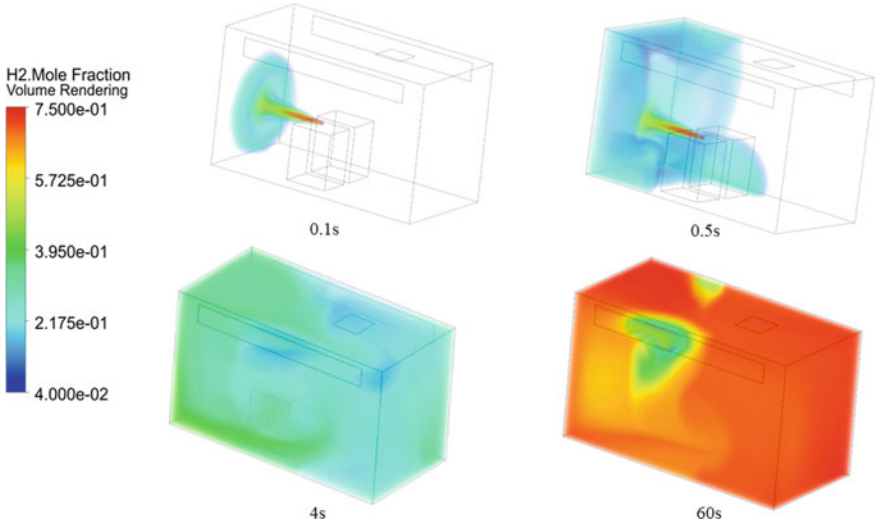

Fig. 6.3 Fuel cell room flammable hydrogen cloud distribution at different moments

of hydrogen increases basically linearly in the first 20 s of time, while the rise in the mass of hydrogen slows down significantly when the time exceeds 20 s, which is due to the further increase in the ability of the window as a pressure outlet to release hydrogen, limiting the increase in the hydrogen mass in the room.

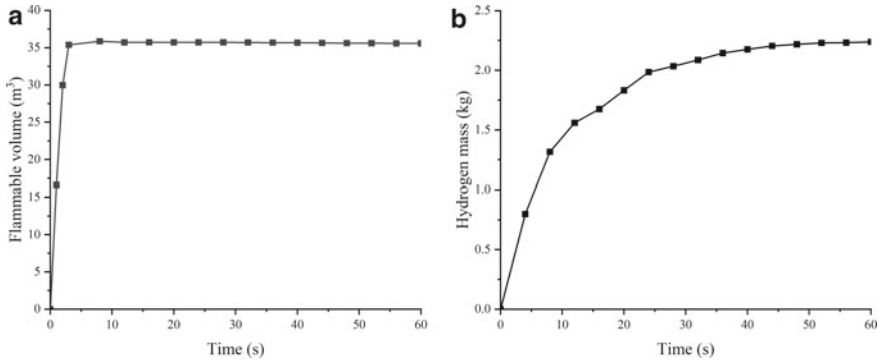

Fig. 6.4 Change of flammable cloud volume (**a**) and hydrogen mass (**b**) with time in the fuel cell room

6.3.2 *Effect of Flow Rate and Ventilation on the Volume and Mass of Flammable Hydrogen*

The SHRS in this study is equipped with an exhaust fan for active ventilation on the top of the room for exhausting leaking hydrogen outside from a safety point of view. However, when hydrogen leaks continuously, flammable hydrogen may still accumulate due to insufficient ventilation, so it is worthwhile to study the effect of exhaust fan ventilation speed on flammable hydrogen gas. In addition, the rate of hydrogen leakage has an equally significant effect on the flammable hydrogen gas. First, in order to analyze the effect of hydrogen leak rate on the mass and volume of flammable hydrogen, three different leak mass flow rates of 0.22834 kg/s, 0.14584 kg/s and 0.06334 kg/s were set for the study.

Figure 6.5a shows the variation pattern of flammable hydrogen volume with time for different leakage mass flow rates. As can be seen from the figure, the effect of the leak rate on the volume of the flammable hydrogen occurs only at the beginning of the leak. When the mass flow rate is 0.22834 kg/s, it takes only 3 s for the room to fill with hydrogen gas in the flammable range. And when the leak rate is 0.14584 kg/s, this process time increases to 7 s. When the leak flow rate is 0.06334 kg/s, the flammable hydrogen takes 15 s of leakage to fill the entire vessel. When the leakage time exceeds 15 s, the volume of flammable hydrogen gas in the three leak rate cases is kept at about 35.7 m^3 by the size of the room. It can be seen that for the smaller room volume of a SHRS, high-pressure hydrogen gas tends to accumulate when it leaks.

Figure 6.5b shows the variation pattern of flammable hydrogen mass with time for different leakage mass flow rates. With the decrease of the leakage rate, the growth rate of the mass of flammable hydrogen at the beginning of the leakage decreases, and the mass of flammable hydrogen in dynamic equilibrium decreases accordingly. The mass of flammable hydrogen is about 2.254 kg at a mass flow rate of 0.22834 kg/s, while at a rate of 0.06334 kg/s, the mass drops to about 1.793 kg.

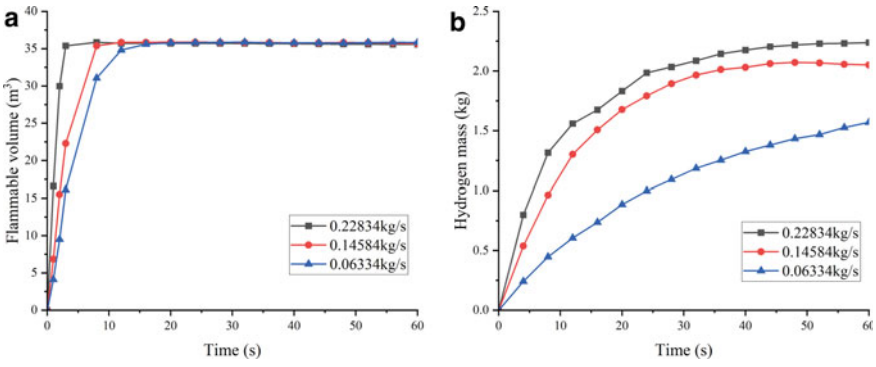

Fig. 6.5. Change of flammable cloud volume (**a**) and hydrogen mass (**b**) with time in the fuel cell room for different mass flow rates

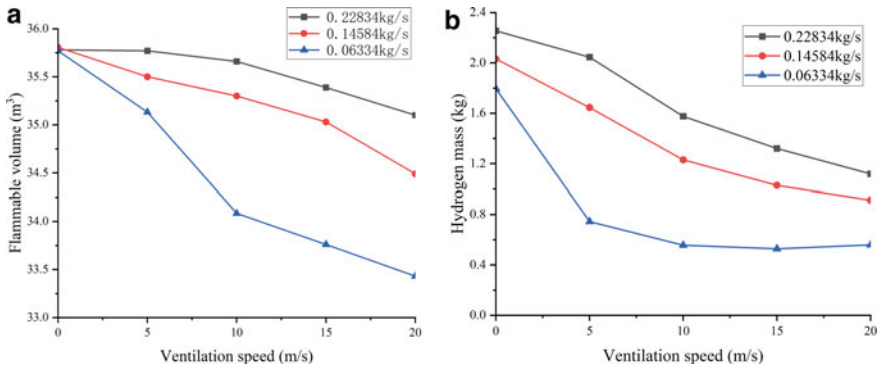

Fig. 6.6 Effect of ventilation speed on flammable cloud volume (**a**) and hydrogen mass (**b**) in fuel cell room at different leakage rates

The effect of exhaust fan air speed on the volume and mass of flammable hydrogen at different leakage rates has also been studied. Figure 6.6a shows the effect of ventilation speed on the volume of the flammable hydrogen. According to the results in the graph, the effect of the ventilation speed on the volume is small, and at a mass flow rate of 0.22834 kg/s, the volume does not start to decrease until the speed is greater than 5 m/s due to the large concentration of hydrogen in the room. And when the rate is 0.06334 kg/s, the volume decreases more, but the volume of the flammable hydrogen in the room is still large.

Figure 6.6b shows the effect of ventilation speed on the mass of the flammable hydrogen. It can be seen that the ventilation air velocity has a significant effect on the mass. At a leakage rate of 0.22834 kg/s, the mass of flammable gas without ventilation was 2.254 kg. As the ventilation volume increased, the mass of hydrogen in the vessel decreased to 1.118 kg at a ventilation speed of 20 m/s. At a leakage rate of 0.14584 kg/s, the mass decreased from 2.031 to 0.912 kg. And when the rate is 0.06334 kg/s, the mass drops even faster, from 1.793 to 0.744 kg at a wind speed of 5 m/s.

6.4 Hydrogen Cloud Explosion Hazard Assessment

6.4.1 TNT Equivalent Method

When hydrogen leaks from a FC, the hydrogen will form a combustible hydrogen cloud in the room. Due to the wide flammable range of hydrogen and the high calorific value generated when hydrogen is ignited, the explosion is inevitable once ignited, especially in SHRS where the space is restricted to a large extent, it is more likely to accumulate in the space to form a flammable cloud. At present, there are many methods for calculating the gas explosion overpressure, the application of more TNO

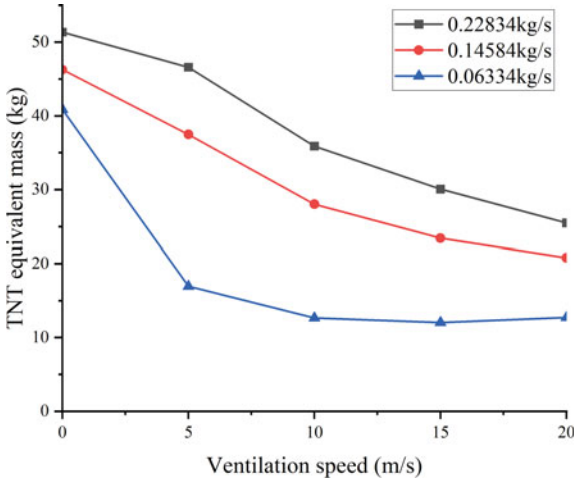

Fig. 6.7 Effect of ventilation rate on TNT equivalent mass at different leakage rates

multi-energy method and TNT equivalent method. The TNT equivalent method is the most classical method of evaluating gas cloud explosions. The TNT equivalent method can be equivalent to replace the explosion energy, the explosion energy of the corresponding mass of TNT to replace the the explosion energy of other combustible gas clouds. Its calculation formula can be expressed as follows:

$$W_{\mathrm{TNT}} = \frac{\alpha A W_h Q_h}{Q_{\mathrm{TNT}}} \tag{6.5}$$

where, W_{TNT} is the TNT equivalent mass, kg; α is the explosion efficiency factor; A ground explosion coefficient; W_h is the mass of flammable hydrogen, kg; Q_h is the heat of combustion of hydrogen, kJ/kg; Q_{TNT} is the explosion energy of TNT, kJ/kg.

The TNT equivalent mass of flammable hydrogen in the FC room can be calculated by Eq. (6.5). Figure 6.7 shows the variation of TNT equivalent mass with wind speed for different leakage velocities. With the increase in wind speed, the TNT equivalent mass at different leakage rates decreases significantly.

6.4.2 Explosion Hazard Analysis of Fuel Cell Rooms

The overpressure generated by the explosion is the main hazard to people and buildings. Tables 6.1 and 6.2 show the correspondence between different overpressure values and human injuries, including direct and indirect injuries. According to the degree of injury, the danger zone can be divided into the death zone, the serious injury zone and the light injury zone. The overpressure of the death radius reaches 241.3 kPa, the overpressure range of the serious injury radius is 34.5–48.3 kPa, and the minor injury radius is 13.8 kPa. The following formula can calculate the hazard

radius:

$$R_d = 13.6\left(\frac{W_{\mathrm{TNT}}}{1000}\right)^{0.37} \tag{6.6}$$

$$R_s = 1.089\left(\frac{P_0}{W_{\mathrm{TNT}} Q_{\mathrm{TNT}}}\right)^{-1/3} \tag{6.7}$$

$$R_m = 1.957\left(\frac{P_0}{W_{\mathrm{TNT}} Q_{\mathrm{TNT}}}\right)^{-1/3} \tag{6.8}$$

where, R_d is death radius; R_s is serious injury radius; R_m is minor injury radius.

According to Eqs. (6.6–6.8), the radius of death, the radius of serious injury and the radius of minor injury can be calculated for different leakage rates in the FC room when ventilation is not activated, as shown in Table 6.3. As can be seen, for the FC room, the potential explosion hazard in the event of a hydrogen leak is large and the interior of the room is all in the dead zone. Table 6.4 shows the hazard range at different ventilation speeds for a leakage rate of 0.22834 kg/s. As the ventilation speed increases, the hazard radius decreases significantly, the radius of death decreases by 1 m, the radius of serious injury decreases by 1.1 m, and the radius of minor injury decreases by 1.9 m.

Table 6.1 Direct damage to people caused by overpressure events (LaChance et al. 2011)

Overpressure (kPa)	Damage description	Overpressure (kPa)	Damage description
13.8	Tympanic membrane rupture threshold	82.7–103.4	Lung hemorrhage threshold
34.5–48.3	50% probability of eardrum rupture	137.9–172.4	50% probability of death from pulmonary hemorrhage
48.3	Threshold of internal injuries caused	206.8–241.3	90% probability of death from pulmonary hemorrhage
68.9–103.4	90% probability of eardrum rupture	482.6–1379	Immediate blast fatalities

Table 6.2 Indirect damage to people caused by overpressure events (LaChance et al. 2011)

Overpressure (kPa)	Damage description	Overpressure (kPa)	Description of damage
6.9–13.8	Skin damage caused by debris	10.3–20	Knocked down by shockwave
13.8	Falling from an obstacle and dying	55.2–110.3	Standing people will be pushed out some distance

Table 6.3 Radius of damage at different rates

Mass flow rate (kg/s)	Death radius (m)	Serious injury radius (m)	Minor injury radius (m)
0.22834	4.5	14.4	25.8
0.14584	4.4	13.9	24.9
0.06334	4.2	13.3	23.9

Table 6.4 Radius of injury at different ventilation wind speeds

Wind speed (m/s)	Death radius (m)	Serious injury radius (m)	Minor injury radius (m)
0	4.5	14.4	25.8
5	4.4	13.9	25.0
10	4.0	12.7	22.9
15	3.7	12.1	21.6
20	3.5	11.3	20.4

6.5 Conclusion

This paper presents a simulation of hydrogen leakage from a FC system room in a SHRS. The changes in the volume and mass of room flammable hydrogen clouds under different leakage conditions were analyzed. Finally, the explosion hazard was evaluated using the TNT equivalent method.

It was found that at a mass flow rate of 0.22834 kg/s, the room was filled with combustible hydrogen in 3 s, and the concentration of hydrogen increased further in 60 s, reaching the upper limit of the flammable range in some areas. The change in the volume and mass of flammable hydrogen in the room shows that after only 3 s, the volume of flammable hydrogen is already roughly equal to the volume of the room. And the mass of flammable hydrogen rose faster at the beginning of the leak, but when the time exceeded 20 s, the mass rose significantly slower.

Due to the small volume of the FC system room in the SHRS, the rate of leakage only affects the growth rate of the flammable hydrogen volume at the beginning of the leakage, and eventually the different rates will all fill the room with flammable hydrogen. And as the rate of the leak decreased, the change in flammable hydrogen was noticeable. When ventilation is on, the volume and mass of flammable hydrogen decrease fastest at a mass flow rate of 0.06334 kg/s. And when the rate is 0.22834 kg/s, the change of the flammable hydrogen volume is small and the mass decreases significantly.

Hazard assessment of room by TNT equivalent method. The results showed that the room was within the dead zone at all three leakage rates. When ventilation was activated, the hazard range was effectively reduced with increasing wind speed.

Acknowledgements This research was funded by the Technology Project of the State Grid Zhejiang Electric Power Company, Ltd., “Research on risk identification and safety protection technology of electric-hydrogen coupling system” (No. B311DS221001).

References

Brennan SL, Makarov DV, Molkov V (2009) LES of high pressure hydrogen jet fire. J Loss Prev Process Ind 22:353–359

Choi J, Hur N, Kang S, Lee ED, Lee K-B (2013) A CFD simulation of hydrogen dispersion for the hydrogen leakage from a fuel cell vehicle in an underground parking garage. Int J Hydrogen Energy 38:8084–8091

Cirrone DMC, Makarov D, Molkov V (2019) Simulation of thermal hazards from hydrogen under-expanded jet fire. Int J Hydrogen Energy 44:8886–8892

Denisenko VPKIA, Korobtsev SV et al (2009) Hydrogen-air explosive envelope behavior in confined space at different leak velocities. In: Proceedings of the third international conference on hydrogen safety. Ajaccio, Corsica, France

Goswami R, Sun B (2022) Study on vapour dispersion and explosion from compressed hydrogen spill: risk assessment on a hydrogen plant. Int J Hydrogen Energy 47:41195–41207

LaChance J, Tchouvelev A, Engebo A (2011) Development of uniform harm criteria for use in quantitative risk analysis of the hydrogen infrastructure. Int J Hydrogen Energy 36:2381–2388

Li F, Yuan Y, Yan X, Malekian R, Li Z (2018) A study on a numerical simulation of the leakage and diffusion of hydrogen in a fuel cell ship. Renew Sustain Energy Rev 97:177–185

Liang Y, Pan X, Zhang C, Xie B, Liu S (2019) The simulation and analysis of leakage and explosion at a renewable hydrogen refuelling station. Int J Hydrogen Energy 44:22608–22619

Pitts WM, Yang JC, Blais M, Joyce A (2012) Dispersion and burning behavior of hydrogen released in a full-scale residential garage in the presence and absence of conventional automobiles. Int J Hydrogen Energy 37:17457–17469

Schefer R, Houf W, Bourne B, Colton J (2006) Spatial and radiative properties of an open-flame hydrogen plume. Int J Hydrogen Energy 31:1332–1340

Venetsanos AG, Papanikolaou E, Cariteau B, Adams P, Bengaouer A (2010) Hydrogen permeation from CGH2 vehicles in garages: CFD dispersion calculations and experimental validation. Int J Hydrogen Energy 35:3848–3856

Yang F, Wang T, Deng X, Dang J, Huang Z, Hu S et al (2021) Review on hydrogen safety issues: Incident statistics, hydrogen diffusion, and detonation process. Int J Hydrogen Energy 46:31467–31488

Chapter 7
Increasing Nozzle Blade Deposition on Steam Turbine C-9015A by Adding Parallel Grooved Surface

Hemati Masood, Nikolay Zabelin, Georgy Fokin, and Nilan Jayasinghe

Abstract This paper presents a grooved surface for improving the nozzle blade C-9015A of wet-steam turbines in modern power plants by increasing the deposition of droplets after impact on the surface with the help of a parallel grooved surface. By putting the grooved surface in the direction of the steam flow on the surface of the nozzle, the angle between the surface and the impact of the droplets decreases. The smaller the angle between the surface and the impact of the drop, the more deposition of a droplet on the surface after impact. This article discusses the physics of droplet impact with different surfaces and droplet movement in steam flow. And finally, the results of the deposition due to the impact of drops with different diameters on the smooth blade surface and a grooved blade surface are compared with each other, and it is concluded from the results that the deposition of drops on the grooved blade surface is more than the deposition on the smooth blade surface.

Keywords Deposition · Grooved blade surface · Effective erosion energy

H. Masood (✉) · N. Zabelin
Higher School of Power Engineering, Peter the Great St. Petersburg Polytechnic University, Saint Petersburg, Russia
e-mail: Masoodhemati97@gmail.com

G. Fokin
Department of Gas Turbine Units for Gas Pumping Stations, Peter the Great St. Petersburg Polytechnic University, Saint Petersburg, Russia

N. Jayasinghe
Higher School of High Voltage Engineering, Peter the Great St. Petersburg Polytechnic University, Saint Petersburg, Russia

Z. Sun and P. K. Das (eds.), *Proceedings of the 10th International Conference on Energy Engineering and Environmental Engineering*, Environmental Science and Engineering, https://doi.org/10.1007/978-3-031-48204-5_7

7.1 Introduction

The modeling and simulations of thermal power plants using steam turbines to increase the electricity production of non-renewable, renewable power plants have recently grown. The share of electricity produced at power plants through turbine installations is about 75% worldwide. Consequently, the improvement and modernization of turbines have become an important topic today in the last decades (Yu et al. 2020; Foroozesh et al. 2020; Lohrmann et al. 2019; Hashemian et al. 2020; Xie et al. 2019). One of the most critical issues in enhancing the efficiency of steam turbines is increasing the turbine lifespan by protecting the rotor and nozzle blades against moisture by decreasing erosion. For this purpose, special protection alloys on their surfaces and moisture separators into and out of steam turbines are applied (Mishnaevsky et al. 2021; Dashtkar et al. 2019; Singh et al. 2021; Zarrouk and Purnanto 2015; Kim et al. 2021). Moisture separators inside steam turbines are usually placed in the last stage of the turbine to separate the moisture before the rotor blades. In this article, it will be shown that using a grooved surface instead of a smooth surface on the surface of the nozzle causes an increase in deposition to occur on this surface and improve the efficiency of the separator surface.

In power plants, the most effective way to prevent steam turbine blades from erosion is to separate moisture from wet steam (Kim et al. 2021; Egorov et al. 2020, 2019). In recent years, separators have been installed inside the steam turbine stages. To achieve the maximum efficiency of these separators, the movement path of moisture is checked in the form of spherical droplets. When a droplet moves in a steam flow, various forces are applied to this droplet. The drag force applied to the drop is much larger than the other forces, so other forces are ignored in most works. With the help of the drag force on the droplet, the droplet's motion equation is obtained. Various works have been done to find the drag coefficient in the drag force (Lin and Palmore 2022; Wang et al. 2021; Fang et al. 2020; Singh et al. 2021).

After a droplet impacts on a surface, the droplet may fall into one of four state regimes: 1- stick, 2- rebound, 3- spread, and 4- splash. The entire drop is deposited after impact in stick and spread regimes, while the whole droplet is reflected in the rebound regime. In the splash regime, a little of the droplet is deposited, and the rest is reflected in several smaller droplets. The rebound regime does not occur in steam turbines (Quetzeri-Santiago et al. 2019; Ashida et al. 2020; Rioboo et al. 2003). The results of experimental works have shown that the boundary of these regimes is defined by dimensionless numbers such as (Re $= \frac{\rho d_0 w_0}{\mu}$), the Ohnesorge number (Oh $= \frac{\mu}{\sqrt{\rho \sigma d_0}}$), the Laplace number)La $= \frac{\rho \sigma d_0}{\mu^2}$ (, the Weber number (We $= \frac{\rho d_0 w_0^2}{\sigma}$), and the surface roughness number (St $= \frac{R_t}{d_0}$), where ρ, μ and σ are liquid density, viscosity, and surface tension at the interface, respectively, is the initial diameter of the drop, is the average height of the surface roughness, and is the initial normal velocity of the droplet to the surface (Mundo et al. 1995; Burzynski et al. 2020; Almohammadi and Amirfazli 2019; Goede et al. 2021). The less the droplet is in the splash regime after

impact and more in the entire deposition regimes, the more efficient the moisture separator is.

In this work, to increase the deposition of the nozzle blade in the last stage of the turbine, a grooved nozzle surface for the blade of C-9015A is suggested. With this replacement on the nozzle surface, the deposition of a droplet spectrum in the impact on a grooved surface is increased. The results calculations for the impact of the droplet spectrum on the smooth surface and the grooved surface of blade C-9015A with different groove angles were performed, and it was shown that the presence of the grooved surface helps to increase the droplet deposition. In this work, all the calculations were done on the geometry of nozzle C-9015A, but the work results are applicable to any nozzle.

7.2 Energy Analysis Equations

When a droplet impacts a grooved surface, if the angle C = 90 ° according to Fig. 7.1, the smallest angle of the droplet with the grooved surface at the time of impact can be found by the formula 7.1, i.e., θ:

$$\sin\theta = \sin\alpha.\sin(\frac{\beta}{2}) \tag{7.1}$$

where the angle β is the angle between the groove.

In this work, the movement of the drop is modeled in the X–Y plane; that is, it is always C = 90. The geometry of the nozzle blade and grooved surface is as follows (Fig. 7.2):

As shown in Fig. 7.3, if the droplet impacts the surface, the boundaries between the regime of spread for complete deposition or the regime of splashing after impact are defined by the value of K and formula 7.2 (Lee and Ryu 2006):

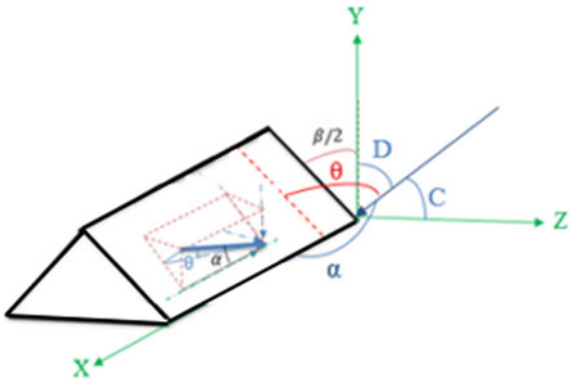

Fig. 7.1 The impact of the drop on the grooved surface

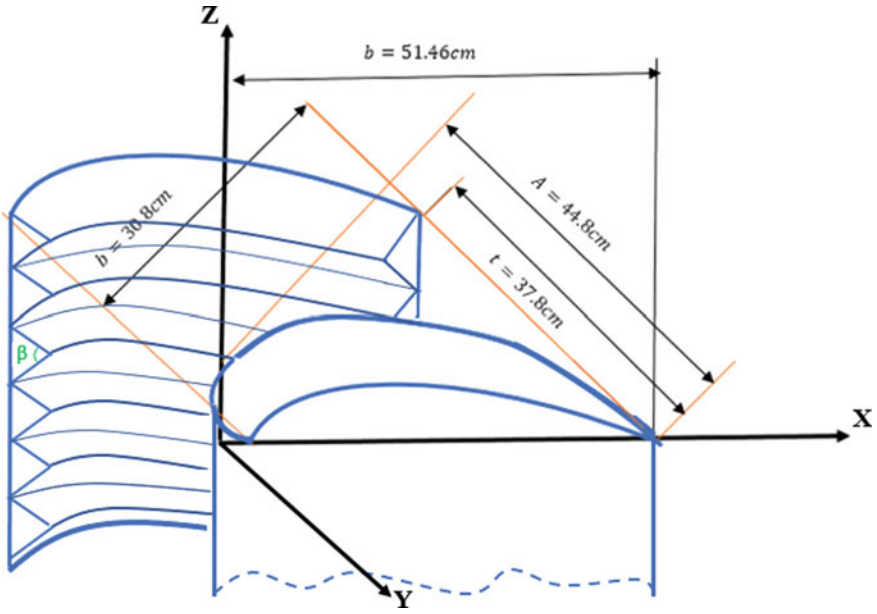

Fig. 7.2 The geometry of the grooved surface of blade C-9015A with grooves parallel to the direction of steam flow

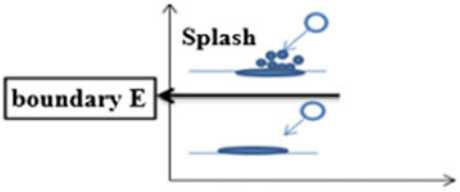

Fig. 7.3 Boundaries of different impact regimes

$$K = We_n \mathrm{Re}_n = 57.7 \tag{7.2}$$

If the value of K for the drop is more than 57.7, after the droplet impacts the surface, splashing occurs, and if this value for the droplet is smaller than 57.7, then the entire drop is deposited.

The drop spectrum is determined by the following formula3, as shown in Fig. 7.4:

$$f(x) = 0.492 + 13.1e^{(1-(\frac{x-60.64}{28.37})-e^{-(\frac{x-60.64}{28.37})})} \tag{7.3}$$

In this work, the moisture of the nozzle is considered to be a range of completely elastic particles. It is assumed that there is no collision and heat transfer between the

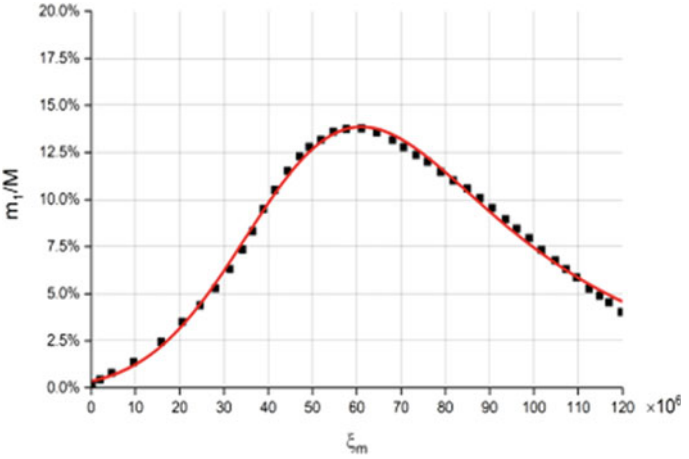

Fig. 7.4 The droplet spectrum distribution function

droplets between the vapor and liquid phases. The equation of the drop movement in the steam flow between the nozzle blade is obtained using the drag force with the following formula:

$$\frac{d\vec{c}_k}{dt} = \frac{3}{4}\frac{\mu_n C_x}{d_K^2 \rho_K}\overline{\mathrm{Re}}_K(\vec{c}_\prod - \vec{c}_k) \tag{7.4}$$

$$\frac{d\overrightarrow{x}_k}{dt} = \vec{c}_k \tag{7.5}$$

Where μ_n—dynamic viscosity of the steam flow; $\vec{c}_\prod$ is the instantaneous speed of the carrier stream; $\overline{\mathrm{Re}}_\kappa$ is the relative Reynolds number of a drop, defined as:

$$\overline{\mathrm{Re}}_K = \frac{\rho_n d_K}{\mu_n}\left|\vec{c}_\prod - \vec{c}_k\right| \tag{7.6}$$

And C_x-drag coefficientthe is accounted from the following equation:

$$\begin{aligned} C_x &= \frac{A_i}{\mathrm{Re}^{n_i}}(i = 1, 2, 3) \\ A_1 &= 24; n_1 = 1; \mathrm{Re} \le 1 \\ A_2 &= 24; n_2 = \frac{3}{5}; 1 \le \mathrm{Re} \le 10^3 \\ A_3 &= 24; n_3 = 0; \mathrm{Re} \ge 10^3 \end{aligned} \tag{7.7}$$

where Re is the Reynolds number of the droplet in the steam flow.

Table 7.1 Comparison of the mass percentage of the spectrum droplets splashed after impact on the smooth nozzle surface and the grooved nozzle surface with different groove angles β for different inlet locations of droplet spectrum at the nozzle inlet

Location (x, cm)	% smooth surface	% β = 60°	% β = 30°	% β = 20°	% β = 15°	% β = 10°	% β = 7°	% d β = 5°
−22	1	1	0.999	0.999	0.973	0.447	0	0
−19	1	1	0.999	0.999	0.995	0.806	0	0
−16	1	1	0.999	0.999	0.999	0.915	0	0
−14	1	1	0.999	0.999	0.999	0.915	0.226	0
−12	1	1	1	1	0.999	0.915	0.226	0
−10	1	1	1	1	0.999	0.915	0.226	0

Table 7.1 shows The results of the impact of the droplet spectrum with the smooth blade surface and the grooved blade surface with groove angles of 60, 30, 15, 10, and 7° if this droplet spectrum enters the nozzle from different inlet locations of the nozzle and in the direction of the steam. As the results of this table show, for all the inlet distances to the nozzle, when the spectrum of droplets impacts the smooth nozzle surface, for all the droplets in the mentioned distances, splashing occurs, and little deposition occurs on the smooth surface. But if the same range of drops impacts the grooved surface under the same conditions, the smaller the angle of the groove becomes, and the percentage of drops splashing after the impact decreases. If the angle of the groove becomes less than ten degrees, the percentage of droplets that are sprayed on the grooved surface after the impact becomes almost zero; that is, every droplet from every nozzle inlet distance moves and hits the grooved surface, the whole droplet after impact deposits on it.

The graph in Fig. 7.5 is the results of Table 7.1. This graph also shows that the more the droplet spectrum at the nozzle entrance is at a distance from the grooved nozzle surface, the more likely the droplets will spray after impact. This result is logical because the droplets located at the nozzle inlet at a greater distance from the grooved surface collide with the grooved surface at a larger angle.

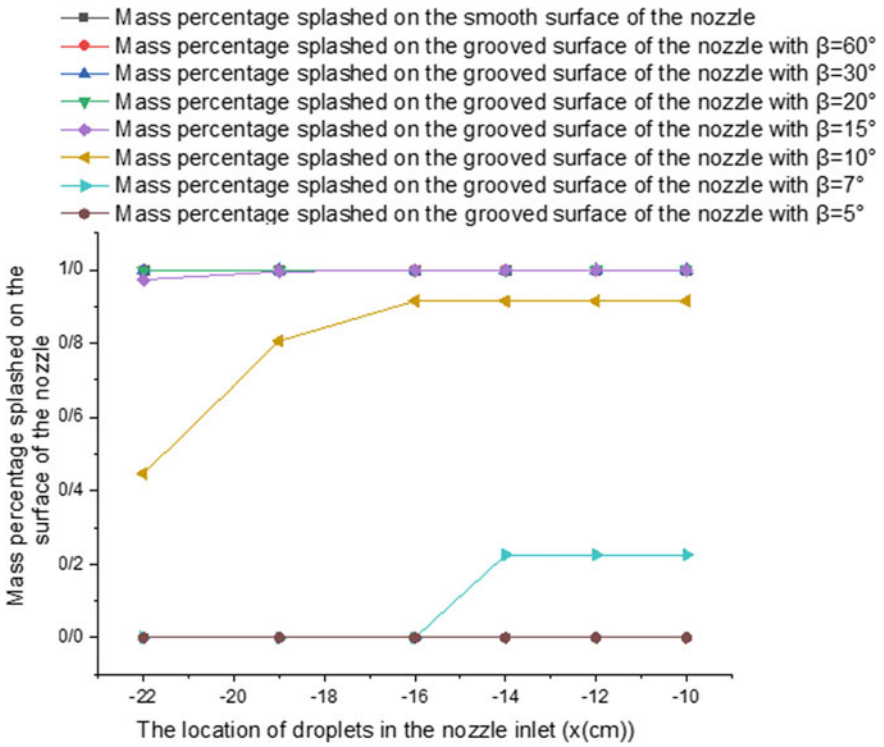

Fig. 7.5 Comparison of the mass percentage of the spectrum droplets that spray(splash) after impact on the smooth surface of the blade and the grooved surface with different groove angles β

7.3 Conclusion

In this work, the impact of a range of droplets from different nozzle inlet distances in the direction of steam on the smooth surface of the nozzle and the grooved surface of the nozzle in the same condition is modeled. The purpose of this work is to investigate if the surface of the nozzle is grooved and if these grooves are in the direction parallel to the movement of steam, then after the impact of the spectrum of droplets on the grooved surface of the nozzle, splashing of the droplets will be less, and the deposit of the droplets will be more. To do this, the geometry of the nozzle blade C-9015A was chosen. If a drop hits a wet surface, according to experimental results, either splashing or complete deposition of the droplet occurs on the surface. The boundary between these two regimes of splashing and complete deposit is determined by the number $K = 57.7$. The smaller the contact angle of the droplet with the surface, the more the droplet is in the entire deposition regime after impact. The grooved surface of the nozzle causes the angle of the droplet impact to be smaller with the surface, and as a result, the drops are more likely to be in the complete deposition regime after the impact. And with the help of the grooved surface, the efficiency of

the separator installed on the nozzle surface can be increased. The modeling results showed that the most suitable groove angle for complete deposition is less than ten degrees. Decreasing the groove's angle makes the groove's width smaller and increases the probability of drops hitting the edge of the groove. For a proper solution to this problem, the grooves' depth should be as high as possible so that the width of the groove increases and more deposition occurs.

References

Almohammadi H, Amirfazli A (2019) Droplet impact: viscosity and wettability effects on splashing. J Colloid Interface Sci 553:22–30

Ashida T, Watanabe M, Kobayashi K, Fujii H, Sanada T (2020) Hidden prompt splashing by corona splashing at drop impact on a smooth dry surface. Phys Rev Fluids 5(1):011601

Burzynski DA, Roisman IV, Bansmer SE (2020) On the splashing of high-speed drops impacting a dry surface. J Fluid Mech 892:A2

Dashtkar A, Hadavinia H, Sahinkaya MN, Williams NA, Vahid S, Ismail F, Turner M (2019) Rain erosion-resistant coatings for wind turbine blades: a review. Polym Polym Compos 27(8):443–475

De Goede T, de Bruin K, Shahidzadeh N, Bonn D (2021) Droplet splashing on rough surfaces. Phys Rev Fluids 6(4):043604

Egorov M, Kalyutik AA, Akhmetova IG, Makoev SO (2019) Heat transfer in coiled type superheater of moisture separator-reheater of turbines at the nuclear power plant. In: IOP conference series: earth and environmental science, vol 288, No. 1. IOP Publishing, p 012080

Egorov M, Kasatkin I, Kovalenko I, Krectunova I, Lavrovskaya N, Litvinova N (2020) The new ways to increase the efficiency of thermal hydraulic processes in systems of separation and reheating of NPP wet steam turbines. In: E3S web of conferences, vol 178. EDP Sciences, p 01029

Fang D, Li L, Li J, Wang M, Yu H, Zhang J, Su GH (2020) Full-scale numerical study on the thermal-hydraulic characteristics of steam-water separation system in an advanced PWR UTSG. Part two: droplets separation process. Progress Nucl Energ 118:103139

Foroozesh F, Khoshnevis AB, Lakzian E (2020) Improvement of the wet steam ejector performance in a refrigeration cycle via changing the ejector geometry by a novel EEC (Entropy generation, entrainment ratio, and coefficient of performance) method. Int J Refrig 110:248–261. https://doi.org/10.1016/j.ijrefrig.2019.11.006

Hashemian A, Lakzian E, Ebrahimi-Fizik A (2020) On the application of isogeometric finite volume method in numerical analysis of wet-steam flow through turbine cascades. Comput Math Appl 79(6):1687–1705. https://doi.org/10.1016/j.camwa.2019.09.025

Kim WS, Lee JB, Kim KH (2021) Development of empirical correlation of two-phase pressure drop in moisture separator based on separated flow model. Energies 14(15):4448

Kim K, Bong Lee J, Kim WS, Choi HS, Kim JI (2021) Development of a prediction model relating the two-phase pressure drop in a moisture separator using an air/water test facility. Nucl Eng Technol 53(12):3892–3901

Lee SY, Ryu SU (2006) Recent progress of spray-wall interaction research. J Mech Sci Technol 20(8):1101–1117

Lin Y, Palmore Jr J (2022) Effect of droplet deformation and internal circulation on drag coefficient. Phys Rev Fluids 7(12):123602

Lohrmann A, Farfan J, Caldera U, Lohrmann C, Breyer C (2019) Global scenarios for significant water use reduction in thermal power plants based on cooling water demand estimation using satellite imagery. Nat Energ 4(12):1040–1048

Mishnaevsky L Jr, Hasager CB, Bak C, Tilg AM, Bech JI, Rad SD, Fæster S (2021) Leading edge erosion of wind turbine blades: understanding, prevention and protection. Renew Energ 169:953–969

Mundo C, Sommerfeld M, Tropea C (1995) Droplet-wall collisions: experimental studies of the deformation and breakup process. Int J Multiph Flow 21(2):151–173

Quetzeri-Santiago MA, Castrejón-Pita AA, Castrejón-Pita JR (2019) The effect of surface roughness on the contact line and splashing dynamics of impacting droplets. Sci Rep 9(1):1–10

Rioboo R, Bauthier C, Conti J, Voue M, De Coninck J (2003) Experimental investigation of splash and crown formation during single drop impact on wetted surfaces. Exp Fluids 35(6):648–652

Singh S, Kharub M, Singh J, Singh J, Jangid V (2021) Brief survey on mechanical failure and preventive mechanism of turbine blades. Mater Today Proc 38:2515–2524

Singh N, Kroells M, Li C, Ching E, Ihme M, Hogan CJ, Schwartzentruber TE (2022) General drag coefficient for flow over spherical particles. AIAA J 60(2):587–597

Wang ZB, Yang ZW, Gou LJ, Zhao RJ (2021) A volume of fluid simulation of the steady deformation and the drag of a single droplet in a flowing gas. J Hydrodyn 33:334–346

Xie J, Liang Z, Zhang X, Zhu L (2019) Efficiency evaluation of thermal power plants in China based on the weighted Russell directional distance method. J Clean Prod 222:573–583

Yu J, Liu P, Li Z (2020) Hybrid modelling and digital twin development of a steam turbine control stage for online performance monitoring. Renew Sustain Energ Rev 133. https://doi.org/10.1016/j.rser.2020.110077

Zarrouk SJ, Purnanto MH (2015) Geothermal steam-water separators: Design overview. Geothermics 53:236–254

Chapter 8
Numerical Simulation Study on the Evolutionary Characteristics of Soil Cavities in Karst Water Mining Area Under Positive Pressure Effect

Zongchun Li, Yongyao Wei, Bo Chen, Hong Yin, Jianxun Xiao, and Jinqi Kong

Abstract As a new mechanism to cause karst collapse, the positive pressure effect causes geological disasters that seriously affect the safety of people's lives and properties in karst areas. If we can understand the characteristics and rules of karst soil cavities in different evolutionary stages from the kinetic point of view, it can play an important role in saving the funds for engineering investigation, reducing the cost of soil cavity treatment and reducing the risk of engineering disasters. Therefore, in this paper, based on the analysis of the damage mechanism of karst soil cavern under the effect of positive pressure, based on the ASCII text provided by FLAC itself, the orthorectified simulation calculation program is prepared and finite element analysis is realized in FLAC3D, focusing on the uneven change of soil displacement, stress redistribution and plastic damage of karst soil cavern in different evolutionary stages under the effect of positive pressure, and summarizing the the stress, strain and damage characteristics and rules of plastic zone in karst soil caverns at different evolutionary stages are summarized. It is hoped that the research results will be of scientific value to deepen the research on the theory of cave-in prevention and control of covered karst soil caverns.

Z. Li
East China Exploration and Development Bureau, Nanjing 210007, China

Y. Wei (✉)
Geological Survey of Jiangsu Province, Nanjing 210049, China
e-mail: weiyongyao@163.com

Key Laboratory of Earth Fissures and Geological Disaster Ministry of Land and Resources, Nanjing 210049, China

B. Chen · J. Kong
The 1St Geological Brigade of Jiangsu Geology and Mineral Exploration Bureau, Nanjing 210041, China

H. Yin · J. Xiao
Jiangsu Geology and Engineering Co, Ltd., Nanjing 210000, China

Z. Sun and P. K. Das (eds.), *Proceedings of the 10th International Conference on Energy Engineering and Environmental Engineering*, Environmental Science and Engineering, https://doi.org/10.1007/978-3-031-48204-5_8

Keywords Positive pressure effect · Karst soil cavern · Evolution · Numerical modeling

8.1 Introduction

Ground surface destabilization due to over-extraction of groundwater in karst areas is the most common phenomenon in karst collapse (Gao 2008). However, when pumping (discharge) is stopped, the groundwater level will undergo the opposite process, i.e., karst groundwater level recovery and the resulting collection of positive pressure, under the action of head pressure. The recovery of water level will be very rapid due to the huge drop depth during pumping and the rapid penetration characteristics of karst medium. If the gas in the void is not released in time, a high pressure will be formed in the soil cavity and will be sufficient to cause the destruction of the soil. The karst collapse caused by this phenomenon is called the "airburst effect" or positive pressure effect (Wei and Sun 2017) (Fig. 8.1).

Especially in recent years, the global awareness of ecological environmental protection has increased, and karst groundwater extraction in some karst areas has been decreasing year by year, along with the emergence of extreme weather (e.g., heavy rainfall and the growth of heavy rainfall time), and the positive pressure effect formed by the karst water level began to rebound sharply leading to frequent karst collapse disasters (He et al. 2017), thus drawing the attention of scholars at home and abroad to this phenomenon. For example, Liu first proposed that karst airburst is

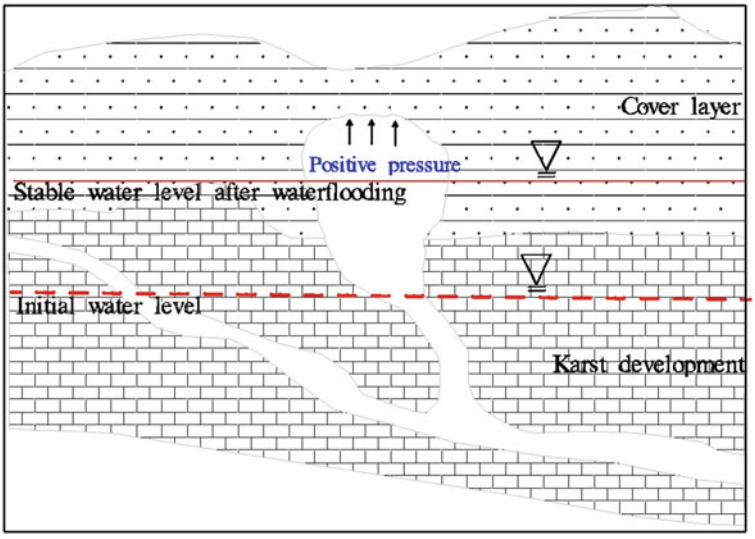

Fig. 8.1 Schematic diagram of positive pressure effects

a new type of collapse (Liu and Han 1995); Hu discussed that the long-term evacuation of mines in karst areas suddenly closes the pit and the water level rises sharply, resulting in karst collapse as the process of positive pressure airburst (Hu et al. 1989); Jiang analyzed the dynamic source of karst collapse induced by monitoring the water (gas) conditions in the karst cavity and its change law (Jiang et al. 2016); Lu emphasized that the karst cave airburst effect should be paid attention to the engineering construction in the karst area, and pointed out that the karst airburst mechanism will also be an important scientific research direction (Yr 2016); Wei studied the influence of the positive pressure effect generated during the rapid rise and fall of karst water level on the evolution of karst soil caves, further revealing the critical conditions of karst soil cave evolution from the mechanical perspective (Wei and Sun 2018).

The above scholars have provided good research ideas for the influence of positive pressure effect on karst soil caverns, but their results mainly focus on the research work carried out on the collapse mechanism, development process, characteristics of collapse and critical conditions of karst soil caverns, while in the process of karst soil cavern evolution, the soil around the overlying karst soil caverns is bound to undergo uneven changes of displacement, redistribution of stress and plastic damage under the effect of positive pressure effect These problems are the important basis for a clear understanding of the mechanical mechanism and critical warning model of karst soil cavern collapse. Therefore, it is especially important to choose suitable numerical simulation software to study the mechanical damage characteristics of stress, strain and plastic zone in different evolutionary stages of soil caverns.

8.2 Analysis of Karst Collapse Mechanism Under Positive Pressure Effect

For the karst development area with thick overburden, the thick overburden is equivalent to the top plate of a closed system, assuming that ideally, the volume and pressure of the gas follow the Boyle-Marriott law when the temperature field is constant. When groundwater extraction is stopped, if the water level recovers more sharply, then there will be a positive pressure increase in earth caves and karst caves, and this force is applied to the top of the earth cave. On the one hand, the higher positive pressure makes the soil pore water flow back and increases the porosity of the soil; on the other hand, it makes the soil around the cave become loose and easy to fall off, and when the positive pressure is large enough, it will directly impact out of the ground after exceeding the collapse resistance of the cover layer and cause the ground to collapse, often with the phenomenon of gas and water spray (Fig. 8.2).

The karst gas explosion effect has three stage process that leads to the karst collapse of an overlying layer (Cheng et al. 2002). Stage 1, if the covered soil layer is thick, especially when the soil layer is clay, permeability is small making it difficult for gas to reach the outside through soil layer, which prolongs air pressure release, hence pressure difference is easily formed. When the water level violently fluctuates

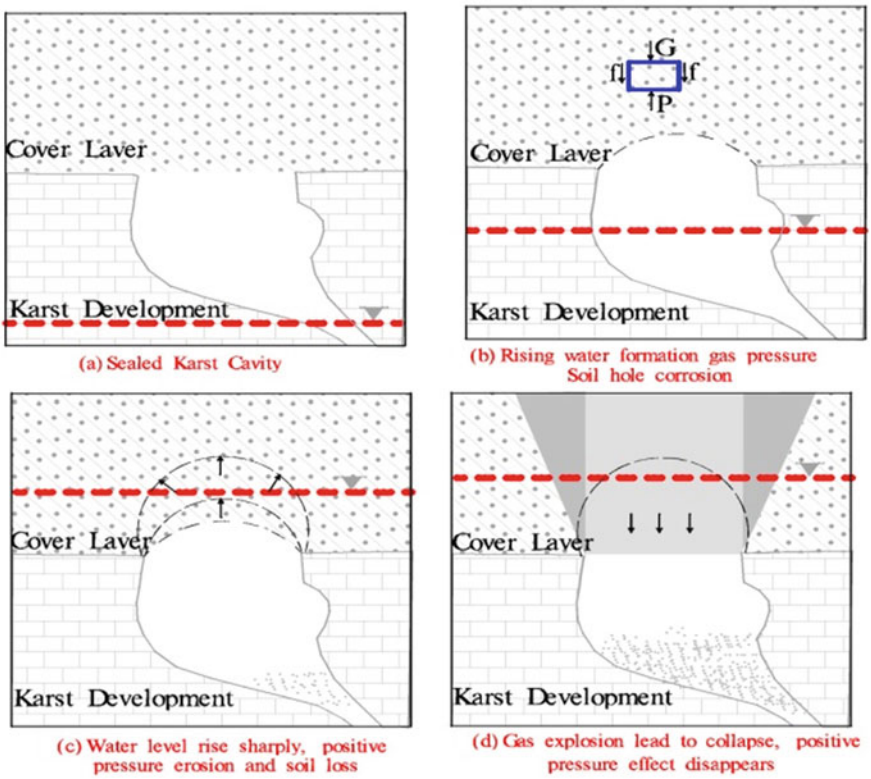

Fig. 8.2 Different evolutionary stages under positive pressure effect

at short notice, the gas permeability of the soil layer can be regarded as 0. When the water level rapidly rises or falls, the pressure difference in the hole rises or falls quickly, forming a large upward force in the soil layer on top of the soil hole, a force that is exactly the opposite of as the direction of the soil layer's gravitation, the result is a rapid equilibrium between positive pressures and the bearing capacity of a covered layer. Stage 2 corresponds to the failure of the soil layer, which means that an ongoing rise in water level brings about an increase in the positive pressure. Once the active force caused by the positive pressure exceeds the bearing capacity of the covered layer, a karst gas explosion or collapse occurs. Stage 3 is the equilibrium stage caused by rapid pressure release. In the case of the failure of an earthen mass structure in the covered layer, gas in the cavity quickly releases to reach a new balanced state.

8.3 Study on Evolution Characteristics of Karst Soil Caves Under Positive Pressure Effect

8.3.1 Selection of Numerical Simulation Software

Since FLAC 3D can highlight the following advantages when simulating the stress, strain and plastic zone changes during the development of karst soil cavities. Firstly, it adopts the "hybrid discrete method" to simulate plastic damage and plastic flow, which is more accurate and reasonable than the "discrete integration method" usually used in the finite element method. Even if the simulated system is static, the dynamic equations of motion are still used, which makes FLAC3D not numerically obstructed in simulating the physical instability process; secondly, the numerical simulation process adopts the "explicit solution" scheme, which takes almost the same time to solve the nonlinear stress–strain relationship as the linear one. The time spent on solving the nonlinear stress–strain relationship is almost the same as that of the linear one, and there is no algorithmic difference between the nonlinear and linear instantonal relationships in the explicit method, so it can save more time for numerical simulation.

8.3.2 Construction of Geological Prototype

In order to make the numerical model more convincing and representative, the overlying karst soil cave collapse frequent area in Xuzhou is taken as the prototype, According to the research results of Wei on the karst collapse area in Xuzhou, China, the average thickness of the upper soil layer in the karst collapse area is 18 m, the soil cave is hemispherical or arched spherical, and the cave opening is rounded (Wei and Sun 2018). In the numerical simulation process, the generalized model length, width, and height dimensions were set as $20 \times 15 \times 20$ m^3, the thickness of the lower tuff was 2 m, and the diameter of the karst cave opening was 4.5 m.

8.3.3 Selection of Parameters

In the process of numerical model construction, the main model parameters were designed as shown in Table 8.1. The design assignment model is a mohr mechanics model, input FLAC3D > model mohr, and define the parameters with the commands FLAC3D > property bulk = xx, shear = xx, friction = xx; FLAC3D > property conesion = xx, tension = xx, etc.

Table 8.1 Summary of model parameters

Category	Volumetric modulus of elasticity (MPa)	Shear modulus (MPa)	Tensile strength (Pa)	Unit weight (kN/m^3)	Angle of internal friction (°)	Cohesion (kPa)	Water content (%)	Porosity
Sandy soil	9.6	3.7		21.4	30.3	8.9	16.5	0.49
Clayey soil	13.5	5.5	4×10^3	19.5	22.5	26	25.2	0.33
Limestone	8700	3700	9.5×10^7	27.55	40.8	10.4		

8.4 Numerical Simulation Results Analysis

8.4.1 Characteristics of Vertical Displacement Change

Under the influence of strong fluctuation of water level, karst soil caverns with cover type will have vertical and horizontal displacement deformation, but compared with vertical displacement, the deformation formed by horizontal displacement is much smaller, and the damage of karst soil caverns is mainly based on vertical displacement deformation. Therefore, when studying the damage characteristics of karst soil caverns, the analysis will focus on vertical displacement.

Due to the positive pressure effect formed when the groundwater level rises rapidly upward, the water (gas) in the karst cavity is compressed sharply, and the positive pressure effect makes the pore water of soil layer flow back, the looseness of soil particles near the soil cavity is strengthened, the soil body becomes loose and easy to fall off, and the development of soil cavity is accelerated. If the air pressure formed by the positive pressure effect is large enough, it will have the tendency to break the overburden layer when it exceeds the gravity and shear strength of the soil layer, and the direction of vertical displacement settlement of the overburden layer changes from downward to upward at this time. According to the numerical simulation results of vertical displacement deformation (Fig. 8.3).

It is found that the strong change of water (gas) dynamic conditions leads to the vertical displacement deformation mainly concentrated in the top of the karst soil cave. Displacement contours are clearly convex, showing cylindrical and funnel-shaped.

If the difference of soil structure is considered, the vertical displacement strain at the center of the overburden surface, the top of the karst soil cave and the foot of the karst soil cave also has a big difference depending on the soil structure. According to the numerical simulation test data, in the early stage when the groundwater level rises rapidly to form the positive pressure effect, the vertical displacement deformation of the surface center is mainly downward, and as the positive pressure effect increases, the single-layer sandy soil type structure is the most sensitive, and the vertical displacement deformation direction changes from vertical downward to upward first. The soil layers of single-layer cohesive soil structure and double-layer upper sand and lower cohesive structure behave similarly in the early stage, and only when the positive pressure effect is large enough, the later vertical displacement deformation is slightly different. At the top of the karst cave, the vertical displacement deformation of sandy soil structure is the largest and fastest, while the vertical displacement deformation curves of single-layer clayey soil structure and double-layer upper sand and lower clay structure are similar in the early stage and slightly different in the later stage because the lower part is clayey soil (Fig. 8.4).

The deformation curves of vertical displacement at the foot of the cave and the top of the cave are similar in shape, but the deformation of vertical displacement at the foot of the cave is much smaller than that at the top of the cave (Fig. 8.5).

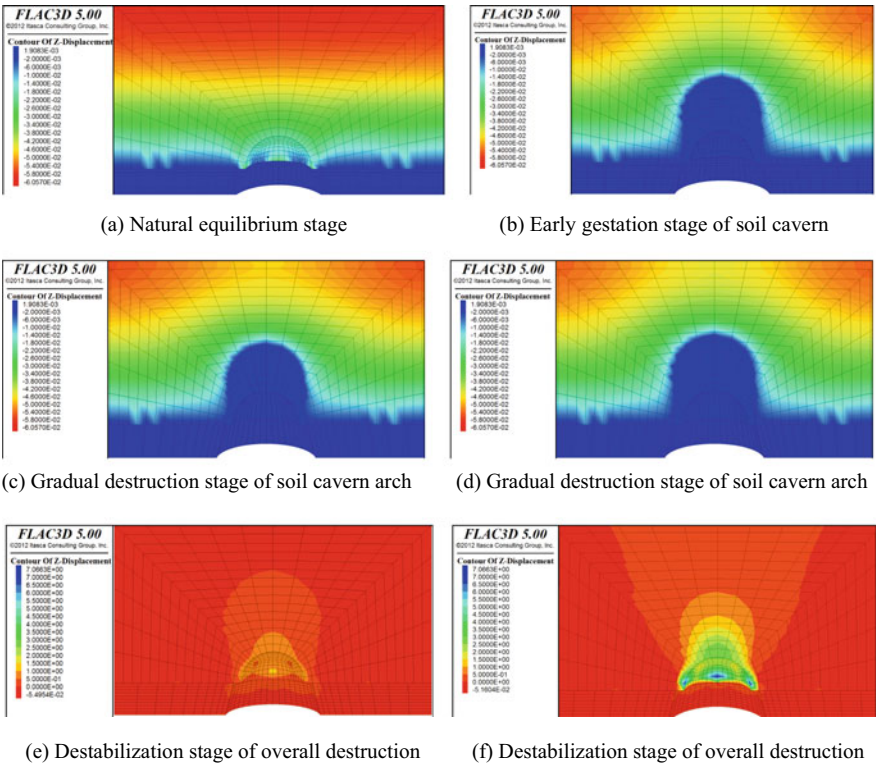

(a) Natural equilibrium stage (b) Early gestation stage of soil cavern

(c) Gradual destruction stage of soil cavern arch (d) Gradual destruction stage of soil cavern arch

(e) Destabilization stage of overall destruction (f) Destabilization stage of overall destruction

Fig. 8.3 Effect of positive pressure effect on vertical displacement

Combining Figs. 8.4, 8.5 and 8.6, it can also be found that the vertical displacement deformation at the top of the cave > vertical displacement deformation at the center of the surface > vertical displacement deformation at the foot of the cave.

8.4.2 Characteristics of Vertical Stress Variation

Under the influence of strong fluctuation of water level in the overburden karst soil cavern, the stresses in all different directional planes at each point in the overburden soil body are different, and the analysis of the vertical stresses can best reflect the stress state when the overburden karst soil cavern is damaged. According to the numerical simulation results, in the natural state, the values of vertical stress around the surface of the overburden layer and the soil cave are small; when the groundwater rises strongly upward to form the positive pressure effect, under the influence of water (gas), the values of vertical stress around the karst soil cave increase, and the contours show hemispherical or semi-ellipsoidal shape, at which time it enters the stage of soil

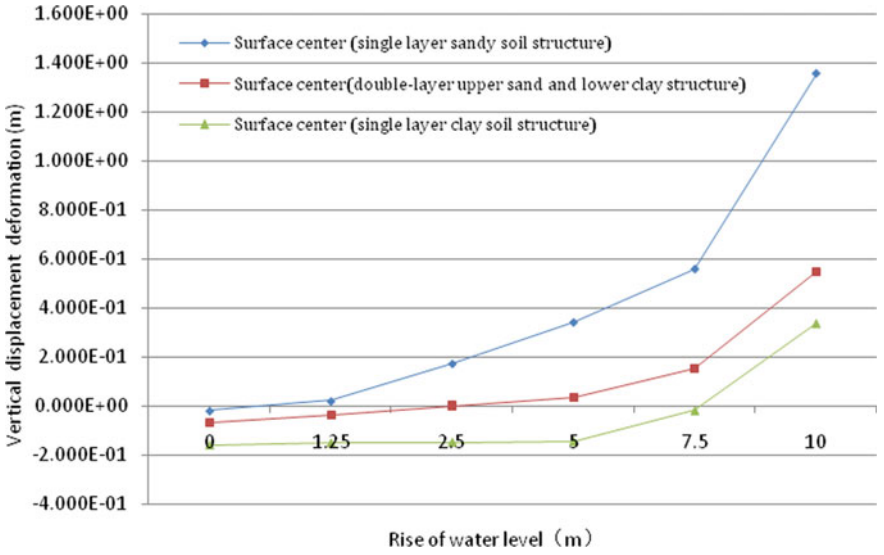

Fig. 8.4 Characteristics and rules of vertical displacement of the surface center

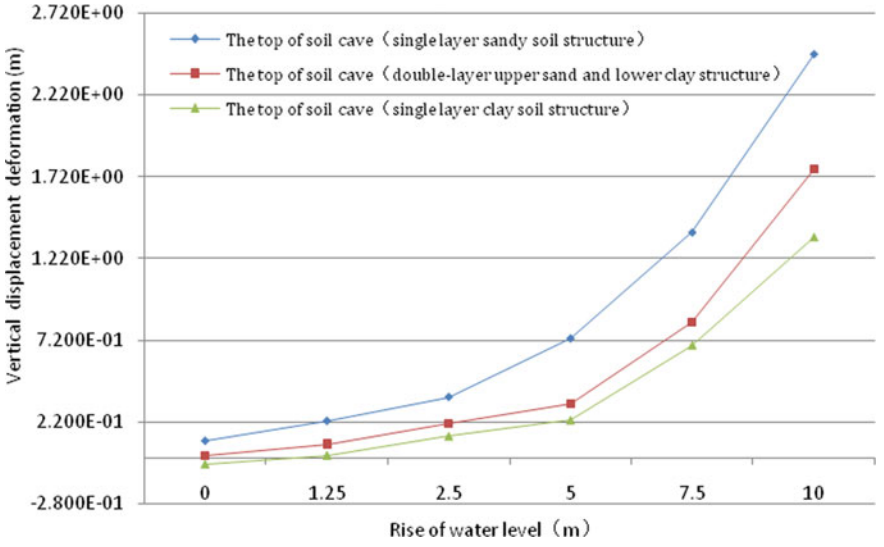

Fig. 8.5 Characteristics and rules of vertical displacement at the top

cave breeding and expansion. If the positive pressure value is close to the collapse resistance of the overlying soil layer, it is obvious that the vertical stress around the karst cavern increases rapidly and enters the stage of overall damage and instability (Fig. 8.7).

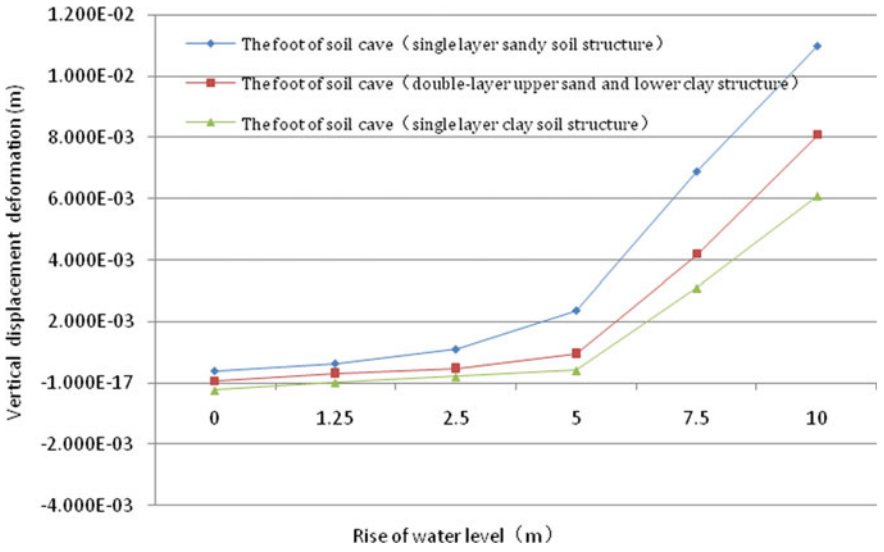

Fig. 8.6 Characteristics and rules of change of vertical displacement at the foot

If the influence of soil structure is considered, the characteristics of vertical stress changes in the surface center of single-layer clayey soil type, single-layer sandy soil type and double-layer upper sand and lower clay type overburden, the top of karst soil cave and the foot of karst soil cave have similarity. The top of the karst soil cave is most obviously affected by the positive pressure effect, and the vertical stress increases with the increase of groundwater rise, while the amount of vertical stress variation in the surface center of the overburden and the amount of vertical stress variation in the foot of the cave are less affected by the groundwater rise and have no obvious fluctuation (Fig. 8.8).

8.5 Conclusions

(1) During the evolution of karst soil caverns, the overburden soil body is bound to experience uneven changes of displacement, redistribution of stress and plastic damage due to the positive pressure effect.
(2) As the positive pressure effect increases, the displacement deformation is mainly concentrated at the top of the karst soil cavern, and the displacement contours show cylindrical and funnel-shaped, while the shape of the displacement contours directly determines the shape of the future karst collapse pit.
(3) With the strengthening of positive pressure effect, the vertical stress contours show hemispherical or semi-ellipsoidal shape and expand from the top of the soil cavern to the surface.

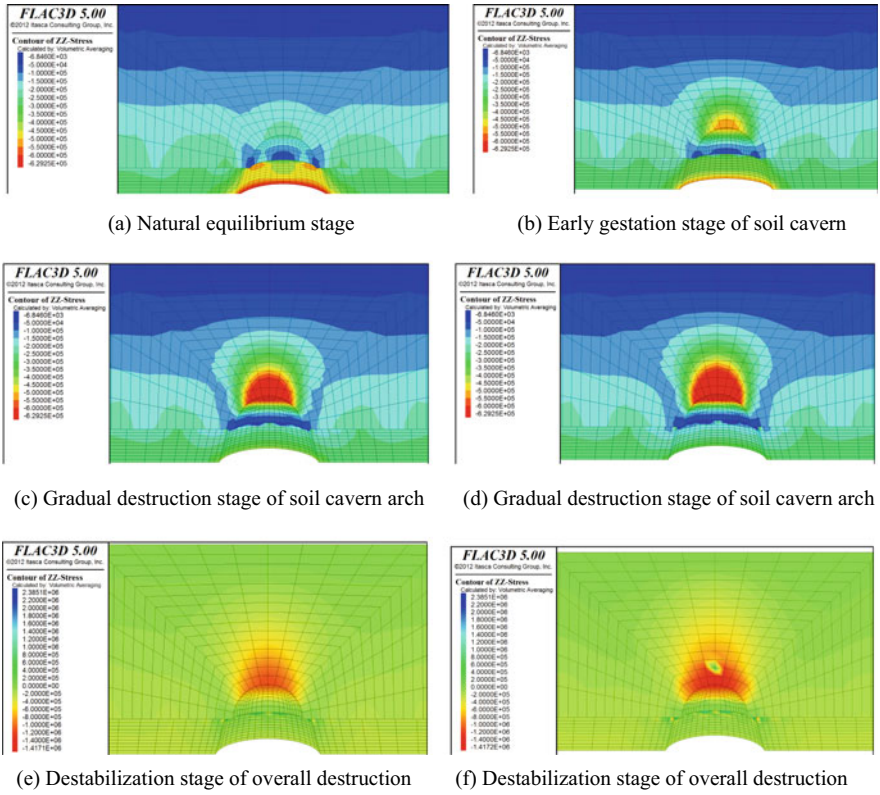

(a) Natural equilibrium stage (b) Early gestation stage of soil cavern

(c) Gradual destruction stage of soil cavern arch (d) Gradual destruction stage of soil cavern arch

(e) Destabilization stage of overall destruction (f) Destabilization stage of overall destruction

Fig. 8.7 Effect of positive pressure effect on vertical stress

(4) There is a critical relationship between the displacement deformation, vertical stress deformation and the magnitude of groundwater level rise at the foot, top and surface center of the karst cave.

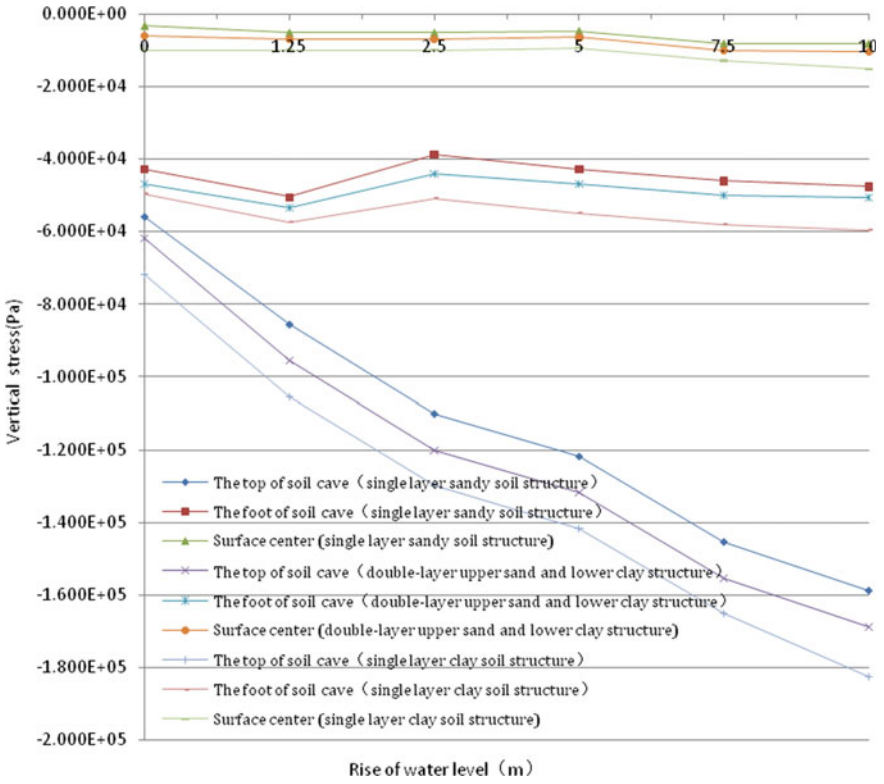

Fig. 8.8 Characteristics and rules of vertical stress in different structures

Acknowledgements The authors gratefully acknowledge the data support provided by the Xuzhou City geological survey projects. The authors also thank Comprehensive geological environment survey projects of key sections in Yellow River flood area of northern Jiangsu province and Comprehensive Development and Utilization Evaluation of Underground Space Resources in Suzhou Based on Multi-source Data Fusion pilot projects for supporting the valuable materials.

References

Cheng X, Huang RQ, Xu PH (2002) A discussion on mathematical model of karst air burst collapse. J Chengdu Univ Technol 29(6):686–689 (in Chinese)

Gao ZJ (2008) Study on the mechanism and cause mode of the karst collapse—taking tai'an-laiwu for example. Eng Sci 10(4):38–43 (in Chinese)

He HZ, Wei YY, Huang JJ (2017) Stability assessment for karst collapse along Xuzhou metro using a comprehensive fuzzy model. Chin J Geol Hazard Control 28(3):66–72 (in Chinese)

Hu P, Hu YL, Ma WT, Yang Y (1989) Analysis of reservoir induced earthquake caused by gas explosion in karst caves. Seismol Geol

Jiang XZ, Lei MT, Guan DD (2016) Character of water or barometric pressure jump within karst conduit in large strong drainage area of karst water filling mine in Dachengqiao, Ningxiang, Hunan. Carsologica Sin 35(2):179–189 (in Chinese)

Liu ZS, Han XG (1995) Investigationof possibility of reservoir-induced earthquake in the Yangtze gorges under new classification. Crustal Deformation Earthq 15(2):51–58 (in Chinese)

Wei YY, Sun SL (2017) Comprehensive critical mechanical model of covered karst collapse under the effects of positive and negative pressure. Bull Eng Geol Env 77(1):177–190

Wei YY, Sun SL (2018) A Study on karst development characteristics and key control factors of collapse in Xuzhou, eastern China. Carbonates Evaporites 33(3):359–373

Yr LU (2016) Karst development mechanism and research directions of developing engineering construction effect. Acta Geoscientica Sin 37(4):419–432 (in Chinese)

Chapter 9
Low Carbon and Clean Design for Garment Industry Based on Environmental Footprint Accounting

Chen Yiding

Abstract Due to its long industrial chain and wide variety of commodities, the garment industry with high carbon emissions and high pollution cannot effectively achieve low-carbon and clean production by upgrading a specific technology. Considering that the impact of the garment industry on the environment is mainly carbon emission, wastewater pollution and chemical pollution, this paper analyzes and lists three kinds of environmental footprints that should be considered most by the garment industry from the perspective of environmental footprint, namely, carbon footprint, water footprint and chemical footprint, and gives the calculation models of the three kinds of footprints. Finally, this paper takes carbon footprint as an example to analyze the carbon footprint of Xiangyun yarn fabric, linen fabric and worsted wool fabric, and gives some suggestions on the low-carbon upgrading of the garment industry. The results show that the worsted fabric has the highest carbon footprint, 24.809 kgCO_2e/kg, and its spinning process and post-treatment process are the two processes with the largest carbon footprint, accounting for 70.6% of the total carbon emissions. This means that for the worsted wool fabric, the improvements of spinning and post-treatment related processes can greatly reduce the level of carbon emissions in the production process and contribute to the low-carbon upgrading of the garment industry.

Keywords Garment industry · Low carbon design · Carbon footprint

9.1 Introduction

In recent years, with the frequent occurrence of extreme weather disasters around the world, people pay more and more attention to environmental protection, energy conservation and emission reduction. Clothes, as the most common items in life, tend

C. Yiding (✉)
Canadian International School of Hong Kong, Hong Kong 999077, China
e-mail: cocochen0612@126.com

Z. Sun and P. K. Das (eds.), *Proceedings of the 10th International Conference on Energy Engineering and Environmental Engineering*, Environmental Science and Engineering, https://doi.org/10.1007/978-3-031-48204-5_9

to cause a lot of carbon emissions and environmental pollution in their entire life cycle. Due to its huge scale and long supply chain, the garment industry produces about 10% of the total carbon emissions and 20% of the industrial wastewater each year (Leal et al. 2022; Kant 2012). In addition, throughout the life cycle of clothing, there will be a series of problems such as chemical pollution and textile waste accumulation (Niinimaki et al. 2020).

Obviously, the high carbon emissions and high pollution of the garment industry can not be ignored at present. In terms of reducing carbon emissions, due to the long industrial chain of the garment industry, a single technological improvement measure is far from effectively promoting the realization of the carbon dioxide emission reduction target of the industry at the macro level. Therefore, considering that the garment industry involves a large number of countries and regions and a wide variety of technical links, it is an effective means to reduce emissions of the garment industry by quantifying carbon emission targets and finding the carbon emission entry point in the life cycle of the garment industry based on carbon footprint accounting. This is because, firstly, it has become an international consensus to jointly promote the reduction of greenhouse gas emissions, and many countries have made up their minds to tackle these problems and set corresponding carbon reduction targets. Germany, for example, plans to reduce carbon emissions from its clothing sector to 65% below 1990 levels by 2030 (Black et al. 2021). Vietnam plans to reduce carbon emissions in the garment sector by 85% below 2014 levels by 2030 (Do and Burke 2021). Secondly, carbon footprint accounting also provides the possibility for the garment industry to fundamentally implement carbon emission reduction, because it can cover all aspects of the garment industry's life cycle, from raw material acquisition to recycling. Therefore, the use of carbon footprint accounting method can provide strong support and guidance for the low carbon upgrading of the garment industry. Similarly, in terms of pollutant emissions, corresponding environmental footprint accounting methods can also be adopted to help the garment industry achieve a clean transition.

Based on the above content, this paper focuses on carbon emission reduction, wastewater emission reduction and chemical pollution, and expounds the method to solve the low-carbon and clean development of the garment industry from a macro perspective, that is, the method to rely on environmental footprint estimation. And this paper analyzes and lists three kinds of environmental footprints that the clothing industry should consider most, namely, carbon footprint, water footprint and chemical footprint, and the calculation models of the three kinds of footprints. With the help of the corresponding footprint accounting, it is helpful to conduct a comprehensive investigation of the environmental indicators of the whole life cycle of the garment industry, and can effectively provide a reference for the optimization direction of the low-carbon and clean development of the garment industry.

9.2 Accounting for Environmental Footprint

9.2.1 Conceptual Definition of Environmental Footprint Accounting in the Garment Industry

Environmental footprint refers to the series of impacts on the environment during the life cycle of a product, including direct and indirect impacts from raw material acquisition, finished product production, use and maintenance, recycling and disposal processes. For the garment industry, during the life cycle of a specific product, the impact on the environment mainly comes from carbon dioxide emissions, water pollution and chemical pollution. Therefore, for the garment industry, it is necessary to conduct carbon footprint accounting, water footprint accounting and chemical footprint accounting for the garment life cycle.

9.2.2 Accounting Boundary

Before calculating the environmental footprint of a product, it is necessary to determine the product accounting boundary. The accounting boundary of a certain product in the garment industry can be divided into time boundary and spatial boundary. For the garment industry, the time boundary of the environmental footprint can be all units of activity between raw material acquisition and recycling, the main units of activity are shown in Fig. 9.1. The spatial boundaries of the environmental footprint refer to the required energy and resource inputs and waste outputs in the areas necessary for these activities. For example, the water and electricity consumed in the garment processing plant, the discharge of industrial wastewater, greenhouse gases and chemical pollutants.

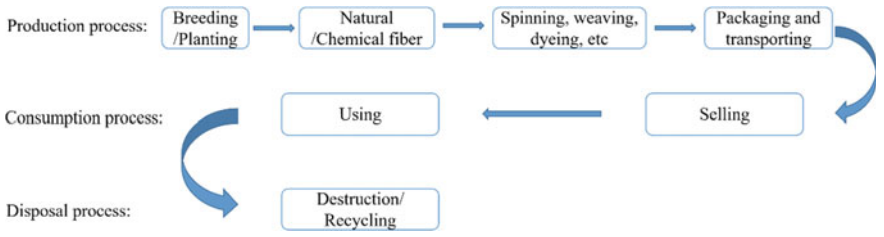

Fig. 9.1 The life cycle of typical products in the garment industry

9.2.3 Carbon Footprint Accounting Model

The carbon footprint calculation is the sum of the carbon dioxide emission ns of the product within a certain accounting boundary, including the direct and indirect part, and other greenhouse gas carbon footprint calculation also needs to be converted to carbon dioxide equivalent, that is, CO_2e. In the calculation process of specific carbon emissions, the emission factor method can often be used, which can usually be calculated by the following formula (Wiedmann and Minx 2009):

$$S_{cf} = \sum_{i=1}^{n} (Q_i + k_i) \tag{9.1}$$

where S_{cf} is the carbon footprint of a product; Q_i is the amount of input or output of a certain activity unit of a product (statistical units, such as kg, m^3, KWh, etc.); k_i is the carbon emission factor (CO_2e/ statistical unit).

9.2.4 Water Footprint Accounting Model

Since the concept of water footprint was proposed by Hoekstra (2009) in 2002, water footprint has become an essential index for evaluating the load of water resources. According to ISO 14046 (Environmental management-water footprint-principles, requirements and guidelines), water footprint can be divided into two categories: water scarcity footprint and water degradation footprint. The water footprint is defined as consumption and an indicator of potential environmental impacts associated with water. The water scarcity footprint is a measure of the amount of fresh water consumed by a product or service over its life cycle in terms of water consumption. The water degradation footprint is the potential environmental impact related to water quality, which can be subdivided into water eutrophication footprint, water acidification footprint, water ecological toxicity footprint, etc.

The water scarcity footprint can be calculated as follow (Ridoutt and Pfister 2010):

$$S_{wsf} = \sum_{i=1}^{n} \left(\frac{WPI_i}{WPI_G} \times V_i \right) \tag{9.2}$$

where S_{wsf} is the water scarcity footprint of a product (m^3 H_2Oe); WPI_i is the water pressure index of a certain unit; WPI_G is the global average water pressure index.; V_i is the water consumption (m^3).

The water degradation footprint is mainly considered as the water eutrophication footprint, the water acidification footprint and the water eco-toxicity footprint, which can be calculated respectively by the following formula (Wanwen et al. 2017):

$$S_{wdf-eu} = \sum_{i=1}^{n} \left(S_{eu,i} \times c_{eu,i} \right) \tag{9.3}$$

$$S_{wdf-ac} = \sum_{i=1}^{n} \left(S_{ac,i} \times c_{ac,i} \right) \tag{9.4}$$

$$S_{wdf-ec} = \sum_{i=1}^{n} \left(S_{ec,i} \times c_{ec,i} \right) \tag{9.5}$$

where S_{wdf-eu} is the water eutrophication footprint (kg$PO_4{}^{3-}$e or kgNO^{3-}e); S_{wdf-ac} is the water acidification footprint (kgSO_2e); S_{wdf-ec} is the water eco-toxicity footprint (m^3H_2Oe); S and c are the quality of pollutants and the characteristic factors of corresponding pollutants, respectively; The subscripts eu, ac and ec are the water eutrophication footprint, the water acidification footprint and the water eco-toxicity footprint, respectively.

9.2.5 Chemical Footprint Accounting Model

The chemical footprint was proposed by Panko and Hitchcock (2011) in a commercial report in 2011. After years of development, chemical footprints can effectively evaluate the environmental load of chemical use. At present, it is considered feasible to calculate chemical footprint with the help of eco-toxic impact characterization factors, which is typically represented by the USE_{tox} model, calculated as follow (Bjorn et al. 2014):

$$S_{chf} = f \times \sum_{i=1}^{n} \left(chf_i \times m_i \right) \tag{9.6}$$

where, S_{chf} is the chemical footprint, representing the score of potential toxic effects on human ecology (Cases) or the score of potential toxic effects on ecology (PAF m^3 day); f is the correction factor for estimating the absolute environmental impact, with a value of 290; chf_i is the characteristic factor (Cases/kg or PAF m^3 day/kg); m_i is the mass of the corresponding pollutant (kg).

9.3 Low Carbon Clothing Industry Life Cycle Design

The production link refers to all the links from raw material acquisition to processing into products, such as cotton planting, fiber synthesis, weaving, dyeing, packaging, etc. For the garment industry, raw materials, as the most basic component, are directly

related to the carbon emissions of the entire production link, so it is crucial to study the carbon footprint of a certain raw material in a specific unit. As shown in Table 9.1, the raw materials of the garment industry can be roughly divided into three categories, namely natural fibers, recycled fibers and synthetic fibers. Among them, natural fibers exist in nature and can be directly obtained, which are divided into plant fibers, animal fibers and mineral fibers according to their sources. Among them, natural fibers exist in nature, that is, plants, animals and minerals exist in nature, which can be divided into cotton fabrics, hemp fabrics, silk fabrics and wool fabrics. Both regenerated fibers and synthetic fibers are chemically synthesized fibers. Among them, the recycled fiber is made of textile fiber after chemical processing with substances containing natural fiber or protein fiber, such as wood, soybean protein fiber and other fiber raw materials that have lost the value of textile processing. Synthetic fibers are made by chemical synthesis and mechanical processing from substances that do not contain cellulose or protein themselves, such as oil, coal, and natural gas.

Due to differences in the origin, processing technology, and management methods of processing enterprises for different fabrics, it is difficult to gradually investigate and obtain information for various fabrics. Therefore, this paper refers to "Greenhouse gas emission coefficient set for the entire lifecycle of Chinese products" (China Product Whole Life Cycle Greenhouse Gas Emission Coefficient Set 2022). The carbon footprint of Xiangyun yarn fabric, worsted wool fabric and linen fabric was collected and analyzed again. Moreover, since the processing technology of each fabric is not completely consistent, it is necessary to make classification when comparing the carbon footprint of different fabrics. In this paper, it is divided into three parts, including raw material acquisition, processing, and other classes, as shown in Fig. 9.2. When judging the carbon footprint of a fabric alone, as shown in Fig. 9.3, the carbon footprint of each process can be listed in order to analyze the optimization direction of the fabric production and promote the low-carbon upgrading of the industry.

Figure 9.2 shows the comparison of the Carbon footprint of three fabrics: the Xiangyun yarn fabric, the worsted wool fabric and the linen fabric. As shown in the figure, the worsted wool fabric has the highest carbon footprint of 24.809 $kgCO_2e/kg$ among the three kinds of fabrics, and the lowest is the Xiangyun yarn fabric of 18.7 $kgCO_2e/kg$. It can also be seen from Fig. 9.2 that in the process of processing raw materials into finished products, the Carbon footprint of the worsted wool fabric is 22.36 $kgCO_2e/kg$, which is 4.97 times of 4.5 $kgCO_2e/kg$ of the Xiangyun yarn fabric and 2.58 times of 8.66 $kgCO_2e/kg$ of the linen fabric respectively. This indicates that the current processing technology of the worsted wool fabrics has a high carbon emission footprint and may have a large carbon reduction potential. Figure 9.3 shows the

Table 9.1 The main categories of raw materials for the garment industry

Natural fiber	Regenerated fiber	Synthetic fiber
Cotton fabric, linen fabric, silk fabric, woolen fabric	Regenerated cellulose fiber, regenerated protein fiber	Dacron, acrylic fiber, polypropylene fiber, etc

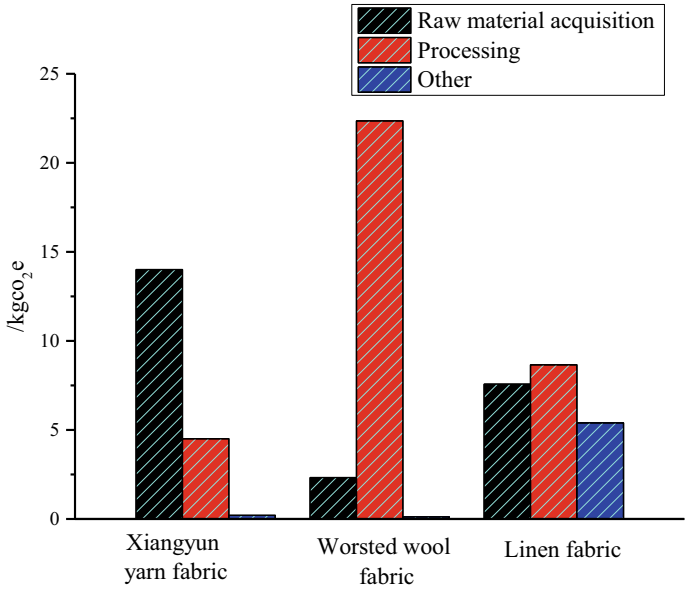

Fig. 9.2 Comparison of the carbon footprint of different fabrics

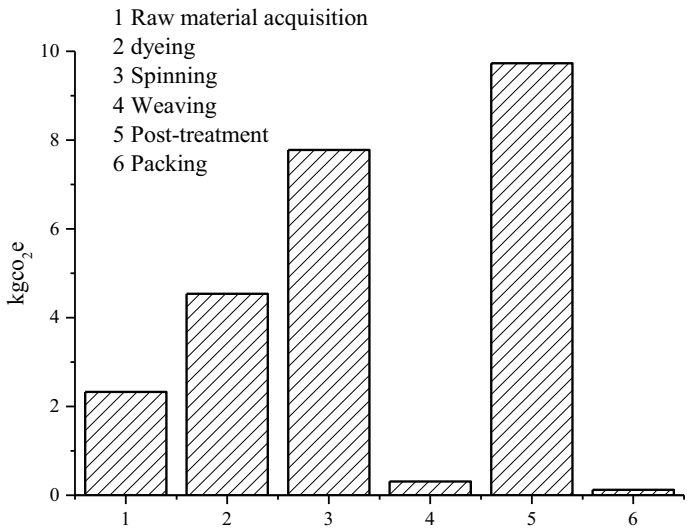

Fig. 9.3 Composition of the carbon footprint of the worsted wool fabric

corresponding carbon footprint of each process of the worsted wool fabric. It can be seen from the figure that the production processes of the worsted wool fabric specifically include raw material acquisition, dyeing, spinning, knitting, post-treatment and packaging. The carbon footprints are 2.329, 4.54, 7.78, 0.31, 9.73 and 0.12 respectively. The processes with the highest carbon emissions are spinning and post-treatment, accounting for about 31.4% and 39.2% respectively, with a total carbon emission of 70.6%. This means that for upgrading the low-carbon industry of worsted wool fabrics, priority can be given to improving spinning and post-treatment related processes.

9.4 Conclusion

The long industrial chain and wide variety of goods in the garment industry determine that the industry needs to analyze and trace the source from the perspective of environmental footprint, so as to hope to fundamentally solve the low carbon and cleanliness of the garment industry. The carbon footprint evaluation results of the worsted wool fabric showed that the carbon footprints of spinning and post-treatment accounted for the largest proportion, which was 70.6% of the total carbon footprint of 24.809 $kgCO_2e/kg$ in the production process. This shows that optimizing the spinning and post-processing related processes has great emission reduction potential for this product. Similarly, the carbon footprint, water footprint and chemical footprint verification of the garment industry can help to provide optimization direction and ideas for the low-carbon and clean development of the industry.

References

China Product Whole Life Cycle Greenhouse Gas Emission Coefficient Set (2022) http://lca.cityghg.com/. Accessed 2 July 2023

Bjorn A, Diamond M, Birkved M et al (2014) Chemical footprint method for improved communication of freshwater ecotoxicity impacts in the context of ecological limits. Environ Sci Technol 48(22):13253–13262

Black MS, Chen MR, Mineshima MA (et al) Scaling up climate mitigation policy in Germany. IMF Working Papers (241):36

Do TN, Burke PJ (2021) Carbon pricing in Vietnam: options for adoption. Energy Clim Change 2:100058

Hoekstra AY (2009) Human appropriation of natural capital: a comparison of eco-logical footprint and water footprint analysis. Ecol Econ 68(7):1963–1974

Kant R (2012) Textile dyeing industry: an environmental hazard. Nat Sci 4(1):22–26

Leal W, Perry P, Heim H et al (2022) An overview of the contribution of the textiles sector to climate change. Front Environ Sci 10:1–5

Niinimaki K, Peters G, Dahlbo H et al (2020) The environmental price of fast fashion. Nat Rev Earth Environ 1(4):189–200

Panko J, Hitchcock K (2011) Chemical footprint ensuring product sustainability. Air Waste Manage Assoc (12):11–15

Ridoutt BG, Pfister S (2010) A revised approach to water footprinting to make transparent the impacts of consumption and production on global freshwater scarcity. Glob Environ Chang 20(1):113–120

Wanwen H, Yi L, Laili W (2017) Water footprint accounting and evaluation of textile and clothing products based on ISO 14046. Print Dyeing 43(17)

Wiedmann T, Minx JA (2009) Definition of 'carbon footprint.' J R Soc Med 92(4):193–195

Chapter 10
Influence of the Abandoned Oil Layer on Heat Mining Performance of U-shape Well Geothermal System

Fengming Li, Wei Zhang, Zhengnan Wei, Shuaidong Qi, and Mingjian Wang

Abstract Regarding the current situation that there are large amounts of high water-cut oil and gas reservoirs, the switching of geothermal development using the available well pattern has become the effective way to control carbon emission. However, the influence of the abandoned oil layer features on geothermal development performance are still unclear. This study combines the exploration of U-shape well geothermal system with the CO_2 geological storage using the oil-extracted layer. Considering the fluid natural convection in porous medium induced by temperature gradients in thermal reservoir, the heat and mass transfer in wellbore and thermal reservoir and the heat transfer between pipes and reservoir are coupled, then the effect of oil layer features on heat mining of the U-shape well geothermal system are discussed. The results show that heat mining performance of closed-well geothermal system can be enhanced by the increase of rock permeability around the well (include the oil and cover layer) due to the strengthen of natural convection. In CO_2 buried oil layer due to the low viscosity of $ScCO_2$ and the sensitivity temperature-independent density, the natural convection of $ScCO_2$ drives the vertical migration of high temperature heat flow. Comparing the water-flooded abandon layer with the $ScCO_2$-flooded abandon layer, the outlet temperature of geothermal system with $ScCO_2$ storage increased by 11.23% and the heat mining rate increased by 17.9% after 10-year exploitation. The increase of the oil layer number and oil layer thickness will enhance the natural convection, which can raise the heat mining performance of U-shape well geothermal development. This research will provide technical support for the site selection and stimulation scheme design for geothermal development and the CO_2 geological storage scheme in abandoned oil reservoirs, and contribute to the carbon reduction in oil and gas field.

F. Li · W. Zhang (✉) · Z. Wei
New-Energy Development Center of Shengli Oilfield, SINOPEC, Dongying 257001, China
e-mail: zhwei1990@sdust.edu.cn

W. Zhang · S. Qi · M. Wang
College of Energy and Mining Engineering, Shandong University of Science and Technology, Qingdao 266590, Shandong, China

Z. Sun and P. K. Das (eds.), *Proceedings of the 10th International Conference on Energy Engineering and Environmental Engineering*, Environmental Science and Engineering, https://doi.org/10.1007/978-3-031-48204-5_10

Keywords Abandoned oil layer · U-shape well geothermal system · Heat mining performance · Natural convection · $ScCO_2$ storage

10.1 Introduction

For the exploitation of geothermal energy in oilfields, the rich geological data, existing wellbore and the advanced fluid extraction technology all provide support for the efficient extraction of geothermal energy (Xin et al. 2012; Zeng et al. 2013; Held et al. 2014). The existing geothermal extraction methods can be mainly divided into open-cycle geothermal system (including geothermal recharge, enhanced geothermal system) and close-cycle geothermal system (including tube-buried heat exchange, single well co-axial heat exchange, gravity heat pipe heat extraction and U-shape well heat extraction). Regarding series problems of pipe corrosion, reservoir damage, high reservoir fracturing cost, and the difficulty in downhole communication of fracturing fractures in open-cycle geothermal systems, the close-cycle heat extraction has gradually attracted the attention of most oilfields (Ammar et al. 2020; Bujakowski et al. 2015; Garcia et al. 2016). Meanwhile, the construction of U-shape geothermal well becomes possible due to the technological advance of downhole well communication and well sealing (Cheng et al. 2013; Adelina et al. 2009). Although scholars have studied the heat mining performance of U-shape well geothermal system, there is no report on the effect of oil layer features on the heat mining performance of close-cycle geothermal system with CO_2 sequestration. In this study, it is proposed to employ the CO_2-flooding to enhance the oil recovery, then based on the oil-extracted abandoned layer to construct the U-shape well geothermal system with $ScCO_2$ storage based on the existing well pattern (Fig. 10.1). Then, the influence of oil layer characteristics and fluid type buried in oil layer on heat mining performance of U-shape well geothermal system was investigated.

For the open-cycle heat extraction, some scholars have carried out the related research (Kumari et al. 2018; Zhao et al. 2017; Guo et al. 2016). Hofmann et al. discovered that the use of natural fracture for shear fracturing has higher economic benefits, and the heat mining performance of horizontal wells is better than that of

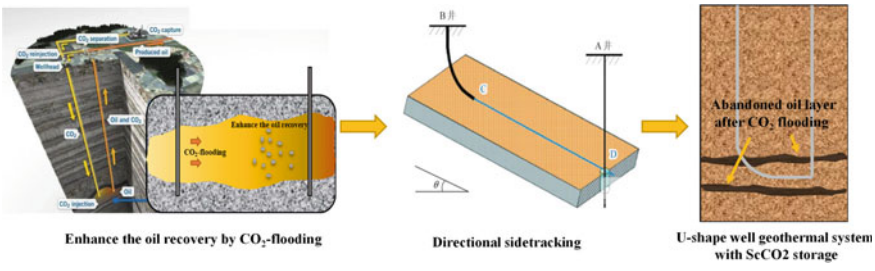

Fig. 10.1 The U-shape well geothermal system with $ScCO_2$ storage

vertical wells (Hofmann et al. 2014). Blöcher et al. analyzed the thermal breakthrough rule of the geothermal project by 3D geological model (Pandey et al. 2017). Based on actual geological data of Soultz geothermal project, Sebastian et al. discussed the development characteristic of fractured geothermal reservoir under different well patterns (Blöcher et al. 2010). Bujakowski et al. evaluated the thermal extraction of sedimentary reservoir in central Poland, and the results show that the heat mining rate is 2–3 MW when the injection flow rate is 55 l/s in the layer at 5500 m with temperature of 170 °C (Bujakowski et al. 2015). Zhang et al. studied the geothermal heat mining performance of horizontal well with staged fracturing (Zhang et al. 2015). Jiang et al. established a three-dimensional TH coupled model to analyze the heat mining performance of three-well geothermal system and general two-well geothermal system, and the result show that the multi-well pattern can prolong the production duration (Jiang et al. 2014). Qu and Zhang et al. discussed the effect of different fracture morphology on heat mining performance and explored the use of water and supercritical CO_2 as heat-carrying medium (Qu et al. 2017).

Although the heat extraction efficiency is high using the open-cycle geothermal system, there are still problems and rules limit its development (Ammar et al. 2020; Omid et al. 2021; Shabnam et al. 2018; Kujawa et al. 2006; Noorollahi et al. 2015). For the close-cycle system, Kujawa et al. (2006) and Noorollahi et al. (2015) conducted numerical simulation of single well co-axial heat transfer for abandoned wells. The results show that the inlet temperature, flow rate and internal pipe insulation will affect the heat mining performance, and the heat mining rate can be 40–360 kW. Sun et al. proposed to use supercritical CO_2 as the circulating medium in U-shape well geothermal system, and the heat mining performance of supercritical CO_2 and water is researched (Sun et al. 2019). Liao et al. concluded that the multi-level sections can improve the heat mining rate by numerical simulation (Liao et al. 2021). Li et al. evaluated the heat transfer performance of U-shape well horizontal section under different injection flow rates and horizontal section lengths through high temperature physical experiments (Li 2020).

Although series of experiments and numerical simulation studies on U-shape well geothermal system have been conducted by scholars, there is no report on the influence of abandoned oil layer features on U-shape well heat extraction. In this study, the natural convection of fluid in porous medium is considered, and the coupled model of heat and mass transfer in wellbore and thermal reservoir as well as the heat transfer between pipes and reservoir is constructed. Firstly, the influence of oil and cover layer permeability characteristics on heat mining performance of U-shape well geothermal system with $ScCO_2$ storage is explored. Then, the influence of fluid type buried in oil layer, oil layer number and oil layer thickness on heat mining performance of U-shape well geothermal system is discussed. The research results will provide important support for the conversion of abandoned oil reservoir to geothermal development.

10.2 Numerical Model

As it was found that the natural convection of fluid in reservoir promotes the heat extraction in the heat mining of close-cycle geothermal system (Huang et al. 2018). Therefore, considering the natural convection of fluid in porous medium, the coupled model of heat and mass transfer in wellbore and thermal reservoir as well as the heat transfer between pipes and reservoir is constructed.

10.2.1 Flow and Heat Transfer Model in Pipeline

The following continuity and momentum equations describe the steady flow in pipeline are:

$$\nabla \cdot (A_{\mathrm{p}u}) \equiv 0 \tag{10.1}$$

$$0 = -\nabla p - f_D \frac{\rho}{2d_h} u|u| + F \tag{10.2}$$

The energy equation for pipeline flow is:

$$\rho A C_{\mathrm{P}} u \cdot \nabla T = \nabla \cdot Ak\nabla T + f_D \frac{\rho}{2d_h} |u|^3 + Q_{wall} \tag{10.3}$$

Q_{wall} is a source/sink term due to heat exchange with the surroundings through the pipe wall.

$$Q_{wall} = hZ(T_{\mathrm{ext}} - T) \tag{10.4}$$

10.2.2 Flow and Heat Transfer Models in Porous Media

Considering the action of mechanical stress and temperature the seepage field governing equation is (Li et al. 2017):

$$-c_1 \frac{\partial \varepsilon_{\mathrm{v}}}{\partial t} - c_2 \frac{\partial T}{\partial t} + -c_3 \frac{\partial p}{\partial t} = \nabla \cdot \left[\frac{k}{\mu} (\nabla_p + \rho_1 g \nabla z) \right] \tag{10.5}$$

$$\begin{cases} c_1 = 1 - \dfrac{K'}{K_\mathrm{s}} \\ c_2 = \phi\alpha_1 + (1-\phi)\alpha_\mathrm{s} - \dfrac{\alpha_\mathrm{T}K'}{K_s} \\ c_3 = \dfrac{\phi}{\beta_1} + \dfrac{1-\phi}{K_\mathrm{s}} \end{cases}$$

Considering the thermal convection and mechanical stress the temperature field governing equation is (Zhang et al. 2022):

$$(\rho C)_\mathrm{M}\frac{\partial T}{\partial t} + (T_0 + T)K'\alpha_\mathrm{T}\frac{\partial \varepsilon_\mathrm{T}}{\partial t} + \rho_1 C_1 (T_0 + T)\frac{k}{\mu}\nabla p = \lambda_\mathrm{M}\nabla^2 T \tag{10.6}$$

10.2.3 Realization of Natural Convection of Fluid in Porous Media

The gravity term and viscosity term in Eq. (10.5) can be used to realize the depiction of the natural convection of fluid in porous medium (Zhang et al. 2022). As shown in Fig. 10.2, the fluid density and viscosity are temperature-dependent parameters, and compared with water the density and viscosity of CO_2 are more sensitive to temperature.

10.3 Heat Mining Performance of U-Shape Well Geothermal System

For the open-cycle geothermal system, the influence of reservoir characteristics on heat mining performance has been investigated by many scholars. While, considering the natural convection of fluids in reservoir, the heat mining performance of U-shape well geothermal system under different reservoir characteristics is still worthy of further study.

10.3.1 Model Establishment

The established geometric model includes the reservoir with the height of 3500 m, the length of 1900 m and the width of 800 m. And the thickness of oil layer is 100 m, the length is 1900 m and the width is 800 m, meanwhile the oil layer has a certain degree of heterogeneity, as shown in Fig. 10.3a. Based on the actual temperature

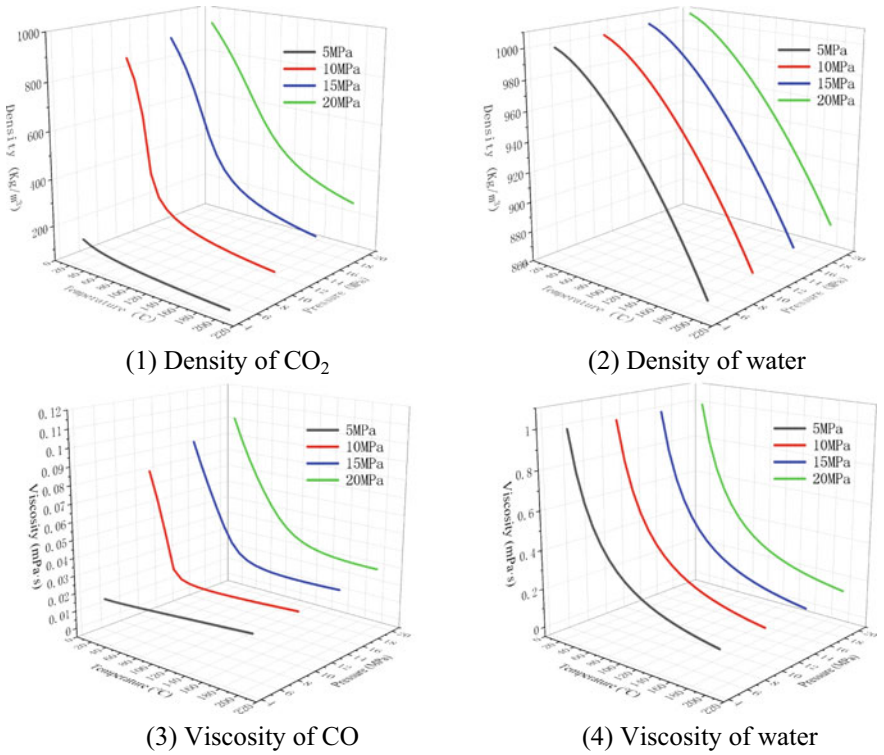

(1) Density of CO_2 (2) Density of water

(3) Viscosity of CO (4) Viscosity of water

Fig. 10.2 The density and viscosity of CO_2 and water

measured downhole, the temperature gradient in model is described by interpolation module. Based on the drilling trajectory design, the horizontal link section of U-shape well is constructed. During geothermal development, water is employed for heat-carrying medium in the U-shape well geothermal system, and the abandoned oil layer is assumed to be the porous with certain saturation. And the porous medium is assumed to filled with water or CO_2 according to the oil layer is water-flooded or CO_2 flooded. The simulation parameters are shown in Table 10.1.

10.3.2 Simulation Scheme

For research of the influence of different reservoir characteristics on U-shape well geothermal system heat mining performance, the various parameters of oil and cover layer are set. In this part, to highlight the function of natural convection in reservoir, the CO_2 is assumed to be buried in the abandoned oil layer. And in the initial state, the water is assumed to be buried in the cover layer. The various parameters of oil and cover layer under different simulation scheme are shown in Table 10.2.

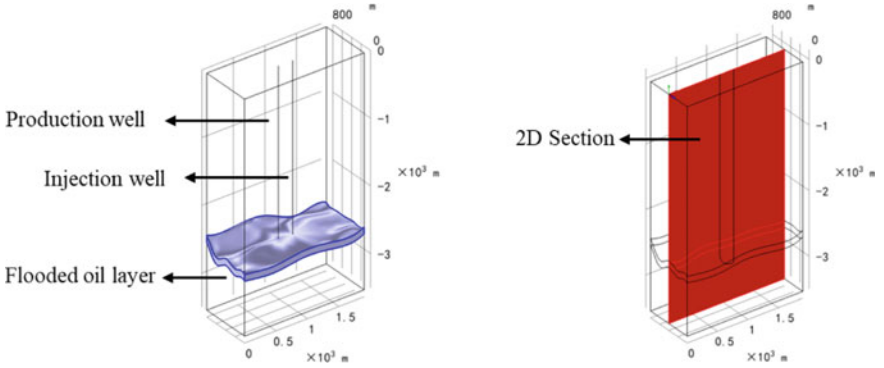

(a) U-shape well geothermal system (b) 2D Section of geothermal system

Fig. 10.3 Geometry of U-shape well geothermal system with abandoned oil layer (the 2D Section will be used to describe the distribution of temperature and flow velocity in reservoir)

Table 10.1 Parameters of the U-shape well geothermal system

h_r m	w_r m	l_r m	φ_o	φ_r	U_{inj} kg/s
3500	800	1900	0.3	0.1	6
C_o W/(m K)	C_r W/(m K)	C_{wi} W/(m K)	C_{wo} W/(m K)	C_{wh} W/(m K)	T_{inj} °C
1.9	2.9	2.45	1	2.45	20

Table 10.2 Parameters of oil and cover layer under different simulation scheme

Item	Oil layer permeability/(m^2)	Cover layer permeability/(m^2)
Case1	100×10^{-15}	1×10^{-15}
Case2	500×10^{-15}	1×10^{-15}
Case3	1000×10^{-15}	1×10^{-15}
Case4	50×10^{-15}	1×10^{-15}
Case5	50×10^{-15}	100×10^{-15}
Case6	50×10^{-15}	500×10^{-15}
Case7	50×10^{-15}	1000×10^{-15}
Case8	1000×10^{-15}	1000×10^{-15}
Case9	$10{,}000 \times 10^{-15}$	1000×10^{-15}

After years of oil extraction, there are large numbers of pores and micro-fractures in oil layer, so the abandoned oil layers usually present the high permeability. Besides, to raise the heat mining performance of U-shape well geothermal system, the reservoir stimulation can also be applied to the oil layer or the cover layer of the abandoned oil reservoirs. As can be seen in Fig. 10.4, when the permeability of cover layer maintains constant (1×10^{-15} m^2), with the increase of oil layer permeability from 50 ×

10^{-15} to 1000×10^{-15} m^2, the outlet temperature and heat mining rate of U-shape well geothermal system presents minor changes. In addition, when the permeability of oil layer maintains constant (50×10^{-15} m^2), with the increase of cover layer permeability from 1×10^{-15} to 1000×10^{-15} m^2, the outlet temperature and heat mining rate of U-shape well geothermal system also presents minor changes. And the temperature and velocity field of Case7 are shown in Figs. 10.5 and 10.6. While when the permeability of both the oil and cover layer raise (as Case8 and Case9), the outlet temperature and heat mining rate present the growing trend. After 120 Ms geothermal development, the outlet temperature of Case8 raises by 9.8% compared with Case1, and the heat mining rate of Case8 raises by 18.8% compared with Case1. The outlet temperature of Case9 raises by 10.9% compared with Case8, and the heat mining rate of Case9 raises by 15.4% compared with Case8. And the temperature and velocity field of Case8 are shown in Figs. 10.7 and 10.8. $ScCO_2$ buried in oil layers moves upward under the action of density difference and brings heat to the upper part of the oil layer. The cover layer around the upper part of the oil layer will be heated, which can generate the natural convection in the overburden thermal reservoir. Furthermore, the heat-carrying medium in wellbore can be heated by the natural convection heat transfer in thermal reservoir. So, the heat mining performance of closed-well geothermal system can be enhanced by the stimulation of rock around the well. With the improvement of the reservoir permeability, the raise of heat mining performance will be larger.

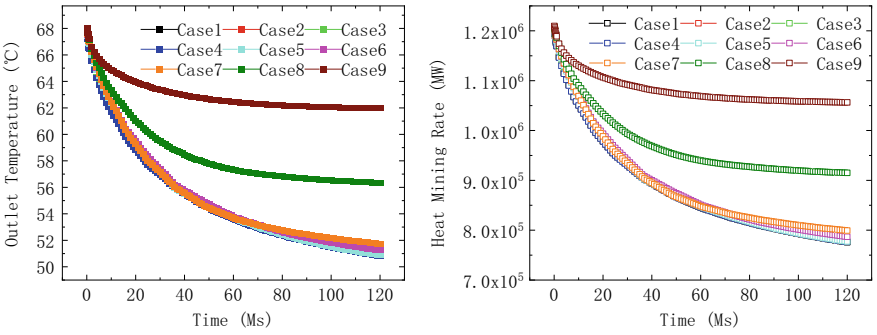

(a) outlet temperature (b) heat mining rate

Fig. 10.4 Heat mining performance of the U-shape well geothermal system under different parameters of oil and cover layer

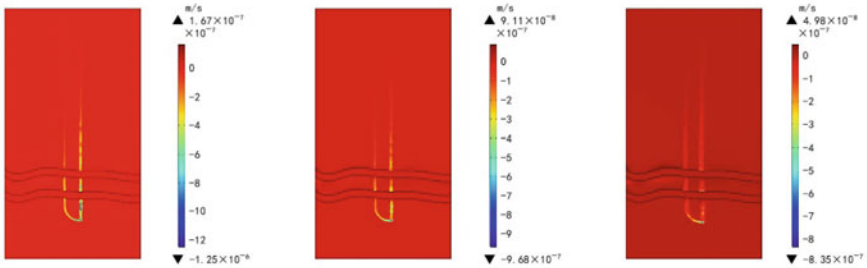

(a) 36Ms (b) 60Ms (c) 120Ms

Fig. 10.5 Flow velocity field of Case7 at different time

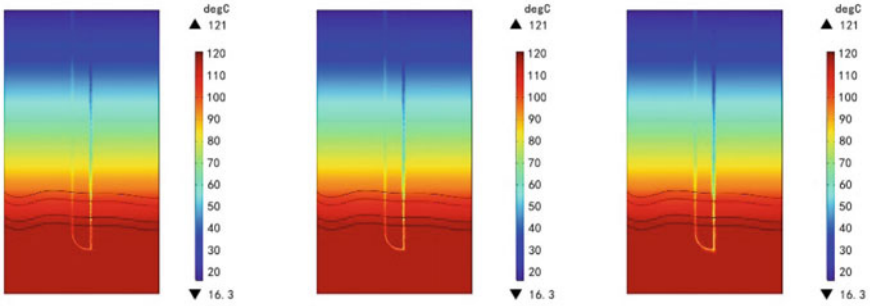

(a) 36Ms (b) 60Ms (c) 120Ms

Fig. 10.6 Temperature field of Case7 at different time

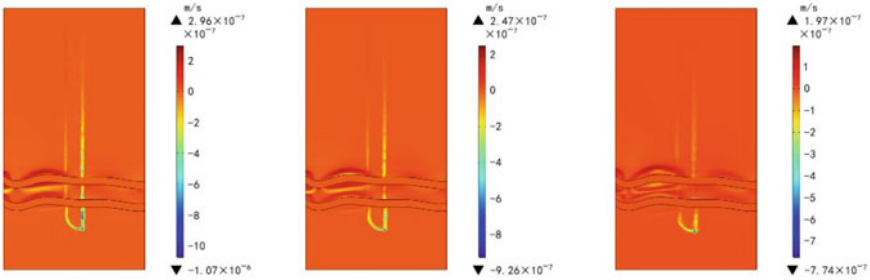

(a) 36Ms (b) 60Ms (c) 120Ms

Fig. 10.7 Flow velocity field of Case8 at different time

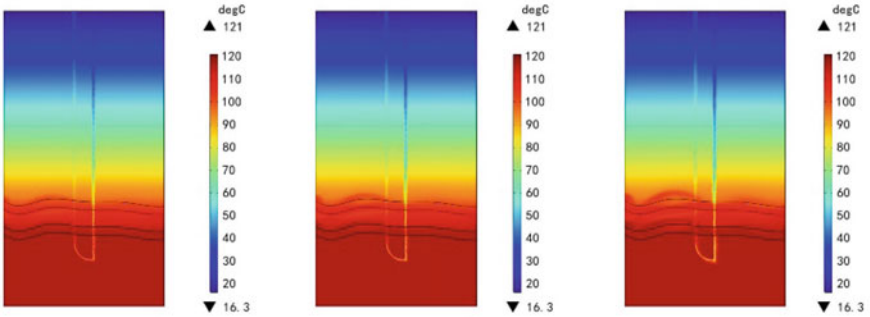

(a) 36Ms (b) 60Ms (c) 120Ms

Fig. 10.8 Temperature field of Case8 at different time

10.4 Influence of Key Parameters on Heat Mining Performance of U-Shape Well Geothermal System

10.4.1 Fluid Type Buried in Oil Layer

The mining of geothermal resources in oil field is usually carried out after the completion of oil and gas exploitation, that is when the oil and gas recovery rate is reduced to almost no economic benefits, a geothermal system will be constructed to extract geothermal energy. And water flooding is commonly used to enhance the output of oil and gas. However, the CO_2 flooding technology proposed in recent years can not only improve the oil and gas recovery, but also play the role of CO_2 geological storage. In fact, under the reservoir temperature and pressure environment, the CO_2 will be in supercritical state. Therefore, the heat mining performance of U-shape well after water flooding and after CO_2 flooding will be discussed by setting the saturation of water or CO_2 in oil layer. In addition, the parameters of oil and cover layer refers to the parameters in Case9.

In terms of the abandoned oil layer after water-flooding and after CO_2-flooding, their heat mining performance with the construction of U-shape well geothermal system is compared. The simulation results show that the outlet temperature and heat mining rate after CO_2-flooding are higher than those after water-flooding under the same operation parameters. As shown in Fig. 10.9, the outlet temperature in geothermal system after CO_2-flooding is 9.1% higher than that after water-flooding, and the heat mining rate is improved by 14.9% after 5-year development. After 10-year development, the outlet temperature of geothermal system after CO_2-flooding increase by 11.23% and the heat mining rate increase by 17.9% compared with the geothermal system after water-flooding. So for the efficient exploitation of U-shape well geothermal system is inclined to choose the abandoned oil layer after CO_2-flooding.

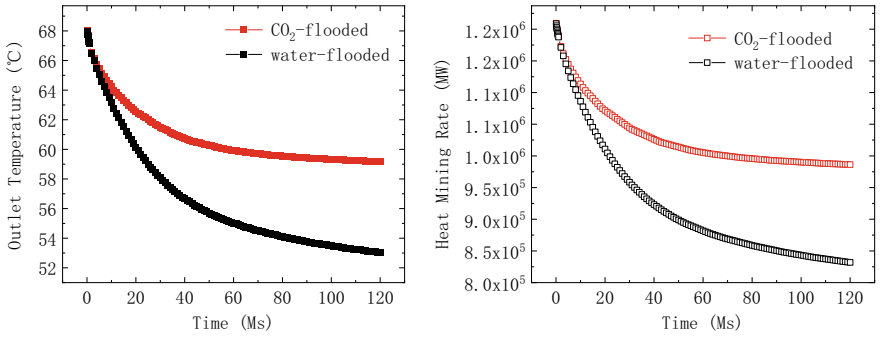

(a) outlet temperature (b) heat mining rate

Fig. 10.9 Heat mining performance comparation of the U-shape well geothermal system with water-flooded and CO_2-flooded

The distribution of temperature and fluid velocity at 36, 60 and 120 months of development is respectively described in Figs. 10.10, 10.11, 10.12 and 10.13. The surrounding temperature around the wellbore decreases with the exploitation of geothermal energy around the wellbore. As the temperature decrease, the fluid density increases and moves downward in the thermal reservoir under gravity action. Meanwhile, the relative hotter fluid with lower density at the deeper zone flows upwards in thermal reservoir driven by buoyancy, which induce the natural convection in thermal reservoir. In addition, the function of natural convection results in the redistribution of reservoir temperature. Since the density and viscosity of CO_2 is lower than water, the CO_2 flow driven by buoyancy has the greater impact on temperature distribution in the abandoned oil layer after CO_2-flooding. Then the cover layer around the oil layer will be heated by the temperature redistribution of oil layer, which plays better role in the heating of heat-carrying medium in U-shape wellbore. Therefore, the output temperature and heat mining rate of U-shape well geothermal system with CO_2 storage are higher.

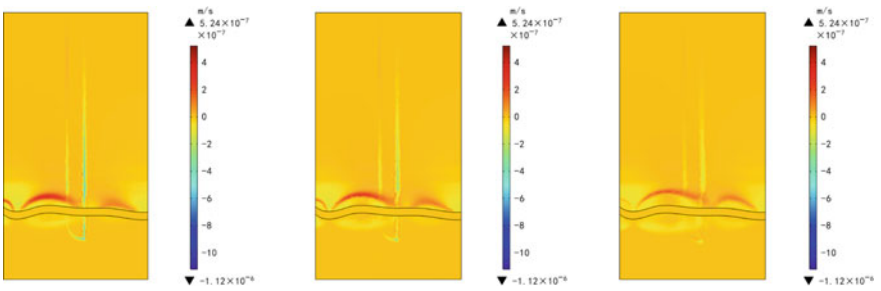

(a) 36Ms (b) 60Ms (c) 120Ms

Fig. 10.10 Flow velocity field of CO_2-flooded reservoir at different time

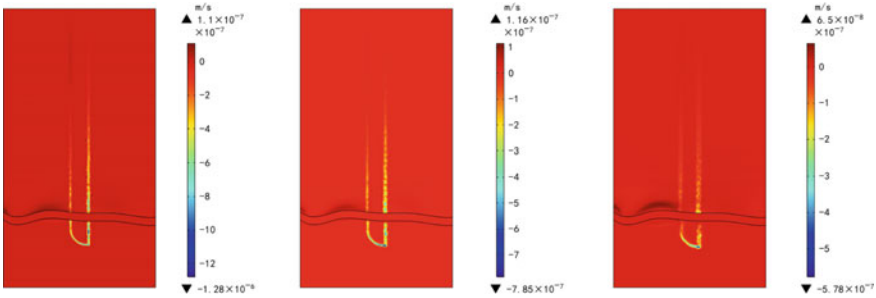

(a) 36Ms (b) 60Ms (c) 120Ms

Fig. 10.11 Flow velocity field of water-flooded reservoir at different time

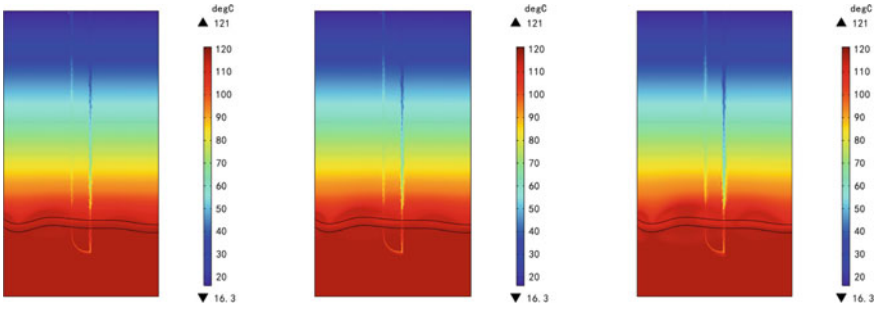

(a) 36Ms (b) 60Ms (c) 120Ms

Fig. 10.12 Temperature field of CO_2-flooded reservoir at different time

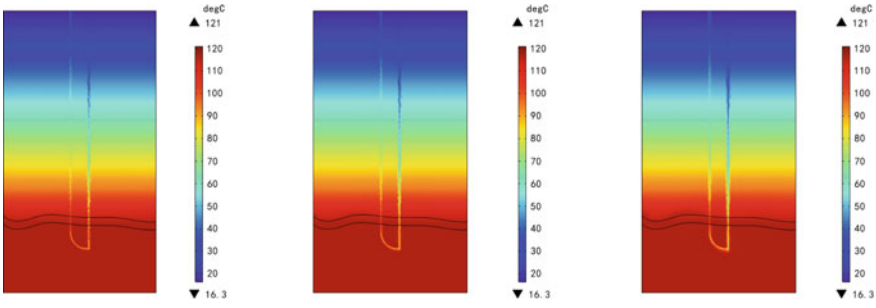

(a) 36Ms (b) 60Ms (c) 120Ms

Fig. 10.13 Temperature field of water-flooded reservoir at different time

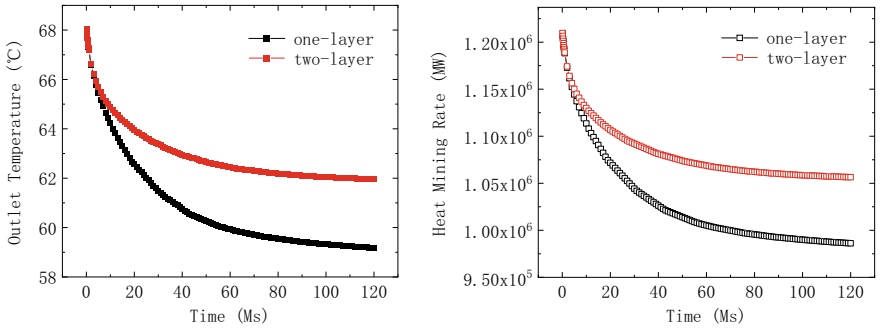

(a) outlet temperature (b) heat mining rate

Fig. 10.14 Heat mining performance comparation of the U-shape well geothermal system with different oil layer number

10.4.2 Oil Layer Number

For the abandoned oil layer that have completed the extraction of oil and gas, multiple oil layers may be transformed into geothermal development reservoirs. In this part, we investigate the influence of oil layer number on heat mining performance of U-shape well geothermal system. Before the development of geothermal system, the abandoned oil layer is flooded by the supercritical CO_2. And the parameters of oil and cover layer refers to the parameters in Case9.

As can be seen in Fig. 10.14, the outlet temperature and heat mining rate will be enhanced with the increase of oil layer number. After 5-year development the outlet temperature in geothermal system with two oil layers is 4.69% higher than that with one oil layer, and the heat mining rate is improved by 6.2%. After 10-year development, compared with the geothermal system with one oil layer, the outlet temperature of geothermal system with two oil layer increase by 5.07% and the heat mining rate increase by 9.3%. As can be seen from Figs. 10.15 and 10.16, with the increase of oil layer number, the natural convection in reservoir is strengthened, which carry the high-temperature resources at the bottom part of reservoir to the shallow part. It can be seen that the increase in the number of abandoned oil layers is beneficial for the development of closed cycle geothermal system.

10.4.3 Oil Layer Thickness

In this part, the influence of oil layer thickness on heat mining performance of U-shape well geothermal system, and the oil layer thickness is set by 50 and 100 m. Before the development of geothermal system, the abandoned oil layer is flooded by the supercritical CO_2. And the parameters of oil and cover layer refers to the parameters in Case9.

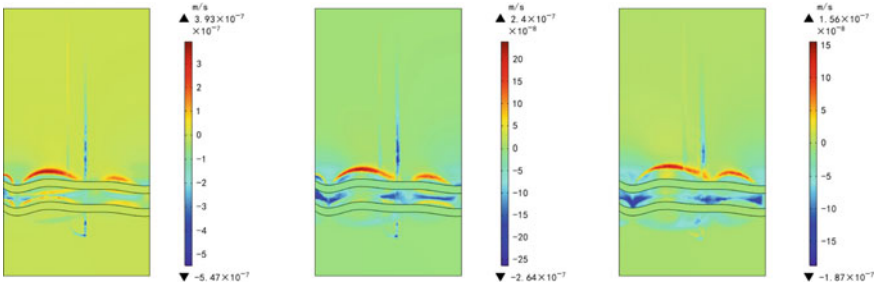

(a) 36Ms (b) 60Ms (c) 120Ms

Fig. 10.15 Flow velocity field of two oil layer at different time

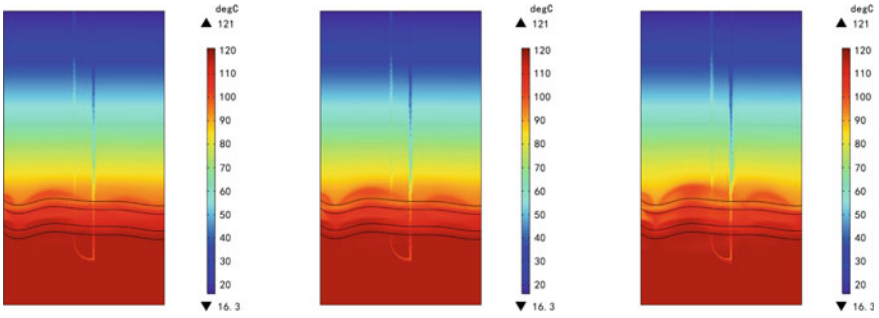

(a) 36Ms (b) 60Ms (c) 120Ms

Fig. 10.16 Temperature field of two oil layer at different time

As can be seen in Fig. 10.17, the outlet temperature and heat mining rate will be enhanced with the raise of oil layer thickness. After 5-year development the outlet temperature in geothermal system with the oil layers thickness of 100 m is 4.16% higher than that with the oil layer thickness of 50 m, and the heat mining rate is improved by 9.3%. After 10-year development, compared with the geothermal system with the oil layer thickness of 50 m, the outlet temperature of geothermal system with the oil layer thickness of 100 m increase by 4.73% and the heat mining rate increase by 12.7%. As can be seen from Figs. 10.18 and 10.19, the increase of reservoir thickness can enhance the natural convection, which can raise the heat mining performance of U-shape well geothermal development. So in the construction of the closed cycle well, it is benefit to choose the thicker abandoned oil layers.

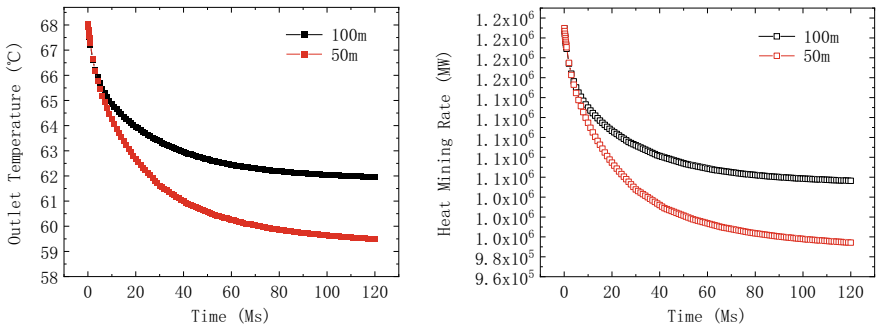

(a) outlet temperature (b) heat mining rate

Fig. 10.17 Heat mining performance comparation of the U-shape well geothermal system with different thickness of oil layer

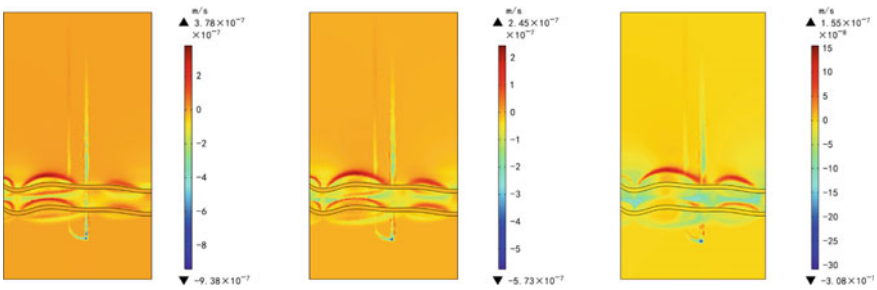

(a) 36Ms (b) 60Ms (c) 120Ms

Fig. 10.18 Flow velocity field of the oil layer with the thickness of 50 m at different time

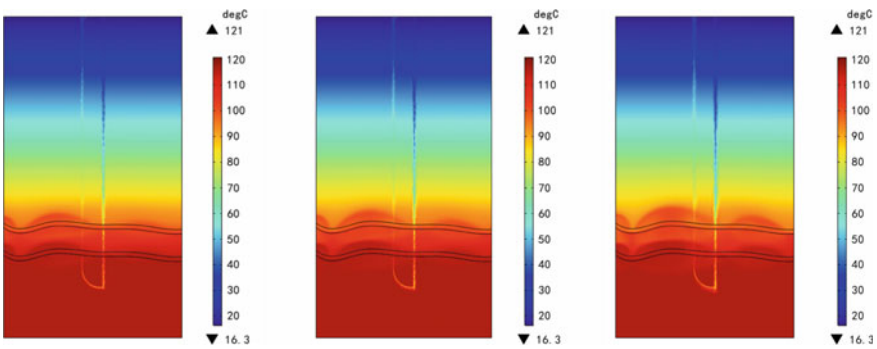

(a) 36Ms (b) 60Ms (c) 120Ms

Fig. 10.19 Temperature field of the oil layer with the thickness of 50 m at different time

10.5 Conclusions

Considering the natural convection, the coupled model of heat and mass transfer both in wellbore and thermal reservoir as well as heat transfer between the linked pipes and the thermal reservoir is established. In this study, firstly, the influence of oil and cover layer permeability characteristics on heat mining performance of U-shape well geothermal system with $ScCO_2$ storage is explored. Then, the influence of fluid type buried in oil layer, oil layer number and oil layer thickness on heat mining performance is discussed. The results show that:

(1) The heat mining performance of closed-well geothermal system can be enhanced by the increase of rock permeability around the well (include the oil and cover layer). $ScCO_2$ buried in oil layers moves upward under the action of density difference and brings heat to the upper part of the oil layer. The cover layer around the upper part of the oil layer will be heated, which can further generate the natural convection in the cover layer. In addition, the heat-carrying medium in wellbore can be heated during the exploitation of U-shape well geothermal energy. Therefore, enhancing the permeability of the abandoned oil layer and the cover layer through reservoir transformation can improve the thermal recovery efficiency of U-shape well geothermal system.
(2) The function of natural convection is enhanced in CO_2-flooded oil layer compared with that in water-flooded oil layer. The CO_2 flow driven by buoyancy lead to the stronger disturbances to reservoir temperature, which increases the temperature gradient near the oil layer. At 10-year development, the outlet temperature and the heat mining rate of the U-shape well geothermal system with $ScCO_2$ storage respectively increases by 11.23% and 17.9%.
(3) The outlet temperature and heat mining rate will be enhanced with the increase of oil layer number. After 10-year development, compared with the geothermal system with one oil layer, the outlet temperature of geothermal system with two oil layer increase by 5.07% and the heat mining rate increase by 9.3%.
(4) The outlet temperature and heat mining rate will be enhanced with the raise of oil layer thickness. After 10-year development, compared with the geothermal system with the oil layer thickness of 50 m, the outlet temperature of geothermal system with the oil layer thickness of 100 m increase by 4.73% and the heat mining rate increase by 12.7%. So in the construction of the closed cycle well, it is benefit to choose the thicker abandoned oil layers.

Acknowledgements This research was supported by the National Natural Science Foundation of China (42102338); China Postdoctoral Science Foundation (2022M712210); Natural Science Foundation of Shandong Province (ZR2020QE115); the Fundamental Research Funds for the Central Universities (27R1902010A); the Opening Fund of Key Laboratory of Unconventional Oil & Gas Development (China University of Petroleum (East China)), Ministry of Education.

References

Adelina P, Michaelides EE (2009) Geothermal power production from abandoned oil wells. Energy, 34: 866–872

Ammar H, Borji M, Ziapour BM et al (2020) Performance analysis of a cascade PCM heat exchanger and two-phase closed thermosiphon: a case study of geothermal district heating system. Sustain Energy Technol Assess 40:100755

Blöcher MG, Zimmermann G, Moeck I et al (2010) 3D numerical modeling of hydrothermal processes during the lifetime of a deep geothermal reservoir. Geofluids 10(3):406–421

Bujakowski W, Barbacki A, Miecznik M et al (2015) Modeling geothermal and operating parameters of EGS installations in the lower Triassic sedimentary formations of the central Poland area. Renew Energy 80:441–453

Cheng WL, Li TT, Nian YL et al (2013) Studies on geothermal power generation using abandoned oil wells. Energy 59:248–254

Garcia J, Hartline C, Walters M et al (2016) The Northwest Geysers EGS Demonstration project, California Part1: characterization and reservoir response to injection. Geothermics 63:97–119

Guo B, Fu PC, Hao Y et al (2016) Thermal drawdown-induced flow channeling in a single fracture in EGS. Geothermics 61:46–62

Held S, Genter A, Kohl T et al (2014) Economic evaluation of geothermal reservoir performance through modeling the complexity of the operating EGS in Soultz-sous-Forêts. Geothermics 51:270–280

Hofmann H, Weides S, Babadagli T et al (2014) Potential for enhanced geothermal systems in Alberta, Canada. Energy 69:578–591

Huang WB, Cao WJ, Jiang FM (2018) A novel single-well geothermal system for hot dry rock geothermal energy exploitation. Energy 162:630–640

Jiang F, Chen J, Huang W et al (2014) A three-dimensional transient model for EGS subsurface thermo-hydraulic process. Energy 72(7):300–310

Kujawa T, Nowak W, Stachel AA (2006) Utilization of existing deep geological wells for acquisitions of geothermal energy. Energy 31:650–664

Kumari WGP, Rangith PG, Perera MSA, Chen BK (2018) Experimental investigation of quenching effect on mechanical, microstructural and flow characteristics of reservoir rocks: thermal stimulation method for geothermal energy extraction. J Petrol Sci Eng 162:419–433

Li X, Wang JH, Elsworth D (2017) Stress redistribution and fracture propagation during restimulation of gas shale reservoirs. J Petrol Sci Eng 154:150–160

Li PF (2020) Research on heat transfer law of horizontal section of U-shaped geothermal well in Caotan District of Xi'an [D]. Xi'an. Xi'an University of Science Technology (in Chinese)

Liao YQ, Sun XH, Sun BJ et al (2021) Geothermal exploitation and electricity generation from multibranch U-shaped well enhanced geothermal system. Renew Energy 163:2178–2189

Noorollahi Y, Pourarshad M, Jalilinasrabady S et al (2015) Numerical simulation of power production from abandoned oil wells in Ahwaz oil field in southern Iran. Geothermics 55:16–23

Omid K, Mohsen P, Edris Y et al (2021) Evaluating and optimizing the geometry of thermal foundation pipes for the utilization of the geothermal energy: numerical simulation. J Energy Storage 37:102464

Pandey SN, Chaudhuri A, Kelkar S (2017) A coupled thermo-hydro-mechanical modeling of fracture aperture alteration and reservoir deformation during heat extraction from a geothermal reservoir. Geothermics 65:17–31

Qu ZQ, Zhang W, Guo TK (2017) Influence of different fracture morphology on heat mining performance of enhanced geothermal systems based on COMSOL. Int J Hydrogen Energy 42:18263–18278

Shabnam G, Emad M, Seyed JHAB et al (2018) Feasibility study of geothermal heat extraction from abandoned oil wells using a U-tube heat exchanger. Energy 153:554–567

Sun XH, Wang ZY, Liao YQ et al (2019) Geothermal energy production utilizing a U-shaped well in combination with supercritical CO_2 circulation. Appl Therm Eng 151:523–535

Xin SL, Liang HB, Hu B et al (2012) A 400 kW geothermal power generator using co-produced fluids from Huabei oilfield. Geothermal Resour Council Trans 36:219–223

Zeng YC, Wu NY, Su Z et al (2013) Numerical simulation of heat production potential from hot dry rock by water circulating through a novel single vertical fracture at Desert Peak geothermal field. Energy 63:268–282

Zhang YJ, Guo LL, Li ZW et al (2015) Electricity generation and heating potential from enhanced geothermal system in Songliao Basin, China: Different reservoir stimulation strategies for tight rock and naturally fractured formations. Energy 93:1860–1885

Zhang W, Wang ZL, Guo TK et al (2022) The enhanced geothermal system heat mining prediction based on fracture propagation simulation of thermo-hydro-mechanical-damage coupling: Insight from the integrated research of heat mining and supercritical CO_2 fracturing. Appl Therm Eng 215:118919

Zhao YS, Feng ZJ, Zhao Y et al (2017) Experimental investigation on thermal cracking, permeability under HTHP and application for geothermal mining of HDR. Energy 32:305–314

Chapter 11
From Ozone Layer Protection to Mitigation of Climate Change: Perspective of Subtropical Regional Actions as "Pure Consumer"

Kaixian Zhu, Hexiao Chen, Rong Dai, Shengping Cao, Fang Ou, and Min Ding

Abstract Ozone Depleting Substances (ODS) are chemicals harmful to the intact state of Ozone Layer and thus to be gradually eliminated and finally phased out as per schedules of Montreal Protocol. Nowadays, China had fulfilled its obligations to eliminate a variety groups of ODS substances according to schemes of the Protocol and had only to focus on phasing out the last remaining group of ODS- Hydrochlorofluorocarbons (HCFCs) by 2030. Meanwhile, the most widely used alternatives for ODS called Hydrofluorocarbons (HFCs) had arose new concerns for their high greenhouse effects, new obligations for reducing HFCs was stated by the Kigali Amendment of Montreal Protocol, for A5 countries including China, the utilization of HFCs would not be freeze until the year 2024. In this study, a survey was carried out on the baseline situations of the year 2014 for domestic consumptions and reclamation capabilities of ODS/HFCs in Guangxi province, China. It was found that eliminated HCFCs consumptions was likely shift to HFCs due to technical convenient and economic interests, since gaseous forms of HCFCs and HFCs are both severe Green House Gas (GHG), banks of GHG may be formed as used HCFCs abandoned and HFCs consumption increased from 2014 to 2023. The purpose of this study is to figure out the policy perspective of regional administration of ODS/alternatives consumptions to minimize potential GHG accumulations by comprehensively consider aspects of consumption, refrigerating service, technical inertia, market interest et al.

Keywords Ozone depleting substance · Green House Gas · Kigali Amendment

K. Zhu · H. Chen (✉) · S. Cao · F. Ou · M. Ding
Scientific Research Academy of Guangxi Environmental Protection, Nanning 530000, China
e-mail: 77609099@qq.com

R. Dai
Nanjing Institute of Environmental Sciences, Nanjing 210042, China

Z. Sun and P. K. Das (eds.), *Proceedings of the 10th International Conference on Energy Engineering and Environmental Engineering*, Environmental Science and Engineering, https://doi.org/10.1007/978-3-031-48204-5_11

11.1 Introduction

Ozone in the earth mainly distributed in the stratosphere region and thus forms Ozone Layer which absorbed large part of ultraviolet radiation of the sunlight to the earth, intact state of the ozone layer is maintaining in a balance between decomposition and forming of ozone molecules (Anwar et al. 2016). In 1970s, some researches began to concern about ozone depleting effects of chemicals such as chlorofluorocarbons (CFC) (Molina and Rowland 1974) which was later confirmed as one of the most common Ozone Depleting Substance (ODS), most types of ODS were developed and manufactured for a variety of economic utilizations (Wachowski et al. 2001). Since 1980s, as the discovery of huge ozone disappearance over Antarctic (Farman et al. 1985) and other reports of ozone layer damage (Zurer 1988) induced panics to international communities, "Vienna Convention" was firstly established in 1985 to protect ozone layer (Morrisette 1989), then 24 countries reached an agreement as "Montreal Protocol" in 1987 to clarify the obligations of ratified countries to eliminate consumption/supplying of ODS substances (Nanda 1989), in a serious Conference of Parties (COP) held afterwards, amendments of Montreal Protocol were made for incorporating additional controlled ODS substances including Hydrochlorofluorocarbons (HCFCs) (Andersen et al. 2018). The international implementation of Montreal protocol had been proven to be successful in significantly reducing the production and consumption of ODS (Canan et al. 2015). However, some studies still concerned about existing large ODS banks (Hurst 2004) and their sizes may even be underestimated (Lickley et al. 2020). Up to the date, the international endeavor is focused to eliminate the last remaining ODS group-HCFCs and their alternatives-Hydrofluorocarbons (HFCs), HFCs are not ODS but possess significant greenhouse effects (Papanastasiou et al. 2018), as interim alternatives of ODS, HFCs are to be eliminated as per Kigali Amendment of Montreal Protocol (Polonara et al. 2017), some HFCs are quite commercial available (Tsvetkov et al. 2020), however, increased consumptions of HFCs have aroused new concerns of high global warming effects (Velders et al. 2012). The most common utilizations of HCFCs and HFCs are refrigerants nowadays, in recent years, new type of alternatives such as hydrocarbons (Powade et al. 2018; Zhang et al. 2017) and hydro-olefins (Mishra and Sarkar 2016) are being introduced as their alternatives.

The severity of substance cause ozone depletion and greenhouse effects are measured by its Ozone Depleting Potential (ODP) values and Global Warming Potential (GWP) values respectively. the ODP of a particular substance is expressed as the number of equivalent mass of chlorofluorocarbon-11 (CFC-11) which has the ability to destroy the same amount of ozone as 1 unit mass of that substance, similarly, Global Warming Potential (GWP) values for a substance is defined as the number of equal mass of CO_2 to 1 unit of this substance for equivalent greenhouse effects on global warming (NASA Principal Center for Clean Air Act Regulations 2006). To calculate a value A of total ODP or GWP consumptions, equations described below are used:

$$A = \sum_{i=ODS}^{n} (P_{ODS} \times ODP) \tag{11.1}$$

$$A = \sum_{i=GHG}^{n} (P_{GHG} \times GWP) \tag{11.2}$$

where P is the mass of production (consumption) of ODS (or GHG), ODP/GWP is the corresponding ODP/GWP values of individual compounds. Reference ODP/GWP values of investigated substances were listed in Table 11.1.

China had formally accepted Kigali Amendment in 2021. According to Montreal Protocol, for developing countries (article 5 parties including China), HCFC should be deducted since 2015 until totally phased out by 1/Jan/2030 and HFCs consumptions would enter into freeze phase during 2024 to 2028 and then to be reduced (Ozone Secretariat, United Nations Environment Programme 2018), to investigate the overall ODS/Alternatives consumptions of the year 2014 to provide consolidate baseline information for further ODS eliminations, Guangxi (see Fig. 11.1) was selected as an typical moderately industrialized province for survey. Guangxi is located in sub-tropical region which naturally leads to significant demand of ODS/alternatives substance in refrigeration. The purpose of this research was to comprehensively analyzed the consumption structures of ODS/alternatives in Guangxi to find out how to optimized regional environmental strategies to minimize relevant ecological impacts caused by their eliminating process.

11.2 Methods and Investigation

The investigation was carried out in 2014 by methodologies including documentary review, sending questionnaires, telephone interviewing, site-visiting et al. The situations of household appliances consumptions/refrigerant reclamation in 14 prefecture cities of Guangxi (see Fig. 11.1), and HCFCs/Alternatives substances utilization for commercial civil utilizations in the capital city-Nanning were surveyed.

Questionnaire forms of verified information of fridges/air-conditioners sales were collected from wholesale/retailers to evaluate the compositions of refrigerants in sold appliances. The information of preference of local consumers in selecting eco-friendly products were synchronizing collected from appliance retailers; Questionnaire forms were also delivered to identified registered entities which are engaged in reclamation of used ODSs and HFCs, entities covered included automobile maintenance providers and other entities involving in refrigeration maintenances, verified data were then collected to evaluate the status of ODS/HFCs reclamation capabilities that had been established in 2014. Commercial civil utilizations of ODS/Alternatives in Nanning city which directly used in refrigeration maintenance of commercial/public service like house-hold appliances repairing and other civil applications such as central air-conditioning, large refrigerating facilities, machinery and

Table 11.1 The information of typical HCFC/HFC substance in this study

HCFC/HFC	Chemicals	ODP	GWP	Principal applications
HCFC-22	$CHClF_2$	0.055 (Ozone Secretariat, United Nations Environment Programme 2018)	1810 (Ozone Secretariat, United Nations Environment Programme 2018)	Air-conditioning; cold store
HCFC-123	$C_2HF_3Cl_2$	0.02 (Ozone Secretariat, United Nations Environment Programme 2018)	77 (Ozone Secretariat, United Nations Environment Programme 2018)	Air-conditioning
HCFC-124	C_2HF_4Cl	0.022 (Ozone Secretariat, United Nations Environment Programme 2018)	609 (Ozone Secretariat, United Nations Environment Programme 2018)	Civil centrifugal chiller
HFC-134a	CH_2FCF_3	0	1430 (Ozone Secretariat, United Nations Environment Programme 2018)	Air-conditioning; automobile/ machinery
HFC-32	CH_2F_2	0	675 (Ozone Secretariat, United Nations Environment Programme 2018)	A component of blends
HFC-143a	CH_3CF_3	0	4470 (Ozone Secretariat, United Nations Environment Programme 2018)	A component of blends
HFC-125	CHF_2CF_3	0	3500 (Ozone Secretariat, United Nations Environment Programme 2018)	A component of blends
R407c	HFC-32/ 125/134a (23/25/52m/ m/m)	0	1773.85[a]	Air-conditioning
R404a	HFC-125/ 143a/134a (44/52/4m/ m/m)	0	3921.6[a]	Air-conditioning; cold store; machinery
R410a	HFC-32/ 125 (50/ 50m/m)	0	2087.5[a]	Air-conditioning; machinery

[a]GWP of blends were calculated according to the mass percentages of individual HFCs

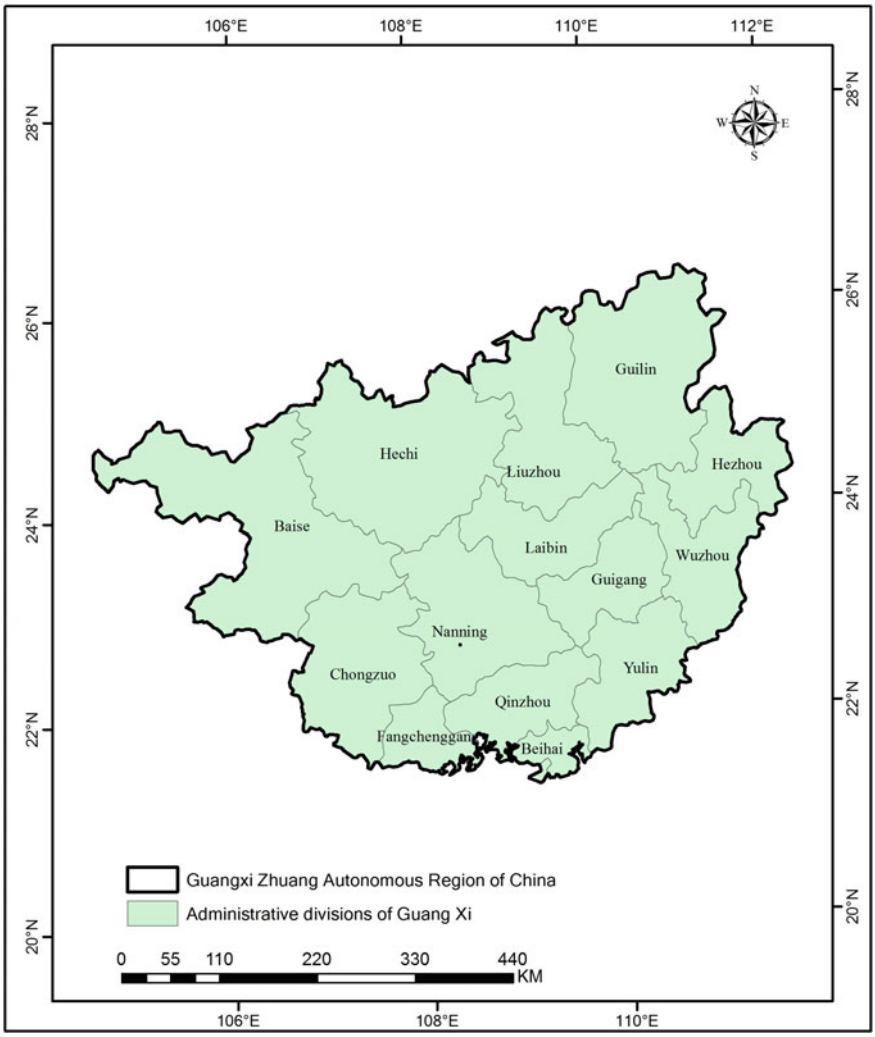

Fig. 11.1 The coordination of Guangxi with 14 prefecture cities

automobile maintenances were surveyed, the survey covered a total of 106 entities of public service (government organs, library, hospitals, schools etc.) and commercial (shopping centers, hotels, banks etc.) in the city.

11.3 Results and Discussion

11.3.1 The Consumptions of Appliances with Relevant Refrigerants in Guangxi

The survey of markets covered most brands and typical specifications of house-hold appliance consumptions in Guangxi. The variations of refrigerants in appliances were summarized in Table 11.2. Since ODS refrigerant had been totally abandoned in the fridges consumptions in 2008 (Lu et al. 2011), it was found that HFC-134a had also been further replaced and dropped from 15% to less than 0.5%. Fridges had thus provided a successful example of traditional refrigerants transforming to hydrocarbon alternatives (R600a). In contrast, majority of refrigerant filled in air conditioners were shifted from HCFC-22 to R410a (increased from 10% to 61.7%).

Holding numbers of air conditioners of urban/rural households were estimated by yearly statistical figures of Guangxi (Guangxi Statistic Bureau 2015) (see Fig. 11.2), the results indicated that air-conditioners in urban/rural areas of Guangxi had been both increased steadily from 2014 to 2021, the estimated holding numbers increased from 4216 thousand to 13,008 thousand units in urban areas and from 1721 to 7266 thousand units in rural areas. considering the rapid growth of air conditioners in Guangxi, the accumulation of GHG banks would be inevitable if their refrigerant types are simply transformed from HCFCs to HFCs, the solution would be relied on technical improvement as more eco-friendly refrigerants (such as R290) acquired in up-streaming productions of air-conditioners (Zhang et al. 2017).

Table 11.2 Variations of refrigerants utilized in household appliances in Guangxi

Appliance	Refrigerant (category)	Mass ratio 2014 (surveyed) (%)	Mass ratio 2008–2009 (Lu et al. 2011) (%)
Fridges	R600a	99.6[a]	85
	HFC-134a	0.4[a]	15
Total	–	100	100
Air conditioners	HCFC-22	38.3[a]	88
	R410a	61.7[a]	10
	HFC-134a	–	2
Total	–	100	100

[a]Estimated figures based on questionnaire data from wholesalers/retailers of the survey

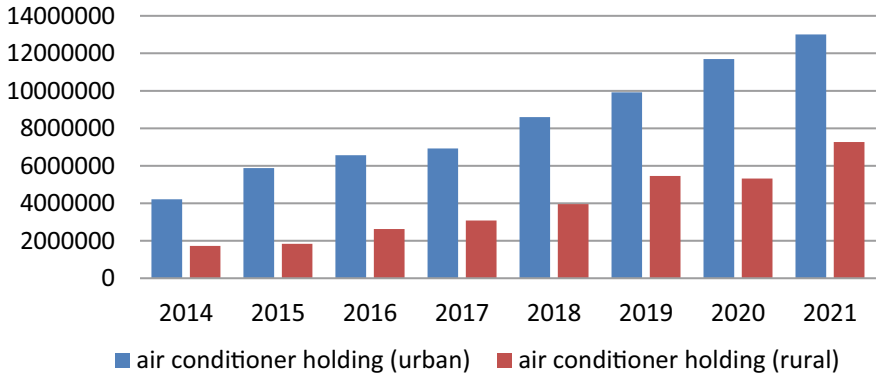

Fig. 11.2 Estimated holding numbers of air conditioners in urban/rural areas of Guangxi by years

11.3.2 Commercial Utilization of ODS/Alternatives in the Capital City-Nanning

Entities involved in utilization of ODS and relative alternatives which included whole-sale distributors, large service facilities (food storage, supermarket/shopping centers, hotel/library, hospital/commercial buildings et al.) and also businesses of refrigerator maintenance (household air-conditioner/freezer repairing and automobile airconditioner/machinary maintaining) in Nanning city were surveyed for their consumptions in 2014. It was found that ODS substance HCFC-22 dominate the usage (28.018 tons) followed by HFC-134a (4.442 tons), while only very small amount of hydrocarbon-R600a (0.032 tons) used in this sector, the CFC-11e Tons and CO_2 e Tons produced by the consumptions of corresponding materials were calculated by Eqs. (11.1) and (11.2) and summarized in Table 11.3. The survey had showed that users/entities of local communities prefer to use HFCs to replace HCFCs particularly in air-conditioning, machinery and automobiles, the amount of HFCs were relatively smaller compared to HCFCs, but the overall GWP imposed by HFCs were higher for equivalent mass. The result of this HFCs preference is particularly obvious in central air-conditioner and large refrigerating system installations while reluctances to adopting alternative refrigerant (e.g. NH_3, LiBr) or advanced technologies (e.g. air-cooled chiller) attributed to technical difficulties or financial barriers. However, more installed refrigerative devices adopting HFC as refrigerant would become problematic as the supplying level of HFC would soon be freezed as per nation-wide implementation framework fulfil the obligation stated by Kigali amendment in 2024.

Table 11.3 Surveyed ODS/alternatives of commercial civil utilizations in Nanning/2014

Substance	Mass	ODP	GWP	Total mass	Total GWP	GWP/mass
	Tons	CFC-11e tons	CO_2 e tons	Tons	CO_2 e tons	
HCFC-22	28.018	1.541	50,712.58	30.142	51,153.832	1697.095
HCFC-123	1.602	0.032	123.354			
HCFC-124	0.522	0.0115	317.898			
HFC-134a	4.442	–	6352.06	8.239	18,907.471	2294.874
R410a	1.259	–	2628.163			
R404a	2.526	–	9905.962			
R407c	0.012	–	21.286			
R600a	0.032	–	Neglect[a]	0.032	–	–

[a]R600a is of very low GWP, it is not a controlled GHG thus its CO_2 e Ton was neglect

11.3.3 Reclamations of Used ODS/Alternatives in Guangxi

Through the registered commercial entities lists, surveys were conducted over entities involved in reclaiming ODS/alternatives accross Guangxi in 2014, many of such entities were found scattered and of relatively small scale, thus only those reclaimed over 10 kg per year were counted for reflecting established scale ODS/alternatives reclamation industrial chain in Guangxi. For automobile service entities, the only reclaimed refrigerant identified was HFC-134a which is aligned with the previous study (Lu et al. 2011). For civil commercial entities, the recovering materials identified included HFC-134a, HCFC-22, HFC-32, R410a from household air-conditioners and other refrigerative systems (Central Air-conditioning, Cold Store etc.), the entities in account were found located in Guigang city (7 entities, 3 ones reclaimed 150 kg +), Hechi city (1 entity), Laibin city (5 entities including 2 hotels, one reclaimed 150 kg +) and Beihai city (3 entities reclaimed 150 kg + , one reclaimed 2720 kg of HCFC-22 and 565 kg of R410a; another one reclaimed 2000 kg of HCFC-22). It was obvious that some regional commercial reclamation industrial chains had been established in some cities, however, the overall reclamation volumes were still insignificant comparing to consumptions. As the recycled HCFCs/HFCs were mostly suitable to be adopted as refrigerants for local consumptions, supplying back to the market is of course the best solution for reducing the building GHG banks, however, some obstacles for their re-entering into consumptions was that local consumers refluctant to accept them with concerns on their quality, suppressed prices then subsequently make entities having less motivative to enlarge reclaim capabilities and reclaiming entities were usually identified clustered in low-income cities. The feasible strategy is to povide more economic incentives (e.g. tax allowance) to help reclamation entities make recycled refrigerants more competitive in prices and quality, thus increased their acceptance.

11.3.4 The Regional Perspective in Scenario of Implementing Kigali Amendment

There is no identified manufacturing of ODS in Guangxi, therefore, eliminating ODS consumption should not confronting common resistance previously reported from relevant manufacture industries (Andrew 1998), However, its sustaining requires public awareness and participations of relevant stakeholders with proper financial supports (Al-Awad et al. 2018). Base on the existing success of Montreal Protocol, the entering into force of Kigali Amendment is a milestone that the action of phasing out ODS and HFC had already become part of global efforts to mitigate GHG emissions and climate change. Under the scheme of Kigali Amendment, China is belonging to A5-Group 1 countries for those the freeze phase of HFC consumption (supplying) would begin in 2024 and then the overall supplying would be gradually deducted since 2029 (Ozone Secretariat, United Nations Environment Programme 2018). Base on the facts identified by this investigation conducted in Guangxi, the roadmap of completely eliminating ODS/high GWP alternatives was outlined (see Fig. 11.3), on its left side, among the controlled substances, HFCs could be considered as an interim solution of replacing HCFCs (Canan et al. 2015). Technically, it is inaccurate to project deducted HCFCs would be replaced by equal mass of HFCs (Powade et al. 2018), but anyway, the scenario provides a intuitionistic estimation of an escalation of GHG banks (of HCFC + HFC) particularly before the compulsory freeze of HFCs in 2024 (cargos of HCFC and HFC are liquid forms, but their boiling points are very low, they would simultaneously become GHGs by leakages at room temperature). It is hypothesized that significant banks (Lickley et al. 2020; Velders et al. 2012) of HCFCs (mostly HCFC-22) and HFCs (mostly R-410a and HFC-134 a) would be formed as there are more and more used refrigerants and scraped air conditioners in the near future. To meet relevant environmental regulations, previous study had suggested efficient procedures to collect used ODS to be delivered to registered agencies for appropriate recycling (reused) or destroying treatments, the process of recycling indeed reduced the overall ODS consumption (Al-Awad et al. 2018). New types of refrigerants like HFOs (Hydrofluoro-olefin) of Low GWP may be suitable alternatives to HFC for their similar physical characteristics (Mishra and Sarkar 2016) but still halted by high costs and limit commercial availability (Gupta et al. 2018) and possible toxicity (Tsvetkov et al. 2020). At this stage, Hydrocarbons (HCs) are suggested to replace common HCFC (Powade et al. 2018) and HFC refrigerants (Mishra and Sarkar 2016), besides their eco-friendly and suitable refrigerate properties (Zhao et al. 2003), another advantage of HCs is that they are easy to be destroyed by simple incineration. On contrary, the destroying procedures of halogenated refrigerants usually involved in high-cost incineration facilities (U.S. EPA 2018) to meet environmental criteria.

Within the roadmap, the process of recycling/reusing plays a role of "dual mandate", firstly, it reducing the banks of abandoned HCFC/HFC and adding

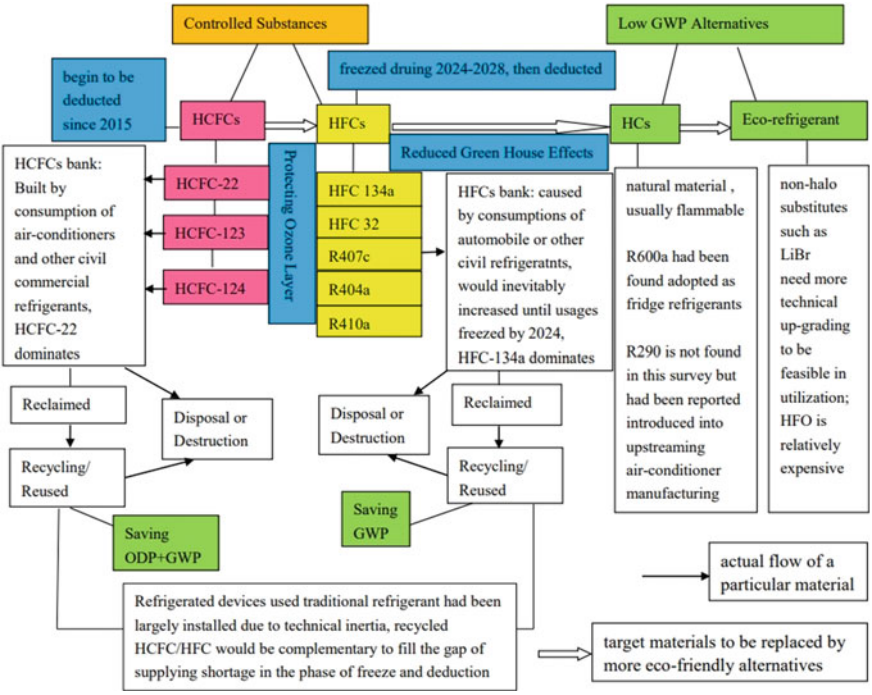

Fig. 11.3 Regional roadmap of transforming HCFCs/HFCs into low-GWP alternatives

economic values to civil utilizations, meanwhile, as mentioned previously, the technical inertia had make refrigerating facilities adopting traditional refrigerant (particularly HFCs) still being installed for civil commercial utilizations, recycled refrigerants should be a good complements to fill the possible gaps of shortages when traditional refrigerant supplying is freeze or even deducted according to the phase out schedules of Kigali/Montreal, this "dual mandate" is thus to achieve a closed circle of environmental protection (reduced GHG banks) and social benefits (economic output).

11.4 Conclusion

The investigation in Guangxi had revealed that ODS had been successfully replaced by eco-friendly alternatives in some products supplying (e.g. fridges), however, in aspects of some civil consumptions like air-conditioning, there is motivations to adopt HFCs replacing HCFCs due to technical convenient and less expense, market interest is obvious based on the cost and present legal policy but ignoring the future changes as the coming of nation-wide implementation of Kigali Amendment in 2024. Considering time-lags of existing HCFCs/HFCs utilizations preference, large

abandoned HCFCs/HFCs banks could be formed which are sources of possible GHG emissions. Meanwhile, large amount of refrigerating facilities adopting HCFC/HFC may face shortage of fresh refrigerant supplying in the future as the overall HFC production would be freeze or even deducted. The ideal environmental strategy is to encourage recycled HCFCs/HFCs to re-enter into local markets. The process of recycling/reused plays a role of "dual mandate" of both environmental and economic interests.

References

Al-Awad TK, Saidan MN, Gareau BJ (2018) Halon management and ozone-depleting substances control in Jordan. Int Environ Agreem Polit Law Econ 18:391–408

Andersen SO, Sherman NJ, Carvalho S, Gonzalez M (2018) The global search and commercialization of alternatives and substitutes for ozone-depleting substances. CR Geosci 350(7):410–424

Andrew J (1998) The ozone endgame: the implementation of the Montreal Protocol in the United Kingdom. Environ Polit 7:23–52

Anwar F, Chaudhry FN, Nazeer S, Zaman N, Azam S (2016) Causes of ozone layer depletion and its effects on human: review. Atmos Clim Sci 06(01):129–134

Canan P, Andersen SO, Reichman N, Gareau B (2015) Introduction to the special issue on ozone layer protection and climate change: the extraordinary experience of building the Montreal Protocol, lessons learned, and hopes for future climate change efforts. J Environ Stud Sci 5(2):111–121

Farman JC, Gardiner BG, Shanklin JD (1985) Large losses of total ozone in Antarctic reveal seasonal ClO_x/NO_x interaction. Nature 315:207–210

Guangxi Statistic Bureau (2015–2022) Guangxi Statistic Yearbook. http://tjj.gxzf.gov.cn/tjsj/tjnj/

Gupta S, Karanam NK, Konijeti R, Dasore A (2018) Thermodynamic analysis and effects of replacing HFC by fourth-generation refrigerants in VCR systems. Int J Air Cond Refrig 26(02):1850013

Hurst DF (2004) Emissions of ozone-depleting substances in Russia during 2001. J Geophys Res 109:D14303

Lickley M, Solomon S, Fletcher S, Velders GJM, Daniel J, Rigby M, Montzka SA, Kuijpers LJM, Stone K (2020) Quantifying contributions of chlorofluorocarbon banks to emissions and impacts on the ozone layer and climate. Nat Commun 11:1380

Lu W, Xiong J, Tang Y, Guo J, Li Z (2011) Analysis on the status Quo of refrigerants use in Guangxi. Refrig Air Cond 25:198–203 (in Chinese)

Mishra S, Sarkar J (2016) Performance characteristics of low global warming potential R134a alternative refrigerants in ejector-expansion refrigeration system. Arch Thermodyn 37(4):55–72

Molina MJ, Rowland FS (1974) Stratospheric sink for chlorofluoromethanes: chlorine atom-catalysed destruction of ozone. Nature 249(5460):810–812

Morrisette PM (1989) The evolution of policy responses to stratospheric ozone depletion. Nat Resour J 29(3):793–820

Nanda VP (1989) Stratospheric ozone depletion: a challenge for international environmental law and policy. Michigan J Int Law 10(2):482

NASA Principal Center for Clean Air Act Regulations (2006) Halocarbons: ozone depletion and global warming overview. https://www.nasa.gov/pdf/355567main_HalocarbonOverview_October 2006.pdf. Accessed 28 Feb 2021

Ozone Secretariat, United Nations Environment Programme (2018) Handbook for the Montreal Protocol on substances that deplete the ozone layer, 12th edn. Ozone Secretariat, UNEP, Nairobi

Papanastasiou DK, Beltrone A, Marshall P, Burkholder JB (2018) Global warming potential estimates for the C1–C3 hydrochlorofluorocarbons (HCFCs) included in the Kigali Amendment to the Montreal Protocol. Atmos Chem Phys 18:6317–6330

Polonara F, Kuijpers L, Peixoto R (2017) Potential impacts of the Montreal Protocol Kigali Amendment to the choice of refrigerant alternatives. Int J Heat Technol 35(Special Issue1):S1–S8

Powade RS, Rane AA, Rane AD, Sutar OS, Bagade VS (2018) Performance investigation of refrigerants R290 and R134a as an alternative to R22. Int J Res Appl Sci Eng Technol 6(4):4668–4676

Tsvetkov OB, Laptev YA, Sharkov AV, Mitropov VV, Fedorov AV (2020) Alternative refrigerants with low global warming potential for refrigeration and air-conditioning industries. In: Conference 2020 (ed) IOP conference series (Mater Sci Eng 905(1):12070)

U.S. EPA (2018) ODS destruction in the United States and Abroad. https://www.epa.gov/sites/default/files/2018-03/documents/ods-destruction-in-the-us-and-abroad_feb2018.pdf. Accessed 6 Dec 2021

Velders GJM, Ravishankara AR, Miller MK, Molina MJ, Alcamo J, Daniel JS, Fahey DW, Montzka SA, Reimann S (2012) Preserving Montreal Protocol climate benefits by limiting HFCs. Science 335(6071):922–923

Wachowski L, Kirszensztejn P, Foltynowicz Z (2001) Ecological replacements of ozone-depleting substances. Pol J Environ Stud 10:415–435

Zhang Z, Chen J, Gao Y, Liu H, Bai J (2017) Analysis on the influence of Kigali Amendment to Montreal Protocol to refrigeration and air-conditioning industry. Refrig Air Cond 17:1–7 (in Chinese)

Zhao Y, Liu B, Zhao H (2003) Experimental study of the inert effect of R134a and R227ea on explosion limits of the flammable refrigerants. Exp Thermal Fluid Sci 28:557–563

Zurer PS (1988) Studies on ozone destruction expand beyond Antarctic. Chem Eng News 66:16–25

Chapter 12
Optimized Energy-Performance of Building Integrated Photovoltaic Systems in Hot and Arid Regions of South Africa

Favour David Agbajor, Modupe Cecilia Mewomo, and Iseoluwa Joanna Mogaji

Abstract Building integrated photovoltaic (BIPV) technologies are practical solutions to counteract the dire menace of global warming on humans and built environment while providing pragmatic principles that enables practitioners and policymakers in designing new and existing buildings. This study seeks to investigate how the energy-performance of this technology in buildings is beneficial to South Africa's hot and arid climate zones due to abundant solar energy. Thus, a hypothetical modelled residential building, designed for Nelspruit and Upington was selected as a case study for parametric simulation. By considering tilt angles (20°, 26° and 30°), installation capacity, and azimuth angles (oriented in east–west direction and northwards), the analysis determined these systems' operating energy performance. The findings indicate that generated energy and power output by the BIPV modules were higher in Upington than Nelspruit. Meanwhile, findings revealed that the lowest energy outputs were recorded at greater inclination angles. The BIPV modules produced the highest amount of energy for residential buildings in both locations, but, at lower tilt angles. Moreover, BIPV systems facing the east–west split outperformed north-ward orientations at very significant rates of about 48% and delivered greater energy outputs. The study concluded that optimized BIPV systems can generate clean energy for buildings' energy efficiency, aid in energy conservation, combat climate change, and help the nation uphold its international

F. D. Agbajor · M. C. Mewomo (✉) · I. J. Mogaji
Department of Construction Management and Quantity Surveying, Durban University of Technology, Durban 4001, South Africa
e-mail: modupem@dut.ac.za

F. D. Agbajor
e-mail: 22175971@dut4life.ac.za

I. J. Mogaji
e-mail: 22176047@dut4life.ac.za

Z. Sun and P. K. Das (eds.), *Proceedings of the 10th International Conference on Energy Engineering and Environmental Engineering*, Environmental Science and Engineering, https://doi.org/10.1007/978-3-031-48204-5_12

climate commitments. The study recommended that large-scale BIPV demonstration projects be built and improved in South Africa's hot and dry regions to show the public and industry stakeholders the benefits and efficacy of these systems.

Keywords Climate change · Building energy efficiency · Solar radiation · BIPV

12.1 Introduction

12.1.1 Motivation and Background

The twenty-first century greatest ecological hazard is realized in natural resources' depletion and climate change acceleration, emanating from the unsustainable use of resources and energy alongside the hiking necessity for raw materials (Jin et al. 2022). Typically, the dire consequence on nature is evident in declining natural vegetation, urban heat island, aquatic habitat extinction and whatnot. In specifics, the built-environment is criticized to be an energy-intensive, resource-consuming, and carbon-emitting sector in its entire lifecycle as it accounts for 25 and 18% of global deforestation, and surface water drawdowns respectively (Marotta et al. 2023; Zuo and Zhao 2014). Similarly, about 40% of global energy use and 40% of carbon emissions are attributed to the built environment while future forecasts indicate that these values may rise much further (Agbajor and Mewomo 2022).

Optimizing energy efficiency is imperative for all concerned stakeholders in the energy, industry and building sectors globally to attain the lofty goal of carbon neutrality by 2060 (Alabi et al. 2023). Thus, buildings that are energy-efficient and climate-resilient are essential on a worldwide scale, particularly in the world's rapidly growing nations like South Africa. Conversely, 40% of South Africa's primary energy use is utilized by the building industry, which strains the country's coal-dependent energy supply grid and often causes power outages (Agbajor et al. 2023). Meanwhile, the concept of building integrated photovoltaic (BIPV) systems, being a recognized revolutionary theory and practice in the construction industry (Martín-Chivelet et al. 2022), is suggested as a solution to the country's ecological challenges. Specifically, locations like Upington with severe temperatures at 41.7 °C (being the fourth-hottest year ever recorded in South Africa) (SAWS 2022), as well as hot interior zones like Nelspruit can utilize this technology to tackle climate change and resource scarcity issues in their domain. However, there is a dearth of research on this subject in the aforesaid locations. Considering its importance, this study seeks to examine the energy performance of BIPVs towards the advancement of ecofriendly energy options for buildings in South Africa's hot and arid regions.

12.1.2 Related Works

BIPVs are systems comprising photovoltaic components that transform incident solar irradiation to produce electrical power with enhanced energy efficiency in buildings (Martín-Chivelet et al. 2022; Yu et al. 2021). Without hesitation, numerous studies on BIPV technology have been carried out. Samarasinghalage et al. (2022) pointed out that PVs are an attractive advancement in solar technology that improves the dual roles of energy conversion efficiency and economically utilizing spaces in building fabrics and rooftops. Happle et al. (2019) opined that BIPV has advanced quickly and has the potential to lessen building operational carbon emissions by up to 50% in regions like Southeast Asia. Similarly, recent study by Taşer et al. (2023) indicated that adopting BIPV technology helps to provide better daylight, thermal comfort and energy-saving potentials of buildings while constituting a sustainable future for cites. However, Martín-Chivelet et al. (2022) revealed that designing BIPV systems requires the consideration of a sizable number of PVs and envelope-related features as well as competing performance standards. Also, it is very crucial to consider the geographical location and climate alongside major design parameters such as tilt angle, orientation angle, installation capacity, BIPV type, and such like. Consequently, these factors significantly influence the energy efficiency of BIPV systems because they could control the amount and intensity of incident solar energy that is available, alongside the ambient temperature and weather, which affect the efficiency of the BIPV modules (Martín-Chivelet et al. 2022; Roux 2016; Li et al. 2023).

12.2 Method and Materials

12.2.1 Building Geometry and Selected Study Locations' Conditions

This study considered a typical five-storey, 25 m × 20 m open-plan residential building. The building is designed to face the four principal geographical compass points (i.e., North, East, South and West). Each storey is presumed designed to have horizontal windows, with a window area occupying around 25% of the entire floor area. Meanwhile, horizontal, or vertical screens were typically employed as shading devices across windows.

Two South African cities, Nelspruit and Upington, were considered in this study's calculations. Nelspruit was selected being the largest city and capital of Mpumalanga province in eastern South Africa with Latitude 25.50°S and Longitude 30.91°E. Meanwhile, Upington is specifically situated at the center of the Northern Cape Province with Latitude 28.41°S and Longitude 21.26°E, making it a region with very high capacity for solar energy generation. These cities' climates are true depiction of the hot and arid weather situations of South Africa, and they correspond to two different climatic zones in Koppen's classification of climate. Due to its Cwa climate,

Nelspruit has dry winters and scorching summers with a mean daily high temperature of roughly 32 °C. Upington is known to have a hot, arid desert environment with a mean daily high temperature of roughly 39 °C due to its Bwh climate.

12.2.2 *Parameters and Case Scenarios for Building Modelling*

This study considered five independent parameters that relates to the studied locations' weather and the BIPV system namely: (i) the location's climatic status—summer and winter seasons; (ii) the BIPV's orientation coordinate at east, north and west; (iii) the BIPV's inclination angle from at 20°, 26° and 30°. Here, six case scenarios were formed (see Fig. 12.1) (iv) the installation capacity of the BIPV (v) the BIPV's installation area.

The 26° inclination angle was selected because it depicts the ideal average inclination angle for both locations. By positioning the BIPV modules perpendicular to the yearly average solar path, this angle can help in maximizing the annual energy production and offers both regions an equitable energy production. Meanwhile, the 20° inclination angle was selected to allow for installation of more BIPV panels. Also, this lower angle can enhance the energy output during summer months for both regions by allowing the modules to absorb a greater amount of light when the sun is at a higher angle. Conversely, an increased inclination angle of 30° was finally chosen to allow for optimal energy production during winter seasons when the sun is at a lower angle and the sunlight intensity drops. Additionally, this angle is suggested as the optimum tilt angle for most South African locations to capture the utmost solar

Fig. 12.1 Hypothesized residential buildings model and six case scenarios

insolation possible (Roux 2016). In the meantime, this study considered the northward orientation to enable the BIPV panels to capture the utmost direct sunlight and optimize their potential of generating energy. However, the east–west orientation was chosen to allow for the flow of electricity generation during the day to be more evenly distributed by the BIPV panels (Roux 2016; Yadav et al. 2020).

To determine the effects of the analysed BIPV systems on solar energy harvesting, potential, and energy savings, two dependent parameters were compared in this study. These include: (i) the BIPV module type and (ii) the distance between the BIPV modules. The BIPV module type could be monocrystalline, polycrystalline, or thin film. In this study, the monocrystalline silicon BIPV module was employed because of its relatively great efficiency and dependability Alhammadi et al. (2022).

For the analyzed cities, meteorological information from the Meteonorm 8 software was used in this study. The simulation software can create a realistic simulation for each hour of the entire year by considering the latest meteorological year climate information, which is typically based on extended periods nearing 30 years. Using the Polysun simulation software, the BIPV power generation installed on residential buildings' rooftops were estimated.

12.3 Results and Discussion

Figure 12.2 illustrates the study results on the total quantity of power generated annually by the BIPV panels for residential buildings in the Nelspruit and Upington. The greatest energy generation in the surveyed cities occurred under Case 4 whenever the BIPV modules were aligned in the east-to-west direction and inclined at 20° with 34.53 MWh/year in Upington and 31.47 MWh/year in Nelspruit. This is because the designed layout made it possible to install more BIPV modules due to the closer spacing between them. Additionally, when the BIPV modules are placed facing east to west, the lower angle increases power production for residential buildings. The next-highest quantity of energy generated is achieved by the BIPV modules with a 26° inclination angle and positioned in the east–west orientation (Case 5). Here, the total energy produced for the hypothesized buildings is 32.66 MWh/year in Upington and 29.53 MWh/year in Nelspruit. Similarly, the values in Case 6 were ranked third as the overall power produced in Nelspruit and Upington are 31.45 and 27.68 MWh/year respectively. In this case, the BIPV panels were placed at an increased tilt angle of 30°. However, whenever the modules are inclined at 20° and 26° northwards, energy generated by these modules was 17.25 and 16.09 MWh/year for Cases 1 and 2 respectively in Nelspruit. The power generation amounted to 18.03 and 17.19 MWh/year for Cases 1 and 2 respectively in Upington. Apparently, the least amount of electricity is generated in Case 3 with 16.72 and 15.14 MWh/year in Upington and Nelspruit respectively when the BIPV modules are tilted at 30°, facing the north. This is because the installed system's capacity in this situation is the smallest.

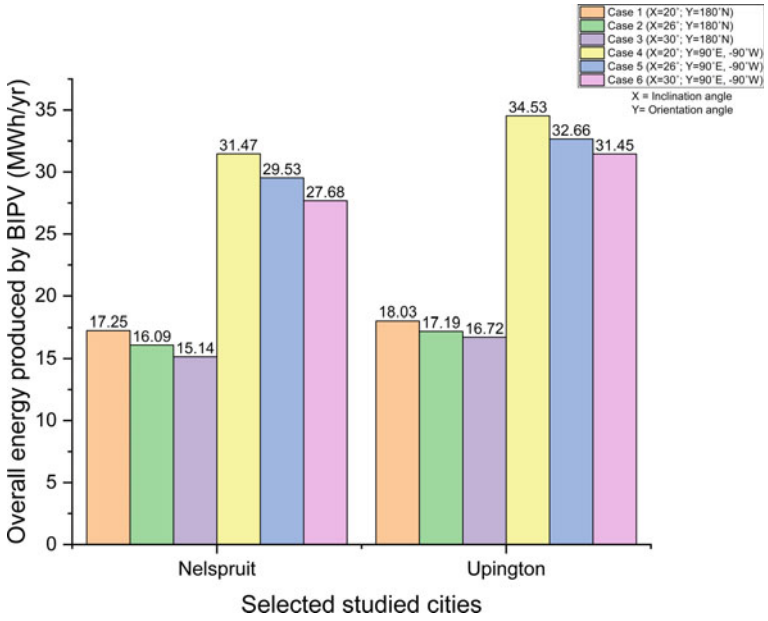

Fig. 12.2 BIPV energy production (MWh/year) for residential buildings in all cases

As illustrated in Table 12.1, analysis from the study showed that based on the three inclination angles considered (20°, 26° and 30°), some marginal drops occurred in the energy produced via the BIPV modules for the domestic buildings in both cities. The percentage difference spanned between 6 to 12% and 3 to 7% for Cases 1–3 when these panels are oriented northwards in Nelspruit and Upington respectively. Similarly, in Cases 4–6 when the BIPV modules are oriented in the east–west split, the percentage decline in energy production ranged from 6 to 12% in Nelspruit and about 4–9% in Upington.

In the meantime, the energy output for building per installed kilowatt peak power output (kWp) is shown in Fig. 12.3. When the BIPV modules are installed with their faces along the east–west split, the highest energy production per kWp is obtained with the lowest inclination angle, (which is 20° in this study), achieving values around 1954 kWh in Upington and 1873 kWh in Nelspruit. This is trailed by Case 5 (26° tilt angle at east–west direction) with 1870 and 1738 kWh/kWp in Upington and Nelspruit respectively. However, the quantity of energy generated with the best inclination angle of 30° occurs when the BIPV modules are mounted towards north, with the higher output of about 1517 kWh/kWp in the arid region of Upington and followed by a value around 1406 kWh/kWp in the hot climatic area of Nelspruit. Moreover, the results revealed that whenever the inclination angle is set to 30° and the rooftop BIPV modules are oriented towards east–west direction, Case 6 produced the least amount of power per installation in any of the situations. In this case, the

Table 12.1 Percentage drop in annual energy produced by BIPV modules

Conditions	Orientation	Cases considered	Percentage drop in energy generated by BIPV modules	
			Nelspruit (%)	Upington (%)
Based on inclination angles (20°, 26° and 30°)	Northwards	Δ (Case 1–Case 2)	5.63	4.66
		Δ (Case 2–Case 3)	5.90	2.85
		Δ (Case 1–Case 3)	12.23	7.26
	East–west direction	Δ (Case 4–Case 5)	6.26	5.42
		Δ (Case 5–Case 6)	6.16	3.70
		Δ (Case 4–Case 6)	12.04	8.92
Based on orientation angles	East–west direction versus Northwards	Δ (Case 4–Case 1)	45.19	47.79
		Δ (Case 5–Case 2)	45.51	47.37
		Δ (Case 6–Case 3)	45.30	46.84

BIPV electrical energy generation is at 1750 and 1622 kWh/kWp for Upington and Nelspruit respectively.

When analyzing the amount of overall energy generated with the amount of energy generated per kWp in each scenario, the findings indicated that when the BIPV is oriented northwards (Cases 1, 2 and 3), Case 1 with the smallest inclination angle produces more overall electric power, despite the fact the amount of power generated

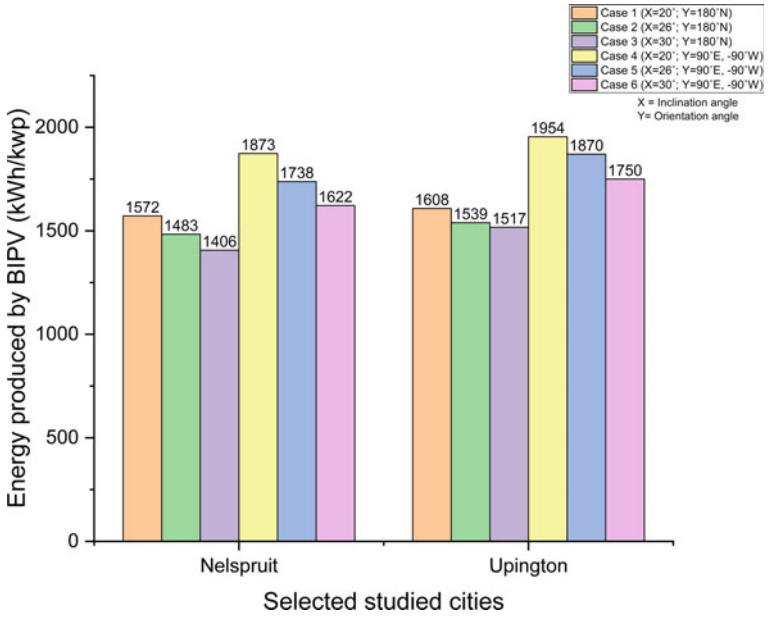

Fig. 12.3 BIPV energy production (kWh/kWp) for residential buildings in all cases

per kWp is lesser. This occurred because Case 1 has the highest installation potential in this aspect. In contrast, the overall amount of power supplied is greater in Case 4 even if the total installed capacity is lower when the BIPV modules are oriented towards east–west direction (Cases 4, 5 and 6). This is so, the reason being that as the BIPV modules capture more sunlight through lower inclination angles, more power is generated per kilowatt peak.

Moreover, this study's findings were expanded by determining the energy output per unit area of the usable rooftop space for the installation of BIPV modules. As depicted in Fig. 12.4, when the BIPV modules were set up over all the building's rooftop in the east–west orientation and lower inclination angle, it produced higher total power generation than the ideal inclination angle and north-facing BIPV modules. Whenever the BIPV modules are positioned at the ideal inclination angle of 30° and north orientation, the modules at Case 3 generated the least amount of energy in buildings, with the overall power/m^2 of rooftop space being 135 kWh in Upington and 107 kWh in Nelspruit. Conversely, in Case 4, the BIPV modules' best electricity output is attained in the residential buildings when they are mounted with a 20° inclination angle towards east–west. This yielded 210 and 202 kWh/m^2 of the building's rooftop space in Upington, and Nelspruit respectively. This is primarily because PV modules oriented towards east–west produce more energy per kilowatt peak at the least angle, and because lesser angles need a smaller distance between the modules, which increases installed capacity and, consequently, energy production.

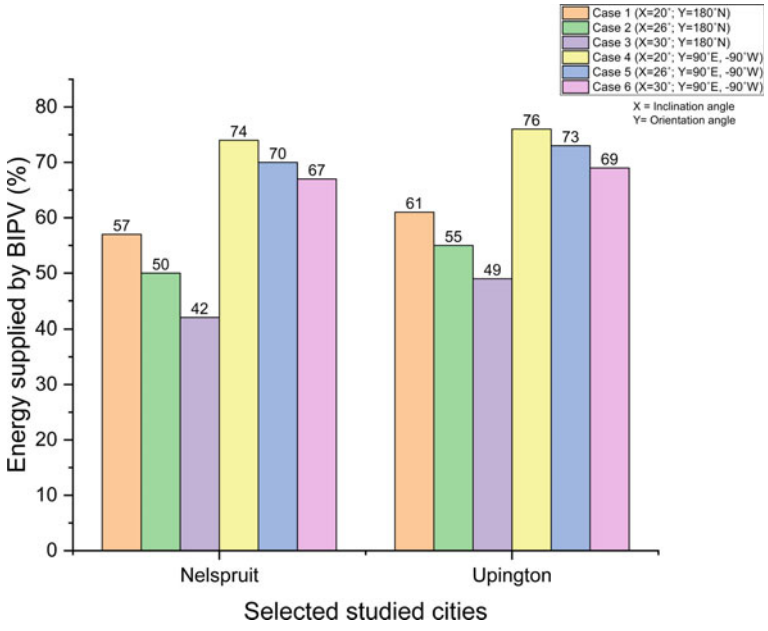

Fig. 12.4 BIPV energy production (kWh/m^2) for residential buildings in all cases

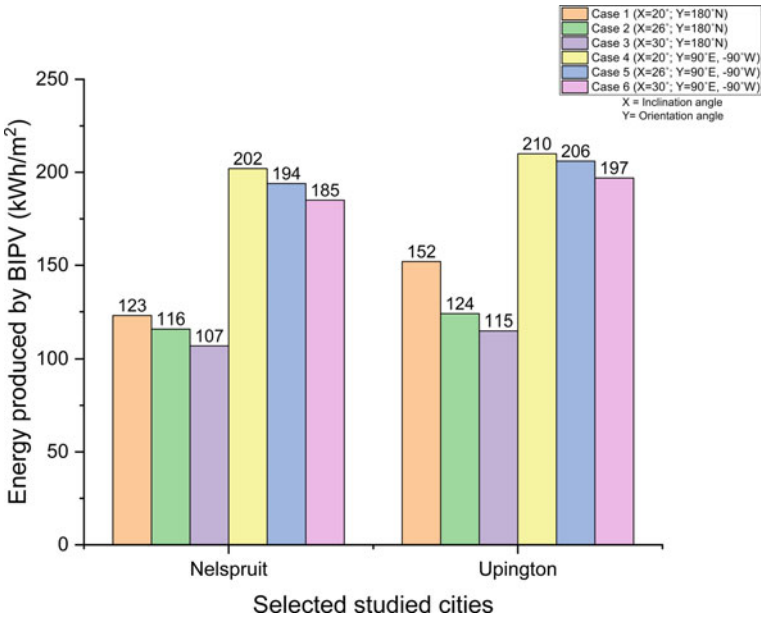

Fig. 12.5 Current percentage of energy demand supplied by BIPV

As revealed in Fig. 12.5, the comparative analysis of energy production and consumption showed that the energy produced by BIPV modules may meet as much as 76% and 74% of the present energy needs of Upington, and Nelspruit, respectively. These maximum values for the two studied cities were attained under Case 4 while these percentages were lowest in Case 3.

12.3.1 Further Discussion

Given Upington and Nelspruit's arid and hot climate respectively alongside the abundance of solar radiation available in the two territories, renewable energy systems can play a substantial role in this respect. This suggests that BIPV technology would be effective if applicably adopted by domestic buildings in any of the two studied locations. Figure 12.6 revealed the impact of daylight durations on energy generation of BIPV technologies in both studied climes. Sunshine hours can reach 9 h in Nelspruit and over 11 h in Upington (highest in South Africa), providing avenues for BIPV systems to reach their maximum power generation capabilities. This implies that the amount of energy the BIPV systems can produce all over the day increases with the length of daylight. This can be helpful in being able to satisfy the building's energy needs and even supply any extra energy back to South Africa's energy grid.

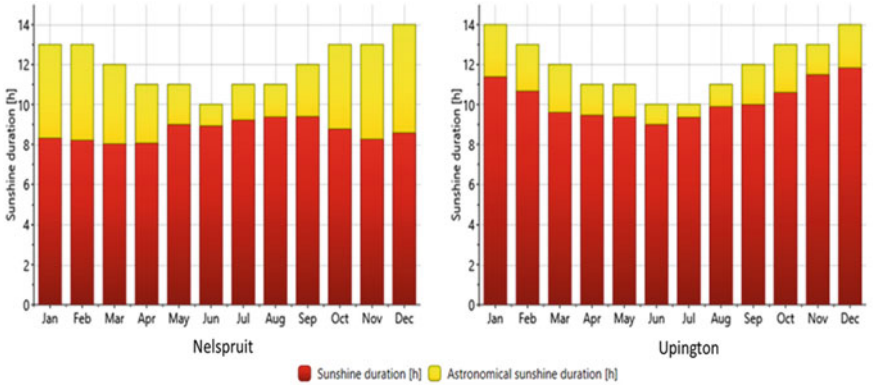

Fig. 12.6 Modelled results on sunshine periods in the study locations

Moreover, results unveiled the essence and impact of inclination angle on BIPV's energy performance. It was observed from the results above that the lowest energy outputs were recorded in higher inclination angles. However, under lower tilt angles, the BIPV modules generated the utmost energy output for residential buildings in both regions. This suggests that the designed layout made it possible to install more BIPV modules because a smaller distance is needed between them. Also, the study's findings indicated the influence of orientation angles on energy performance of BIPV in all cases as both north and east–west directions were considered. It was observed that north facing BIPV systems produced lower energy output when compared to east–west orientations. The east–west split outperforms northward orientations at very significant rates of about 48%. This is because BIPV systems oriented in the east–west direction have a dual contextual advantage of harnessing more sunlight from morning to late afternoon hours which could favorably help to meet the energy demand profiles from building occupants in Nelspruit and Upington all over the day.

12.4 Conclusion

The study pragmatically examined the incorporation of green BIPV systems in the hot interior and arid interior climate zones of South Africa which were studied on hypothetically modelled residential buildings using Nelspruit and Upington as case studies.

In all considered case scenarios, findings showed that the generated energy and power output by the BIPV modules were higher in Upington than Nelspruit, affirming the assertion that the amount of solar radiation that a specific place receives frequently has a direct impact on how much energy BIPV systems produce. Moreover, there are opportunities for BIPV systems to reach their optimum power generating potential because of long sunshine hours in both locations. Furthermore, as both north and

east–west directions were taken into consideration, the data showed that orientation angles influenced BIPV's energy performance in all circumstances. When compared to east–west orientations, BIPV systems with a northward facing were shown to yield less energy. Similarly, it was also revealed that higher inclination angles generated lower energy outputs, while lower tilt angles produced the highest energy output for domestic buildings in both locations from the BIPV modules.

In sum, the following conclusions were arrived at based on the findings: (i) BIPVs can maximize occupant comfort and wellbeing while ensuring optimum energy efficiency and ecological performance; (ii) The improved BIPV systems can alleviate over-dependence on conventional energy supply for buildings in such regions, while achieving greater energy conversion efficiency; (iii) Optimized BIPV systems can produce clean power for building energy performance while helping with energy conservation, climate change mitigation in the studied regions and beyond.

It is recommended that large-scale BIPV demonstration projects be developed and enhanced in South Africa's hot and arid regions to illustrate the efficacy and merits of these systems to the public and industry stakeholders. Also, the enactment of beneficial regulations, including feed-in tariffs and tax incentives should be promoted to foster the use of BIPV systems and eco-friendly construction techniques. Going forward, future research can examine the effects of additional electrical components on buildings and BIPV modules. Also, prospective studies could investigate practical measures that can reduce the likely overheating and fire risk of BIPV panels.

References

Agbajor FD, Mewomo MC, Umoh VB, Makanjuola SA (2023) Building energy management system research in South Africa—a decade overview. Energy Rep 9:33–39. https://doi.org/10.1016/j.egyr.2023.05.056

Agbajor FD, Mewomo MC (2022) Green building research in South Africa: a scoping review and future roadmaps. Energy Built Environ. https://doi.org/10.1016/j.enbenv.2022.11.001

Alabi TM, Agbajor FD, Yang Z, Lu L, Ogungbile AJ (2023) Strategic potential of multi-energy system towards carbon neutrality: a forward-looking overview. Energy Built Environ 4(6):689–708. https://doi.org/10.1016/j.enbenv.2022.06.007

Alhammadi N, Rodriguez-Ubinas E, Alzarouni S, Alantali M (2022) Building-integrated photovoltaics in hot climates: experimental study of CIGS and c-Si modules in BIPV ventilated facades. Energy Convers Manage 274:116408

Happle G, Shi Z, Hsieh S, Ong B, Fonseca JA, Schlueter A (2019) Identifying carbon emission reduction potentials of BIPV in high-density cities in Southeast Asia. J Phys Conf Ser 1343(1):012077

Jin Y, Hu S, Zhang Z, Zhu B, Bai D (2022) The path to carbon neutrality in China: a paradigm shift in fossil resource utilization. Resour Chem Mater 1(1):129–135. https://doi.org/10.1016/j.recm.2022.01.003

Le Roux WG (2016) Optimum tilt and azimuth angles for fixed solar collectors in South Africa using measured data. Renew Energy 96:603–612

Li C, Zhang W, Tan J, Liu W, Lyu Y, Tang H (2023) Energy performance of an innovative bifacial photovoltaic sunshade (BiPVS) under hot summer and warm winter climate. Heliyon 9(8):e18700. https://doi.org/10.1016/j.heliyon.2023.e18700

Marotta A, Porras-Amores C, Rodríguez Sánchez A (2023) Are green buildings an indicator of sustainable development? Appl. Sci. 13(5). https://doi.org/10.3390/app13053005

Martín-Chivelet N et al (2022) Building-integrated photovoltaic (BIPV) products and systems: a review of energy-related behavior. Energy and Buildings 262:111998

Samarasinghalage TI, Wijeratne WMPU, Yang RJ, Wakefield R (2022) A multi-objective optimization framework for building-integrated PV envelope design balancing energy and cost. J Clean Prod 342:130930

SAWS (2022) Annual State of the climate of South Africa 2022. South African Weather Service. https://www.weathersa.co.za/Documents/Corporate/Annual%20State%20of%20the%20Climate%202022_31032023102536.pdf. Accessed 13 July 2023

Taşer A, Koyunbaba BK, Kazanasmaz T (2023) Thermal, daylight, and energy potential of building-integrated photovoltaic (BIPV) systems: a comprehensive review of effects and developments. Sol Energy 251:171–196

Yadav S, Panda SK, Hachem-Vermette C (2020) Optimum azimuth and inclination angle of BIPV panel owing to different factors influencing the shadow of adjacent building. Renew Energy 162:381–396. https://doi.org/10.1016/j.renene.2020.08.018

Yu G, Yang H, Yan Z, Kyeredey Ansah M (2021) A review of designs and performance of façade-based building integrated photovoltaic-thermal (BIPVT) systems. Appl Thermal Eng 182:116081

Zuo J, Zhao Z-Y (2014) Green building research–current status and future agenda: a review. Renew Sustain Energy Rev 30:271–281

Chapter 13
An Investigation on Promotional Strategies to Green Building Adoption in a Developing Economy

Modupe Cecilia Mewomo, Favour David Agbajor, and Iseoluwa Joanna Mogaji

Abstract Green buildings (GB) have been identified as a feasible solution to the ecological problems emanating from the construction industry. Diverse themes within this subject matter have been made known to most world regions. Nonetheless, the availability of promotional strategies that can ampler its implementation is lacking in Nigeria's built environment. Thus, for the first time, this study provided an overview of existing promotional strategies adopted among developing and developed countries with a view to deducing solution roadmaps for the adopting GB in Nigeria. A total of 50 questionnaires was obtained from knowledgeable experts in Nigeria's construction industry and forthwith analyzed. Four topmost strategies were identified to boost this auspicious approach while recommending on their essence of they are implemented with immediate effect.

Keywords Green building · Promotion strategy · Barriers · Drivers · Nigeria

M. C. Mewomo (✉) · F. D. Agbajor · I. J. Mogaji
Department of Construction Management and Quantity Surveying, Durban University of Technology, Durban 4001, South Africa
e-mail: modupem@dut.ac.za

F. D. Agbajor
e-mail: 22175971@dut4life.ac.za

I. J. Mogaji
e-mail: 22176047@dut4life.ac.za

Z. Sun and P. K. Das (eds.), *Proceedings of the 10th International Conference on Energy Engineering and Environmental Engineering*, Environmental Science and Engineering, https://doi.org/10.1007/978-3-031-48204-5_13

13.1 Introduction

13.1.1 Motivation and Background

The construction industry is known to constitute major global ecological hazards through its diverse anthropogenic activities as it accounts for 40% of energy use and 40% of CO_2 emissions globally (Agbajor and Mewomo 2022). Green building (GB), being an efficacious approach to alleviate these hitches, have witnessed vast pragmatic adoption via standards, policies, financing schemes, innovations, and whatnot, while it has been a cynosure of all eyes for built-environment's scholars and practitioners due to the myriads of merits it offers (Debrah et al. 2022). A holistic survey of extant literature revealed diverse aspects of research themes regarding the subject matter, including, GB policies and certification systems, drivers, barriers, critical success factors, GB technologies, post-occupancy evaluation, GB incentives, GB design, materials, and marketing, among others, each contributing to the overarching goal of enhancing GB initiative worldwide (Wuni et al. 1992).

Promisingly, sub-Saharan African nations are adopting the GB initiative with prominent interests and acceptance from Ghana, South Africa, Egypt and Nigeria (Mushi et al. 2022). For Nigeria in particular, the GB initiative is crucial owing to rapid urban sprawl, increased housing demand and such like. By and large, several initiatives were launched by the Nigerian government and allied organizations such as the National Building Code, Green Building Council of Nigeria, National Adaptation Strategy and Plan of Action, alongside National Building Energy Efficiency Code, all with the prime aim of enhancing GB development in Africa's most populous and fastest urbanizing region (Abisuga et al. 2020). Similarly, some research endeavours were earlier conducted by Nigerian scholars as indicated in Abisuga et al. (2020), Dalibi et al. (2017), Ebekozien et al. (2022a) and Olawumi and Chan (2021). Meanwhile, these studies are veered towards GB assessments, GB barriers, in the country whereas, the promotional strategies (PS) towards GB remains unexplored as just one study considered the issue from the standpoint of GB certification only (Ebekozien et al. 2022b). While it is vital to consider the drawbacks to and benefits of GB growth, the recognition of PS is imperative as it can offer blueprint for breakthroughs in this area.

13.1.2 Related Works

Notably, some researchers have delved into the subject of PS for GB adoption across some world regions with their outputs offering solution roadmaps for GB barriers. For instance, the study of Darko et al. (2017), Darko and Chan (2018), Hwang et al. (2017), Li et al. (2014) and van Doren et al. (2016) all identified the topmost ways of promoting GB adoption in the United States, Ghana, Singapore, China and Netherlands respectively. Ideally, these aforesaid PS for GB could have granted profound

merits to those regions (see Table 13.1 [PS01-PS15]) but may not all apply to Nigerian context having its social, economic, environmental peculiarities. On this wise, this study seeks to address this sparse research upshot via an exploratory investigation from Nigerian perspective which is hoped to offer invaluable insights and aid decision and policy making for researchers and built environment practitioners in Nigerian and beyond.

13.2 Research Method

This study aims to empirically evaluate the strategies to promote GB adoption in Nigeria. Thus, the research method consists of (i) questionnaire design and (ii) data collection and analysis. A brief discussion on these is provided below.

13.2.1 Questionnaire Design

The adopted approach comprised an online field survey of construction project stakeholders with sound knowledge of and experience in GB. After an in-depth overview of extant scholastic publications, a well-structured questionnaire, comprising 5 sections, was designed with the goal of providing answers to the study's objective. Section 13.1 presented the research overview, contact details along with respondents' informed consent and anonymity. Section 13.2 enquired respondents' background information and project characteristics. Questions regarding barriers to and benefits of GB adoption in Nigeria were asked in Sects. 13.3 and 13.4 respectively while Sect. 13.5 focused on the PS for GB adoption. It is noteworthy that Sects. 13.3 and 13.4 (not part of this paper's purview) were excluded as they will be demystified in future research. Thus, the current study centered on other sections with Sect. 13.5's questions hinged on 25 identified promotional strategies listed in Table 13.1. A Likert-scale (using a 5-point rating scale: 1 = not important; 2 = less important; 3 = moderately important; 4 = important; 5 = very important) approach was employed since it is devoid of ambiguity and allow respondents to easily rank their responses (Darko et al. 2017). Prior to the questionnaire distribution, pilot study/interview was conducted to ensure the appropriateness of the research instrument.

13.2.2 Data Collection and Analysis

Questionnaires were distributed via an online google form as it is user friendly, enables informed consent and allow for tracking the response progress. Based on the study's objective, the non-probability sampling method of "purposive sampling" is found suitable for selecting the qualified specialists as it aligns with previous

Table 13.1 Identified list of promotion strategies from literature

Code	Strategies for promotion	References							
		Chan et al. (2017)	Hwang et al. (2017)	Darko et al. (2017)	Li et al. (2014)	Darko and Chan (2018)	Zhang (2015)	Darko et al. (2018)	Ebekozien et al. (2022b)
PS01	Financial and further market-based incentives for GBs adoption	✓	✓	✓	✓	✓	✓		
PS02	Compulsory GB policies and regulations	✓	✓	✓	✓	✓	✓	✓	✓
PS03	Green rating and labelling programs	✓		✓	✓	✓	✓	✓	✓
PS04	Better enforcement of GB policies after they have been developed	✓		✓	✓	✓		✓	
PS05	Low-cost loans and subsidies from government and financial institutions	✓		✓	✓	✓	✓		
PS06	Public environmental awareness creation through workshops, seminars, conferences	✓		✓	✓	✓	✓		
PS07	More publicity through media (e.g., print media, radio, television and internet)	✓		✓		✓	✓		
PS08	GB-related educational and training programs for developers, contractors and policymakers	✓	✓	✓		✓	✓		

(continued)

Table 13.1 (continued)

Code	Strategies for promotion	References							
		Chan et al. (2017)	Hwang et al. (2017)	Darko et al. (2017)	Li et al. (2014)	Darko and Chan (2018)	Zhang (2015)	Darko et al. (2018)	Ebekozien et al. (2022b)
PS09	Availability of better information on cost and benefits of GB	✓	✓	✓	✓	✓			
PS10	Availability of competent and proactive GB promotion teams	✓		✓		✓		✓	
PS11	Availability of institutional framework for effective GB implementation	✓	✓	✓		✓			
PS12	Strengthened GB research and development	✓	✓	✓	✓	✓	✓		
PS13	Acknowledging and rewarding GB adopters publicly					✓			
PS14	Executive management support					✓			
PS15	More GB adoption advocacy to promote GB					✓			
PS16	Public awareness of GB benefits								✓
PS17	Developing awareness of clients about the benefits								✓

(continued)

Table 13.1 (continued)

Code	Strategies for promotion	References							
		Chan et al. (2017)	Hwang et al. (2017)	Darko et al. (2017)	Li et al. (2014)	Darko and Chan (2018)	Zhang (2015)	Darko et al. (2018)	Ebekozien et al. (2022b)
PS18	New efficient processes and by learning new roles								
PS19	Availability of information on beneficial operational costs of GB								✓
PS20	Financial incentives and innovative fiscal arrangement								✓
PS21	Intense interdisciplinary collaboration of construction professionals								
PS22	Greater understanding of GB innovation process								✓
PS23	Developing able and willing technology experts to champion GB innovations								✓

(continued)

Table 13.1 (continued)

Code	Strategies for promotion	References							
		Chan et al. (2017)	Hwang et al. (2017)	Darko et al. (2017)	Li et al. (2014)	Darko and Chan (2018)	Zhang (2015)	Darko et al. (2018)	Ebekozien et al. (2022b)
PS24	Developing innovative GB promotion actors via coordination and network building								✓
PS25	Higher commitment from the client								

References: Chan et al. (2017), Hwang, et al. (2017), Darko et al. (2017), Li et al. (2014), Darko and Chan (2018), Zhang (2015), Darko et al. (2018), Ebekozien et al. (2022b)

construction management studies (Chan et al. 2017). Survey participants were urged to share the data to their fellows who are veterans in the construction industry in a bid to improve the sample size during the data collection period. After 3 months' duration, a total of 50 valid responses were collected. Obviously, the sample size could be adjudged as satisfactory as relevant extant works in the construction, engineering and management (CEM) domain affirmed a minimum sample size of 30 is significant for conducting statistical analysis (Darko and Chan 2018). More so, pragmatic adoption of GB being at its budding stage in Nigeria could have resulted in such sample size. The collected data were curated using Excel spreadsheet and forthwith exported into SPSS 28.0 statistical software for requisite analysis.

Regarding respondents' demographic details, architects hold 54% (27 people (P)), quantity surveyors, builders and engineers accounted for 26% (12P), 12% (6P) and 4% (2P) of participants respectively, while anonymous participants represented 4% (just 2P) of the total survey partakers. A per job titles, 48% (24P), 14% (7P) and 8% (4P) of the respondents identified themselves as project managers, construction managers and contract managers respectively. In contrast, directors of firms and unnamed job titles contains 12% (6P) and 18% (9P) separately. Besides these data, 11 (22%) contracting firms, 17 (34%) consultancy firms, and 20 (40%) government agencies and developers signified the respondents' organization type, although 2 (4%) firms/companies were undisclosed. Moreover, Fig. 13.1i indicated that 19 respondents (38%) had less than 5 years' work experience in the construction industry, compared to 5 (10%), 6 (12%), 8 (16%) and 12 (24%) respondents who had beyond 5 years, ranging between 6–10 years, 11–15 years, 16-20 years and above 20 years of experience respectively. Contrariwise, Fig. 13.1ii illustrated 90% of the respondents (i.e. 36P (72%) and 9P (18%) with 4–6 and 6–10 years respectively) have less than 10 years of experience in GB while a sparse number (5P, 10%) of

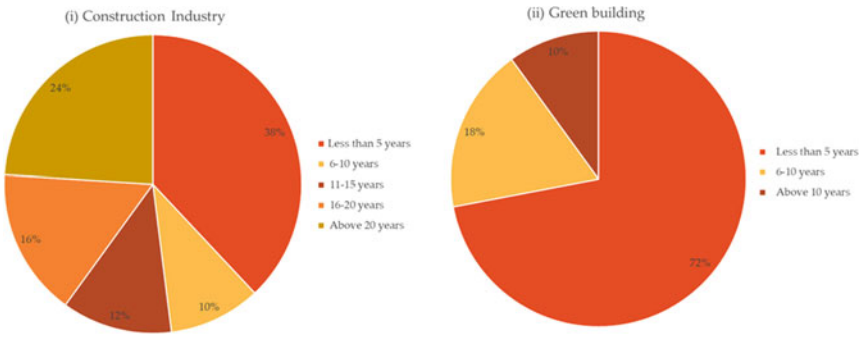

Fig. 13.1 Presentation on respondents' year of experience in: **i** Construction industry; **ii** Green building

respondents had 10 years of experience. This indicates the dilatory and slow adoption of GB in Nigeria when compared to the emergence of its concept since in the early '80s (Wuni et al. 1992). Nonetheless, this outcome could be viewed as sensible given the little GB initiatives that have been implemented in Nigeria in recent years.

Meanwhile, our study employed six inferential statistical analysis approach which is akin to related scholarly works in the CEM field as highlighted in Chan et al. (2017) namely:

i. Cronbach's alpha coefficient test—to evaluate the collected data's reliability for subsequent analysis via assessment of the data's internal consistency (value ranges between 0 and 1).
ii. One sample t-test—to determine the significance of the mean scores for the significance of the PS for GB.
iii. Mean score ranking—to ascribe the corresponding weight and rank for the proposed PS for GB adoption.
iv. Kendall's W—this concordance test (referred to as Kendall's coefficient of concordance) was employed to find out the ultimate agreement among the examined professionals within a particular group.
v. Mean difference analysis—employed to ascertain the precise values of the mean score differences of GB PS.
vi. One-way analysis of variance (ANOVA)—this test is an ideal approach for comparative analysis of more than two groups. Thus, this study utilized it to determine substantial statistical variations in the weighted averages of the GB PS among various professional categories.

13.3 Results and Discussion

Firstly, retrieved data from the administered questionnaire was tested for reliability via the Cronbach's alpha test for internal consistency. Ideally, this study obtained Cronbach's alpha value of 0.965 which is beyond the threshold of 0.7 as asserted in Chan et al. (2017).

Table 13.2 provides an overview of results from data collected on the relative significance of the PS. Evidently, the mean value of all the data is statistically above the test value of 3.00 which is the average value for the questionnaire's rating scale. Moreover, all but the last five PS have p-values lower than 0.05 as gotten from the one sample t-test. Thus, it could be inferred that the results are reckoned to be substantially essential for statistical analysis.

The PS "More publicity through media (e.g., print media, radio, television & internet)" (PS07) tops the poll with a mean value of 3.78, By and large, this is a type of PS that can assist develop a positive image for a product, arouse the populace to use it, communicate its advantages, raise consumer awareness, and boost demand for the GB (Darko and Chan 2018). This is very effective and efficient, especially in emerging countryside where new housing demand is increasing. Such communication could introduce GB and educate the public about its benefits and the need to adopt this initiative. Moreover, avenues such as expert panel discussion on radio and television, on-point analysis and interviews with the top leaders on GB adoption could prove helpful in this regard.

The PS "availability of better information on cost and benefits of GB" (PS09) ranks second with a mean value of 3.72. This is an auspicious approach as it can stimulate people aversion to adopting this technology about its essence. Actually, the initial investment outlay or capital cost of could be high, nonetheless, a clear and convincing analysis on its payback period than conventional buildings are essential. For instance, it was recently reported that GB can save about 30% of energy demand and consequently reduce carbon emissions (Himmetoğlu et al. 2022). Extensively, this information can be shared between the knowledgeable and those with little/no idea. In the meantime, it is vital to disburse such information in a convincing manner in a bid to alleviate the age-long apathy on about the future financial benefits of GB.

The PS "availability of competent and proactive GB promotion teams" (PS10) having mean value of 3.70 comes third. With the fast-paced implementation of GB worldwide, it is crucial that competent personnel should be readily available to enhance its adoption. Also, experts that can strategically optimize the potentials of GB particularly in North-eastern part of Nigeria which are promising areas for raising GB development are essential.

Fourthly, the PS "Developing able and willing technology experts to champion GB innovations", with a mean value of 3.66 trails behind the top three strategies. It is essential to fruitfully train and produce able-ready fellows that can spearhead the inaction of GB ideas, construction of iconic eco-friendly infrastructures and whatnot using the cutting-edge innovative technique such as green roofs, eco-friendly localized GB materials, advanced construction approaches and so on. This have proven

Table 13.2 Overview of survey results on PS for GB

Code	All respondents				Group 1			Group 2			Group 3			Diff. (1–2)	Diff. (2–3)	Diff. (1–3)	ANOVA
	M	SD	R	*p*-value	M	SD	R	M	SD	R	M	SD	R				
PS07	3.78	1.32	1	0.000	3.83	1.42	1#	3.76	1.20	3#	3.47	1.51	6#	0.24	− 0.17	0.07	0.827″
PS09	3.72	1.25	2	0.000	3.65	1.36	6	3.76	1.35	3#	3.57	1.23	1#	− 0.14	− 0.17	− 0.31	0.928″
PS10	3.70	1.20	3	0.000	3.38	1.02	15#	3.71	1.21	6#	3.57	1.43	1#	0.04	− 0.23	− 0.18	0.780″
PS23	3.66	1.29	4	0.001	3.38	1.24	15#	3.82	1.29	2	3.25	1.67	13	− 0.07	0.02	− 0.05	0.776″
PS12	3.62	1.35	5	0.002	2.77	1.52	25	3.88	1.11	1	3.57	1.49	1#	− 0.51	− 0.05	− 0.56	0.236″
PS06	3.60	1.34	6#	0.003	3.27	1.26	20	3.53	1.33	13#	3.47	1.43	6#	0.35	− 0.40	− 0.06	0.601″
PS25	3.58	1.13	6#	0.001	3.83	1.30	1#	3.71	1.10	6#	3.03	1.22	22#	0.29	0.24	0.53	0.361″
PS08	3.58	1.39	8	0.005	3.38	1.14	15#	3.47	1.42	17#	3.50	1.45	5	0.28	− 0.53	− 0.25	0.666″
PS15	3.56	1.25	9	0.003	3.48	1.52	11#	3.65	1.00	9#	3.27	1.48	11#	− 0.02	− 0.09	− 0.11	0.816″
PS16	3.54	1.30	10#	0.005	2.92	1.47	23	3.59	1.06	12	3.53	1.36	4	− 0.09	− 0.28	− 0.37	0.579″
PS05	3.54	1.30	10#	0.005	3.19	1.25	21	3.65	1.27	9#	3.43	1.32	8	− 0.27	− 0.22	− 0.49	0.730″
PS11	3.52	1.13	12	0.002	3.31	1.32	18	3.76	0.97	3#	3.33	1.21	9	− 0.14	0.30	0.16	0.814″
PS22	3.52	1.28	13	0.006	3.54	1.21	9	3.53	1.12	13#	3.27	1.56	11#	0.22	− 0.20	0.02	0.773″
PS17	3.50	1.16	14	0.004	3.58	1.34	7#	3.65	1.06	9#	3.17	1.34	17#	− 0.02	0.11	0.09	0.831″
PS21	3.50	1.28	15	0.008	3.79	1.02	4	3.47	1.42	17#	3.07	1.36	20#	0.78	0.14	**0.92**	0.449″
PS19	3.48	1.15	16	0.005	3.83	1.30	1#	3.53	1.07	13#	3.20	1.23	16	0.47	0.33	0.80	0.728″
PS04	3.46	1.33	17	0.018	2.85	1.47	24	3.71	1.21	6#	3.30	1.44	10	− 0.33	0.11	− 0.26	0.637″
PS13	3.42	1.13	18	0.011	3.77	1.04	5#	3.53	1.18	13#	3.10	1.30	19	− 0.03	0.13	0.10	0.827″
PS01	3.40	1.25	19	0.028	3.50	1.20	10	3.18	1.38	25	3.23	1.32	14#	**0.82**	− 0.29	0.53	0.607″
PS24	3.40	1.28	20	0.032	3.42	1.11	14	3.35	1.17	20#	3.07	1.50	20#	0.15	− 0.38	− 0.23	0.542″
PS14	3.36	1.27	21	0.051*	3.29	1.51	19	3.41	1.06	19	3.23	1.34	14#	− 0.16	− 0.05	− 0.22	0.989″

(continued)

Table 13.2 (continued)

Code	All respondents				Group 1			Group 2			Group 3			Diff. (1–2)	Diff. (2–3)	Diff. (1–3)	ANOVA
	M	SD	R	*p*-value	M	SD	R	M	SD	R	M	SD	R				
PS20	3.32	1.27	22	0.081*	3.44	1.00	13	3.35	1.22	20#	2.97	1.40	25	0.52	0.02	0.54	0.647″
PS02	3.32	1.36	23	0.103*	3.58	1.47	7#	3.29	1.21	22	3.03	1.51	22#	0.21	− 0.17	0.33	0.861″
PS18	3.30	1.25	24	0.096*	3.48	1.42	11#	3.24	1.09	23#	3.17	1.41	17#	0.39	− 0.10	0.29	0.967″
PS03	3.24	1.00	25	0.096*	3.08	1.11	22	3.24	1.21	23#	3.03	1.51	22#	0.83	0.04	0.26	0.902″

Legend: M = mean; SD = standard deviation; R = rank; Group 1 = contractors; Group 2 = consultants; Group 3 = government agency and developers
The asterisk (*) depicts the data with non-significant one-sample t-test ($p > 0.05$) (2 tailed); Kendall's W = 0.051; Chi-square (χ^2) = 60.990; df = 24; Level of significance = 0.000

efficacious in advanced countries where approach have gained ground. Implementing such in an emerging economy like Nigeria can go a long way to raise the pragmatic reality of GB adoption.

The fifth most significant promotional strategy, "strengthened GB research and development" (PS12), with a mean value of 3.62. This strategy highlights the essential role of research and development (R&D) in advancing green building practices in Nigeria's developing economy. Investing in R&D initiatives is essential to foster innovation, improve performance, and tackle the country's particular issues. By doing so, stakeholders can create tailored solutions that align with Nigeria's unique context, ultimately encouraging the widespread adoption of green building practices. It is noteworthy that Li et al. (2014) and Anzagira et al. (2022) have also suggested that a reinforced GB research and education framework within an adequate institutional framework is essential for promoting green building adoption in the construction industry. Robust research and development efforts will contribute to the growth of Nigeria's green building industry, paving the way for a more sustainable future.

"Public environmental awareness creation through workshops, seminars, conferences" (PS06) with a mean value of 3.60, making it the sixth most important promotional strategy for green building adoption in Nigeria's developing economy. These events effectively educate various audiences, such as professionals, policymakers, industry experts, and the public, about the benefits of green building practices and their positive effects on the environment and society. Workshops, seminars, and conferences provide a platform for knowledge exchange, the dissemination of best practices, and interactive discussions, allowing participants to gain valuable insights, exchange ideas, and form networks. Furthermore, these events encourage stakeholder collaboration, promoting partnerships and creating opportunities for collective action towards sustainable development. Aminu Umar and Khamidi (2012) suggested the development of public awareness to transform the way of living, conserve water resources, reduce waste, and support the implementation of practical guidelines and approaches. This recommendation aligns with the importance of public environmental awareness creation through workshops, seminars, and conferences in advancing green building adoption.

13.4 Conclusion

This work presents an overview and exploratory analysis of GB promotional strategies in Nigerian construction industry. By and large, the article provided 25 PS coined out from literature to enhance GB adoption. Therefrom statistical analysis of retrieved data obtained from 50 respondents revealed the top four PS which are the crux of the matter in Nigeria setting. A real-time implementation of these PS can enhance decision and policy making for researchers and built environment practitioners in Nigerian and allied African nations facing similar challenge.

References

Abisuga AO, Okuntade TF (2020) The current state of green building development in Nigerian construction industry: policy and implications. In: Gou Z (ed) Green building in developing countries: policy, strategy and technology. Springer International Publishing, Cham, pp 129–146

Agbajor FD, Mewomo MC (2022) Green building research in South Africa: a scoping review and future roadmaps. Energy Built Environ. https://doi.org/10.1016/j.enbenv.2022.11.001

Aminu Umar U, Khamidi DMF (2012) Determined the level of green building public awareness: application and strategies

Anzagira LF, Duah D, Badu E, Simpeh EK, Marful AB (2022) Stimulation strategies to promote green building uptake in developing countries: the case of Ghana. J Eng Des Technol ahead-of-print(ahead-of-print). https://doi.org/10.1108/JEDT-12-2021-0719

Chan APC, Darko A, Ameyaw EE (2017) Strategies for promoting green building technologies adoption in the construction industry—an international study. Sustainability 9(6). https://doi.org/10.3390/su9060969

Dalibi SG, Feng JC, Shuangqin L, Sadiq A, Bello BS, Danja II (2017) Hindrances to green building developments in Nigeria's built environment: "the project professionals' perspectives". IOP Conf Ser Earth Environ Sci 63(1):012033. https://doi.org/10.1088/1755-1315/63/1/012033

Darko A, Chan APC (2018) Strategies to promote green building technologies adoption in developing countries: the case of Ghana. Build Environ 130:74–84. https://doi.org/10.1016/j.buildenv.2017.12.022

Darko A, Chan APC, Ameyaw EE, He B-J, Olanipekun AO (2017) Examining issues influencing green building technologies adoption: the United States green building experts' perspectives. Energy Build 144:320–332. https://doi.org/10.1016/j.enbuild.2017.03.060

Darko A, Chan APC, Yang Y, Shan M, He B-J, Gou Z (2018) Influences of barriers, drivers, and promotion strategies on green building technologies adoption in developing countries: the Ghanaian case. J Cleaner Prod 200:687–703. https://doi.org/10.1016/j.jclepro.2018.07.318

Debrah C, Chan APC, Darko A (2022) Artificial intelligence in green building. Autom Constr 137:104192. https://doi.org/10.1016/j.autcon.2022.104192

Ebekozien A, Ayo-Odifiri SO, Nwaole ANC, Ibeabuchi AL, Uwadia FE (2022a) Barriers in Nigeria's public hospital green buildings implementation initiatives. J Facil Manag 20(4):586–605. https://doi.org/10.1108/JFM-01-2021-0009

Ebekozien A, Ikuabe M, Awo-Osagie AI, Aigbavboa C, Ayo-Odifiri SO (2022b) Model for promoting green certification of buildings in developing nations: a case study of Nigeria. Prop Manag 40(1):118–136. https://doi.org/10.1108/PM-05-2021-0033

Himmetoğlu S, Delice Y, Kızılkaya Aydoğan E, Uzal B (2022) Green building envelope designs in different climate and seismic zones: multi-objective ANN-based genetic algorithm. Sustain Energy Technol Assess 53:102505. https://doi.org/10.1016/j.seta.2022.102505

Hwang B-G, Zhu L, Tan JSH (2017) Green business park project management: Barriers and solutions for sustainable development. J Cleaner Prod 153:209–219. https://doi.org/10.1016/j.jclepro.2017.03.210

Li Y, Yang L, He B, Zhao D (2014) Green building in China: needs great promotion. Sustain Cities Soc 11:1–6. https://doi.org/10.1016/j.scs.2013.10.002

Mushi FV, Nguluma H, Kihila J (2022) A critical review of African green building research. Build Res Inf. **50**(6):610–627. https://doi.org/10.1080/09613218.2021.2015276

Olawumi TO, Chan DWM (2021) Green-building information modelling (Green-BIM) assessment framework for evaluating sustainability performance of building projects: a case of Nigeria. Architect Eng Design Manag 17(5–6):458–477. https://doi.org/10.1080/17452007.2020.1852910

van Doren D, Giezen M, Driessen PPJ, Runhaar HAC (2016) Scaling-up energy conservation initiatives: barriers and local strategies. Sustain Cities Soc 26:227–239. https://doi.org/10.1016/j.scs.2016.06.009

Wuni IY, Shen GQP, Osei-Kyei R (2019) Scientometric review of global research trends on green buildings in construction journals from 1992 to 2018. Energy Build 190:69–85. https://doi.org/10.1016/j.enbuild.2019.02.010

Zhang X (2015) Green real estate development in China: state of art and prospect agenda—a review. Renew Sustain Energy Rev 47:1–13. https://doi.org/10.1016/j.rser.2015.03.012

Chapter 14
Lead Exposure in Primitive E-Waste Recycling and Its Dose-Dependent Effects on Health

Haoqian Hu, Kun Liu, Haoyi Yang, and Yuanzhe Li

Abstract This comprehensive study investigates the potential health hazards associated with unsophisticated electronic waste (e-waste) recycling in Guiyu, China, particularly emphasizing the effects of lead exposure on children's health and behavior. Utilizing methodologies such as the Parent Temperament Questionnaire, physical examinations, and residential surveys, the research uncovers a significant association between e-waste recycling and elevated levels of lead in cord blood in Guiyu. Furthermore, children in this region show an increased prevalence of adverse reproductive outcomes like stillbirths and preterm births. Notably, an age-dependent increase in blood lead levels was identified, indicating a continuous risk of lead exposure. However, the study falls short in directly assessing behavioral changes stemming from lead exposure or providing age-specific comparisons of blood lead levels. Alongside the observational findings, the research presents an in-depth review of the health risks posed by lead exposure, the mechanisms of occupational exposure, exposure assessment, and toxicological risk assessment, ultimately suggesting strategic interventions for controlling exposure. The critical public health implications unveiled through this study underscore the pressing necessity for improved waste management practices, policy interventions, and further exploration into the effects of other e-waste toxins on human health.

H. Hu
Institut Supérieur du Commerce, 22 Boulevard du Fort de Vaux, 75017 Paris, France

K. Liu
Faculty of Law, The University of Buenos Aires, C1111AAI Buenos Aires, Argentina
e-mail: rbk@vip.163.com

H. Yang · Y. Li (✉)
NUS College of Design and Engineering, National University of Singapore, Singapore 118429, Singapore
e-mail: yuanzhe001@e.ntu.edu.sg

Y. Li
Carbon Neutrality Research Lab, China Academy of Art, Hangzhou 310002, China

Z. Sun and P. K. Das (eds.), *Proceedings of the 10th International Conference on Energy Engineering and Environmental Engineering*, Environmental Science and Engineering, https://doi.org/10.1007/978-3-031-48204-5_14

Keywords Lead · Human exposure · E-waste processing · Risk management · Exposure control

14.1 Introduction

Electronic waste (e-waste), a burgeoning environmental issue, encompasses obsolete electronic devices such as computers, televisions, mobile phones, and toys. Globally, an estimated 20–50 million tons of e-waste are generated yearly, with annual increases anticipated at 3–5% (Julander et al. 2014). This waste is composed of various materials, including plastics and metals. Predominantly practiced in countries like Nigeria, China, Thailand, Ghana, the Philippines, India, and Vietnam, informal recycling involves disassembling obsolete electronics to reclaim valuable components. However, due to the lack of appropriate technology, this process exposes workers to toxic and hazardous compounds, including heavy metals like antimony, arsenic, beryllium, cadmium, chromium, cobalt, indium, lead, mercury, nickel, and thallium (Grant et al. 2013). Lead, among these toxins, is particularly alarming given its potential detrimental health impacts, particularly on children. Lead exposure can lead to developmental issues, behavioral problems, lower IQ scores, and harm to the nervous system, kidneys, and blood cells. Children are most susceptible to the harmful effects of lead, and exposure can occur through ingestion of contaminated soil, dust, or water, or inhalation of lead particles. Informal e-waste recycling has been associated with elevated blood lead levels (BLL) in workers and local residents. Guiyu, a town in China, has been dubbed the "e-waste capital of the world," with an estimated 80% of the world's e-waste processed there (Liu et al. 2013). Research in Guiyu revealed significantly elevated BLL in children living near e-waste recycling sites, with BLL in some children exceeding 10 micrograms per deciliter (μg/dL), the threshold for lead poisoning in children according to the United States guidelines. Given its health implications, high exposure levels associated with informal e-waste recycling, and the need for effective interventions, much of the e-waste research has rightfully focused on lead. Research is ongoing into the health effects of lead exposure at informal e-waste recycling sites, identification of risk factors for elevated BLL in workers and local residents, and evaluation of interventions to minimize exposure to lead and other toxic compounds in e-waste recycling. The examination of lead in e-waste research is crucial due to its potential harm to human health, the high levels of exposure associated with informal e-waste recycling, and the urgent need for effective interventions to mitigate exposure and protect workers and local communities.

14.2 Blood Lead Levels (Pb-B) and Health Effects

14.2.1 Lead Property

Lead is a heavy metal with atomic number 82, represented by the symbol Pb. Its low melting point and exceptional corrosion resistance have made it a popular material in a variety of industries, including plumbing, electronics, and construction. However, lead is highly toxic and can cause severe health issues when ingested or inhaled. Lead exists in three oxidation states: metallic Pb(0), Pb(II), and Pb(IV). While lead can form stable Pb(II) compounds, the majority of lead's chemistry involves the tetravalent (+4) oxidation state. Contrary to some misconceptions, lead, despite its thickness and extreme malleability, is not an efficient conductor of electricity. Its high corrosion resistance is impressive, as exemplified by the enduring use of lead water pipes installed by the ancient Romans. When exposed to air and water, lead forms protective layers of lead sulfate, lead oxide, and lead carbonate. These films act as a barrier, preventing the metallic substrate from undergoing regular corrosion. It's also noteworthy that lead is amphoteric; it reacts with both acids and bases, forming various lead salts.

14.2.2 Pb-B Exposure and Health Effects

Blood lead levels (Pb-B) reflect the amount of lead present in a person's bloodstream. The relationship between Pb-B exposure and the activity of the enzyme delta-aminolevulinic acid dehydratase (ALAD) is generally inverse, with ALAD activity decreasing as Pb-B levels increase. ALAD activity tends to plateau at low enzyme activity for higher Pb-B levels. A 'no-effect' level of Pb-B exposure, particularly for iron-deficient children, is generally considered to be approximately 4 μg/dL. For workers, a Pb-B level of 10 μg/dL or above is typically considered as the 'no-effect' level. However, some reports suggest a minor decrease in hemoglobin occurs at a median Pb-B level around 5 μg/dL. For nephropathy to occur, prolonged exposure to Pb-B concentrations greater than 7 μg/dL is typically necessary. Preclinical neuropathy appears to occur at Pb-B levels between 4 and 5 μg/dL. Acute or chronic encephalopathy is observed at Pb-B concentrations of about 6–7 μg/dL in children and > 8 μg/dL in adults. Pb-B levels of 9–10 μg/dL have been associated with aminoaciduria, indicating reduced amino acid transport via the renal tubules. However, the effects on children may not be noticeable for months or years after initial exposure, making correlations challenging. Some studies report no associations between Pb-B levels and changes in blood components such as calcium, phosphorus, glucose, cholesterol, total proteins, serum albumins, alkaline phosphatase, lactate dehydrogenase, and urea nitrogen. However, others report slight increases in pyruvate levels after glucose administration in children with Pb-B levels between

4 and 6 μg/dL. The lack of temporal correlation between Pb-B exposure measurement and impact detection hinders establishing a definitive 'no-effect' level. Future studies should consider additional variables such as nutrition, socioeconomic status, and parental care.

14.2.3 Regulatory Limits

The Centers for Disease Control and Prevention (CDC) defines an elevated blood lead level as 5 μg/dL or higher. However, some studies suggest that even lower levels of lead exposure may be associated with health problems, particularly in children. The parameters included in Table 14.1 are carcinogenicity classification, oral slope factor, reference concentration, reference dose, and biological exposure indices. The carcinogenicity classification for lead compounds inorganic is listed as Group 2A by the International Agency for Research on Cancer (IARC) in 2004, which means it is "probably carcinogenic to humans." In contrast, lead compounds organic are classified as Group 3 by the World Health Organization (WHO) in 2000, which means they are "not classified as carcinogenicity to humans." Lead, on its own, is classified as Group A3 by the American Conference of Governmental Industrial Hygienists (ACGIH) as a confirmed animal carcinogen with unknown relevance to humans. It is also listed as Group B2 by the United States Environmental Protection Agency (EPA) in 2005, which means it is a probable human carcinogen. The oral slope factor (OSF), reference concentration (RfC), and reference dose (RfD) values for lead compounds inorganic and lead are not available. However, the EPA has classified lead compounds inorganic as a probable human carcinogen based on other available evidence. The biological exposure indices (BEIs) for lead in the blood are listed as 30 μg/dL for adults and 10 μg/dL for children by the Agency for Toxic Substances and Disease Registry (ATSDR). BEIs are guidelines for the interpretation of biological monitoring results, indicating the levels of exposure at which an individual may experience adverse health effects.

14.3 Bioassays Studies from E-Waste Recycling Sites

14.3.1 River State, Illoabuchi

Water samples contaminated by e-waste leachate, particularly enriched with heavy metals such as lead, were taken from River State near an e-waste recycling facility in Illoabuchi. The concentration of lead in these samples varied from 0.72 to 18.48 mg/L. These samples were tested on onions, catfish, and mice to observe the effects. Results showed that exposure to the e-waste leachate led to cytogenotoxicity in catfish, as observed by an increase in the frequency of micronuclei. The onion bulbs,

Table 14.1 Regulatory limits of lead compounds in inorganic and organic phases

Parameter		Information	Classification	Regulatory Bodies
Carcinogenicity classification	Lead compounds, inorganic	Group 2A[a]	Probably carcinogenic to humans	IARC 2004
	Lead compounds, organic	Group 3[b]	Not classified as carcinogenicity to humans	WHO 2000
	Lead	Group A3[c]	Confirmed animal carcinogen with unknown relevance to humans	ACGIH
		Group B2[d] Oral slope factor—not available RfC—not available RfD—not available	Probable human carcinogen	EPA (IRIS 2005)
Biological exposure indices (Pb-B)		30 μg/dL 10 μg/dL for children	NA	ATSDR

[a]Group 2A: IARC classified lead compounds as "probably carcinogenic to humans" in 2004 due to sufficient animal but limited human evidence
[b]Group 3: WHO categorized lead compounds in 2000 as unclassifiable for carcinogenicity due to inadequate evidence in both humans and animals
[c]Group A3: ACGIH labeled lead as a "confirmed animal carcinogen with unknown human relevance" due to strong animal evidence but unclear human relevance
[d]Group B2: EPA's IRIS classified lead as a "probable human carcinogen" in 2005 because of sufficient animal evidence and limited human evidence

when exposed to the e-waste leachate, demonstrated a dose-dependent increase in chromosomal aberrations, suggesting a clear link between increased leachate exposure and chromosomal damage. Mice exposed to the contaminated water exhibited signs of oxidative stress, marked by an increase in malondialdehyde (MDA) levels and a decrease in glutathione (GSH) levels in the liver. Furthermore, the mice showed indications of DNA damage, as denoted by increased tail length, tail moment, and olive tail moment in the comet assay. These results suggest the formation of reactive oxygen species (ROS) due to the presence of lead, leading to DNA damage. The findings underscore the potential risks associated with e-waste recycling sites and underscore the need for effective waste management practices to mitigate environmental and health impacts. The results also indicate cytogenotoxicity in catfish (*Clarias gariepinus*) and onions (*Allium cepa*), as well as oxidative stress in mice, all attributable to lead exposure from the e-waste (Babatunde and Anabuike 2015).

14.3.2 Lagos, Nigeria

E-waste leachate from two electronic marketplaces in Lagos, Nigeria, was examined for its potential cytotoxic and genotoxic effects. A range of assays were conducted on mice to analyze bone marrow micronucleus formation, bone marrow chromosome aberration, sperm chromosome aberration, sperm morphology, and sperm count. Results indicated that the chromosome aberration tests for bone marrow and spermatogonia showed a decrease in the mitotic index and an increase in various types of chromosome aberrations. Specifically, the bone marrow micronucleus assay showed a significant rise in the frequency of micronucleated polychromatic erythrocytes in mice, from $6.00 \pm 1.41‰$ in the control group to $14.67 \pm 1.70‰$ and $25.33 \pm 1.70‰$ in the two leachate-exposed groups, respectively. The bone marrow chromosome aberration assay revealed a significant decrease in the mitotic index (MI) in mice, from $3.10 \pm 0.26‰$ in the control group to $1.73 \pm 0.10‰$ and $1.36 \pm 0.12‰$ in the two leachate-exposed groups, respectively. There was also a significant increase in the frequency of various types of chromosome aberrations such as chromatid breaks, chromosomal fragments, and centromeric fusions in the leachate-exposed groups compared to the control group. In the sperm morphology assay, abnormal sperm morphology significantly increased from $5.60 \pm 1.35\%$ in the control group to $26.00 \pm 4.83\%$ and $35.00 \pm 3.36\%$ in the two leachate-exposed groups, respectively. The sperm count assay showed a significant decrease in the number of spermatozoa, from $63.60 \pm 5.84 \times 10^6$ in the control group to $33.80 \pm 3.20 \times 10^6$ and $18.40 \pm 3.19 \times 10^6$ in the two leachate-exposed groups, respectively. In the sperm chromosome aberration assay, the frequency of various types of chromosomal aberrations, such as chromatid breaks, chromosomal fragments, and centromeric fusions, increased significantly in the leachate-exposed groups compared to the control group. These results suggest DNA chain breakages, possibly caused by free radicals from the leachate or changes in pH that alter DNA structure (Alabi and Bakare 2011).

14.3.3 Nanyang River and Lianjiang River, Guiyu China

WIn Guiyu, a hub for e-waste recycling, comprehensive evaluations were conducted across multiple trophic levels and exposure phases at two local rivers. One of the primary focuses of this study was the concentration of metals such as lead in river sediments. Wang et al. (2009) investigated the environmental impact of e-waste recycling in Guiyu, China, with a specific focus on the Nanyang and Lianjiang rivers. Their findings revealed that the water and sediment samples collected from the Nanyang River exhibited substantially higher concentrations of heavy metals like lead, copper, and nickel, as compared to those from the Lianjiang River. Specifically, the lead, copper, and nickel levels in the water samples from the Nanyang River were 4.4, 4.9, and 3.3 times higher, respectively, than those in the Lianjiang River. In addition, sediment samples from the Nanyang River contained 15 times

more lead, 5 times more copper, and 6 times more nickel than the samples from the Lianjiang River. The study also encompassed an analysis of the levels of persistent organic pollutants (POPs) in sediment samples. The sediment samples from the Nanyang River revealed significantly higher concentrations of polychlorinated biphenyls (PCBs) and polycyclic aromatic hydrocarbons (PAHs) than those from the Lianjiang River. Specifically, the total concentration of PCBs in the Nanyang River's sediment samples was 11 times higher than that in the Lianjiang River. Similarly, the total concentration of PAHs in the Nanyang River's sediment samples was 5 times higher than that in the Lianjiang River. These results demonstrate that the e-waste recycling activities in Guiyu, particularly those occurring near the Nanyang River, have led to significant contamination of both heavy metals and POPs in the local aquatic and sediment ecosystems (Wang et al. 2009).

14.3.4 Epidemiological Studies

Numerous epidemiological studies have investigated the health risks associated with exposure to e-waste recycling sites. These studies have consistently shown that certain populations are at an increased risk of exposure, including the elderly, fetuses, pregnant women, people with impairments, and personnel who work in informal e-waste recycling sites. However, studies have consistently found that children are the most vulnerable group due to various exposure routes such as breastfeeding and placental exposures. Additionally, children often engage in high-risk activities such as hand-to-mouth behaviors, which increases the ingestion route exposure. Moreover, dermal contact with parents who work at e-recycling plants can also lead to increased exposure. Table 14.2 provides an overview of several epidemiological studies that have been conducted and categorized.

14.4 Lead Exposure Assessment in Guiyu E-Waste Site: Factors, Indicators, and Challenges

14.4.1 Lead Sources, Effects, and Assessment

Guiyu, located in Guangdong Province, China, hosts around 5500 companies involved in the recycling of obsolete electronics to recover valuable metals such as lead, gold, and copper. This industry engages tens of thousands of individuals and annually processes approximately 1.5 million pounds of electronic waste, including laptops, phones, and televisions. The lead exposure in Guiyu presents a significant public health concern, and numerous studies have explored the health impact of such exposure. The blood-lead (Pb-B) curve reflects the dynamic equilibrium between lead intake, blood lead concentration, and tissue deposition of lead, including in the

Table 14.2 Summary of Lead epidemiological studies conducted and categorized

Year of study	Exposure setting	Exposed population	Health effect
Reproductive health			
Xu et al. (2012) • A higher prevalence of low birth weight infants (< 2500 g) was found in the e-waste recycling area (10.6%) compared to the control area (6.2%), but this difference was not statistically significant	Informal recycling	Newborn infants (n = 531)	• Lead levels in cord blood were significantly higher (10.87 vs. 2.25 μg/dL, $p < 0.01$) in the recycling area
Growth			
Zheng et al. (2008) • Guiyu had significantly higher BLLs in children than the control area, with a statistically significant upward trend in BLLs with age ($p = 0.01$) • The mean child height in Guiyu was significantly shorter than in the control area ($p = 0.01$)	Ecological: exposed versus control	Children (1–7 years old, n = 154)	• In Guiyu, 70.8% of the people had Blood Lead Levels (BLLs) > 10 μg/dL, while in the control group, 20.1% of kids had BLLs > 2 μg/dL
• No significant difference in head diameter, chest circumference, height, or weight between the two groups was found	Ecological: exposed versus. control	Children (< 6 years old, n = 226)	• Blood lead levels were significantly higher in the exposed group (15.3 vs. 9.94 μg/dL, $p = 0.01$)

(continued)

Table 14.2 (continued)

Year of study	Exposure setting	Exposed population	Health effect
Mental health/nervous			
Liu et al. (2011) • There was no significant correlation between activity level, adaptation, disengagement approach temperament ratings, and elevated blood pressure	Ecological: exposed versus control	Children (aged 3–7 years, n = 303)	• Blood lead levels were significantly higher in the exposed group compared to the control group (13.2 vs. 8.3 μg/dL, $p < 0.001$)
Li et al. (2008) • Cord blood lead levels were significantly higher in the exposed group (11.3 vs. 6.0 μg/dL, $p < 0.001$) compared to the control group • Negative correlations were found between meconium lead levels and neonatal behavioral neurological assessment (NBNA) scores (38.45 vs. 38.93, $p = 0.043$) as well as behavioral clusters (10.91 vs. 11.29, $p = 0.012$) for activity tone and behavioral scores	Ecological: exposed versus control	Newborn babies (n = 152)	• Meconium lead levels were higher in the exposed group (2.5 vs. 1.2 mg/kg)

(continued)

Table 14.2 (continued)

Year of study	Exposure setting	Exposed population	Health effect
DNA Damage			
	Recycling activity	Recycle workers versus not exposed (n = 104)	Binucleated cells had 4.0% versus 1.0% chromosomal aberrations, $p < 0.01$. Serum IgE levels and binucleated cell micronuclei showed a positive correlation
Lung function			
Zeng et al. (2015) • Blood lead levels and cough were positively correlated with living in Guiyu (odds ratio 2.37; 95% confidence interval 1.30–4.32; $p = 0.01$) and B = 0.196, respectively	Ecological: exposed versus control	Children (3–8 years, n = 800)	• Children in Guiyu had higher rates of respiratory symptoms compared to those in Haojiang (cough, phlegm, dyspnea, and wheezing) with a p-value less than 0.05

bones. Though data is lacking on the precise metrics of the recycling operations, it is proposed that the lead levels likely fluctuate following the inhalation of a soluble lead compound. After initial exposure, lead is quickly eliminated in the urine and deposits in the tissues at a slower rate, followed by a redistribution in accordance with lead metabolism. Over an extended period, a steady-state equilibrium develops with absorption, deposition, and excretion of lead occurring at a constant rate. Irregular variations in lead dose can complicate the determination of how rapidly this equilibrium (and Pb-B level) changes. The amount of lead excreted in the urine either spontaneously or after the administration of a chelating agent can serve as an indicator of the quantity of lead absorbed. However, estimating an individual's absorbed lead quantity solely from urine excretion can be challenging. The urinary excretion of lead is influenced by numerous factors, including the blood lead level, which is an indicator of absorption. Lead elimination following chelation therapy is thought to reflect the body's total lead burden and is more sensitive to over-exposure and excess absorption than the blood lead level. Long-term lead exposure can be inferred from examining lead levels in bones, teeth, hair, and other tissues. Blood delta-aminolevulinic acid dehydratase (ALAD) activity, urinary excretion of aminolevulinic acid (ALA) and coproporphyrin (CP), and erythrocyte protoporphyrin IX levels serve as indicators of disrupted porphyrin metabolism. Although blood lead level influences ALA and CP excretion, it doesn't impact their production. Their excretion declines immediately upon cessation of exposure, indicating a measure of average long-term exposure level. Early signs of renal and neurological damage can be detected through the presence of basophilic stippling and increased hemoglobin levels during hematological examination. The majority of studies only provide conclusions about differences between groups with varying exposure, which complicates the determination of a non-observable or lowest observable adverse effect level (NOAEL or LOAEL). Furthermore, given the limited number of workers exposed to lead, drawing definitive conclusions has been challenging. When blood lead level measurements are used in large populations, effects may become discernible even at low exposures. The concurrent use of sensitive methods further complicates the assessment of whether observed impacts should be considered detrimental, indicative of health risks, and relevant for risk assessment.

14.4.2 Dose–Effect Relationships and Effects of Lead Exposure on Different Body Systems

Lead exposure, a public health concern, is assessed via blood-lead (Pb-B) levels. But Pb-B levels alone don't indicate exposure mode. For prolonged exposure, dose–effect correlations based on Pb-B levels are necessary. Despite limited data for reliable dose–effect curves, the dose–effect relationship of lead exposure can be estimated for certain effects. The inverse relationship between Pb-B concentrations and ALAD levels has been observed, and increased Pb-B corresponds to decreased ALAD.

Similarly, Pb-B levels correlate with ALA levels exponentially. No-effect levels are challenging to determine due to lacking reference data, especially below 9–10 μg/dL Pb-B. High Pb-B can cause erythrocyte membrane damage and nephropathy above 7 μg/dL. Subclinical peripheral alterations and cerebral malfunction may occur at 4 μg/100 ml and 5 μg/dL in children and seniors respectively. Acute or chronic encephalopathy can occur in children at 6 μg/dL and adults over 8 μg/dL. Yet, establishing links between Pb-B levels and effects in children can be challenging due to delayed onset of effects. Future studies need to consider factors like diet, socioeconomic status, and childcare to establish solid dose–effect and dose–response connections. The current no-effect values seem conservative, but solid dose–response data are lacking.

Table 14.3 presents no-effect concentrations of Pb-B in terms of μg/dL in blood for different effects and populations. Figure 14.1 summarizes available knowledge on dose–response relationships based on observed relative frequencies of effects at specific dose levels, highlighting 5% response levels. However, more research is needed to determine Pb-B levels for 0.5 and 1% response rates.

Zielhuis (1975) provides further analysis of response rates, aligning with Hernberg's (1975) predictions. Dose–response relationships consider the relative frequency of an effect's occurrence at a specific dose level. While some data is available, more comprehensive studies are needed to improve understanding of lead's dose–response relationships. An observed relative frequency of an effect's occurrence in a collection of participants at a specific dose level is considered in a dose–response relationship. Similar to dose–effect relationships, there is either insufficient

Table 14.3 List of no-effect concentrations in terms of Pb-B μg/dL of blood

No detected effect level of Pb-B (μg/dL)	Effect	Population
Less than 1	Erythrocyte ALAD inhibition FEP	Children, Adults Children
2–2.5	FEP	Adults (female)
2–3	FEP	Adult (male)
2.3–3.5	Erythrocyte ATPase inhibition	General
3–4	ALA exertion in urine	Children, Adults
4	Coproporphyrin (CP) excretion in urine	Adults, children
4	Anaemia	Adult
4–5	Peripheral neuropathy	Adult
5	Anaemia	Children
5–6	Minimal brain dysfunction	Adult
6–7	Minimal brain dysfunction encephalopathy	Children
8 and above	Encephalopathy	Adults

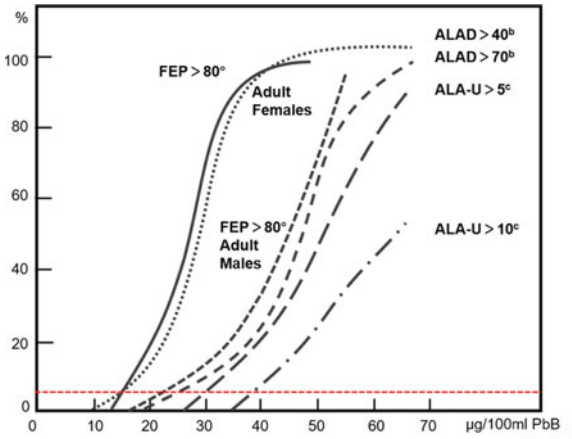

Fig. 14.1 Dose–response relationships for some effects of lead Hernberg's (1975)

or no data to assess a dose–response relationship. Figure 14.1, the dose–response relationships for various effects of lead, summarize the knowledge on dose–response relationships that is currently available. These relationships are based on observed relative frequencies of each effect's occurrence in a collection of participants at specific dose levels. The figure highlights the 5% response levels, which represent the amount of Pb-B at which not more than 5% of the total cohort is expected to demonstrate the stated intensity of a defined effect. While these levels provide valuable information, additional investigations are needed to determine the Pb-B levels that correspond to 0.5 and 1% response rates. Such investigations would increase the available data volume and improve our understanding of the dose–response relationships for lead. For further information, Zielhuis (1975) provides an analysis of response rates in Table 14.4 that concurs with Hernberg's (1975) predictions.

Table 14.4 Pb-B concentrations below which 5% or less of the population will exhibit the given degree of effect Zielhuis (1975)

Biochemical effect	Intensity of effect	Population	Pb-B (µg/dL)
ALAD inhibition	Perceptible inhibition	Adults, children	1
	> 40% inhibition	Adults	1.5–2
	> 70% inhibition	Adults	3
	> 70% inhibition	Children	2.5–3
ALA-U	Perceptible increase	Adults, children	4
	> 10 mg/L	Adults, children	5
FEP	Perceptible increase	Adults (male)	3
		Adults (female)	2.5
		Children	2

14.5 Risk Assessment of Lead Exposure in Guiyu E-Waste Site

14.5.1 Risk Assessment

Risk assessment encompasses qualitative and quantitative evaluation, with dose–response analysis crucial for examining a substance's adverse effects. Quantitative assessment combines exposure assessment and dose–response analysis. The E.U. expert committees utilize the Margin of Safety (MoS) or Margin of Exposure (MoE), comparing the No Observable Adverse Effect Level (NOAEL) in animals to the human exposure level, to gauge acceptable exposure (Nordberg et al. 2014). Safe exposure levels should prioritize vulnerable groups such as children and pregnant women, as their data are vital for risk management and regulation development.

Severity Analysis of Lead Exposure
Lead exposure can cause severe effects like coma, anemia, colic, neuropathy, nephropathy, infertility, and sterility. Most of the lead combines with erythrocytes, disseminates to soft tissues, and remains stored in bones for 10–20 years (Abadin et al. 2007; Nordberg et al. 2014). However, stored lead can reenter the body and affect organs. The Permissible Exposure Limit (PEL) is set at 0.5 g/m^3, with 95% of exposed individuals having blood lead levels under 5 g/dL after around 40 years of occupational exposure. During the first year of exposure, lead levels increase drastically but eventually stabilize, primarily accumulating in bones. Guiyu, China, infamous for its uncontrolled e-waste processing, serves as our case study. An estimated 60–80% of local households participate in this industry (Guo et al. 2010), resulting in high lead concentrations in the area's dust and silt (Leung et al. 2008; Wong et al. 2007).

Possibility Analysis of Lead Exposure
Careless practices like burning e-waste or dissolving it in strong acids without sufficient protection can release considerable amounts of lead. Lead from cathode ray tubes, printed circuit boards, light bulbs from obsolete TVs, and batteries is released into the environment due to these reckless practices. Lead exposure can occur through inhalation, ingestion, and skin absorption (Grant et al. 2013). This increases the risk of lead exposure for residents, particularly seniors, working adults, and children. Figure 14.2 illustrates the intake of lead from electronic waste.

14.5.2 Lead Exposure Modeling

The risk assessment of lead (Pb) exposure significantly depends on available data to evaluate the population's adverse effects. There are three primary models to assess Pb

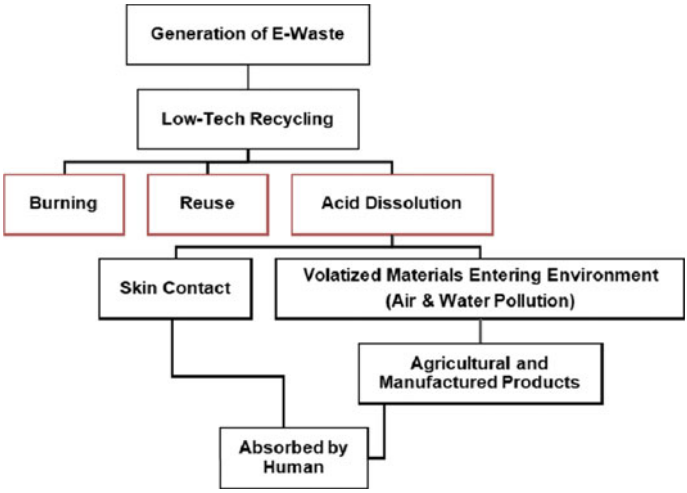

Fig. 14.2 Route of Pb absorbed from e-waste to humans

exposure, namely the O'Flaherty, Integrated Exposure Uptake BioKinetic (IEUBK), and Leggett models (Table 14.5).

Table 14.5 Models of lead exposure

Model	O'Flaherty (National Academics of Science, Engineering, and Medicine 2020)	Integrated exposure uptake BioKinetic (IEUBK) (Moon et al. 2020)	Leggett (1993)
Simulates	Pb kinetics from birth through adulthood	Pb in children	Pb kinetics from birth through adulthood
Methods applied by model	Physiological base on volume, flows, composition, and metabolic activity on blood and bone	Multicompartmental kinetic data from animal and human studies used to calculate lead's age-specific transmission rate coefficients	Model not explained
Rate of uptake (Pb absorbed per unit time)	Uptake = Intake Dosage × Frequency (Intake)	Model not explained	Model not explained

14.5.3 Hazard Quotient (HQ) Calculation

The HQ is calculated as the dose over the reference dosage. HQ scores above 10 indicate a significant chronic risk, a HQ of 1 implies unlikely adverse health impacts, and a HQ > 1 suggests potential health risks (Leung et al. 2008). The tolerable daily Pb intake for an adult with an average body mass of 60 kg and an oral RfD of 3.5 μg/kg/day (Ara and Usmani 2015) is 210 μg. The HQ for adults is 100.41, while for a child, it is a staggering 200.91. In other words, Pb exposure levels are 10–20 times higher than levels representing chronic risk.

14.5.4 Calculations of Lead Exposure to Adults and Children at Guiyu

The potential dangers of inhaled dose, skin contact dose, and per-day dose (ingestion) have been evaluated. The formulas for these calculations are adapted from the EPA's guidelines and Ara and Usmani's (2015) work. The person breathed a dose of the substance. However, the dose absorbed by skin contact with polluted river sediments is described by the equation above. Finally, the quantity of lead consumed can be determined by solving for the Average Daily Dose (ADD). For this analysis, InhR = 7.6 m^3 day^{-1} (Bowers 2021). Dust ingestion rates, IngR, are conservatively estimated at 100 mg/day for adults and 200 mg/day for children. The exposure duration (ED) of 6 years is estimated to be an average of 2190 days. In this study, SA = 2800 cm^2 for skin exposure, and SL (Skin Adhesion Factor) is calculated to be 0.2 mg cm^2 day^{-1}. In this study, the dermal absorption factor was set at 0.001, and the particle emission factor was calculated to be 1.36×10^9 m^3 kg^{-1} (Ara and Usmani 2015). The average body weight (BW) was considered to be BW = 15 kg for children and BW = 60 kg for adults (Leung et al. 2008). The hazard quotient measures the non-carcinogenic risk of lead metals. The 'RfD' is the chronic reference dose of lead (mg kg^{-1} d^{-1}), and the 'CDI (E)' is the chronic daily intake (exposure) (Liu et al. 2013). The Pb content in a PCB recycling factory is calculated using the dose determined by Leung et al. (2008), which was 61,200–110,000 mg/kg.

14.5.5 Root Cause Analysis

A study on lead poisoning situations in China, conducted by interviewing personnel from four provinces, revealed several causes for the persistent problem of lead poisoning in rural areas (Cohen and Amon 2012). The primary reason was ignorance. Many households in high-lead areas could learn about the dangers of lead and how to prevent or treat lead poisoning, yet failed to do so. Information was primarily spread by word of mouth, leading to a lack of detail and uncertainty. Excessive

government suppression and harassment of environmental activists, journalists, and parents of lead-affected children were highlighted as the second cause. Chinese law's 2008 Measures on Open Environmental Information require that complaints made to Environmental Protection Bureau websites, and the outcomes of any investigations into those complaints, be made public. However, government authorities often fail to take immediate action in resolving lead pollution accusations or fail to publicize the investigation findings as required by law. Finally, the execution of environmental remediation, compensation, and relocation methods was often insufficient and partial. Depending on the province, residents in lead-contaminated areas may be offered a one-time payment to settle any potential claims against the company for medical expenses, lost wages, or relocation costs. However, this often isn't enough to help a family recover after moving.

14.6 Conclusion

Lead exposure in e-waste recycling areas in Guiyu, China represents a significant public health threat, particularly for children. Even though the reduction of lead in fuels and paints has been implemented in many places, e-waste recycling activities have led to persistent lead poisoning. Scientific evidence suggests that even low levels of lead in the blood can negatively impact children's cognitive abilities and growth. Lead exposure continues to pose urgent public health issues, especially for children. Therefore, implementing stricter manufacturing processes controls, improving workers' health protections, enhancing health education, and improving diagnostic and therapeutic options are necessary. Taking these steps will be pivotal in mitigating lead poisoning in rural China and protecting the health and well-being of its residents.

Competing Interests All authors declare no Competing Financial or Non-Financial Interests.

Data Availability The data that support the findings of this study are available from the corresponding author upon reasonable request.

Conflicts of Interest Statement This study received funding from Enerstay Sustainability Pte. Ltd. (Singapore) Grant Call (Call 1/2022)_GHG (Project ID VS1-001), Singapore. The funder was not involved in the study design, collection, analysis, interpretation of data, the writing of this article or the decision to submit it for publication. All authors declare no other competing interests.

References

Abadin H, Ashizawa A, Stevens Y-W, Llados F, Diamond G et al (2007) Bicological profile for lead: agency for toxic substances and disease registry (U.S.), Atlanta (G.A.); Damstra T (1977) Oxicological properties of lead

Alabi OA, Bakare AA (2011) Genotoxicity and mutagenicity of electronic waste leachates using animal bioassays. Toxicol Environ Chem 93(5):1073–1088. https://doi.org/10.1080/02772248.2011.561949

Ara A, Usmani JA (2015) Lead toxicity: a review. Interdisc Toxicol 8(2):55

Babatunde T, Anabuike F (2015) In vivo cytogenotoxicity of electronic waste leachate from lloabuchi electronic market, Diobu, Rivers State, Nigeria on *Allium cepa*. Challenges (20781547) 6(1):173–187. https://doi.org/10.3390/challe6010173

Bowers TS (2021) Relating environmental lead and arsenic exposure to observed levels in humans. Pract Appl Med Geol 263–286

Cohen JE, Amon JJ (2012) Lead poisoning in China: a health and human rights crisis 14(2):74–86; Schnur J, John RM (2014) Childhood lead poisoning and the new centers for disease control and prevention guidelines for lead exposure. J Am Assoc Nurse Pract 26(5):238–247. https://doi.org/10.1002/2327-6924.12112

Grant K, Goldizen FC, Sly PD, Brune M-N, van den Neira M, Berg M, Norman RE (2013) Health consequences of exposure to e-waste: a systematic review. Lancet Glob Health 1(6):e350–e361. https://doi.org/10.1016/52214-1098(13)70101-3

Guo Y, Huo X, Li Y, Wu K, Lu J, Huang J, Xu X (2010) Monitoring of lead, cadmium, chromium and nickel in placenta from an e-waste recycling town in China. Sci Total Environ 408(16):3113–3117. https://doi.org/10.1016/j.scitotenv.2010.04.018

Julander A, Lundgren L, Skare L, Grander M, Palm B, Vahter M, Liden C (2014) Formal recycling of e-waste leads to increased exposure to toxic metals: an occupational exposure study from Sweden. Environ Int 73:243–251. https://doi.org/10.1016/j.envint.2014.07.006

Leggett RW (1993) An age-specific kinetic model of lead metabolism in humans. Environ Health Perspect 101(7):598–616

Leung AOW, Duzgoren-Aydin NS, Cheung KC, Wong MH (2008) Heavy metals concentrations of surface dust from e-waste recycling and its human health implications in southeast China. Environ Sci Technol 42(7):2674–2680. https://doi.org/10.1021/es071873x

Li Y, Xu X, Wu K, Chen G, Liu J, Chen S, Gu C, Zhang B, Zheng L, Zheng M, Huo X (2008) Monitoring of lead load and its effect on neonatal behavior neurological assessment scores in Guiyu, an electronic waste cycling town in China. J Environ Monit 10(10):1233–1238. https://doi.org/10.1039/8804959j.neuro.2011.03.012

Liu J, Xu X, Wu K, Plao Z, Huang J, Guo Y, Li W, Zhang Y, Chen A, Huo X (2011) Association between lead exposure from electronic waste recycling and child temperament alterations. NeuroToxicology (4):458–464. https://doi.org/10.1016/j.neuro.2011.03.012

Liu X, Song Q, Tang Y, Li W, Xu J, Wu J, Brookes PC (2013) Human health risk assessment of heavy metals in soil-vegetable system: a multi-medium analysis. Sci Total Environ 463–464:530–540. https://doi.org/10.1016/scotenv.2013.06.064; Mason LH, Harp JP, Han DY (2014) Pb neurotoxicity: neuropsychological effects of lead toxicity

Moon WK, Atique U, An KG (2020) Ecological risk assessments and eco-toxicity analyses using chemical, biological, physiological responses, DNA damages and gene-level biomarkers in Zebrafish (*Danio rerio*) in an urban stream. Chemosphere 239:124754

National Academies of Sciences, Engineering, and Medicine (2020) Committee's review of the DoD-O'Flaherty model. In: Review of the department of defense biokinetic modeling approach in support of establishing an airborne lead exposure limit. National Academies Press, USA

Nordberg GF, Fowler BA, Nordberg M (2014) Handbook on the toxicology academic press of metals. BioMedearch International; Oflaherty EJ (1993) Physiologically based models for bone-seeking elements. Toxicol Appl Pharmacol 118(1):16–29. https://doi.org/10.1006/taap.1993.1004

Wang F, Leung AOW, Wu SC, Yang MS, Wong MH (2009) Chemical and ecotoxicological analyses of sediments and elutriates of contaminated rivers due to e-waste recycling activities using a diverse battery of bioassays. Environ Pollut 257(7):2082a090. https://doi.org/10.1016/j.envpol.2009.02.015

Wong CSC, Duzgoren Aydin NS, Aydin A, Wong MH (2007) Evidence of excessive releases of metals from primitive e-waste processing in Guiyu, China

Xu X, Yang H, Chen A, Zhou Y, Wu K, Liu J, Huo X (2012) Birth outcomes related to informal e-waste recycling in Guiyu, China. Reprod Toxicol 33(1):94–98. https://doi.org/10.1016/j.reprotox.2011.12.006

Zeng X, Xu X, Zheng X, Reponen T, Chen A, Huo X (2015) Heavy metals in PM2.5 and in blood, and children's respiratory symptoms and asthma from an e-waste recycling area. Environ Pollut 210:346–353. https://doi.org/10.1016/j.envpol.2016.01.025

Zheng L, Wu K, Li Y, Qi Z, Han D, Zhang B, Gu C, Chen G, Liu J, Chen S, Xu X, Huo X (2008) Blood lead and cadmium levels and relevant factors among children from an e-waste recycling town in China. Environ Res 10(1):15–20. https://doi.org/10.1016/j.envres.2008.04.002

Chapter 15
Evaluation Method of Rural Revitalization Boosted by Water Conservancy

Guofang Wu, Tian Zhang, Bin Liu, Tianpeng Ruan, Fei Chen, and Baijun Liang

Abstract Water conservancy is a fundamental guarantee for implementing national strategies such as rural revitalization in China. Previous studies mainly focused on water resources of rivers and lakes, while studies about water conservancy promoting rural revitalization were rare. In this study, a set of scientific evaluation method of rural water conservancy construction is formulated based on the five objectives of the rural revitalization strategy by using analytic hierarchy process (AHP) and fuzzy membership function method. The results indicate that the typical case of Jingning County in China can meet the general requirements of the national rural vitalization strategy and prompt the construction and development of beautiful rivers and lakes in Zhejiang Province of China. This study provides theoretical guidance and practical basis for implementing the strategy of rural revitalization boosted by water conservancy.

Keywords Water conservancy · Rural revitalization · Analytic hierarchy process · Fuzzy membership function method

G. Wu · T. Ruan · F. Chen · B. Liang (✉)
Shaoxing Water Conservancy and Hydropower Survey and Design Institute Co., Ltd., Shaoxing 312000, China
e-mail: 45993804@qq.com

T. Zhang
National Research Institute for Rural Electrification, Hangzhou 310012, China

B. Liu
School of Traffic and Transportation Engineering, Changsha University of Science and Technology, Changsha 410114, China

Z. Sun and P. K. Das (eds.), *Proceedings of the 10th International Conference on Energy Engineering and Environmental Engineering*, Environmental Science and Engineering, https://doi.org/10.1007/978-3-031-48204-5_15

15.1 Introduction

Water conservancy is not only the lifeblood of rural revitalization strategy development, but also the critical factor of modern agriculture and rural development, and even the important indicator of national economic and social development (Adeel 2017). Water conservancy plays a very important guiding and supporting role in resisting drought and flood disasters, ensuring the safety of drinking water in rural areas, accelerating the development of rural industries, optimizing rural living environment, deepening and inheriting rural culture and civilization (Anderson et al. 2019; Ladson et al. 1999). The significance of implementing the strategy of rural vitalization issued by the Chinese government puts forward the general goals of rural vitalization of "Thriving Industry, Livable Ecology, Civilized Rural Custom, Effective Governance and Prosperous Life", which gives new meaning, new orientation and new direction to rural water conservancy work in the new period (Le and Qiu 2002). Therefore, establishing a set of scientific and reasonable evaluation index system of water-conservancy-assisted rural revitalization to evaluate the degree and level of rural revitalization can not only provide data support for the evaluation, prediction and correction of the progress of rural revitalization boosted by water conservancy, but also provide basis and reference for the implementation of the strategic plan (Chuan 2000; Babel and Shinde 2020).

The evaluation of water conservancy high-quality development is a multi-level comprehensive evaluation. Yang et al. (2020) carried out a study on river health and water resources management in 2021. However, there are few studies on rural revitalization boosted by water conservancy. At present, most scholars stay in the research of river & lake health and water resources (Huang et al. 2015; Jia 2016; Sadat et al. 2020; Gain and Giupponi 2015), or just make a summary discussion from the perspective of water resources policy, planning and management (Doolan and Hart 2017; Liu et al. 2022). Studies have also been conducted on the relationship between river health and human activities. However, few scholars have studied the ability of rural revitalization boosted by water conservancy.

15.2 Materials and Methods

15.2.1 Index System Construction

The research innovation of this article is based on the study of human-water relations (see Fig. 15.1), constructing an evaluation system for the ability of water conservancy to promote rural revitalization. Through field investigation and referring to relevant literature (Zhai et al. 2016; Wang and Xu 2016), the main index factors of rural water conservancy construction are selected preliminarily, the relevance and representativeness between evaluation index and each criterion layer are statistically sorted out, and the indicators with overlapping functions are merged.

Fig. 15.1 Human-water relationships concept map

Effective Governance, Civilized Rural Custom (Luo et al. 2018), Livable Ecology (Cheng et al. 2018), Thriving Industry and Prosperous Life (Friesen et al. 2017) are the five Criterion Layers that are finally The technical route adopted in this paper is shown in Fig. 15.2.

15.2.2 Study Area and Data Source

Jingning County is located in the southwest mountainous area of Zhejiang Province, China, as shown in Fig. 15.3.

15.2.3 Assessment Process

(1) Judgment matrix construction

The evaluation index judgment matrix compares the importance of each index to a factor in the upper layer in pairs, where A is the judgment matrix, *Aij* represents the comparison result of the importance of factor *i* to factor *j*. The importance can be reflected by quantitative digital scale from 1 to 9, and the proportion of each index in the target layer can be determined by the expert scoring method, as shown Table 15.1.

The judgment matrix of the five criterion layers and the weight vectors of their index layers are shown in Tables 15.2, 15.3, 15.4, 15.5 and 15.6.

(2) Membership calculation

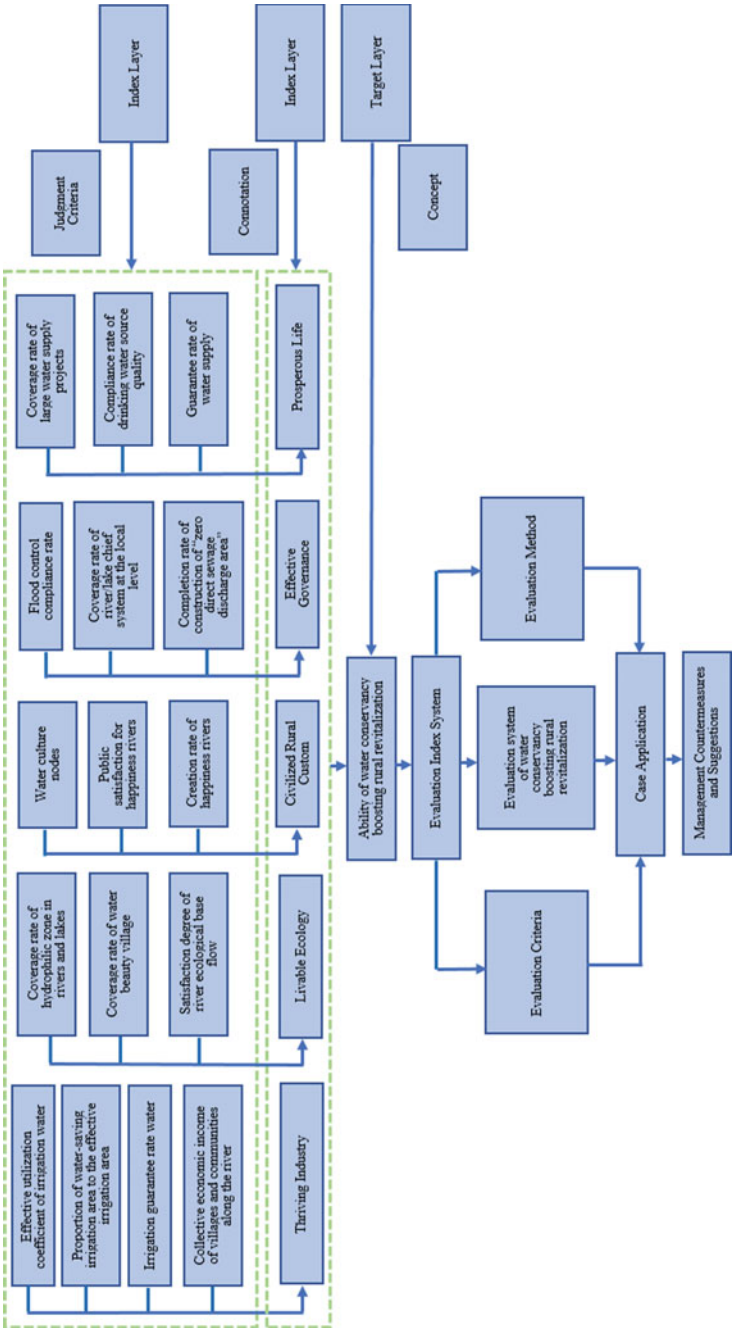

Fig. 15.2 Framework of evaluation index system for rural revitalization boosted by water conservancy

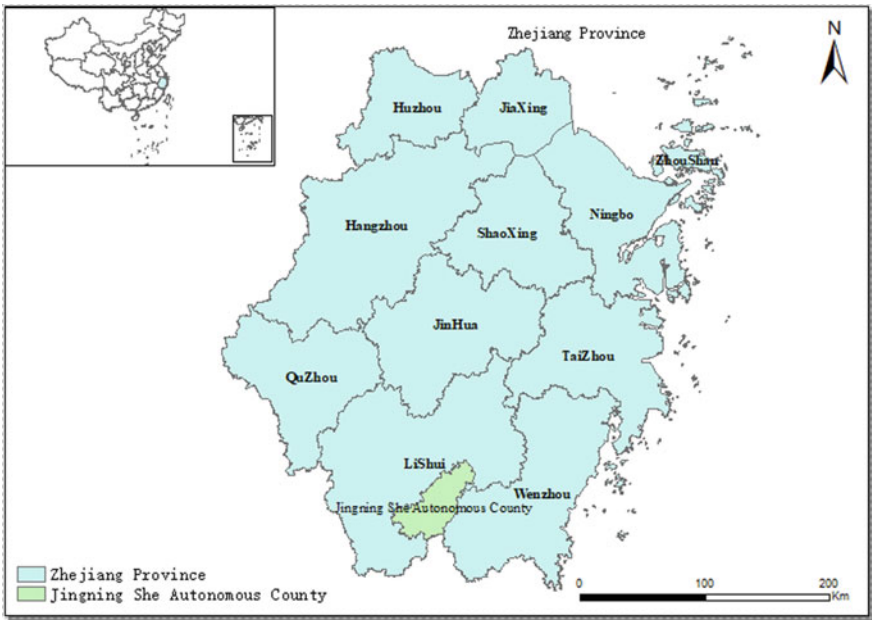

Fig. 15.3 Geographic location map

Table 15.1 Judgment matrix of five items in the criterion layer (A)

A	A1	A2	A3	A4	A5
A1	1	3	5	1	1
A2	1/3	1	3	3	1
A3	1/5	1/3	1	1/3	1/5
A4	1	1/3	3	1	1
A5	1	1	5	1	1

Table 15.2 Judgment matrix of 4 items in thriving industry (A1)

Thriving industry	A11	A12	A13	A14
A11	1	1	1	1/3
A12	1	1	1	1/3
A13	1	1	1	1/3
A14	3	3	3	1
$\omega_{11} = 0.1667, \omega_{12} = 0.1667, \omega_{13} = 0.1667, \omega_{14} = 0.5$				

Table 15.3 Judgment matrix of 3 items in livable ecology (A2)

Livable ecology	A21	A22	A23
A21	1	1	1/3
A22	1	1	1/3
A23	3	3	1
$\omega_{21} = 0.2, \omega_{22} = 0.2, \omega_{23} = 0.6$			

Table 15.4 Judgment matrix of 3 items in civilized rural custom (A3)

Civilized rural custom	A31	A32	A33
A31	1	1	1
A32	1	1	1
A33	1	1	1
$\omega_{31} = 0.33, \omega_{32} = 0.33, \omega_{33} = 0.33$			

Table 15.5 Judgment matrix of 3 items in effective governance (A4)

Effective governance	A41	A42	A43
A41	1	3	3
A42	1/3	1	1
A43	1/3	1	1
$\omega_{41} = 0.6, \omega_{42} = 0.2, \omega_{43} = 0.2$			

Table 15.6 Judgment matrix of 3 items in prosperous life (A5)

Prosperous life	A51	A52	A53
A51	1	1	1
A52	1	1	1
A53	1	1	1
$\omega_{51} = 0.33, \omega_{52} = 0.33, \omega_{53} = 0.33$			

The fuzzy membership function method is used to map all indexes to [0,1] (Liu et al. 2022), and the membership values corresponding to the feature node values are 0, 0.3, 0.6, 0.8 and 1.0 respectively. The membership function value of each single index is calculated in Tables 15.7 and 15.8.

15.3 Results

The calculation results (see Fig. 15.4) show that in rural revitalization of Jingning County Thriving Industry ($\omega_1 = 0.3005$) is the most important basic factor, followed by Livable Ecology ($\omega_2 = 0.2318$), Prosperous Life ($\omega_5 = 0.2299$), Effective Governance ($\omega_4 = 0.1829$), and Civilized Rural Custom ($\omega_3 = 0.0549$) is the last.

Table 15.7 Characteristic value and membership degree of evaluation index of rural revitalization boosted by water conservancy

Index layer	Scoring criteria					Membership degree
	Optimal value e(f)	Better value d(g)	Pass value c(h)	Worse value b(i)	Worst value a(j)	
A11 Effective utilization coefficient of irrigation water	1	0.65	0.55	0.5	0.45	0.7
A12 Proportion of water-saving irrigation area to the effective irrigation area	100	85	70	50	30	0.6
A13 Irrigation guarantee rate	100	90	80	65	50	0.8
A14 Collective economic income of villages and communities along the river	100	95	50	10	5	0.8
A21 Coverage rate of hydrophilic zone in rivers and lakes	86	85	75	65	50	0.7
A22 Coverage rate of water beauty village	86	85	75	65	50	0.7
A23 Satisfaction degree of river ecological base flow	100	98	90	80	60	0.9
A31 Water culture nodes	9	8	6	3	1	0.7
A32 Public satisfaction for happiness rivers	100	95	80	60	30	0.7
A33 Creation rate of happiness rivers	100	95	80	60	30	0.7
A41 Flood control compliance rate	100	95	80	75	50	0.8
A42 Coverage rate of river/lake chief system at the local level	100	95	80	65	50	0.7
A43 Completion rate of construction of "zero direct sewage discharge area"	100	95	80	65	50	0.9
A51 Coverage rate of large water supply projects	100	95	80	60	40	0.8
A52 Compliance rate of drinking water source quality	100	98	85	75	60	0.7
A53 Guarantee rate of water supply	100	95	80	65	50	0.9

Based on the membership value of the single index, the comprehensive evaluation results of the five criterion layers are obtained according to the weighted calculation. The calculation formula is as follows (Sadat et al. 2020; Liu et al. 2021):

$$I_x = \sum_{i=1}^{n_1} w_{1i} G_1^i \tag{15.1}$$

Table 15.8 Evaluation index and standard value of water conservancy boosting rural revitalization

Target layer	Criterion layer	Index layer	Index characteristics	Unit	Grade I (Excellent)	Grade II (Good)	Grade III (Pass)	Grade IV (Poor)	Grade V (Very poor)
Ability of water conservancy boosting rural revitalization	A1 Thriving Industry	A11 Effective utilization coefficient of irrigation water	Positive	%	≥ 0.65	[0.55, 0.65)	[0.5, 0.55)	[0.45, 0.5)	< 0.45
		A12 Proportion of water-saving irrigation area to the effective irrigation area	Positive	%	[85, 100]	[70, 85)	[50, 70)	[30, 50)	< 30
		A13 Irrigation guarantee rate	Positive	%	[90, 100]	[80, 90)	[65, 80)	[50, 65)	< 50
		A14 Collective economic income of villages and communities along the river	Positive	10,000 RMB	≥ 95	[50, 95)	[10, 50)	[5, 10)	< 5
	A2 Livable ecology	A21 Coverage rate of hydrophilic zone in rivers and lakes	Positive	%	≥ 85	[75, 85)	[65, 75)	[50, 65)	< 50
		A22 Coverage rate of water beauty village	Positive	%	≥ 85	[75, 85)	[65, 75)	[50, 65)	< 50
		A23 Satisfaction degree of river ecological base flow	Positive	%	[98, 100]	[90, 98)	[80, 90)	[60, 80)	< 60
	A3 Civilized rural custom	A31 Water culture nodes	Positive	Pieces	≥ 8	[6, 8)	[3, 6)	[1, 3)	0
		A32 Public satisfaction for happiness rivers	Positive	%	[95, 100]	[80, 95)	[60, 80)	[30, 60)	< 30
		A33 Creation rate of happiness rivers	Positive	%	[90, 100]	[80, 90)	[60, 80)	[30, 60)	< 30

(continued)

Table 15.8 (continued)

Target layer	Criterion layer	Index layer	Index characteristics	Unit	Grade I (Excellent)	Grade II (Good)	Grade III (Pass)	Grade IV (Poor)	Grade V (Very poor)
	A4 Effective governance	A41 Flood control compliance rate	Positive	%	[95, 100]	[80, 95)	[75, 80)	[50, 75)	< 50
		A42 Coverage rate of river/lake chief system at the local level	Positive	%	[95, 100]	[80, 95)	[65, 80)	[50, 65)	< 50
		A43 Completion rate of construction of "Zero direct sewage discharge area"	Positive	%	[95, 100]	[80, 95)	[65, 80)	[50, 65)	< 50
	A5 Prosperous life	A51 Coverage rate of large water supply projects	Positive	%	[95, 100]	[80, 95)	[60, 80)	[40, 60)	< 40
		A52 Compliance rate of drinking water source quality	Positive	%	[98, 100]	[85, 98)	[75, 85)	[60, 75)	< 60
		A53 Guarantee rate of water supply	Positive	%	[95, 100]	[80, 95)	[65, 80)	[50, 65)	< 50

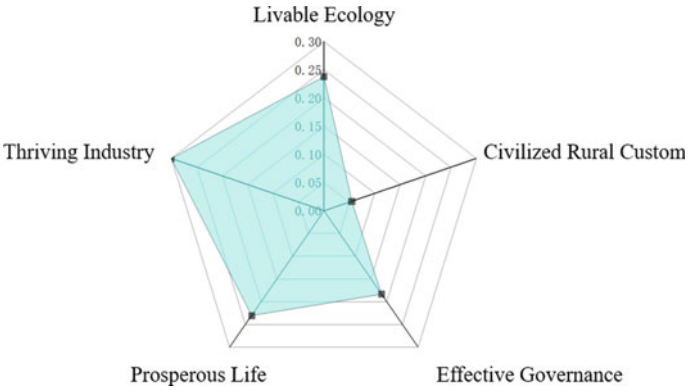

Fig. 15.4 Evaluation impact result diagram

where n_1, n_2, n_3, n_4, n_5 refers to the number of evaluation indexes in the five criterion layers of Thriving Industry, Livable Ecology, Civilized Rural Custom, Effective Governance and Prosperous Life respectively; w_{1i}, w_{2j}, w_{3k}, w_{4l}, w_{5m} respectively are the weights of indicators in each criterion layer relative to this criterion layer; G_1^i, G_2^j, G_3^k, G_4^l, G_5^m are the membership values of Index i, j, k, l and m in the criteria layer of Thriving Industry, Livable Ecology, Civilized Rural Custom, Effective Governance and Prosperous Life respectively.

$$I_{TI} = 0.75, I_{LE} = 0.82, I_{CRC} = 0.70, I_{EG} = 0.80, I_{PL} = 0.8$$

For each criterion layer index, see Fig. 15.5. Where w_1, w_2, w_3, w_4, w_5 are the weights corresponding to the five criteria of Thriving Industry, Livable Ecology, Civilized Rural Custom, Effective Governance and Prosperous Life under the target layer respectively.

$$w_1 = 0.3005, w_2 = 0.2318, w_3 = 0.0549, w_4 = 0.1829, w_5 = 0.2299$$

Combined with Formula 1–5, the value of I_{wcrr} is calculated.

$$I_{wcrr} = I_{TI}w_1 + I_{LE}w_2 + I_{CRC}w_3 + I_{EG}w_4 + I_{PL}w_5 = 0.78$$

This evaluation system is mainly used to evaluate the rural revitalization capacity in different regions and at different times, and to identify key constraints. The index of rural revitalization boosted by water conservancy in Jingning is 0.78, indicating that the capacity is relatively strong.

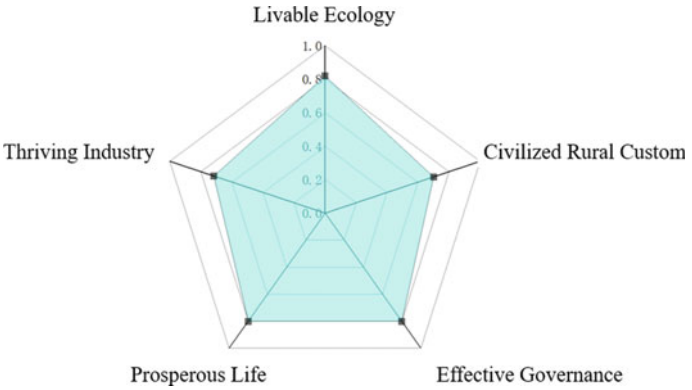

Fig. 15.5 Criterion layer index results graph

15.4 Conclusions

The hilly areas represented by Jingning have a relatively strong rural revitalization capacity boosted by water conservancy. Thriving Industry is the most important basic factor in rural revitalization boosted by water conservancy, and the collective economic income of villages and communities along the river has the greatest impact on Thriving Industry. The indicators under the criterion layer of Civilized Rural Custom are most easily ignored because their current effect of helping rural revitalization is not obvious.

The evaluation system of water conservancy boosting rural revitalization should be a dynamic evaluation process, and the evaluation index system needs to be further improved and modified.

References

Adeel ZA (2017) Renewed focus on water security within the 2030 agenda for sustainable development. Sustain Sci 12:891–894

Anderson EP, Jackson S, Tharme RE et al (2019) Understanding rivers and their social relations: a critical step to advance environmental water management. Wiley Interdisc Rev Water 6(6):1381

Babel MS, Shinde VR et al (2020) Measuring water security: a vital step for climate change adaption. Environ Res 185:109

Cheng X, Chen L, Sun R, Kong P (2018) Land use changes and socio-economic development strongly deteriorate river ecosystem health in one of the largest basins in China. Sci Total Environ 616:376–385

Chuan T (2000) Review on environment indicator research. Res Environ Sci 13(4):53

Doolan J, Hart B (2017) Water resource policy, planning and management in Australia—an overview. Decis Making Water Resour Policy Manag 3–19

Friesen J, Sinobas LR, Foglia L et al (2017) Environmental and socio-economic methodologies and solutions towards integrated water resources management. Sci Total Environ 581:906–908

Gain AK, Giupponi C (2015) A dynamic assessment of water scarcity risk in the Lower Brahmaputra River Basin: an integrated approach. Ecol Ind 48:120–131
Huang H, Xu Z, Li Y (2015) River health based on cloud model of multi-level fuzzy comprehensive diagnosis: in Nanchang section of Ganjiang River. Resour Environ Yangtze Basin 24:62–69
Jia L (2016) River health assessment based on multi-factor model: a case study on water quality of Suzi River. Yangtze River Sci Res Inst 33:28–32
Ladson AR, White LJ, Doolan JA et al (1999) Development and testing of and index of stream condition for water management in Australia. Freshw Biol 41(2):453–468
Le J, Qiu Z (2002) Analysis on the adaptation relationship between water conservancy investment and national economic development. Water Conservancy Econ 05:45–50
Liu B, Zhang F, Hwang FJ (2021) Comfort value of water: natural-artificial dual-structured analytical framework for comfort assessment of regional water environment and landscape system. Water Resour Manag 35(14):4747–4768
Liu B, Fang H, Zhang F, Zhong Z, Chen Y (2022) Spatiotemporal affordability evaluation of water services in China: a functional cost-price model. Adv Sustain Syst 6(1):2100284
Luo Z, Zuo Q, Shao Q (2018) A new framework for assessing river ecosystem health with consideration of human service demand. Total Environ 640:442–453
Sadat MA, Guan Y, Zhang D et al (2020) The associations between river health and water resources management lead to the assessment of river state. Ecol Ind 109:105814
Wang W, Xu X et al (2016) Assessment of river health based on projection pursuit extension set theory. Water Resour Water Eng 27:122–127
Yang Z, Yang K, Su L et al (2020) Two-dimensional grey cloud clustering-fuzzy entropy comprehensive assessment model for river health evaluation. Hum Ecol Risk Assess Int J 26(3):726–756
Zhai J, Xu G, Guo S, Wang Y (2016) Research on river health assessment method based on coordinated development degree. Hydraul Eng 47:1465–1471

Chapter 16
Implementation of Online Digital Twin Framework for Thermal Power Plant

Shiqi Guan, Wenshan Hu, and Hong Zhou

Abstract Power system is the largest, most complex, capital and technology-intensive artificial composite system in all industrial systems in the world so far, and is one of the most important achievements in the history of the science of human engineering. Considering safety and stability, the design and management of power systems are becoming increasingly important. With the breakthrough in network technology, information technology, modeling, and optimization technology, digital twins are expected to be applied in practical systems to solve the problems mentioned above. The proposed framework follows a front-end and back-end separation approach, providing support for seamless integration with web pages, mini programs, and mobile apps through plug-in access. This unified framework offers a comprehensive set of functionalities, including status synchronization, parameter tuning, web-based algorithm design, visual configuration of customized user interfaces, and real-time control using online digital twin control strategies. This paper contributes to the design and implementation of a unified and adaptable online digital twin framework that covers the entire control system process for thermal power plants. Through a case study conducted on an operational thermal unit, it is demonstrated that the implemented online digital twin framework can effectively support various daily management and training tasks.

Keywords Digital twin · Thermal power plant · Online control · Unified framework

16.1 Introduction

Despite the continuous development of new energy in recent years, its proportion is constantly increasing. As energy demand continues to increase, the importance of coal-fired power plants is becoming more and more prominent. At the same time,

S. Guan · W. Hu (✉) · H. Zhou
Wuhan University, Wuhan 430072, P. R. China
e-mail: Wenshan.hu@whu.edu.cn

Z. Sun and P. K. Das (eds.), *Proceedings of the 10th International Conference on Energy Engineering and Environmental Engineering*, Environmental Science and Engineering, https://doi.org/10.1007/978-3-031-48204-5_16

how to improve the safety and efficiency of thermal power plants and reduce environmental pollution has become an important issue. The emergence of digital twin technology provides new ideas for the intelligent management of thermal power plants.

Digital twin is based on physical simulation and computer models, which can construct a real and refined virtual world. In thermal power plants, digital twin technology can construct a complete virtual thermal power plant model. By simulating actual operations, remote monitoring and management can be achieved, faults can be predicted, and preventive measures can be taken in a timely manner.

The implementation of digital twin technology offers significant benefits to thermal power plants, enhancing safety and reducing the occurrence of accidents. Additionally, it improves the overall efficiency of power plants by optimizing equipment installation and operation. By leveraging digital twin technology, design and development processes can be expedited, resulting in reduced time-to-market. Moreover, cost reduction can be achieved through efficient maintenance planning and predictive analytics enabled by digital twins. Digital twin technology can also be used in conjunction with other intelligent systems to achieve intelligent operation and management of thermal power plants, greatly improving production efficiency.

This article presents a comprehensive discussion on a unified and flexible online digital twin framework specifically designed for thermal power plants. The methodologies and implementations of this framework are detailed, with its ability to facilitate massive access and integration of cutting-edge technologies highlighted.

The structure of the remainder of this paper is as follows: Sect. 16.2 provides an overview of the online digital twin system, Sect. 16.3 introduces the architecture of the online digital twin system, Sect. 16.4 explores the control strategy employed to demonstrate the implementation of the digital twin, and finally, Sect. 16.5 concludes the paper.

16.2 Requirements of Online Digital Twin System for Engineering

Since the concept of digital twins was proposed, digital twin technology has been constantly evolving rapidly and has had a huge driving effect on product design, manufacturing, and services. In order to achieve a unified digital twin system framework, its development and needs need to be analyzed with emphasis in this section.

16.2.1 Digital Twin

The idea of digital twins was first introduced by Professor Michael Grieves of the Florida Institute of Technology at the 2002 meeting of the Society of Manufacturing

Engineers (Michael 2014). The concept states that by utilizing the data from physical equipment, a virtual entity and subsystem capable of representing the physical equipment can be constructed within a virtual (information) space. Furthermore, this connection is not limited to being one-way and fixed, but rather it remains interconnected throughout the entire lifespan of the product. Shafto and Vickers, among others, definitively defined the term "Digital Twin" in NASA's roadmap a decade ago and successfully implemented it within the aviation industry.

Researchers have developed a variety of digital twin system architectures. A three-dimension model for the DT is described in Article (Michael 2014), which includes the physical space, virtual space, and the relationship between these two components. A comprehensive DT with five dimensions—physical component, virtual portion, connection, data, and service—was proposed by Tao et al. (2017). The initial proposal for an online DT architecture for power grid online analysis was made in 2019 (Zhou et al. 2019). In 2020, a six-layer design was suggested for the digital twin (Redelinghuys et al. 2020). Regardless of how the DT architecture has been developed, the fundamental objective of the DT system is to establish a bidirectional connection between the physical space and the virtual space. As time has progressed, DT has become increasingly linked with CPS, thereby enhancing the utilization of CPS in various applications (Lei et al. 2022a). Integrated methods in production, smart manufacturing (Tao et al. 2019), production systems (Liu et al. 2020), micro punching systems (Zhao et al. 2019), and other areas are provided by certain publications that combine CPS with DT. DT is now employed and evaluated in a variety of scientific areas. Aircraft, road mapping (Shafto et al. 2010), and air force vehicles (Glaessgen and Stargel 2012) have all benefited greatly from NASA's efforts. DT's data modeling and communication methods was investigated by Schroeder et al. (2016). In 2020, a Soc-based DT system is envisioned (Wang et al. 2020). Additionally, DT can be used in the process of tweaking the parameters (Song et al. 2020).

Fundamentally, digital twins can be defined as dynamic and evolving digital representations of physical objects or processes. They capture historical and current behavioral data, aiming to optimize business performance. The digital twin model relies on extensive, real-time, and real-world data measurements across multiple dimensions, culminating in a large-scale cumulative database. Although it is difficult to have a unified standard for digital universal definitions due to different requirements in different scenarios, all definitions emphasize two important features: (1) Digital twins are digital replicas of living or inanimate physical entities; (2) Data may be smoothly transported between the physical and virtual worlds, allowing virtual and real-world objects to cohabit.

16.2.2 Digital Twin Architecture

To implement the above goal of digital twin system, the function architecture is shown in Fig. 16.1.

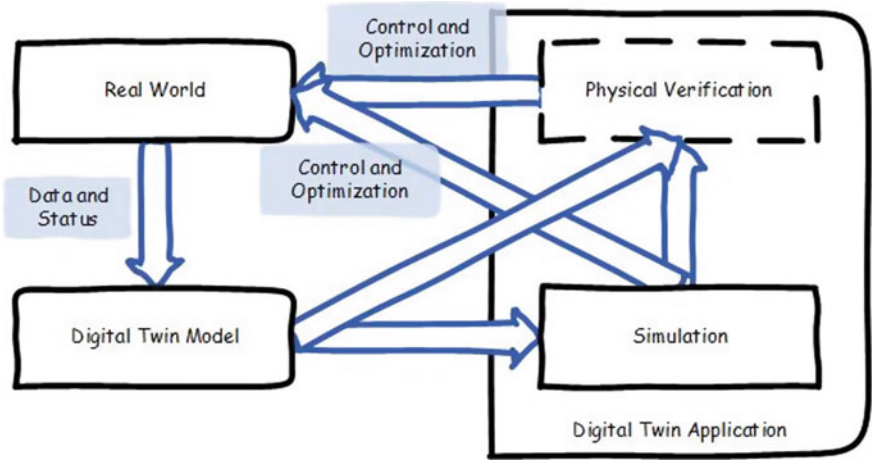

Fig. 16.1 Digital twin system paradigm

Real world and twin world can be distinguished in a digital twin system. The actual world serves as the foundation for the digital twin system since it provides all of the data and status. Digital twin models and their applications make up the twin world. Through algorithms, an accurate digital twin model of the control object can be obtained from data and system state. While, the digital twin model is not limited to mathematical models, but can also be a mathematic model or a physical device. The digital twin model's parameters need to be adjusted in accordance with reality. As a result, more experiments can be run using more precise system models. And control and optimization schemes may be applied to the actual system based on simulation and physical verification. It is important to note that the real system does not need to be shut down and won't be impacted during the modelling and simulation process.

If real-time data interaction between real world and twin world can be achieved through synchronization technology, real-time optimization of real world can be realized. This is an online digital twin system.

16.2.3 Digital Twin in Power Plant

The digital twin system can be widely applied in the operation and maintenance stages of the life cycle of power production and transmission and distribution units. Virtual sensors will capture a large amount of real-time data for subsequent processing and analysis. Virtual sensors refer to applications that can obtain non-measurable information about the current state of a process from the underlying layers of digital twins.

A digital power plant built upon digital twins must possess three key features: holographic replication (HR), twin interaction (TI), and virtual-real iteration (VRI).

(1) HR: Digital power plants employ highly realistic modeling to accurately replicate the ontology of physical power plant equipment in the digital twin power grid. Leveraging extensive sensor deployment across a wide area, twin power plants achieve comprehensive perception and dynamic monitoring of physical power plants, enabling holographic digital descriptions and precise information expression.
(2) TI: In the global digital world, virtual images based on HR enable the operation, management, and services of power plants to move from real to virtual. Twin power plants achieve modeling and simulation, learning and interpretation, knowledge mining, evaluation and prediction, as well as spatiotemporal deduction of complex characteristics within power grids. Feedback from the virtual realm guides the operation trajectory and resource allocation of physical power plants, forming a twin interactive complex system that facilitates virtual-real fusion and collaboration.
(3) VRI: Through IoT perception and ubiquitous networks, the twin power plant correction model continuously monitors and tracks new elements, trends, and issues in the physical world, ensuring spatiotemporal consistency. Simulations anticipate potential risks resulting from changes in the physical world. Guidance outcomes from these simulations are fed back to the twin power plants by the physical power plant, enabling seamless iteration between the virtual.

16.3 Online Digital Twin Architecture

According to the characteristics and requirements of the digital twin system, the architecture can be improved and applied on the basis of remote-control laboratories—Networked Control System Laboratory (NCSLab). NCSLab was initially established at the University of Glamorgan (now known as the University of South Wales) in 2006. Over the course of 17 years of development, the NCSLab framework has undergone continuous enhancements with the addition of new features and supporting technologies. These additions have contributed to the increased power and reliability of the NCSLab framework. NCSLab mainly provide remote experiment platform for control engineering student.

16.3.1 Digital Twin System Implementation Architecture

As shown in Fig. 16.2, a four-layer network structure has been designed and implemented (Lei et al. 2022b, 2021). They are the frontend user interface, central servers cluster, regional controllers, and test rigs. For more details about the online digital twin platform, article (Lei et al. 2021) can be referred to.

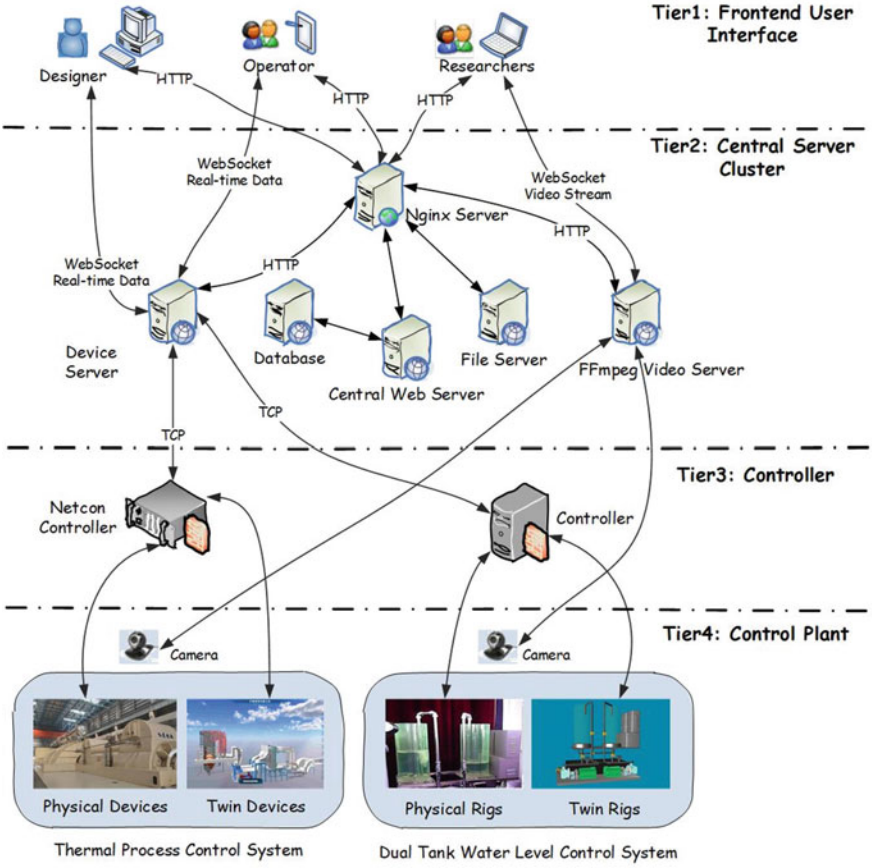

Fig. 16.2 Architecture of the online digital twin system

The online digital twin system is deployed with a four-tier architecture, enabling the seamless integration of diverse devices located at different locations through a unified web interface.

Frontend User Interface: The frontend is encapsulated as a single-page web application, which facilitates the retrieval of various types of data including configuration data, real-time data, and live video streams. These data sources are obtained from the backend servers deployed in Tier 2 during the experimental processes. Client-side can be distributed in any place around the world with an intelligent terminal connected to the Internet. And software is mainstream browsers and mobile applets, such as Fire-fox, Microsoft Edge, and Google.

Central Server Cluster: The Central Server Cluster serves as the core component of the system, primarily responsible for coordinating the front-end and back-end operations, including experimental allocation, data transmission, and other related tasks. The experimental servers and Video Servers are also included in this tier, which

establishes real-time data channels between the frontend user interface and remote experimental processes.

Controller: This tier contains different kinds of controllers for various industrial equipment. The controller is closely connected to the device server. Frequent data exchange to ensure accurate sending and response of instructions.

Control Plant: The process control tier is responsible for implementing engineering processes. Each plant is represented in two forms: the real plant and twin models, which include digital models and physical simulators. Two online control modes are supported. In cases where the physical plants are connected to practical test rigs, remote control is utilized. Alternatively, if the processes are simulated using mathematical models, the digital twin model provides real-time 3D visualization on the frontend user interface.

16.3.2 Supporting Technologies

To establish a sophisticated and comprehensive online laboratory that encompasses multiple design objectives, NCSLab has incorporated various cutting-edge web technologies. These technologies have been adopted to ensure the robust functioning and effectiveness of the laboratory.

(1) React frontend. The frontend of the system is built using React, a JavaScript library specifically designed for constructing user interfaces. React serves as a foundation for developing single-page or mobile applications. It excels at efficiently fetching and managing rapidly changing data that requires real-time updates and recording.
(2) Multiple UI modules. The NCSLab system incorporates multiple UI modules, leveraging the modular React framework to facilitate seamless development of inter-active user interfaces. A wide range of existing open source UI modules can be easily integrated into the system, including Ant Design, React Router, ECharts, Three.js, Unity, and React Sublime Video. This integration allows frontend developers to take advantage of these modules to enhance the functionality and visual appeal of the NCSLab system.
(3) 3-D rendering and visualization. 3-D visualization is an important feature for recent online experimental services, especially for the case of virtual experimentation, in which there is no real experimental process and the results are represented through 3-D animation. NCSLab adopts Three.js as the 3-D engine. The 3-D models are recreated inside the web apps and synchronized with the real-time data through internet.
(4) Nginx reserve proxy. Nginx serves as an HTTP and reverse proxy server, offering versatile backend deployment options for online experimental services. It allows for the simultaneous deployment of different backend service providers like PHP and Tomcat behind the Nginx Server. These services can share a single

HTTP(s) server port, providing seamless integration and efficient utilization of server resources.

(5) WebSocket Real-time communication. By leveraging WebSocket, the experimental services can establish true full-duplex communication channels between the web-based user interface and remote experimental processes. This enables seamless and efficient communication between these components in real-time scenarios.

(6) UDP communication. UDP (User Datagram Protocol) plays a vital role in the interconnection of hardware devices and controllers within thermal power plants. It exhibits compatibility with a wide range of equipment in such plants and demonstrates robust stability. The utilization of UDP guarantees the promptness and precision of instruction and data transmission, thus ensuring efficient and accurate communication in these systems.

16.4 Implementation of Online DT Thermal Power Plant System

The three key procedures for an online digital twin model are mathematical modeling, three-dimensional modeling, and online rendering. While mathematical modeling serves as the foundation for 3D interaction and 3D motion control, 3D modeling also covers the creation of 3D scenes and digital twin devices. Specific 3D sceneries, digital twins, abstract 3D interactivity, and 3D motion control are all included in online rendering. The mathematical model, which incorporates the twin system control algorithm and the twin model, forms the basis of the aforementioned procedure.

In this paper, the combustion system is chosen as a case study to demonstrate the implementation of digital twin control. The thermal process involved in this system presents numerous nonlinear and multiple-coupled variables, making it impractical to rely solely on conventional control methods. Challenges arise due to factors such as mechanical properties, transmission latency, and other thermal engineering-related issues. Additionally, the combustion system exhibits scattered parameter properties, adding complexity to its control. Furthermore, there are higher demands placed on the engineering index and control of the heat process in this system.

16.4.1 Online Control Strategies in Digital Twin

With bidirectional data interactions, synchronization is a crucial issue with digital twins. Data between the physical system, DT system, and DT identification module in particular. Since the majority of the data in the DT system comes from the identifying module or physical system. Additionally, in a perfect world, the DT system would work both dynamically and steadily in order to follow the physical outputs in time.

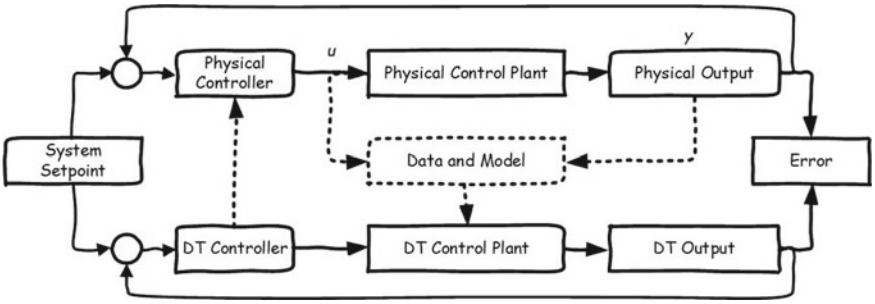

Fig. 16.3 Control strategy of the online digital twin system

The control strategy of the online digital twin system focused on controlling plants is created in Fig. 16.3 to handle the synchronization. The system consists of three parts: the physical loop, the digital twin loop, and the data exchange links. The physical loop is a physical closed-loop feedback control system with a real plant and controller. The virtual loop is a digital closed-loop feedback control system with a digital plant and controller. The data links connect the physical loop and the digital loop.

The input and output of the twin object are combined to create the twin model when the physical system is functioning normally. And the input from the physical system is used as the input value of the twin model to create the digital twin system. Real-time operation data is gathered during the continuous operation process to adjust the twin model's parameters and lessen the output variance between the twin model and the physical system.

16.4.2 Mathematical Model-Based Control Strategy

This study divides typical types of power plant equipment and subsystems into two categories: mathematical model-based systems and equipment status response-based systems (Guan et al. 2021).

Despite the presence of significant time delays, non-linear characteristics, strong coupling, and time-variant behavior in combustion control processes, they can be effectively approximated as transfer function matrices. As illustrated in Fig. 16.4, the combustion system can be modeled as a three-input-three-output system, allowing for an abstraction that facilitates control analysis and design.

In Fig. 16.4, data and system status collected by thousands of distributed sensors are transmitted to model analysis subsystem. Then, a 3I3O time-varying transfer function matrix can be structured for further control usage. After the proper parameters have been set and their characteristics are verified in the twin system by using the mathematical model. These parameters may be transferred to the actual system, and all signals in this process will be monitored and visibly shown as needed. The

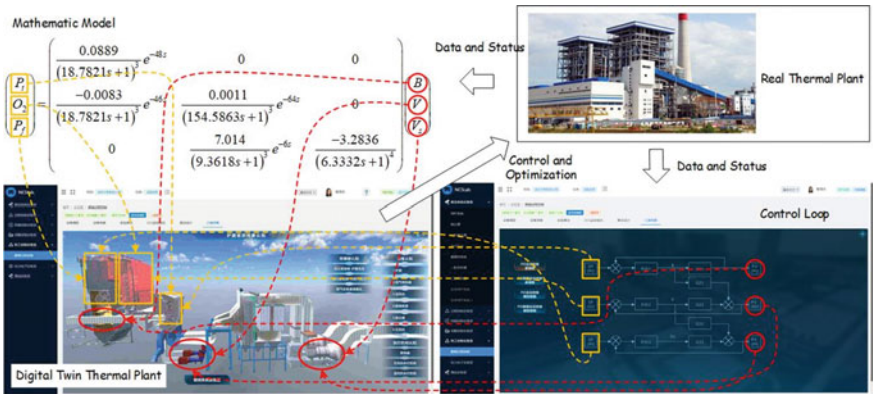

Fig. 16.4 Data links of the online digital twin system

data corresponding links among the real thermal plant, the mathematical model, the control loop and the digital twin 3D scene are marked out in Fig. 16.4.

16.4.3 Device Status Response-Based Control Strategy

In practical applications, not all devices can be accurately expressed through transfer functions. Therefore, a control mechanism based on device state response has been established. By requesting device status through the front-end, the device management system receives instructions, reads the device status, and sends it back to the server. This forms an information control loop based on device status.

Figure 16.5 illustrates the communication information request-response process in a power plant. When a user sends a status request through the monitoring interface, the instruction is transmitted to the requested device via the TCP/IP protocol by the device server. In Fig. 16.5, real-time images of local communication equipment and the operational status of communication lines are requested separately. Upon receiving the request, the device management system makes requests using the UDP protocol to collect necessary data from each device. The collected data is then organized into a specified format and sent back to the server. After receiving the data, the server performs transcoding and data verification before displaying it in the online digital twin system using visual components.

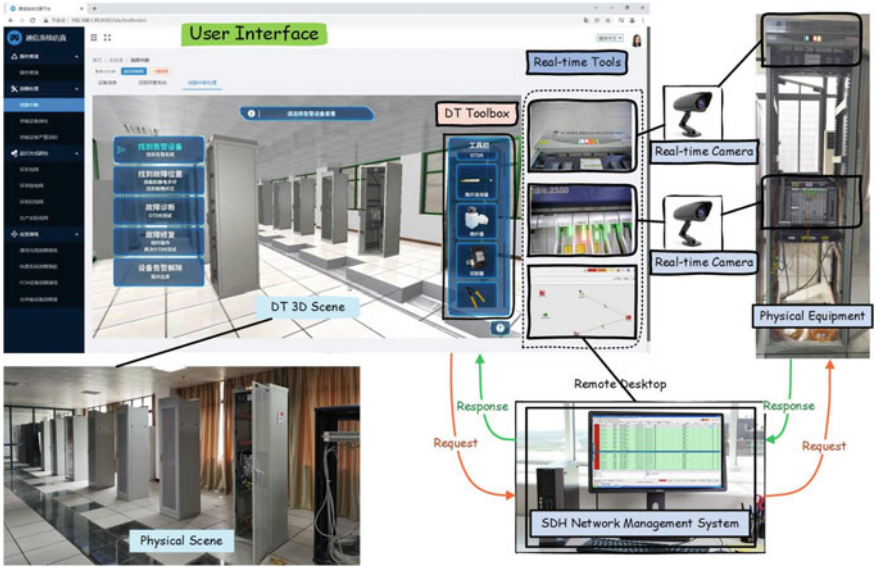

Fig. 16.5 Device status response-based control strategy of the online digital twin system

16.5 Conclusion

This article introduced a novel online digital twin architecture that offers flexibility and scalability. It integrates multiple new open source technologies to support the digital twin system. The proposed framework successfully addresses the requirements outlined in Sect. 16.2, enabling a unified online digital twin architecture that allows for customization of monitoring interfaces, parameter tuning, and real-time monitoring and control of engineering processes. The methodology presented in this paper serves as a foundation and provides insights for the design and research of digital twin systems in various engineering applications. In the future, the digital twin architecture is expected to be utilized with advanced systems, considering additional system status variables and further research.

Acknowledgements This work was supported in part by the National Natural Science Foundation of China under Grant 62073247.

References

Glaessgen EH, Stargel DS (2012) The digital twin paradigm for future NASA and U.S. Air force vehicles. In: Collection of technical papers—AIAA/ASME/ASCE/AHS/ASC structures, structural dynamics and materials conference

Guan S, Hu W, Zhou H, Lei Z, Feng X, Liu GP (2021) Design and implementation of virtual experiment for complex control system: a case study of thermal control process. IET Gener Transm Distrib 15:3270–3283

Lei Z, Zhou H, Hu W, Liu GP, Deng Q, Zhou D (2021) Unified 3-d interactive human-centered system for online experimentation: current deployment and future perspectives. IEEE Trans Industr Inf 17(7):4777–4787

Lei Z, Zhou H, Hu W, Liu GP, Guan S, Feng X (2022a) Toward a web-based digital twin thermal power plant. IEEE Trans Ind Inform 18(3):1716–1725

Lei Z, Zhou H, Hu W, Liu GP (2022b) Unified and flexible online experimental framework for control engineering education. IEEE Trans Industr Electron 69(1):835–844

Liu C, Jiang P, Jiang W (2020) Web-based digital twin modeling and remote control of cyber-physical production systems. Robot Comput Integr Manuf 64:101956

Michael G (2014) Digital twin: manufacturing excellence through virtual factory replication. White Pap 11:1–7

Redelinghuys AJH, Basson AH, Kruger K (2020) A six-layer architecture for the digital twin: a manufacturing case study implementation. J Intell Manuf 31(6):1383–1402

Schroeder GN, Steinmetz C, Pereira CE, Espindola DB (2016) Digital twin data modeling with automation ML and a communication methodology for data exchange. IFAC-PapersOnLine 49(30):12–17

Shafto M, Conroy M, Doyle R, Glaessgen E (2010) DRAFT modeling, simulation, information technology and processing roadmap. Technol Area 1–27

Song X, Jiang T, Schlegel S, Westermann D (2020) Parameter tuning for dynamic digital twins in inverter-dominated distribution grid. IET Renew Power Gener 14(5):811–821

Tao F, Qi Q, Wang L, Nee AYC (2019) Digital twins and cyber–physical systems toward smart manufacturing and industry 4.0: correlation and comparison. Engineering 5(4):653–661

Tao F, Zhang M (2017) Digital twin shop-floor: a new shop-floor paradigm towards smart manufacturing. IEEE Access 5:20418–20427

Wang C, Xu J, Wang K (2020) SoC-based digital twin of power system simulation. In: Proceedings of 2020 5th Asia conference on power and electrical engineering (ACPEE 2020), pp 185–191

Zhao R, Yan D, Liu Q, Leng J, Zhang X (2019) Digital twin-driven cyber-physical system for autonomously controlling of micro punching system. IEEE Access 7:9459–9469

Zhou M, Yan J, Feng D (2019) Digital twin and its application to power grid online analysis. CSEE J Power Energ Syst 5(3):391–398

Chapter 17
Mini-Review of Opportunities and Challenges of Carbon Capture and Storage (CCS) Technology in Addressing Climate Change

Bowen Luo, Haoqian Hu, Kun Liu, Daphne Khee Chong, and Yuanzhe Li

Abstract The pressure of global warming leads to an increasing emission of greenhouse gases, among which carbon dioxide emissions are the most serious, posing serious threats to the earth's ecosystem and biodiversity. Among many emission reduction strategies, Carbon Capture and Storage (CCS) technology has gradually received attention. CCS technology separates carbon dioxide from industrial production and energy consumption processes and transports it to a dedicated location for long-term isolation. However, in the process of reducing global carbon emissions, the application of CCS technology still faces political, economic, and social risks. In specific applications, CCS technology is regarded by some industrial countries as a solution to continue to rely on coal, which requires a deep assessment of its sustainability and benefits. At the same time, developing countries seem unwilling to promote CCS technology. In addition, the balance issue between CCS technology and sustainable energy requires deeper research. There are certain limitations in the public's understanding of CCS technology, and there is a need to strengthen

B. Luo
School of FESTU Transport, Dalian Jiaotong University, Dalian 116028, China
e-mail: rocky_y200109@163.com

H. Hu
Institut Sup.Rieur du Commerce, 75017 Paris, France
e-mail: hqhu245@163.com

K. Liu
Faculty of Law, The University of Buenos Aires, C1111AAI Buenos Aires, Argentina
e-mail: rbk@vip.163.com

D. K. Chong · Y. Li (✉)
Nanyang Technological University, Singapore 639798, Singapore
e-mail: yuanzhe001@e.ntu.edu.sg

Y. Li
School of Civil and Environmental Engineering, University of Auckland, Auckland 1010, New Zealand

Carbon Neutrality Research Lab, China Academy of Art, Hangzhou 310002, China

Z. Sun and P. K. Das (eds.), *Proceedings of the 10th International Conference on Energy Engineering and Environmental Engineering*, Environmental Science and Engineering, https://doi.org/10.1007/978-3-031-48204-5_17

social science research and interdisciplinary research. In general, CCS technology has potential in emission reduction strategies, but in dealing with uncertain risks and long-term impacts, its sustainability and practical effects need to be fully considered.

Keywords Global warming · Greenhouse gas emissions · Carbon dioxide · Carbon Capture and Storage (CCS) · Emission reduction strategies · Sustainability

17.1 Introduction

Global warming continues to spur an increase in greenhouse gas emissions, particularly carbon dioxide. This escalating trend poses severe threats to the Earth, leading to drastic shifts in ecosystems, a loss of biodiversity, and other far-reaching complications (Bäckstrand et al. 2011). Despite continuous global efforts to curb climate change over the years, achieving substantive improvements on a global scale remains challenging. Currently, over 85% of the world's energy demand is still met by the fossil fuel industry (Metz et al. 2005). Although the implementation of renewable energy facilities is on the rise, and they are receiving substantial government support, fully transitioning global energy needs to rely solely on renewable sources will take time (Palm and Hansson 2006). Thus, it is crucial during this transitional period to identify effective carbon dioxide reduction strategies and policies. Against this backdrop, emission reduction technologies like Carbon Capture and Storage (CCS) have been garnering increasing attention over the past decade (Rood 2014; Buck 2016). A report by the Intergovernmental Panel on Climate Change (IPCC) defines CCS as a process that "involves the capture of carbon dioxide (CO_2) from industrial and energy-related sources, transport to a storage location and long-term isolation from the atmosphere" (The Australian Government 2020). The panel of experts asserts that while no single technology can solve the climate issue, CCS can complement other emission reduction measures to help stabilize global carbon emissions (Cook 2017). Scientists, including those from the IPCC, have pointed out that even if humanity immediately halts carbon emissions, existing atmospheric carbon emissions will still cause a minimum temperature rise of 0.6 °C (Ende et al. 1998). Without CCS, limiting the global temperature increase to below 2 °C will be difficult (Edge et al. 2011). Many national governments, scientists, and the IPCC recommend CCS as a viable means of mitigating climate change. This report outlines the technology. Through the application of key technology assessment, this report seeks to answer whether the technology proposed is a morally appropriate solution to the problem of carbon dioxide emission reduction (The Global CCS Institute 2017).

Since the emergence of technology assessment (TA) in the 1960s, societal attention to the larger social and environmental responsibilities brought about by the widespread application of technology, such as computers, smartphones, and the internet, has grown. Consequently, the comprehensive evaluation of the impact of new technologies, including their social, economic, environmental, and ethical dimensions, has become a significant research topic (Folger 2013). In addressing this issue,

the assessment framework for CCS technology has demonstrated diverse characteristics, encompassing three key dimensions: scientific and engineering assessment, social science assessment, and ethical technology assessment (eTA). The scientific and engineering assessment primarily focuses on the basic working principles, efficiency, and safety of CCS technology, as well as its emission reduction effects and potential risks. Table 17.1 shows how various ethical issues can be analyzed from the perspectives of science and engineering, social science, and ethical technology when assessing CCS technology (Table 17.1).

Social science assessment explores the potential social, political, and economic challenges that may arise from the practical application of CCS technology. This includes the degree of public acceptance, difficulties in policy formulation and implementation, and the trade-off between economic costs and benefits. These two dimensions construct a panoramic view of the impacts of CCS technology (Global CCS Institute 2020). However, to gain a more comprehensive understanding, the role of eTA cannot be overlooked. eTA aims to adopt an ethical perspective throughout the lifecycle of the technology, maintaining a connection with technology developers throughout the development process to identify potential ethical issues related to the assessed technology. These issues range from the dissemination and use of information, control, influence and power, impact on social interaction patterns, privacy, sustainability, human reproduction, gender, minority groups and justice, international relations, and the impact on human values. This comprehensive assessment framework embodies the perspective of "constructive technology assistance" (Constructive TA), which posits that technological progress is largely influenced by social processes, while also incorporating the method of "backcasting", i.e., creating ideal future scenarios for assessment. The three dimensions interconnect, forming a comprehensive assessment network, which provides a more in-depth and comprehensive understanding of CCS technology. This comprehensive assessment approach allows for an integrated evaluation of the application of CCS technology, thereby providing policymakers with scientific and empirical evidence, while also offering new insights and directions for further research (Táíwò and Buck 2019).

Through a comprehensive assessment of CCS technology from the perspectives of science and engineering, social science, and ethical technology assessment, this report provides a balanced and multidimensional understanding of CCS technology. While CCS technology has the potential to make a significant contribution to climate change mitigation, it also involves various challenges and ethical issues that need to be addressed (Karayannis et al. 2014). Therefore, it is essential to foster an ongoing dialogue among scientists, policymakers, stakeholders, and the public to ensure the responsible development and deployment of CCS technology.

Table 17.1 Ethical issue analysis of CCS technology: perspectives from science and engineering, social science, and ethical technology assessment

Ethical issue	Science and engineering assessment	Social science assessment	Ethical technology assessment (eTA)
Information dissemination and use	Technical evaluation of the dissemination and use of information involved in the design and implementation of CCS technology	Research on the impact of information dissemination on social dynamics, perceptions, and acceptance	Research on ethical issues that may arise from the dissemination and use of information, such as fairness, transparency, etc
Control, influence, and power	Technical evaluation of control and power distribution in the process of technology development and implementation	Discussion on how social and political factors affect the distribution of control and power	Research on ethical issues that may arise from the distribution of control and power, such as fairness, abuse of power, etc
Impact on social interaction patterns	Analysis of possible changes to social interaction patterns due to CCS technology	Research on the impact of changes in social interaction patterns on social behavior, interaction, and culture	Exploration of potential ethical issues arising from changes in social interaction patterns, such as isolation, discrimination, etc
Privacy	Technical evaluation of potential infringements on privacy due to CCS technology	Discussion on the impact of privacy infringements on society and individuals	Research on ethical issues in privacy, such as respect for personal information, balance of power, etc
Sustainability	Scientific and engineering evaluation of the sustainability of CCS technology	Discussion on the impact of sustainability on society and the economy	Research on ethical considerations of sustainability, such as environmental justice, fair resource distribution, etc
Human reproduction	Research on the potential impact of CCS technology on human reproductive health	Discussion on the impact of reproductive health issues on society and culture	Exploration of potential ethical issues related to human reproduction, such as respect for life, autonomy, etc
Gender, minority groups, and justice	Evaluation of the potential impact of CCS technology on different groups	Research on the impact of issues related to gender, minority groups, and justice on social structures and dynamics	Exploration of potential ethical issues related to gender, minority groups, and justice, such as fairness, equality, etc

(continued)

Table 17.1 (continued)

Ethical issue	Science and engineering assessment	Social science assessment	Ethical technology assessment (eTA)
International relations	Evaluation of the potential impact of CCS technology on international relations	Discussion on the impact of changes in international relations on the global political and economic landscape	Exploration of potential ethical issues related to international relations, such as fair trade, fair technology transfer, etc
Impact on human values	Evaluation of the potential impact of CCS technology on human values	Discussion on the impact of changes in values on society and culture	Exploration of potential ethical issues related to human values, such as respect, justice, human rights, etc

17.2 Carbon Capture and Storage (CCS) Technology

In the battle against global warming, Carbon Capture and Storage (CCS) technology has become an indispensable tool. Numerous technologies can be used to capture and separate carbon dioxide from gas mixtures and the atmosphere, but the extent of their application and developmental status varies greatly. Some have been successfully applied in commercial environments, such as technologies that use specific equipment to extract carbon dioxide from the exhaust gases of power plants and high-emission industrial factories. Others, such as Direct Air Capture (DAC) technology, are still under development and not widely applied. An exhaustive overview of the technological options for carbon dioxide capture is illustrated in the following Fig. 17.1.

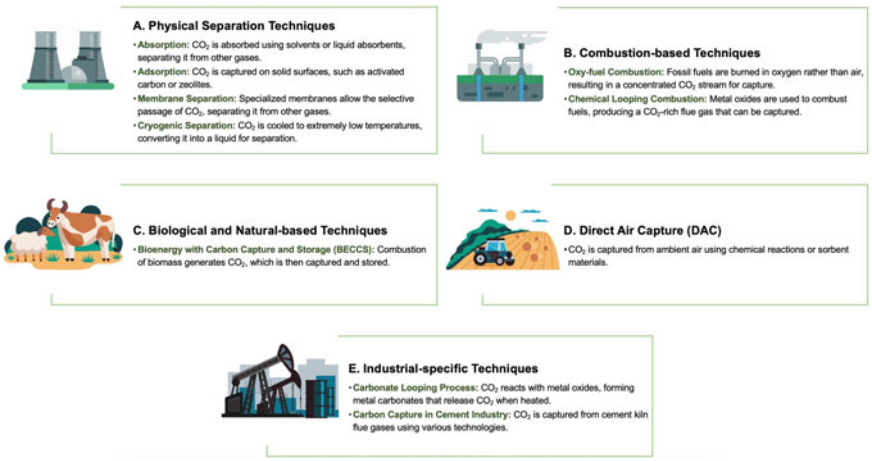

Fig. 17.1 Technological options for capturing carbon dioxide

Research into Carbon Capture and Storage technology can be traced back to 1972 at a natural gas processing plant in Val Verde, Texas, according to the Global CCS Institute (GCCSI) (The Australian Government 2020). By 2020, about 16 facilities worldwide could store approximately 30 million tons of carbon dioxide annually, and an additional 6 facilities were under development. It is expected that by 2020, these 22 facilities will be storing 40 million tons of carbon dioxide each year (Táíwò and Buck 2019; Wilberforce et al. 2018). The application of CCS technology is mainly concentrated in the fossil fuel industry and these technologies are divided into pre-combustion and post-combustion systems based on whether the carbon dioxide is removed before or after the combustion of the fuel. Another technology that does not require capture equipment is known as oxyfuel combustion or all-oxygen combustion, which is still under development (Kusmer 2020). It's worth mentioning that even though the Intergovernmental Panel on Climate Change (IPCC) and the International Energy Agency (IEA) have both recognized Carbon Capture and Storage (CCS) as an important emission reduction strategy, its development and application still face many challenges. Current estimates indicate that by 2050, under the critical value of a 2 °C increase in temperature, the global storage of carbon dioxide will be less than 1 trillion tons. This implies that to keep the global warming within safe thresholds, the development of CCS technology must be elevated at least two orders of magnitude higher than the current level. Undoubtedly, this is an extremely daunting task, but it is also a challenge that humanity must face in combating global climate change and achieving sustainable development (Palm and Hansson 2006). The follows will explain the technical details of three current Carbon Capture and Storage (CCS) technologies.

17.2.1 Pre-combustion CO_2 Capture Process

In Carbon Capture and Storage (CCS) technology, the pre-combustion process is an important method aimed at converting and removing carbon from the fuel before the combustion process begins. The core of the pre-combustion process is to convert the fuel into a form that makes it easy to remove carbon. In a coal-fired power plant, for example, to achieve this goal, coal needs to react with steam and oxygen under high temperature and high pressure conditions. This reaction process is called partial oxidation, which results in a gas composed of carbon monoxide and hydrogen. This way of generating power from the gas is called Integrated Gasification Combined Cycle (IGCC). After the partial oxidation process, special impurities in the gas are removed. Afterward, the gas is introduced into a device called a "shift reactor", where carbon monoxide is converted into carbon dioxide by reacting with water vapor. After completing this step, the carbon dioxide is captured by a chemical solvent. It's worth noting that the remaining gas is primarily almost pure hydrogen. This hydrogen can be combusted in a combined cycle power plant to generate electricity, as shown in Fig. 17.2 (Buck 2016; Karayannis et al. 2014).

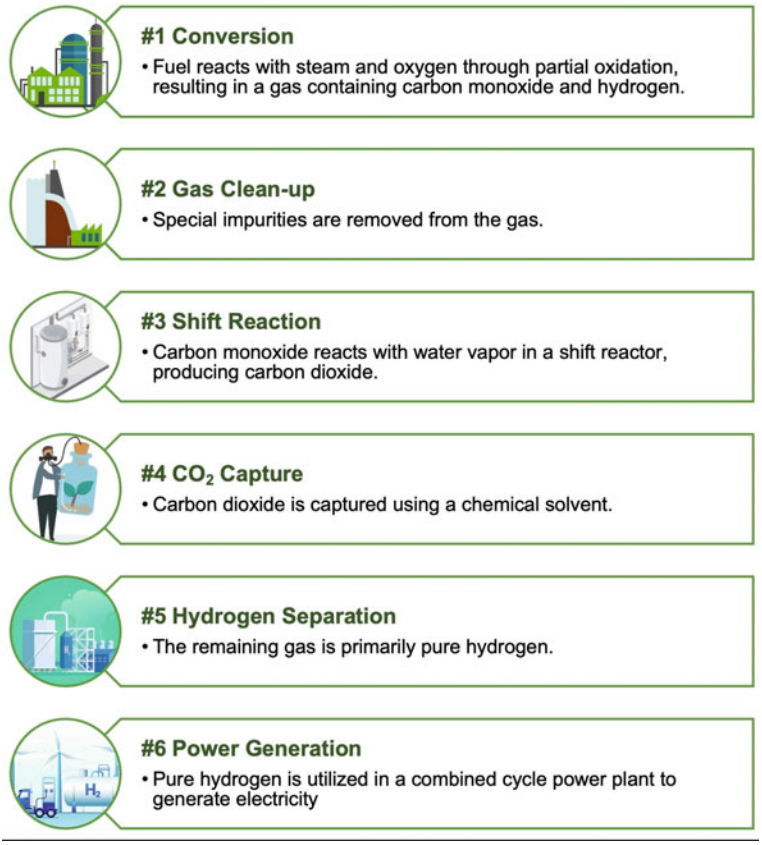

Fig. 17.2 Pre-combustion process for CO_2 capture process

17.2.2 Oxyfuel Combustion CO_2 Capture Process

Oxyfuel combustion is another important method in Carbon Capture and Storage (CCS) technology. Although its level of development in current carbon dioxide capture methods is relatively low, its potential cannot be ignored. This system was initially designed and developed as an alternative to post-combustion systems. In the oxyfuel combustion process, fossil fuels are burned in a mixture of oxygen and recirculated flue gas, producing a new flue gas rich in water and carbon dioxide. As the name suggests, this process uses a large amount of oxygen and removes a large amount of nitrogen from the gas stream (Fig. 17.3). After the removal of certain substances, the flue gas mainly consists of carbon dioxide, water vapor, and residual pollutants (Leung et al. 2020). To obtain a nearly pure carbon dioxide stream, the flue gas needs to be cooled and compressed to remove the water vapor (Ende et al. 1998). Then, other air pollutants are removed, resulting in a nearly pure carbon dioxide

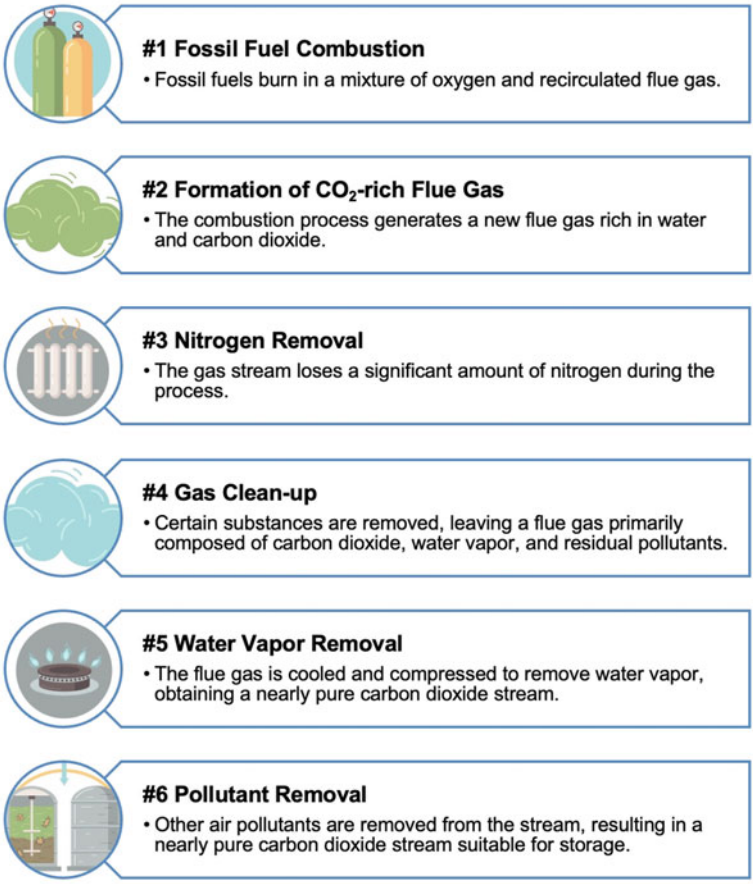

Fig. 17.3 Oxyfuel combustion for CO_2 capture process

stream that can be stored to achieve carbon capture and storage. The following figure provides a detailed depiction of the oxyfuel combustion process.

17.2.3 Post-combustion CO_2 Capture Process

Post-combustion carbon dioxide capture systems are specifically designed to capture carbon dioxide produced during the production process of fossil fuels or other carbon-containing substances (like biomass). Taking a modern coal-fired power plant as an example, the combustion process mixes coal dust with air and burns it in a boiler to release heat to produce steam, which then drives the turbine generator. In this process, the main gases emitted by the boiler include nitrogen from the air, a small amount of

water vapor, carbon dioxide, and other trace impurities formed during combustion. To meet environmental standards, air pollutants must be removed from these exhaust gases. The capture of carbon dioxide can be achieved by chemically reacting with an organic solvent (such as monoethanolamine) (Fig. 17.4). In practical operation, the exhaust gases are introduced into an absorber to contact the amine solution, which can capture about 85–90% of the carbon dioxide. Subsequently, the solution containing carbon dioxide is transported to another container. In this container (also known as a desorber), the solution is heated to release the captured carbon dioxide. This step produces a high-concentration stream of carbon dioxide, which is then compressed and transported via pipeline to a predetermined, safe storage location. It is worth noting that in the entire process, the used solvent is recollected and returned to the absorber for recycling, which not only reduces operating costs but also minimizes environmental impact (Zhu et al. 2023).

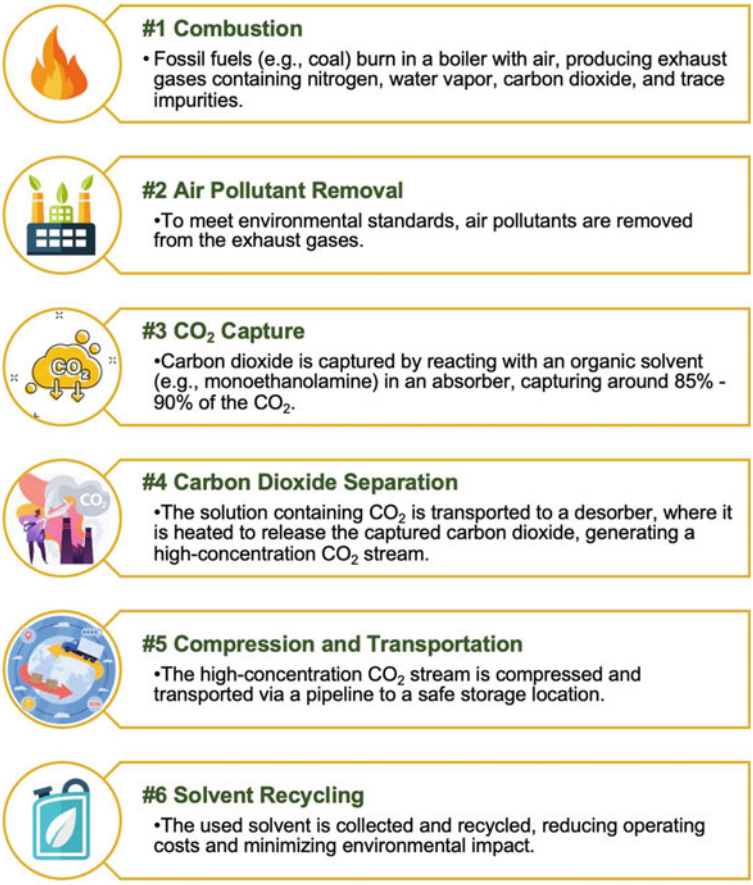

Fig. 17.4 Post-combustion process for CO_2 capture process

Table 17.2 Modes of CO_2 transportation and their cost-effectiveness

Transportation mode	Cost per ton of CO_2 (USD)
Ship tanker	7.48
Rail tanker	12.64
300 km pipeline	7.05

17.2.4 Transportation of CO_2 and Its Cost-Effectiveness

After successfully capturing carbon dioxide, the next critical step is to transport it safely to the storage location or industrial use site. The mode of transportation mainly depends on the volume of carbon dioxide to be handled, including road tankers, ships, or pipeline transportation. At present, pipeline transportation is considered the most feasible solution because it can transport large amounts of carbon dioxide over long distances. The cost of transportation largely depends on the regional economic conditions and maximizing the mass/volume ratio. It should be noted that carbon dioxide is usually transported in the form of liquid dense phase. A cost analysis study from China indicates that in the case of transporting 4000 tons of carbon dioxide per day, the cost of using ship tankers is $7.48 per ton of carbon dioxide, using rail tankers costs $12.64 per ton, and using a 300 km pipeline costs $7.05 per ton of carbon dioxide. It is important to emphasize that monitoring the carbon dioxide stream during transportation is very important, especially in pipeline transportation (Table 17.2). This is because impurities can change the pressure and temperature envelope boundaries in the carbon dioxide single-phase flow. Fortunately, the accident rate involving carbon dioxide pipelines is relatively low. To realize the commercial application of Carbon Capture and Storage (CCS) projects, we need to develop a wide network of pipelines to meet transportation needs.

17.2.5 Geological Storage and Deep Ocean Storage

Geological storage of carbon dioxide is the safe storage of captured carbon dioxide within the Earth, mainly relying on four types of geological formations: depleted oil and gas reservoirs, unminable coal seams, saline aquifers, and basalt. Each type of storage structure has its unique characteristics, providing the possibility for the safe storage of carbon dioxide. Choosing the ideal geological storage site requires a detailed assessment. Assessment factors include the porosity, thickness, and permeability of the reservoir rock to ensure that it can accommodate a large amount of carbon dioxide. At the same time, the storage area must have a good seal to ensure that carbon dioxide does not escape. In addition, a stable geological environment is an important factor, which can prevent carbon dioxide leakage caused by geological activities such as earthquakes. In addition to geological storage, there is a method of deep ocean storage. This method is to store carbon dioxide in the deep ocean to

isolate it from the atmosphere for hundreds of years. Although this method seems an attractive option to many scientists and the Intergovernmental Panel on Climate Change (IPCC), it has also aroused widespread concern and discussion among the public. Especially considering its potential ecological impact, more in-depth research and assessment are needed (Zhu et al. 2023).

17.3 Global Development and Practice of CCS Technology

In the global fight against climate change, Carbon Capture and Storage (CCS) technology is playing a crucial role. This technology is widely used in many countries, and different regional, policy, and resource backgrounds provide a rich sample of its application. Among them, the United States, China, and Australia are leading the world in the development and promotion of CCS technology, and the governments of these three countries have provided strong support for the research and development activities of CCS technology. For instance, Australia, as a country heavily dependent on coal for electricity and exports, holds a special significance for the application of CCS technology. To this end, the Australian government invested AUD 11.5 million in the "Carbon Capture and Storage Flagship Program" in 2017 to encourage and support the application of CCS technology in industrial production. This flagship program focuses mainly on capturing carbon dioxide from industrial production processes, constructing and maintaining related transportation infrastructure, and safely storing captured carbon underground. These demonstration projects have not only promoted the application of CCS technology in Australia but also provided a reference for other regions globally.

17.3.1 The United States: Pioneering CCS Technology

The United States has long been a pioneer in the field of CCS technology. The Department of Energy's (DOE) Carbon Storage Program aims to develop and advance technologies to enable safe, cost-effective, and permanent geologic storage of carbon dioxide (CO_2). The program conducts research and development work on CO_2 capture technologies, as well as the infrastructure needed for implementation. For example, the Petra Nova project in Texas, which is currently the world's largest post-combustion carbon capture facility, captures more than 1.6 million tons of CO_2 annually.

17.3.2 China: Scaling up CCS Deployment

China, the world's largest emitter of CO_2, recognizes the importance of CCS in achieving its climate goals. The country has been scaling up its efforts in deploying CCS technologies, particularly in coal-dependent sectors. China's most notable CCS project is the Sinopec Qilu Petrochemical CCS project, which captures CO_2 from a coal-to-hydrogen plant and uses it for urea production. As of 2023, China has several large-scale CCS projects either in operation or under construction, making it one of the global leaders in this field.

17.3.3 Australia: Leveraging Natural Resources for CCS

Australia, rich in coal and natural gas, has a unique position in the world of CCS. The Australian government's Carbon Capture and Storage Flagship Program is driving CCS research and implementation. One of the notable projects under this program is the Gorgon Project in Western Australia, one of the world's largest natural gas projects and the largest single source of CO_2 storage to date. The Gorgon Project is expected to store approximately 3.4–4 million tons of CO_2 per year.

17.3.4 Canada: A Leader in Commercial CCS Applications

Canada has been a leader in the commercial application of CCS, especially in the oil and gas sector. The Weyburn-Midale field in Saskatchewan is one of the best-known projects where CO_2 is injected into the reservoir for enhanced oil recovery (EOR) while simultaneously storing CO_2 underground. In Alberta, the Shell Quest project has been successfully storing over 1 million tons of CO_2 per year since 2015.

17.3.5 Norway: Advancing Offshore CCS

Norway, with its extensive offshore oil and gas industry, has been a pioneer in offshore CCS. The Sleipner field in the North Sea, operated by Equinor, has been storing CO_2 since 1996, making it the longest-operating CCS project in the world. More recently, the Norwegian government has been supporting the "Northern Lights" project, which aims to transport CO_2 from onshore sources and store it beneath the seabed. This project is part of a broader initiative called "Longship," reflecting Norway's commitment to advancing CCS technology.

17.3.6 United Kingdom: Strategic Approach to CCS

The United Kingdom has adopted a strategic approach to CCS, focusing on industrial clusters. The government has been investing in CCS research and development as part of its Clean Growth Strategy. One notable initiative is the Acorn project in Scotland, which aims to capture CO_2 from the St Fergus Gas Terminal and store it in offshore geological formations.

By looking at these countries, the implementation of CCS technology is proved to be influenced by various factors such as natural resource availability, industrial structure, and government policy. Despite the challenges, these examples show that with commitment and strategic planning, CCS can play a significant role in the global effort to combat climate change. Still, CCS technology is considered a significant strategic tool aimed at limiting global temperature rise to within 2 °C and achieving net-zero emissions in the global energy system in the future. Although the application of CCS technology is most extensive in the power industry, its potential for decarbonization in industrial processes is also attracting attention. Industries such as steel, cement, and chemicals can apply CCS technology to achieve a green transformation of the industrial structure. Additionally, the captured carbon dioxide can be stored or even converted into other valuable products such as beverages, fuel, cement, and even shoes. Therefore, CCS technology is not only of great significance for reducing carbon emissions but can also open up new growth points for economic development (The Australian Government 2020). For countries like China, the United States, and India, which currently account for half of the world's carbon dioxide emissions, the promotion and application of CCS technology are particularly important. Therefore, understanding and exploring the application of CCS in different regions and industries is an important path to achieving global carbon neutrality.

17.4 Social, Economic, and Environmental Impacts of Carbon Capture and Storage (CCS) Technology

Despite some exploration and research into CO_2 capture technology, its application scale hasn't reached the breadth recommended by experts. Therefore, its effect in combating global warming is not yet significant. This section will delve into the social, economic, and environmental impacts of Carbon Capture and Storage (CCS) technology.

Table 17.3 Economic challenges of CCS

Challenge	Remark
High operational costs	The cost of capturing, transporting, and storing CO_2 is high, making it less competitive without financial incentives
Significant energy demands	Energy is required to capture CO_2, compress it, transport it to the storage site, and inject it underground. This is known as the "energy penalty" of CCS

17.4.1 Economic Impact: High Operational Cost and Energy Demand

The primary challenge for the implementation of CCS technology lies in its high operational costs and significant energy demands. These two factors currently pose major obstacles to the widespread application of CCS technology. Despite the objective of CCS technology being to facilitate cleaner energy use and remove carbon dioxide from the atmosphere, if the application itself becomes an energy-intensive activity, the impact on the overall energy balance becomes questionable. To address this issue, in-depth research and development are required to improve technical efficiency and reduce costs, along with substantial government support, including financial and policy support, to promote the commercialization process of CCS technology (Table 17.3).

17.4.2 Environmental Impact: Need for Life-Cycle Impact Studies

A more in-depth study is also needed on the full lifecycle impacts of CCS on the environment. This includes all potential environmental issues that may arise from the capture, transport, and storage processes, including impacts on biodiversity, groundwater contamination, and potential seismic risks. In the process of assessing and managing these risks, public participation and oversight are critical. The environmental implications of CCS technology are multifaceted, encompassing potential impacts at each stage of the process (Table 17.4).

- **Capture**: The capture process itself can have environmental implications. For instance, the chemicals used in post-combustion carbon capture may have environmental and health impacts if not properly managed.
- **Transportation**: The transportation of carbon dioxide, most commonly via pipelines, could potentially impact ecosystems, especially in the event of leaks or failures.
- **Storage**: The most significant environmental concerns are associated with the storage phase of CCS. There is potential for leaks from storage sites, which

Table 17.4 Factors influencing social acceptance of CCS

Factor	Remark
Awareness and understanding	Greater awareness and understanding of CCS typically leads to higher acceptance
Trust	Trust in the organizations implementing CCS projects and in the regulatory frameworks governing these projects influences public acceptance
Local impacts	Concerns about local environmental impacts can influence public acceptance
Perceived fairness	If local communities bear the risks of CCS projects but perceive they do not share in the benefits, this can lead to opposition

could lead to the release of CO_2 back into the atmosphere, undermining the purpose of CCS. Additionally, there is a risk of induced seismicity (human-caused earthquakes) from the injection of CO_2 into geological formations.

17.5 Discussion and Considerations

Risk From a global perspective on climate change challenges, Carbon Capture and Storage (CCS) technology as a potential emission reduction strategy is widely regarded as valuable. This view is not only a consensus in the scientific community, but has also been recognized by governments around the world and numerous international conventions such as the Intergovernmental Panel on Climate Change and other non-governmental organizations (Global CCS Institute 2020). However, even if this technology theoretically has tremendous value, it needs to be treated cautiously within the existing framework of power, economics, and politics, as well as the ethical, environmental, and social risks that may arise from its widespread application.

In this section an in-depth critical analysis of CCS technology using Electronic Technology Assessment (eTA), Constructive Technology Assessment (CTA), and Backcasting is conducted (Fig. 17.5). Under the framework of "Constructive Technology Assessment" and "Backcasting," we note that some industrial and energy production countries heavily reliant on coal, such as the United States, China, and Australia, are seeing CCS technology as a solution to continue relying on coal while reducing carbon dioxide emissions. However, it's worth pondering whether this coal-dependent strategy is merely an interim step towards a transition to renewable energy, or whether it could potentially mask significant funding flowing into CCS research instead of supporting renewables. Furthermore, whether continued coal combustion will lead to resource depletion and scarcity also requires further research and assessment.

Industrialized countries have contributed significantly to the current climate issues over the past few centuries, and therefore, they bear a significant responsibility in

Fig. 17.5 Comprehensive analysis of challenges in implementing CCS technology

international coordination and governance to help mitigate the current climate crisis. However, compared to industrialized countries, developing countries often seem less ambitious in researching CCS policies, mainly relying on case studies from individual countries. Designating carbon capture and storage as a "Clean Development Mechanism project" may expose developing countries to the complex circumstances of the experimental phase, including leakage, monitoring, and unresolved liability issues. From a perspective of sustainable development and information utilization, combining the use of fossil fuels with CCS technology and claiming this combination is sustainable is a debatable standpoint. When there's an opportunity to produce energy through renewable sources like wind and solar power, CCS technology might only be a temporary solution. Further discussions are needed on the comparison and trade-offs between sustainable energy and CCS technology. Public understanding and perceptions of CCS technology are diverse and uncertain, indicating that the social and environmental impacts of CCS technology have not been fully understood and communicated. Therefore, there is a need for more in-depth and broad research on the social science aspects of CCS and strengthening comparative studies of CCS technology across disciplines.

17.6 Conclusion

This paper comprehensively explores the development prospects and potential limitations of Carbon Capture and Storage (CCS) technology from multiple dimensions. On the one hand, CCS technology is widely regarded as an important emission reduction strategy, which can effectively reduce the content of carbon dioxide in the atmosphere and plays a significant role in the global challenge of combating climate change. However, on the other hand, there are certain degrees of skepticism and concern in the academic and industrial communities regarding the sustainability and actual utility of CCS technology. Therefore, future research and development need to delve into and evaluate the potential and risks of CCS technology from the perspective of technology, as well as a broader range of disciplines including society, economics, ethics, and others. If CCS technology is to be widely and comprehensively adopted, it is crucial to fully recognize the uncertainties and risks it may entail, including potential impacts on long-term intergenerational relationships, society, and the environment. This is not a simple decision-making problem; it requires us to actively seek and practice a holistic solution that intertwines and balances diverse factors such as science and society, technology and environment, economics and ethics when dealing with the climate crisis. The future development of CCS technology can only realize its true potential in solving the climate crisis with the collective effort of the entire society.

Competing Interests All authors declare no Competing Financial or Non-Financial Interests.

Data Availability
The data that support the findings of this study are available from the corresponding author upon reasonable request.

Conflicts of Interest Statement
This study received funding from Enerstay Sustainability Pte Ltd (Singapore) Grant Call (Call 1/2022)_GHG (Project ID VS1-001), Singapore. The funder was not involved in the study design, collection, analysis, interpretation of data, the writing of this article or the decision to submit it for publication. All authors declare no other competing interests.

References

Bäckstrand K, Meadowcroft J, Oppenheimer M (2011) The politics and policy of carbon capture and storage: framing an emergent technology. Glob Environ Chang 21(2):275–281

Buck H (2016) Rapid scale-up of negative emissions technologies: social barriers and social implications. Clim Change 139(2):155–167

Cook P (2017) CCS research development and deployment in a clean energy future: lessons from Australia over the past two decades. Engineering 3(4):477–484

Edge P, Gharebaghi M, Irons R, Porter R, Porter R, Pourkashanian M, Smith D, Stephenson P, Williams A (2011) Combustion modelling opportunities and challenges for oxy-coal carbon capture technology. Chem Eng Res Des 89(9):1470–1493

Folger P (2013) Carbon capture: a technology assessment. Congressional Research Service, p 99
Global CCS Institute (2020) Understanding CCS—Global CCS Institute. [Online]. Available at: https://www.globalccsinstitute.com/why-ccs/what-is-ccs/. Accessed 13 Aug 2020
Karayannis V, Charalampides G, Lakioti E (2014) Socio-economic aspects of CCS technologies. Procedia Econ Finan 14:295–302
Kusmer A (2020) Can direct air capture make a real impact on climate change? [Online]. The world from PRX. Available at: https://www.pri.org/stories/2020-07-03/can-direct-air-capture-make-real-impact-climate-change?fbclid=IwAR0Eh1KnqDfTg0Pkx5mNO2SppB1541LXCghAsBfSTTt_0bXIrZ7nziFIuhs. Accessed 13 Aug 2020
Leung D, Caramanna G, Maroto-Valer M (2020) An overview of current status of carbon dioxide capture and storage technologies
Metz B, Davidson O, de Coninck H, Loos M, Meyer L (2005) Carbon dioxide capture and storage. Intergovernmental Panel on Climate Change, New York, p 443
Palm E, Hansson S (2006) The case for ethical technology assessment (eTA). Technol Forecast Soc Chang 73(5):543–558
Rood R (2014) What would happen to the climate if we stopped emitting greenhouse gases today? [Online]. The conversation. Available at: https://theconversation.com/what-would-happen-to-the-climate-if-we-stopped-emitting-greenhouse-gases-today-35011#:~:text=So%20even%20if%20carbon%20emissions,ocean%2C%20will%20continue%20to%20melt. Accessed 12 Aug 2020
Táíwò O, Buck H (2019) Capturing carbon to fight climate change is dividing environmentalists. [Online]. The conversation. Available at: https://theconversation.com/capturing-carbon-to-fight-climate-change-is-dividing-environmentalists-110142. Accessed 14 Aug 2020
The Australian Government (2020) Department of Industry, Science, Energy and Resources—Carbon Capture Storage Flagships. [Online]. Available at: https://www.industry.gov.au/funding-and-incentives/carbon-capture-storage-flagships#:~:text=The%20Australian%20Government%20contribution%20of,costs%20and%20risks%20in%20Australia. Accessed 14 Aug 2020
The Global CCS Institute (2017) The Global Status of CCS, p 43
Van Den Ende J, Mulder K, Knot M, Moors E, Vergragt P (1998) Traditional and modern technology assessment: toward a toolkit. Technol Forecast Soc Chang 58(1–2):5–21
Wilberforce T, Baroutaji A, Soudan B, Al-Alami A, Olabi A (2018) Outlook of carbon capture technology and challenges. Sci Total Environ 657:56–72
Zhu S, Hu H, Yang H, Qu Y, Li Y (2023) Mini-review of best practices for greenhouse gas reduction in Singapore's semiconductor industry. Processes 11:2120. https://doi.org/10.3390/pr11072120

Chapter 18
Studying the Physical Environment of the Chengdu-Demian Economic Circle on Combination Game Theory

Yu Jiang, Xiang Fan, and Yulin Zhang

Abstract A vital component of the urban system, the urban physical environment plays a critical role in information delivery, and the quality of it directly impacts on the viability of cities. Based on the Chengdu-Demian Economic Circle, a more systematic evaluation index system for the urban physical environment was developed in this research. The Combination game theory (CMG) and the improved TOPSIS were adopted to assess the condition of the physical environment in the area. The results of the study revealed that the quality of the physical environment in the Chengdu-Demian Economic Circle was negatively affected by the local natural environment, particularly the scarcity of water resources. Over the study period, there was a pulsating upward trend in the level of geo-environmental conditions in Chengdu-Demian, primarily related to enhancements in water quality, greening levels and sewage treatment capacity. However, the overall state of the physical environment in the Chengdu-Demian Economic Circle is generally unsatisfactory, especially in Deyang, where the average environmental quality remains consistently poor. In conclusion, the physical environment in the Chengdu-Demian Economic Circle exhibited certain issues and challenges that necessitate further efforts in environmental protection and urban greening.

Keywords Urban physical environment · Chengdu-Demian economic circle · Combination game theory (CMG) · Dynamic TOPSIS

Y. Jiang (✉) · X. Fan · Y. Zhang
School of Architecture and Engineering, Tianfu College, Southwestern University of Finance and Economicsrsity, Mianyang 621000, China
e-mail: jiangyu@tfswufe.edu.cn

X. Fan
e-mail: fanxiang@tfswufe.edu.cn

Z. Sun and P. K. Das (eds.), *Proceedings of the 10th International Conference on Energy Engineering and Environmental Engineering*, Environmental Science and Engineering, https://doi.org/10.1007/978-3-031-48204-5_18

18.1 Introduction

Over the past few decades, cities around the world have grown rapidly, with China being no exception. Over 60% of the population lives in China's urban areas currently, with approximately 13–15 million individuals migrating to cities each year. In the next 20 years, the urban population in China will projected to reach about 80% of the total population (Cao et al. 2012). As major consumers of scarce resources, urban areas, contribute to various issues such as a cross-contamination and global pollutant emissions (Sruthi Krishnan and Mohammed Firoz 2020). Recent research indicates that 23% of global deaths are connected to the environment in which people live. The growing prominence of urban disease phenomena like traffic congestion, haze pollution and garbage siege, raises the likelihood of imbalances in non-living components of urban ecosystems. The physical environment within urban areas, a part of the urban system, serves as a medium for conveying information such as light, wind, rain, heat and sound. Abnormal transmission media may hinder a blockage in the functioning of information transmission, directly or indirectly interfering with the normal functioning of the internal and other components of the urban ecosystem (Tai et al. 2020). When this adverse impact exceeds the self-regulation threshold of the ecosystem, may also trigger a chain reaction, even affecting the normal operation of the entire urban system. Therefore, effective measurement and quantification of the urban physical environment are essential for enhancing citizen satisfaction with their living environment and promoting sustainable urban development (Su et al. 2017).

Over the past few decades, most studies have extensively investigated and examined how to evaluate the urban physical environment. These studies have primarily focused on various aspects of building environments, including natural ventilation, lighting and thermal environment, to assess the operational performance inside the building (Yilan et al. 2020; Chong and Haibo 2013). With rapid economic development, large-scale urban construction has resulted in the emergence of city-specific physical environmental problems, such as haze, heat island, etc. (Mills 2008). Researchers, therefore, have gradually begun to shift their attention to the influence of urban form and structure on the urban environment, concerning the urban system as the object. For example, investigating the influence of urban morphology on the wind environment to adjust and optimize the layout of wind channels, as well as exploring the effects of expansion in artificial surfaces on the urban thermal environment, and so on. Research on the urban physical environment the successes of previous studies has provided significant support for decision-making in urban planning and management. While several challenges continue to be faced in this field.

18.2 Construction the Evaluation System

Regarding the urban physical environment, a uniform definition has not yet been established. The urban physical environment is commonly considered to be the physical and built environment within a community, along with the environment providing a place for human activities (Kang et al. 2020). There are interactions as well as constraints between the urban physical environment and human life (Pingyu et al. 2008). Thus, this article is to establish a comprehensive system of assessment indicators from the perspectives of both the "natural environment" and the "built environment", to represent the basic ecological environment in the urban material environment and the main aspects of human activities respectively. The specific indicator system is as follows:

In assessing the fundamental ecological conditions of the urban physical environment, we initially referred to consulted two environmental assessment tools, namely Environmental Performance Index (EPI) developed by the U.S. and Environmental Quality Index (EQI) proposed. We specifically selected the categories of "air quality" "water resources" "noise pollution" and "light environment" when assessing the basic ecological conditions in the urban physical environment (see Table 18.1 for details). Given the rising frequency and intensity of extreme weather events (e.g., heavy rainfall, storms, droughts, etc.), we have also incorporated an indicator for "annual extreme maximum temperature". It is essential to note that the urban physical environment encompasses the natural surroundings but also the physical structure and infrastructure of the city (Kang et al. 2020; Ewing 2005). Therefore, to comprehensively assess the degree of the physical environment, we assessed the built environment in terms of urban land use, greening level, and infrastructure operation.

18.3 Methods

In this study, the weights for each evaluation index were determined using Combination game theory (CMG). Then, the environmental quality index (EQI) for the study area was calculated using an enhanced dynamic TOPSIS method. The construction of the EQI involved the following sequential steps:

Step1: Imputation of Missing Data—We aim to infer missing data by examining the dataset to detect any missing values and subsequently employ linear interpolation techniques to impute the absent values.
Step2: Normalization Processing—Since the data contained variables with different units, all variables were normalized using data standardization to mitigate the impact of varying scales on the analysis. Using the following formula (18.1)–(18.2).

For positive indicators:

Table 18.1 Index weight of urban physical environment evaluation system

System layer	Weights (%)	Indicator layer	Explanation	Index properties	Weights (%)
Natural environment	50.86	Per capital water resources	Reserves of urban water resources (Cbm)	+	9.24
		Proportion of surface water quality classes I–III	Degree of urban surface water pollution (%)	+	7.98
		Days with AQI index level exceeding level 2	Urban air quality	+	8.10
		Average ambient daytime noise in the area	Degree of urban noise pollution	−	8.70
		Per capital water resources	Reserves of urban water resources (Cbm)	+	9.24
		Proportion of surface water quality classes I–III	Degree of urban surface water pollution (%)	+	7.98
		Days with AQI index level exceeding level 2	Urban air quality	+	8.10
		Average ambient daytime noise in the area	Degree of urban noise pollution	−	8.70
		Annual total sunshine hours	Sunshine level (h)	+	8.64
		Extreme maximum temperature of the year	Extent of impact of extreme weather events on cities (°C)	−	8.20
Physical environment	49.14	Proportion of urban built-up land to urban area	Urban land-use situation (%)	+	9.10
		Percentage of green area in developed areas (%)	Greening level of urban built-up areas (%)	+	8.45

(continued)

Table 18.1 (continued)

System layer	Weights (%)	Indicator layer	Explanation	Index properties	Weights (%)
		Per capital area of roads	Urban road traffic conditions (m^2)	+	8.39
		Sewage treatment rate	Wastewater treatment in cities (%)	+	7.70
		Density of water supply pipes in built-up areas	Urban water supply capacity (Cbm)	+	7.64
		Gas penetration	Gas supply capacity of cities (%)	+	7.86

$$r_{ij}^{+} = \left(x_{ij} - \min\{x_i\}/\max\left\{x_j\right\} - \min\left\{x_j\right\}\right) \tag{18.1}$$

For negative indicators:

$$r_{ij}^{-} = \left(\max\left\{x_j\right\} - x_{ij}/\max\left\{x_j\right\} - \min\left\{x_j\right\}\right) \tag{18.2}$$

Step3: Weighting and Aggregation—It is required to give these diverse indicators weights in order to meaningfully combine them into a composite index. The relative relevance of each indicator is indicated by its weight, which has a significant influence on how the index is constructed (Lindén 2018). It is challenging to avoid bias when using a singular method to ascertain the weight value of an attribute (Bin et al. 2014). Three unique and independent methodologies were used to ensure the objectivity of the weights: the entropy method, the coefficient of variation method, and the CRITIC method. Utilizing these methods enables the determination of weights for each evaluation index in a way that produces mutually independent evaluation results. However, conflicting conclusions may arise from the different evaluation methods. Therefore, this paper aims to employ game theory in order to reconcile the contradicting conclusions found by various methods. It proposes a strategy to pool the weights obtained from different methods, allowing for coherence between them, while also introducing competition among them (Jialiang 2003).

Based on the weights calculated by n different methods, the corresponding weight vectors can be obtained and represented by the vector W. The weight vector calculated by method i is then represented by W_i as follows:

$$W_i = \omega_{i1}, \ldots, \omega_{ij} (i = 1, \ldots, N) \tag{18.3}$$

where ω_{i1} ij is the weight of evaluation indicator j based on method i and N is the number of competing methods.

In order to minimize and balance the conflicts, then any linear combination of the weight vector W_c, i.e., the final weights, can be expressed as follows:

$$W_g^i = \sum_{i=1}^{n} \alpha_i W_i (\alpha_i > 0) \tag{18.4}$$

where α_i is the W_i corresponding weight factor.

Step4: Construction of EQI—After determining the weights, we use the improved TOPSIS method to evaluate the relative merits of different objects. The traditional TOPSIS method only applies to the relative merits and demerits among the evaluation objects at a certain point in time, and cannot reflect the time change trend of the evaluation objects. Therefore, this paper adopts a fixed positive (negative) ideal solution to optimize the TOPSIS method in order to calculate the actual EQI value.

$$EQI_i(k) = \overline{d_i^-}(k) / \left(\overline{d_i^-}(k) + \overline{d_i^+}(k) \right) \tag{18.5}$$

$EQI_i(k)$ K is the composite rating of the subject i in year j. $\overline{d_i^{\pm}}(k)$ is the distance of the improved positive (negative) ideal solution, and k is year.

Natural breaks classification method was used to categorize the entire study area in five different classes based on the EQI values: very good quality, good quality, moderate quality, poor quality and very poor quality (Brewer and Pickle 2002; Zou and Yoshino 2017).

18.4 Results

18.4.1 Weight Analysis

The Combination game theory (CMG) was utilized to determine the weights of the indicators, with the results shown in Table 18.1. The primary cause for the bound of the physical environment in the Chengdu-Demian Economic Circle can be attributed to the local natural environment. Water resources are one of the most vital factors affecting the natural environment, weighing in at 9.24%, as well as a severe threat to urban sustainability. The majority of the three cities, namely Chengdu, Deyang, and Mianyang, are situated inland, quite distant from major water sources. Furthermore, the hot and dry climatic conditions during the summer months accelerated evaporation rates and increased water loss, thereby severely limiting the groundwater reserves of the city. In particular, the Per capital water resources in Chengdu and Deyang cities have consistently been far behind the national average. In particular,

Chengdu and Deyang cities consistently lagged significantly behind the national average in terms of per capital water resources.

18.4.2 Analysis of the EQI

During the study period, the levels of the physical environment in the Chengdu-Demian Economic Circle exhibited a pulsating increase (refer to Fig. 18.1a). The main driver of this trend was the improved urban water quality conditions, greening levels, and sewage treatment capacity, providing solid support for the physical environment in the area. These positive changes could be attributed to the implementation of the Water Pollution Prevention and Control Law, which enforces stringent water pollution control requirements and a system of accountability. Simultaneously, China has also significantly increased investment in water environment protection, with approximately 200 billion yuan invested between 2010 and 2022. Consequently, the proportion of water quality conditions in the Chengdu-Demian Economic Circle that meet the functions of surface water class I to III has progressively increased, indicating a noticeable enhancement in the safety and health of the water environment. Moreover, the promotion of urban greening has led to an increase in vegetation cover, thereby providing more ecological resources and positively impacting the living environment of the residents. Despite these improvements, the overall level of the physical environment in the Chengdu-Demian Economic Circle remains substandard (refer to Fig. 18.1b). Specifically, Chengdu and Mianyang only achieved a moderate quality rating of approximately 0.5 to 0.6 over a span of 13 years, while Deyang consistently performs at a poor quality level.

Mianyang had the highest level of physical environment among all cities, with an average score of 0.578, and sustained a medium quality stage (see Fig. 18.2). Its favorable geographical location near the Minshan Mountains and the Tibetan

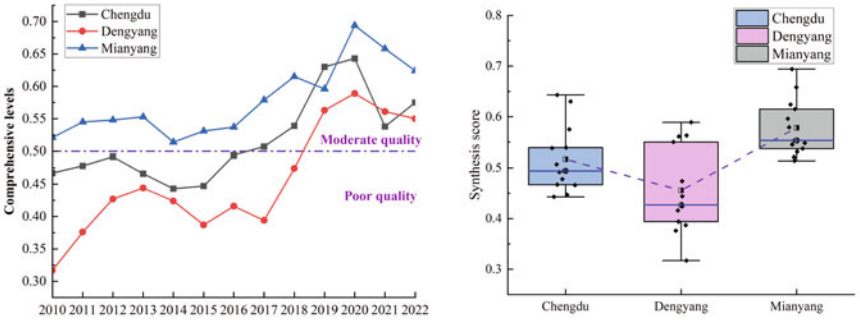

Fig. 18.1 Levels of the urban physical environment in the Chengdu-Demian economic circle over a 13-year period

Plateau, coupled with ample rainfall resources and nourishment from multiple rivers, contribute to the region's abundance of water resources. Furthermore, the city of Mianyang is home to several rivers and reservoirs, including the Shenluo and Pengjiang Rivers, which collectively form a comprehensive water resource system. It should be noted, however, that the development of Mianyang's physical environment has been constrained by scarcity of green space in urbanized areas. Throughout the study period, Mianyang exhibited a green coverage rate of just 39.54%, consistently falling below the national average. The insufficient green cover indicates a dearth of vegetation capable of providing shade and absorbing heat, thereby contributing to the occurrence of extreme heat events in Mianyang. This was evident from the record-high temperature of 32 °C in 2022.

Chengdu successfully transitioned from a stage characterized by the poor quality stage to the medium environment stage during the study period, similar to the situation in Deyang. In the process of urban planning and construction, Chengdu has implemented several greening projects, most notably the Tianfu Greenway and the Panda Greenway, contributing to a gradual increase in overall greening coverage over the years. By 2022, the green coverage rate has already reached an impressive

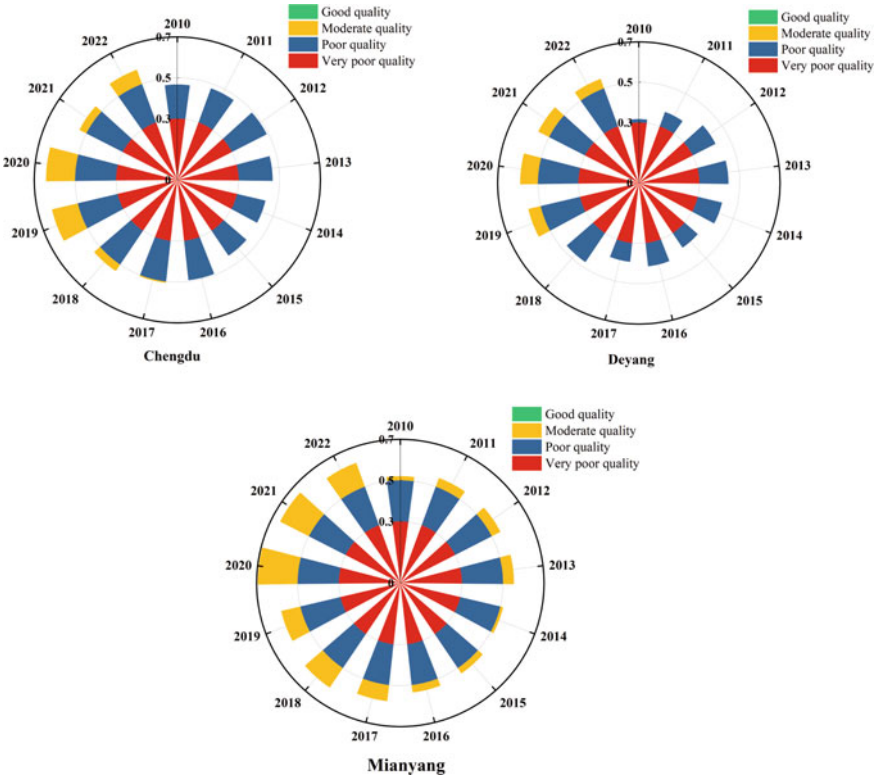

Fig. 18.2 The tendency of each city's physical environment development

44.61%, at a high level among the sub-provincial cities in China. As the capital city of the province and the center of central and western China, Chengdu's appeal to the population has been steadily growing. Consequently, its population share in Sichuan Province has witnessed a sharp rise, with the resident population surpassing 20 million in 2022. However, the increase in population density has given rise to certain challenges. The intensification of the heat island effect in industrial, transportation, and densely populated areas has caused heat to accumulate in the city. This issue was manifested in an upward trend in extreme maximum temperatures and a significant exacerbation of noise pollution.

Deyang faced significant challenges in its physical environment, primarily related to the deterioration of the water environment and insufficient water supply capacity. Being an industrial city, Deyang houses numerous factories and enterprises, resulting in the pollution of the water environment due to wastewater and exhaust emissions from these industrial activities. Meanwhile, agriculture sector, a key industry in Deyang, has further exacerbated the water environment problems with the excessive use of chemical fertilizers and pesticides. Consequently, the superimposed effect of these two factors made the proportion of surface water in Deyang reaching the function of Class I–III waters increase to only 64.34% in 13 years. Compared to other cities, Deyang has experienced relatively slow urban development, inadequate water supply infrastructure, and strained water supply capacity, so water shortages and impaired water quality may occur frequently. However, with the progression of urbanization, Deyang has increased efforts in constructing and renovating wastewater treatment facilities. The construction and renovation of new wastewater treatment plants, wastewater pipeline networks, and other related facilities have significantly enhanced the capacity and effectiveness of wastewater treatment, a major determinant for the improvement of Deyang's physical environment.

18.5 Consultation

The urban physical environment indicator system for the Chengdu-Demian Economic Circle was constructed in this paper, and it was thoroughly analyzed using the CMG and the improved dynamic entropy weight-TOPSIS. During the study period, the physical environment in the Chengdu-Demian Economic Circle showed a pulsing upward trend, which can be attributed to the Water Pollution Prevention and Control Law's implementation and the rise in national investments in the protection of the water environment. In the Chengdu-Demian Economic Circle, the percentage of water quality conditions that meet the requirements of surface water classes I to III has gradually increased, and the security and well-being of the aquatic environment have been significantly improved. Furthermore, the encouragement of urban greening has brought positive impacts on the living environment of the residents.

Despite some encouraging developments throughout the course of the study, the Chengdu-Demian Economic Circle continues to struggle with a subpar physical environment. Both the natural environment and human activities have an impact on the

physical environment's quality. The physical environment in the area is generally poor due to a combination of natural elements including water scarcity, heat, and drought, as well as human activity like agricultural pollution, industrial effluent, and other environmental issues. In particular, while Deyang's average level was still subpar, the physical environment levels in Chengdu and Mianyang were only at the stage of medium grade. Enhancing the protection of water resources, expanding green space, expanding the capacity of sewage treatment, and upgrading water supply infrastructure are all important to improve the physical environment's quality. Furthermore, to support sustainable growth, it is also necessary to improve environmental management and monitoring and to create tougher environmental protection rules.

Funding This paper be fund by Tianfu College, Southwestern University of Finance and Economics (TFXY2023YB05).

References

Bin Y et al (2014) A novel combination weighing method and its application in sluice safety evaluation. J Yangtze River Sci Res Inst 31(10):108–113

Brewer CA, Pickle L (2002) Evaluation of methods for classifying epidemiological data on choropleth maps in series. Ann Assoc Am Geogr 92(4):662–681

Cao G et al (2012) Urban growth in China: past, prospect, and its impacts. Popul Environ 33:137–160

Chong X, Haibo Y (2013) Simulation analysis of the implementation strategy of the architecture schematic design using Ecotect software. Industr Constr 43(08):157–160+28

Ewing R (2005) Can the physical environment determine physical activity levels? Exerc Sport Sci Rev 33(2):69–75

Jialiang C (2003) Research on portfolio empowerment evaluation method based on Game Theory. Fujian Comput 09:15–16

Kang Y et al (2020) A review of urban physical environment sensing using street view imagery in public health studies. Ann GIS 26(3):261–275

Lindén D (2018) Exploration of implicit weights in composite indicators: the case of resilience assessment of countries' electricity supply

Mills G (2008) Luke Howard and the climate of London. Weather 63(6):153–157

Pingyu Z et al (2008) Coordination degree of urban population, economy, space, and environment in Shenyang since 1990. China Popul Resour Environ 18(2):115–119

Sruthi Krishnan V, Mohammed Firoz C (2020) Regional urban environmental quality assessment and spatial analysis. J Urban Manage 9(2):191–204

Su S et al (2017) Area social deprivation and public health: analyzing the spatial non-stationary associations using geographically weighed regression. Soc Indic Res 133:819–832

Tai X, Xiao W, Tang Y (2020) A quantitative assessment of vulnerability using social-economic-natural compound ecosystem framework in coal mining cities. J Clean Prod 258:20969

Yilan N, Jiang H, Hongjuan L (2020) Measurement investigation of the physical environment in the entrance hall of an exhibition building. J Guangxi Univ (Nat Sci Ed) 45(01):210–220

Zou T, Yoshino K (2017) Environmental vulnerability evaluation using a spatial principal components approach in the Daxing'anling region, China. Ecol Indicators 78:405–415

Chapter 19
Research on Urban Renewal Strategies in China from the Perspective of Carbon Neutrality

Jianxin Tang and Yingjian An

Abstract In China's "dual carbon" strategy, the time interval between achieving carbon peak and carbon neutrality is relatively short, and achieving carbon neutrality goals is a short and heavy task. According to analysis, China's carbon emissions mainly from cities. Urban renewal, as an important way for the further development of cities, is of great significance for achieving green and sustainable development. Fully considering carbon neutrality in the process of urban renewal is of great significance for achieving China's "dual carbon" goals. This article will analyze strategies for reducing carbon emissions and increasing carbon sinks in the process of urban renewal from the perspective of carbon neutrality. We mainly conducted sorting and research on the renovation of old residential areas and urban ecological restoration.

Keywords Carbon emissions · Carbon neutrality · Urban renewal · Building energy efficiency · Carbon sink

19.1 Introduction

With the rapid development of the economy, China's total carbon emissions are also rapidly increasing. In the face of increasingly severe international emission reduction pressure, China's carbon emissions have become one of the focuses of global attention. Carbon neutrality is the main tone of future global development, and China has a long way to go in terms of carbon neutrality (Caicai et al. 2021). As of the end of 2020, a total of 44 countries and economies around the world have officially announced carbon neutrality goals, including countries and regions that have achieved the goals, have written them into policy documents, and have proposed or completed legislative procedures. China plans to peak its carbon dioxide emissions by 2030 and achieve carbon neutrality by 2060.

J. Tang · Y. An (✉)
Shanghai Construction Management Vocational College, Shanghai 201702, China
e-mail: 1279820353@qq.com

Z. Sun and P. K. Das (eds.), *Proceedings of the 10th International Conference on Energy Engineering and Environmental Engineering*, Environmental Science and Engineering, https://doi.org/10.1007/978-3-031-48204-5_19

Urban renewal is a redevelopment process that must be experienced after a certain stage of urban development. With the advancement of urbanization and the tremendous changes in living methods in China, people's requirements for living environment and urban ecology are also increasing. Especially at present, China's economic transformation is shifting from high-speed to high-quality, which also requires the development trend of urban renewal to be in line with it, moving towards a more meaningful and high-quality development stage, and contributing more efforts to the better life of the people (Yan 2022; Lizheng and Yumin 2022). Therefore, urban renewal itself contains the concept of "carbon neutrality".

According to statistics, cities are the main source of carbon emissions. If the "carbon" issue is fully considered in the process of urban renewal, it is of great significance for China to achieve the "dual carbon" goal. Among them, the renovation of old residential areas and urban ecological restoration, as important contents of urban renewal, can effectively reduce carbon emissions and increase carbon sinks. On the basis of analyzing the current situation of urban renewal, this article summarizes how to achieve sustainable and green development of urban renewal from the perspective of carbon neutrality, and proposes corresponding strategies.

19.2 Current Situation of Urban Renewal in China

From the perspective of foreign development history, urban renewal can be simply divided into four basic stages after the end of World War II: demolition and reconstruction, community renewal, old city development, and organic renewal. During the evolution process, the purpose of renewal has shifted from solving a single problem to achieving the establishment of a multi-objective comprehensive system, and the behavioral characteristics have shifted from large-scale demolition and construction to a model that combines size and scale with advance planning and reasonable layout, The update mechanism has shifted from government led to a diversified co governance of the public, enterprises, and government, with a value oriented shift from improving material space to protecting and enhancing public interests.

The concept of urban renewal mentioned earlier in China was more about the "three old" renovation, which refers to the release of a large amount of land through the renovation of old towns, factories, and villages to meet the needs of road opening and building. But urban development does not expand space through one-on-one land replacement, but rather requires upgrading and upgrading the industrial structure in order to maintain sustainable social and economic development. Overall, the current urban renewal in China includes the renovation of old cities and the renovation of shantytowns. Old city renovation is a form of contemporary urban renewal, and shantytown renovation belongs to the broad category of old city renovation. Therefore, urban renewal also starts from the perspective of people-oriented urbanization quality improvement and rational utilization of urban culture in existing urban areas. It steadily updates public facilities, existing buildings, and existing construction land in urban areas in a scientific, reasonable, and effective manner, in accordance with

the principles of improving the quality of urban development and balancing the improvement of residential conditions and the coordinated development of urban culture.

Urban renewal can be generally divided into demolition and construction, renovation, and preservation categories based on the degree of renovation. The retention category includes two situations: one is the dimension of the current situation, and the other is to assign new uses to existing buildings on the basis of retaining them. Urban renewal can be divided into three categories according to development models: government led, market led, and government market cooperation. Under these three major categories, they are further divided into nine sub categories based on different development models, including collection and storage models, rural collective self improvement models, and land consolidation models. Compared to before, urban renewal now places more emphasis on overall urban spatial planning, land use, balance of resource allocation, and improvement of living environment. The content and mode of urban renewal are increasingly diversified and enriched. In the new era, the main tasks of urban renewal include optimizing urban spatial layout, completing urban ecological restoration and functional improvement projects, strengthening the renovation of old urban communities, and promoting the construction of new urban infrastructure.

19.3 Current Status of Carbon Emissions in Chinese Cities

At present, China's carbon emission intensity is higher than the global average. According to relevant data statistics, the energy consumption per unit of GDP in China in 2019 was 3.4 tons of standard coal. This value is 1.5 times the global average, indicating that China's energy utilization efficiency is low (Yuping et al. 2022). The major carbon emitters in China are electricity, industry, transportation, and construction, accounting for almost 90% or more of the country's carbon emissions.

From the perspective of energy terminal carbon emissions, the construction sector accounts for a considerable amount of carbon emissions, ranking fourth. From the perspective of carbon emissions throughout the entire construction process, the construction department has become the department with the highest carbon emissions. Figure 19.1 shows the carbon emissions of buildings in China in 2019. The carbon emissions from the entire construction process accounted for 51.3% of the total carbon emissions, while the production and operation stages of building materials accounted for 28.3% and 21.96% respectively. It can be seen that vigorously developing green buildings is an important means for China to achieve carbon neutrality goals. The implementation of green buildings significantly improves energy utilization efficiency and reduces building energy consumption levels through passive technology and renewable energy technologies. In urban renewal, the proportion of building renewal is the highest, including the renewal of new and old buildings, which needs to be given priority consideration.

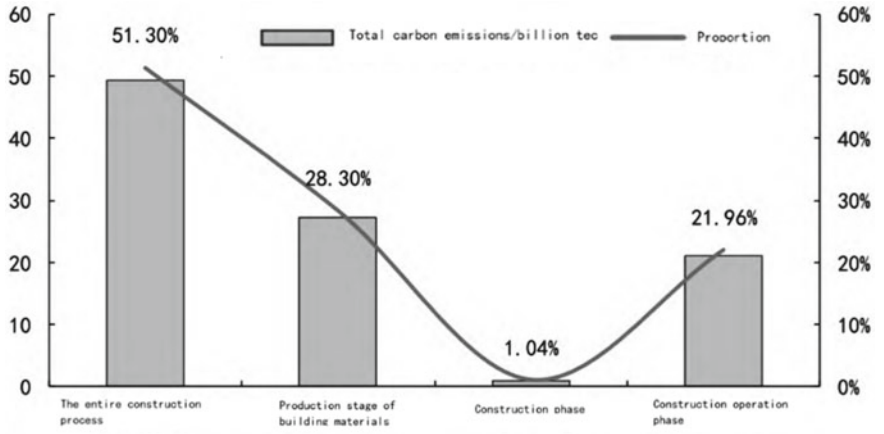

Fig. 19.1 Carbon emissions from Chinese buildings in 2019

19.4 Carbon Neutrality Strategy in Urban Renewal Process

Urban renewal has two important contents: building construction, renovation and expansion, and urban ecological restoration. Among them, in the process of building construction, renovation and expansion, it is necessary to consider how to save energy, and fully utilize emerging building methods to achieve "production capacity", giving buildings a new connotation of "energy conservation + production capacity"(Jingzhi and Hong 2022). In addition, with the gradual improvement of China's carbon trading market system, urban forestry carbon sinks will also be gradually put on the agenda, which is also in line with urban ecological restoration. Therefore, in urban renewal, we can focus on reducing carbon emissions and increasing carbon sinks from the following three aspects.

19.4.1 Vigorously Developing Photovoltaic Buildings

Photovoltaic buildings are a typical type of green building, as shown in Fig. 19.2. It is a new application field of solar power generation, which integrates photovoltaic power generation systems with building external structures to achieve energy conservation and consumption reduction in buildings. It is one of the important means to achieve low energy consumption passive buildings (Li and Yanmei 2022). According to the difference in integration level, photovoltaic buildings can be divided into: rear mounted photovoltaic power generation roof system (BAPV), which generally refers to the installation of solar photovoltaic power generation systems on existing buildings, utilizing idle space in the building to generate electricity, and mostly used for renovation of existing buildings; The Integrated Photovoltaic Building System

Fig. 19.2 Photovoltaic building

(BIPV) is a solar photovoltaic power generation system that is designed, constructed, and installed simultaneously with the building, and integrated with the building, taking into account both power generation efficiency and building appearance. BAPV and BIPV are respectively targeted at newly built and renovated buildings, both of which are involved in the urban renewal process.

19.4.2 Increase the Proportion of Garden Carbon Sink

Urban green space is an effective way to absorb carbon dioxide and reduce the "greenhouse effect" in the medium to long term, and is an important cause for optimizing ecology and meeting people's sense of happiness. Although the policy of absorbing carbon dioxide through urban green space is not yet clear, under the medium to long-term goal of carbon neutrality, urban green space is likely to become one of the important means and is expected to improve the medium to long-term demand expectations of the landscaping industry. In the context of carbon neutrality, the increase in carbon sequestration demand will also bring new development opportunities to the ecological landscape industry. At the same time, in the future, with the continuous improvement and refinement of market-oriented forestry carbon sequestration project management mechanisms and policies, it will be more conducive to the development

of the landscape industry. In the carbon emissions trading market, the carbon sink trading model has gradually formed, and forestry carbon sink trading has created a new business model for ecological garden construction, enhancing the economic value of ecological products. Forestry carbon sequestration trading refers to trading the carbon sequestration capacity of trees as a commodity: when the carbon emission quota of enterprises is insufficient, they can purchase carbon quotas or CCER (China Certified Emission Reduction) circulating in the carbon market. Due to the carbon sequestration value of trees, carbon sequestration assets can be traded as financial products in the carbon emission trading market, generating carbon sequestration profits (Xiaoming et al. 2022). In the future, carbon sequestration can be considered as one of the indicators for urban renewal.

19.4.3 Fully Utilize Digital Technology

Digital technology can provide networked, digital, and intelligent technological means for the green development of the economy and society, empower the construction of a clean, low-carbon, safe, and efficient energy system, assist in industrial upgrading and structural optimization, promote green changes in production and lifestyle, and promote the reduction of overall energy consumption in society. During the operation of buildings, a large amount of carbon emissions will be generated, and digital technology can greatly reduce building energy consumption. In the construction operation and maintenance phase, the application of digital technology is mainly reflected in real-time monitoring and response of the entire building through the Internet of Things, big data, cloud computing platforms, etc., to reduce the overall energy consumption of operation and maintenance. For example, through the Internet of Things technology, corresponding sensors can be installed inside the building to monitor real-time data such as PM2.5, volatile pollutants, carbon dioxide concentration, air humidity, temperature, etc. inside the building. Unified calibration can be carried out through cloud computing platforms, and then corresponding electrical equipment (such as air conditioning, fresh air systems, etc.) can be manipulated through the Internet of Things for adjustment. For example, digital technology can improve the energy efficiency of buildings through energy management systems. Specifically, using furniture and appliances in buildings as carriers, IoT technology and machine learning technology are used to provide energy monitoring, energy management, energy analysis, energy services, etc. for buildings, achieving unified scheduling and optimized balance of overall energy in buildings.

19.5 Conclusion

China's "dual carbon" policy and urban renewal are both major strategies designed at the top level of the country, playing an important role in achieving sustainable development. The analysis shows that the two are not contradictory, but can be organically combined. In the process of urban renewal, measures such as vigorously developing photovoltaic buildings, increasing the proportion of garden carbon sinks, and fully utilizing digital technology can effectively reduce carbon emissions and increase carbon sinks. In the future urban renewal process, the effective integration of "dual carbon" is of great significance for the development of cities in China.

References

Caicai Z, Dongbo H, Chengye J et al (2021) The connotation and path of world energy transformation and its significance for carbon neutrality. J Petrol (2):233–247

Jingzhi S, Hong S, Rong T (2022) The enlightenment of urban renewal development research and green and low carbon concept on yanjiao urban renewal. Mod Hortic (22):167–169+172

Li X, Yanmei C (2022) Research on green transformation of buildings in urban renewal areas. Urban Archit Space (12):228–229

Lizheng Z, Yumin Y (2022) 40 years of renewal governance of urban villages: evolution and prospects of academic thought. Urban Plann (5):103–114

Xiaoming Z, Guobing W, Zhiwei G et al (2022) The main principles and approaches for enhancing forestry carbon sequestration. J Nanjing Uni (6):167–176 (Natural Science Edition)

Yan T (2022) Key dimensions and strategy analysis of urban renewal system construction in china. Int Urban Plann (1):1–8

Yuping D, Hongjun W, Ge R et al (2022) Measurement Challenges Faced by the Path to Carbon Neutrality in the Construction Industry. Refrg Air Conditioning (6):944–949 (Sichuan)

Chapter 20
Alternative Building Materials for a Sustainable Built Environment: A Literature Review

Jocelyn A. Rivera-Lutap, Orlean G. Dela Cruz, Jhun M. Jacinto, Leslie Mae D. Vael, and Manuel M. Muhi

Abstract The Industrial Revolution altered how people worked, the technologies at their disposal, and, in many cases, where they lived. It made life easier for many people; however, it must be considered that more needs and wants would result in unending changes in our built environment. Several building typologies have been derived to address the people's demands. At the same time, the construction methods have changed significantly, and the materials used in construction sourced from our natural resources have remained the same for centuries. While research has constantly shown us the construction industry's impact on the environment, people have remained adamant until they have felt the effects of climate change. The review of Alternative Building Materials (ABM) aims to demonstrate why the building industry must consider this substitute to protect the environment and humanity. The study investigated the various ABMs, their characteristics, acceptability, and the importance of exploring these possibilities on a small scale of the built environment but on a scale where it can have the most significant impact.

Keywords Alternative building materials · Materials waste · Built environment · Construction materials · Construction methods

J. A. Rivera-Lutap
College of Architecture, Design, Built and Environment, Polytechnic University of the Philippines, Sta Mesa, Manila, Philippines
e-mail: jarlutap@pup.edu.ph

J. M. Jacinto
School of Engineering, Aurora State College of Technology, Aurora, Philippines

O. G. Dela Cruz (✉) · M. M. Muhi
Graduate School, Polytechnic University of the Philippines, Manila, Philippines
e-mail: ogdelacruz@pup.edu.ph

M. M. Muhi
e-mail: mmmuhi@pup.edu.ph

O. G. Dela Cruz · L. M. D. Vael · M. M. Muhi
Department of Civil Engineering, Polytechnic University of the Philippines, Manila, Philippines

Z. Sun and P. K. Das (eds.), *Proceedings of the 10th International Conference on Energy Engineering and Environmental Engineering*, Environmental Science and Engineering, https://doi.org/10.1007/978-3-031-48204-5_20

20.1 Introduction

The "Calendar effect," on the other hand, is widely dismissed by meteorologists. However, it was not until 1965 that a US President Advisory Committee panel warned of the greenhouse effect as a "real concern." It took nearly a decade for this concern to be raised at the United Nations, paving the way for establishing The United Nations Environment Programme (UNEP) in 1972. The first United Nations Environment Conference was still concerned with chemical pollution, nuclear testing, and whaling. Only in 1987, at a UNEP meeting, was the Montreal Protocol agreed upon, limiting chemicals that deplete the ozone layer. The Kyoto Protocol, adopted in 1997, puts into action the United Nations Framework Convention on Climate Change by engaging industrialized countries and economies in development to limit and decrease greenhouse gas emissions through agreed-upon individual objectives. The Convention only requires those countries to implement mitigation policies and measures and report regularly.

Sea-level rise has consistently indicated global warming, ozone depletion, and climate change. These are inextricably linked to human activities such as deforestation and the use of fossil fuels usage, as well as construction. Construction is recognized as a critical factor, drivers who promotes greenhouse gas emissions on a large scale in various activities such as material production, land clearing, and engine maintenance. Emissions, demolition, combustion, and hazardous chemicals, among other things (Labaran et al. 2022). The built environment contributes approximately over half of annual worldwide CO_2 emissions, according to Architecture 2030. Construction activities account for 27% of total emissions, with materials and construction (embodied carbon) accounting for the remaining 20%. Construction consumes approximately fifty percent of all energy and raw materials utilized globally (International Energy Agency 2018). Land clearing, equipment engine emissions, demolition, burning, and the use of hazardous chemicals all contribute to environmental pollution (Philips Akinyemi et al. 2019). Global energy intensity—an important measure of the economy's energy efficiency—is predicted to improve (decrease) by 1.9% in 2021, after improving by only 0.5% in 2020.

However, following the worst year in a decade, the requirement to double for net zero by 2050 is predicted to return to their ten-year average. To match the IEA Net Zero Emissions by 2050 Scenario, the pace of progress must double from current levels. Over the last five years, energy intensity has increased by 1.3% per year on average, down from 2.3% between 2011 and 2016, and far below the 4% predicted in the Net Zero Emissions by 2050 Scenario for 2020–2030 (Net Zero by 2050, 2021).

The significance of Alternative Building Materials (ABM) involves environmental protection through decreased energy consumption and CO_2 emissions, affordable housing, energy conservation, meeting the growing need for housing stock, job opportunities, and the advancement and propagation of the traditional technological creativity and skills of our local people. ABMs are environmentally friendly materials because they help to reduce environmental impact. ABMs can improve construction

sustainability by saving energy and resources (energy-efficient, resource-efficient, etc.) and lowering the structure's embodied energy (Josiah Marut et al. 2020).

20.2 Methodology

This literature review is similar to the study of Dela Cruz et al. (Dela Cruz and Dajac 2021; dela Cruz and Ongpeng 2022; Dela Cruz et al. 2021a, b; Roxas et al. 2023; Bernabe et al. 2023) which data analyses that use a Latent Dirichlet Allocation (LDA). Topic models are probabilistic techniques that can investigate high-level text relationships. Each text and subject is represented by topic modeling as a collection of themes and phrases.

20.3 Discussion

20.3.1 Alternative Materials for Building Materials

Building materials, technologies, and practices in earlier times were limited by the availability of materials in the neighborhood and the skills of the homeowners and the community. Stones, mud, thatch made from leaves and reeds, and timber have evolved into more durable building materials. Brick burning to use metal products represents increased energy consumption of manufactured building materials. Today's construction materials include bricks, cement, steel, aluminum, plastic products, paints, polished stones, ceramic products, and the like. These materials are energy-intensive and must travel long distances before being used in construction (Reddy 2004).

Bricks have been utilized for the construction and building process for thousands of years. Since both cement and lime-based calcium-silicate-hydrate bricks are likewise not environmentally friendly, geopolymerisation is a better option for making bricks; nonetheless, cost–benefit assessments for relevant research are required. Clay-based geopolymer bricks may be the focus of future brick research, with the main difficulty being to improve clay reactivity at a cheap cost (Zhang et al. 2018). The geopolymeric approach was used to provide a better option for high-strength pervious concrete as a replacement for conventional concrete. The samples' aggregate size and aggregate binder ratio were changed. The compressive strength was 39.9 MPa and the flexural strength was 2.2 N/mm^2 with a void of 37.7% and a density of 1988.14 kg/m^3. Previous study on pervious concrete has found a correlation between void content and compressive strength. An optimum void-to-strength ratio with environmental benefits validates its use in various buildings (Wijeratne et al. 2021).

The sand was first utilized in the construction industry after the introduction of cement. Sand is used as fine aggregate in concrete worldwide, and an estimated 40

billion tons of natural sand are used each year. This enormous consumption depletes the water table and destroys biodiversity, flora, and fauna. As a result, identifying alternative construction materials for natural sand plays a vital role for built environment practitioners in achieving a sustainable environment through the optimum percentage of replacement with waste products to alter the fine aggregate. Natural sand demand is stabilized by modifying new construction materials. Waste material with properties like natural sand reduces waste. Natural sand demand is stabilized by modifying new construction materials. Waste material with properties like natural sand reduces waste. The effective use of alternative fine aggregate improves the mechanical properties of the concrete. When compared to natural sand, copper slag is widely available on the market at a low cost (Hamid et al. 2021).

Regarding physical properties, species Ochroma pyramidal, a fast-growing tree, is a good alternative for producing wood-cement boards because all water absorption and thickness swelling values were lower than those reported in the literature and met manufacturer requirements. Nonetheless, the boards demonstrated mechanical properties compatible with literature data but lower than what manufacturers require for commercial products. Another advantage is that there is no need for particle treatment, which reduces production costs (Setter et al. 2020).

20.3.2 Characteristics of Alternative Building Materials

The effect of SHA and RCA on density, compressive strength, and hydraulic properties of PC made with natural aggregate (NA) was investigated in order to create a more environmentally sustainable and cost-efficient structure. SHA was employed as a partial replacement for cement at various amounts, and its effect on PC mixes created with NA and RCA was examined. Finally, the sustainability and cost-effectiveness of employing wastes, SHA, and RCA in PC manufacturing were established. The study revealed the effect of using SHA as a fractional substitute for cement and RCA as a substitute for NA on improving hydraulic characteristics at acceptable strength and lowering CO_2 emissions. The cost effectiveness of PC production was also proven (Poornima et al. 2021).

Using crumb rubber and copper slag aggregates as partial substitutes in industrial brick production. Rubber waste has a significant impact on the environment. Regarding solid waste management, the disposal of copper slag is a concern. Reusing and recycling these wastes as a partial substitution in the production of industrial brick will undoubtedly make a significant contribution to the economy and the environment by reducing the adverse effects of accumulated rubber debris and copper slag (Ameri et al. 2020; Tijani et al. 2022; Chithra and Praburanganathan 2022).

The study evaluated at how Mussel shell ash (MSA) and ground granulated blast furnace slag (GGBS) performed as partial cement replacements in concrete. The experimental results lead to the following conclusions: employing GGBS and MSA as partial cement replacements in concrete reduces concrete density significantly when compared to ordinary concrete. It could be because GGBS has a lower specific

gravity than OPC, making it less dense than traditional concrete. Concrete samples containing 40% GGBS and 5% MSA had higher compressive strength after 90 days, with an increase of roughly 1.8%. The concrete sample comprising 50% GGBS and 5% MSA had the lowest compressive strength test results (Hamid et al. 2021; Martínez-García et al. 2021).

Granite powder was utilized as a partial replacement for copper slag fly ash in various percentages, while crumb rubber was used as a partial replacement for stone dust. There are investigations on mechanical, durability, morphology, Fourier transforms infrared (FTIR), the preferred method of infrared spectroscopy, and Ultrasonic pulse velocity (UPV). The bricks of a prototype mix design formed of granite waste and copper slag with a suitable amount of fly ash and lime-gypsum binder provide improved strength and durability, according to the findings. The proposed bricks have two advantages: they are environmentally beneficial because they are created from sustainable waste and can be used for load-bearing structural components; and they can be used for load-bearing structural elements (Chithra and Praburanganathan 2022). Table 20.1 shows the assessment and performance of Alternative Building Materials.

20.3.3 Acceptability of the Alternative Building Materials

The main factors influencing alternative building material buying decisions were perceived health problems and environmental concerns during the production or disposal of insulating boards. Two subgroups' acceptance characteristics were established, with health and environmental factors influencing acceptance decisions the examination of Carbon Capture and Utilization (CCU) technologies. The use of CCU-based insulating boards provided useful insights into potential consumers' perspectives, acceptability levels, and decision-making patterns, resulting in tangible recommendations for promoting CCU technology and CO_2-based products. The general evaluation of CCU insulating boards was favorable, with environmental benefits recognized but countered by—slight—worries about the CCU technology's limited sustainability. The findings contribute to a better understanding of the public's response to the development of sustainable technologies and goods, as well as a better alignment of their development and communication with the demands of the population and future consumers. Understanding could inform research and industry about acceptance aspects at an early stage, allowing technological development and product rollout to be optimized on technical, economic, and ecological characteristics while also incorporating critical acceptance parameters (Arning et al. 2021). These are initial investment costs and construction cost savings, material costs, end-user awareness of the material or technology, result, user perspective, ease of use of technology, training requirements, cost reduction, ABM pollution, durability, structural strength/capability of the materials installation speed, overall construction time reduction, environmental regulations (Occupational Safety and Health Administration and other Public Health Act), building codes, and material accessibility handling and storage

Table 20.1 Assessment and performance of alternative building materials

Category	Key results	References
Bamboo	• Its lightweight and superior physical and mechanical properties have attracted the attention of civil engineers, architects, academics, designers, and artists • Far has proven that the use of bamboo in construction indeed will promote sustainable construction because bamboo has many environmental benefits that can entice people to use it to improve their socio-economic standing • Adding bamboo to cement has been reported as strengthening concrete structures, with great potential for the mass construction of inexpensive dwellings, or as an excellent material for building structures with remarkable resiliency to earthquakes and landslides • Lightweight and high-strength, it is an alternative and renewable construction material that has earned the name of 'vegetal steel'	Chaowana et al. 2021; Manandhar et al. 2019; Borowski et al. 2022)
Recycled concrete aggregates (RCA)	• Reduced waste quantities, improved environmental friendliness, preservation of natural resource base, steel recapture during recycling, and reduced waste disposal costs • Represents a 22–65% reduction in the emissions from natural aggregate production • Construction does not make the pavement unbearably susceptible to moisture damage when the construction is done at the optimum moisture content of the particular RCA asphalt mix • Preservation of natural materials and help meet the challenges of solid waste disposal • RCA would allow for better binder drain-down performance at higher OBC when utilized for asphalt mixtures	Maduabuchukwu Nwakaire et al. 2020; Nwakaire et al. 2020; Nwakaire et al. 2022; Fardin and Santos 2020)
Mycelium	• Fungi have dense mycelium, grow fast at locally available media, and have no toxicity level • The material has also shown great fire-retardant properties, making it safer for construction applications	Alemu et al. 2022; Javadian et al. 2020; Girometta, et al. 2019)
Green roof	• The costs for extensive green roofs are lower compared to traditional flat roofs • Green roofs usually have lower environmental impacts due to reduced energy demand and increased membrane lifespan	Rosasco and Perini 2019; Mihalakakou et al. 2023; Rizzo et al. 2023)

requirements deemed critical in the acceptance of ABM for walling (Odongo 2019). Attempts to replace conventional construction materials are derived from utilizing materials with less carbon footprint than their counterparts. While some by-products have achieved this goal, the materials developed have shown different drawbacks.

20.3.4 Importance of Alternative Materials

Alternative Building Materials must be recognized by the construction sector. The 11th of the United Nations Sustainable Development Goals, Sustainable Cities and Communities, is interpolated throughout the organization's other goals. The construction industry is regarded as one of the world's primary sources of pollution. It has massive direct and indirect environmental effects. The top ten most significant ecological impact factors identified by all respondents are as follows: Consumption of raw materials, generation of noise and vibration, removal of vegetation, interference with ecosystems, water consumption, electricity consumption, edaphic soil loss, dust generation from machinery, and routine waste and energy consumption. The findings also revealed that all respondents agreed that the resource. The most influential environmental impact was the consumption group. The effects on biodiversity were regarded as the second most important cause of environmental deterioration after the effects of local issues (Ansah 2015).

One of the biggest environmental implications seems to be the consumption of renewable and nonrenewable resources. This can be interpreted as the construction process consuming a large amount of raw materials such as sand, gravel, clay, calcium carbonate, water, aggregate, wood, iron, bitumen, aluminum, and vehicle gasoline (Enshassi et al. 2014). Several of the industrial waste that is typically disposed of in landfills pose environmental risks. However, studies demonstrate that this waste can be used as a natural aggregate replacement in concrete/mortar, however this greatly increases material density, production, and handling costs (Chithra and Praburanganathan 2022).

20.4 Research Gaps

Environmental issues such as global warming, ozone depletion, erosion, natural depletion of natural resources, solid waste generation, and indoor air quality are exacerbated by the construction sector (Tatari and Kucukvar 2012). For current and future generations, preserving our environment and its environmental assets is paramount (Palmeira et al. 2021). The expensive cost of conventional construction materials has prompted researchers to explore and discover sustainable and environmentally friendly alternatives (Alabi 2020). Alternative building materials can potentially decrease construction's environmental impact, which is one of their benefits. Conventional building materials, such as concrete and steel, are resource-intensive

and can result in a substantial carbon footprint. Alternative building materials have gained attention in recent years due to concerns about sustainability and the environmental impact of traditional construction materials. While some research has been conducted in this area, several gaps in knowledge still need to be addressed. Table 20.2 summarizes recent studies' challenges concerning alternative building materials research advancement.

Six (6) identified difficulties must be overcome to maximize the utilization of alternative building materials. It was determined that the most significant research gaps in the field of alternative building materials are the establishment of standard requirements for ABM, additional studies on the environmental consequences of ABM, and construction industry awareness regarding the use of ABM. Many research studies emphasize the importance of developing and utilizing alternative construction materials and the architectural, structural, and environmental benefits of incorporating such materials. Developing new manufacturing techniques for alternative building materials can improve quality and reduce production costs. Quality assurance and control processes are essential for ensuring alternative building materials' safety, quality, and performance.

Even with challenges, using alternative building materials comes with challenges. Architects, engineers, and constructors need familiarity with these materials to handle

Table 20.2 Challenges imposed on ABM

Challenges	References
Technological process advancement of alternative building materials	Philips Akinyemi et al. 2019; Zhang et al. 2018; Tahmasebinia et al. 2021; Ameh et al. 2019; Meddah et al. 2019; Kumar and Agrawal 2019)
Awareness of the construction industry on alternative building materials	Philips Akinyemi et al. 2019; Josiah Marut et al. 2020; Reddy 2004; Ansah 2015; Tatari and Kucukvar 2012; Ameh et al. 2019; Rathod et al. 2021; Adegoke et al. 2019; Margarido 2015)
Development of alternative building materials specifications	Philips Akinyemi et al. 2019; Reddy 2004; Zhang et al. 2018; Wijeratne et al. 2021; Ameri et al. 2020; Martínez-García et al. 2021; Tahmasebinia et al. 2021; Azad 2022; Praburanganathan et al. 2022; Qin et al. 2021; Nunes and Borges 2021; Ganiron 2013)
Environmental impact assessment in using the alternative building materials	Reddy 2004; Arning et al. 2021; Ansah 2015; Enshassi et al. 2014; Palmeira et al. 2021; Tijani et al. 2022; Alsaif et al. 2022; Bigolin et al. 2021; Palmeira et al. 2021)
Availability of raw materials for ABM	Reddy 2004; Wijeratne et al. 2021; Ameri et al. 2020; Ameh et al. 2019; Meddah et al. 2019; Tijani et al. 2022)
Limited alternative building materials for different parts of the buildings	Odongo 2019; Qin et al. 2021; Nunes and Borges 2021)

them. It can result in a lack of confidence in using specific materials and a reluctance to experiment with novel construction approaches.

20.5 Conclusion

Alternative building materials are an essential issue of discussion in the construction industry. There are benefits to utilizing these materials; however, there are also challenges that must be addressed. Alternative building materials are anticipated to become more prevalent in the construction sector as the need for sustainable building methods increases. Therefore, a research study or evaluation of adopting alternative building materials in the construction industry will enhance the acceptability of such materials and ensure that they will be efficiently utilized. Likewise, undertaking a research project to evaluate that alternative building materials are available locally. Additionally, it is strongly advised to do a thorough investigation into the physical and mechanical properties of alternative building materials to assure the material's reliability. Technological advancement and research innovation must be achieved to ensure the long-term sustainability of utilizing these alternative building materials.

References

Adegoke DD, Ogundairo TO, Olukanni DO, Olofinnade OM (2019) Application of recycled waste materials for highway construction: prospect and challenges. J Phys: Conf Ser. https://doi.org/10.1088/1742-6596/1378/2/022058

Alabi SA (2020) The potential of recycled aggregates and coconut fiber in the production of concrete. Int J Integr Eng 12(8):303–309. https://doi.org/10.30880/IJIE.2020.12.08.029

Alemu D, Tafesse M, Mondal AK (2022) Mycelium-based composite: the future sustainable biomaterial. Int J Biomater 2022. https://doi.org/10.1155/2022/8401528

Alsaif AS, Abdulrahman A, Albidah S (2022) Compressive and flexural characteristics of geopolymer rubberized concrete reinforced with recycled tires steel fibers. Mater Today Proc 65:1230–1236. https://doi.org/10.1016/j.matpr.2022.04.182

Ameh J, Soyingbe A, Oyediran O (2019) Acceptability and use of innovative bamboo products for the construction of residential buildings in Nigeria. Int J Technol 10(4):648–656. https://doi.org/10.14716/ijtech.v10i4.2574

Ameri F, Shoaei P, Reza Musaeei H, Alireza Zareei S, Cheah CB (2020) Partial replacement of copper slag with treated crumb rubber aggregates in alkali-activated slag mortar. Constr Build Mater 256. https://doi.org/10.1016/j.conbuildmat.2020.119468

Ansah SK (2015) Impacts of construction activities on the environment: the case of Ghana. J Environ Earth Sci 5(3) [Online]. Available at: www.iiste.org

Arning K, Offermann-van Heek J, Ziefle M (2021) What drives public acceptance of sustainable CO_2-derived building materials? A conjoint-analysis of eco-benefits vs. health concerns. Renew Sustain Energy Rev 144. https://doi.org/10.1016/j.rser.2021.110873

Azad AM et al (2022) Pervious geopolymer concrete as sustainable material for environmental application. Mater Lett 318. https://doi.org/10.1016/j.matlet.2022.132176

Bernabe GO, Dela Cruz OG, Angeles APD, Pauya JPJ, Dajac JS (2023) A review on building information modeling in construction risk management, p 020001. https://doi.org/10.1063/5.0162413

Bigolin M, Danilevicz ÂDMF, Weiss MA, Silva Filho LCP (2021) Sustainable New Product Development: a decision-making tool for the construction industry. Int J Sustain Eng 14(4):618–629. https://doi.org/10.1080/19397038.2021.1920642

Borowski PF, Patuk I, Bandala ER (2022) Innovative industrial use of bamboo as key 'green' material. Sustainability (Switzerland) 14(4). https://doi.org/10.3390/su14041955

Chaowana K, Wisadsatorn S, Chaowana P (2021) Bamboo as a sustainable building material—culm characteristics and properties. Sustainability (Switzerland) 13(13). https://doi.org/10.3390/su13137376

Chithra S, Praburanganathan SC (2022) Stimulus on strength and durability of granite powder in the waste-based masonry units with copper slag and crumb rubber as partial substitute of fine aggregate

Dela Cruz G, Dajac JS (2021) Virtual reality (VR): a review on its application in construction safety. Turk J Comput Math Educ 12(11):3379–3393

dela Cruz G, Ongpeng JMC (2022) Building information modeling on construction safety: a literature review, pp 89–102. https://doi.org/10.1007/978-3-031-11232-4_8

Dela Cruz G, Padilla JA, Victoria AN (2021) Managing road traffic accidents: a review on its contributing factors. IOP Conf Ser Earth Environ Sci 822(1):012015. https://doi.org/10.1088/1755-1315/822/1/012015

Dela Cruz G, Mendoza CA, Lopez KD (2021) International roughness index as road performance indicator: a literature review. IOP Conf Ser Earth Environ Sci 822(1):012016. https://doi.org/10.1088/1755-1315/822/1/012016

Enshassi A, Kochendoerfer B, Rizq E (2014) An evaluation of environmental impacts of construction projects. Evaluación de los impactos medioambientales de los proyectos de construcción [Online]. Available at: www.ricuc.cl

Fardin HE, dos Santos AG (2020) Roller compacted concrete with recycled concrete aggregate for paving bases. Sustainability (Switzerland) 12(8). https://doi.org/10.3390/SU12083154

Ganiron TU (2013) Sustainable management of waste coconut shells as aggregates in concrete mixture [Online]. Available at: www.jestr.org

Girometta A et al (2019) Physico-mechanical and thermodynamic properties of mycelium-based biocomposites: a review. Sustainability (Switzerland) 11(2). https://doi.org/10.3390/su11010281

Hamid NAA et al (2021) Utilization of Ground Granulated Blast Furnace Slag (GGBS) and Mussel Shell Ash (MSA) as partial cement replacement in concrete. In: Lecture notes in civil engineering. Springer, pp 13–19. https://doi.org/10.1007/978-981-16-2187-1_2

Javadian A, Le Ferrand H, Hebel DE, Saeidi N (2020) Application of mycelium-bound composite materials in construction industry: a short review [Online]. Available at: www.symbiosisonlinepublishing.com

Josiah Marut J, Alaezi JO, Obeka IC (2020) A review of alternative building materials for sustainable construction towards sustainable development. J Mod Mater 7(1):68–78. https://doi.org/10.21467/jmm.7.1.68-78

Kumar A, Agrawal A (2019) Revisiting the role of architecture for 'surviving' development. A review paper. Emerging conversions of food-agro waste into building & construction material

Labaran YH, Mathur VS, Muhammad SU, Musa AA (2022) Carbon footprint management: a review of construction industry. Clean Eng Technol 9. https://doi.org/10.1016/j.clet.2022.100531

Maduabuchukwu Nwakaire C, Poh Yap S, Chuen Onn C, Wah Yuen C, Adebayo Ibrahim H (2020) Utilisation of recycled concrete aggregates for sustainable highway pavement applications: a review. Constr Build Mater 235. https://doi.org/10.1016/j.conbuildmat.2019.117444

Manandhar R, Kim JH, Kim JT (2019) Environmental, social and economic sustainability of bamboo and bamboo-based construction materials in buildings. J Asian Archit Build Eng 18(2):52–62. https://doi.org/10.1080/13467581.2019.1595629

Margarido F (2015) Environmental impact and life cycle evaluation of materials. In: Materials for construction and civil engineering: science, processing, and design. Springer, pp 799–835. https://doi.org/10.1007/978-3-319-08236-3_18

Martínez-García C, González-Fonteboa B, Carro-López D, Pérez-Ordóñez JL (2021) Assessment of mussel shells building solutions: a real-scale application. J Build Eng 44. https://doi.org/10.1016/j.jobe.2021.102635

Meddah MS, Benkari N, Al-Busaidi M (2019) Potential use of locally and traditionally produced bending construction material. IOP Conf Ser: Mater Sci Eng. https://doi.org/10.1088/1757-899X/471/4/042008

Mihalakakou G et al (2023) Green roofs as a nature-based solution for improving urban sustainability: progress and perspectives. Renew Sustain Energy Rev 180. https://doi.org/10.1016/j.rser.2023.113306

Nunes VA, Borges PHR (2021) Recent advances in the reuse of steel slags and future perspectives as binder and aggregate for alkali-activated materials, Construction and Building Materials, vol. 281. https://doi.org/10.1016/j.conbuildmat.2021.122605.

Nwakaire CM, Yap SP, Onn CC, Yuen CW, Moosavi SMH (2022) Utilisation of recycled concrete aggregates for sustainable porous asphalt pavements. Baltic J Road Bridge Eng 17(1):117–142. https://doi.org/10.7250/bjrbe.2022-17.554

Nwakaire CM, Yap SP, Yuen CW, Onn CC, Koting S, Babalghaith AM (2020) Laboratory study on recycled concrete aggregate based asphalt mixtures for sustainable flexible pavement surfacing. J Clean Prod 262. https://doi.org/10.1016/j.jclepro.2020.121462

Odongo EW (2019) Acceptance criteria of alternative building materials and technologies for walling: a case study of Nairobi City County. B53/7431/2017. A research project submitted in partial fulfilment of the requirements for the award of degree of masters of arts in construction management of University of Nairobi

Palmeira EM (2016) Sustainability and innovation in geotechnics: contributions from geosynthetics [Online]. Available at: https://www.researchgate.net/publication/308549796

Palmeira EM, Araújo GLS, Santos ECG (2021) Sustainable solutions with geosynthetics and alternative construction materials—a review. Sustainability (Switzerland) 13(22). https://doi.org/10.3390/su132212756

Philips Akinyemi A, Adekunle AO, Joseph O, Anthony AI, Dabara DI (2019) The need for green building rating systems development for Nigeria: the process, progress and prospect. Acad J Sci

Poornima V, Vasanth Kumar K, Hridhi Nandu PP (2021) Comparative study on fly ash based AAM concrete with GGBS, rice husk ash and sugarcane bagasse ash

Praburanganathan S, Chithra S, Divyah N, Sudharsan N, Reddy YBS, Vigneshwaran (2022) Value-added waste substitution using slag and rubber aggregates in the sustainable and eco-friendly compressed brick production. Revista de la Construccion 21(1):5–20. https://doi.org/10.7764/RDLC.21.1.5

Qin D, Hu Y, Li X (2021) Waste glass utilization in cement-based materials for sustainable construction: a review. Crystals (Basel) 11(6). https://doi.org/10.3390/cryst11060710

Rathod N, Chippagiri R, Gavali HR, Ralegaonkar RV (2021) Development of sustainable masonry blocks using industrial rejects and alkali activation. In: RILEM bookseries. Springer, pp 357–368. https://doi.org/10.1007/978-3-030-51485-3_24

Reddy BVV (2004) Sustainable building technologies [Online]. Available at: https://www.jstor.org/stable/24109393

Rizzo G, Cirrincione L, La Gennusa M, Peri G, Scaccianoce G (2023) Green roofs' end of life: a literature review. Energies 16(2). https://doi.org/10.3390/en16020596

Rosasco P, Perini K (2019) Selection of (green) roof systems: a sustainability-based multi-criteria analysis. Buildings 9(5). https://doi.org/10.3390/buildings9050134

Roxas ALC et al (2023) Design for Manufacturing and assembly (DfMA) and design for deconstruction (DfD) in the construction industry: challenges, trends and developments. Buildings 13(5):1164. https://doi.org/10.3390/buildings13051164

Setter C, de Melo RR, do Carmo JF, Stangerlin DM, Pimenta AS (2020) Cement boards reinforced with wood sawdust: an option for sustainable construction. SN Appl Sci 2(10). https://doi.org/10.1007/s42452-020-03454-y

Tahmasebinia F et al (2021) Sustainable architecture creating arches using a bamboo grid shell structure: numerical analysis and design. Sustainability (switzerland) 13(5):1–25. https://doi.org/10.3390/su13052598

Tatari O, Kucukvar M (2012) Eco-efficiency of construction materials: data envelopment analysis. J Constr Eng Manag 138(6):733–741. https://doi.org/10.1061/(asce)co.1943-7862.0000484

Tijani MA, Ajagbe WO, Agbede OA (2022) Combined reusing of sorghum husk ash and recycled concrete aggregate for sustainable pervious concrete production. J Clean Prod

Tijani MA, Ajagbe WO, Agbede OA (2022) Combined reusing of sorghum husk ash and recycled concrete aggregate for sustainable pervious concrete production. J Clean Prod 343. https://doi.org/10.1016/j.jclepro.2022.131015

Wijeratne SD, Devapriya KAK, Gallage SD (2021) Applicability of polymer building materials for productivity enhancement and cost reduction in Sri Lankan building industry. In: World construction symposium, Ceylon Institute of Builders, pp 110–121. https://doi.org/10.31705/WCS.2021.10

Zhang Z, Wong YC, Arulrajah A, Horpibulsuk S (2018) A review of studies on bricks using alternative materials and approaches. Constr Build Mater 188:1101–1118. https://doi.org/10.1016/j.conbuildmat.2018.08.152

Chapter 21
Comparative Assessment of Raw and Peroxide-Aeration Recycled Cassava Effluent on Soil Heavy Metal Content

O. A. Omotosho, A. C. O. Uthman, A. T. Atta, J. A. Osunbitan, and G. A. Ogunwande

Abstract This research investigates the levels of heavy metal contamination in soils exposed to raw and peroxide-aeration recycled cassava processing effluent and potential impact on soil quality and environmental health. Cassava processing effluent treated using the peroxide-aeration treatment method in a fabricated pilot scale plant. The treated effluent was thereafter subjected to potted experiment to determine its effect on heavy metal contamination at different concentrations (25, 50, 75 and 100%), groundwater as well as raw effluent. The treatment was applied on 10 kg soil pots at the rate of 0.9 L/day over a period of 90 days. Heavy metal content in the soil was analysed using recommended laboratory methods. The maximum values of Cr, Ni, Fe, Pb and Zn ion pollution reduction of 85.00, 86.29, 71.69, 57.03 and 88.73% respectively was recorded during the treatment, it was however observed that there was a total removal of heavy metals when the treated effluent was supplied at 25% concentration. Cr, Ni and Fe concentration in the soil after the treatment were however observed to be not significantly ($p > 0.05$) different for control, 25 and 50% treated effluent concentrations. Enrichment factor (EF) of heavy metals in the soil ranged from 1.01 to 2.73 showing that the considered heavy metal concentrations measured were due to a combination of both the soil parent material and the cassava processing wastewater. The study concludes that treatment at 25% concentration resulted in the best attenuation of heavy metal pollution soil although higher concentrations also gave acceptable pollution levels.

O. A. Omotosho (✉) · A. C. O. Uthman
Land and Water Resources Management Programme, Institute of Agricultural Research and Training, Obafemi Awolowo University, Moor Plantation, Ibadan, Oyo State, Nigeria
e-mail: akintoshforever@gmail.com

A. T. Atta
Kenaf and Jute Improvement Programme, Institute of Agricultural Research and Training, Obafemi Awolowo University, Moor Plantation, Ibadan, Oyo State, Nigeria

J. A. Osunbitan · G. A. Ogunwande
Department of Agricultural and Environmental Engineering, Faculty of Technology, Obafemi Awolowo University, Ibadan, Osun State, Nigeria

Z. Sun and P. K. Das (eds.), *Proceedings of the 10th International Conference on Energy Engineering and Environmental Engineering*, Environmental Science and Engineering, https://doi.org/10.1007/978-3-031-48204-5_21

Keywords Heavy metal · Soil contamination · Wastewater reuse · Peroxide-aeration · Environmental impact

21.1 Background

Recent rapid expansion in industrial and agricultural activities has led to increased worries about environmental pollution, notably heavy metal contamination. One of the industries that have been under scrutiny for its potential contribution to heavy metal pollution is cassava processing (Okereke et al. 2020; Osakwe 2012). Cassava is a major staple crop in many tropical regions; it however requires various processing steps to be safely converted into the various cuisines. There is however the issue of effluent generated during these processing operations which has been noted to contain elevated levels of heavy metals, which, when indiscriminately discharged into the environment, can accumulate in soils thereby adversely affecting soil quality.

Conservation of soil quality is a very salient issue which requires concerted efforts because once contaminated it will not only affect agricultural productivity but also pose a threat to human health via the food chain (Zhao et al. 2014). The issue of light and heavy metal pollution of soils is therefore one of global concern as a result of its potential impact on the environment and to human health. The potentially toxic nature of heavy metals like Cd, Pb, Zn, Cu, Cr and Ni in soil, plant and animal tissue have given them wide attention. According to Barbieri (2016) and Emurotu and Onianwa (2012), most biologically active trace elements such as Pb, Cr, Cd, Ni, Ag, and Zn reach man through plants and animals by bioaccumulation from the soil.

Heavy mental content in soil is in most cases influenced by anthropogenic factors such as construction, industrial and food processing as well as waste disposal. The assessment of heavy metal contamination in soils affected by cassava processing effluent is a critical area of research to understand the extent of this environmental issue and its potential consequences. Moreover, exploring the efficacy of remediation techniques to mitigate heavy metal pollution is essential to safeguarding environmental and human health. According to Omotosho and Ewemoje (2020), one of the methods that have been put forward for tackling the menace of cassava processing wastewater is the peroxide-aeration treatment method. This treatment method has been identified to present a viable prospect of water conservation for reuse purposes especially with the current unstable rainfall patterns experienced globally.

Therefore, the main objective of this study was to investigate effect of peroxide-aeration treatment of effluent from cassava processing on heavy metal content of receiving soil. Outcomes of this research will contribute valuable insights into the environmental impacts of cassava processing effluent and its role in heavy metal contamination of soils. Ultimately, this research aims to provide a scientific basis for informed decision-making and the implementation of targeted measures to safeguard soil health and environmental sustainability in cassava-producing regions.

21.2 Materials and Methods

21.2.1 Research Area

The study was conducted at the Obafemi Awolowo University's Institute of Agricultural Research and Training, Ibadan (7°23′ N, 3°51′ E) Nigeria. The study area has a tropical humid climate with bimodal rainfall distribution; the mean annual rainfall is 1423.4 mm based on a 10 year estimate. Rainfall peaks in June and September while the temperature ranges from 22.2 to 31.2 °C.

21.2.2 Peroxide-Aeration Treatment Process

The treatment process (Fig. 21.1) involved the construction of a 1000 L/day pilot scale peroxide-oxidation treatment plant for processing of cassava wastewater by connecting a 250 L plastic tank to a pre-fabricated aeration tank incorporating a paddle system powered by a 1.5 hp electric motor. Cassava processing effluent was collected from an industry near the Institute of Agricultural Research and Training in airtight opaque containers and transported to treatment site. The pH of the wastewater was thereafter adjusted to an alkaline range of between 10.8 and 11 by adding 0.5 M of NaOH to it. Hydrogen peroxide at 50% concentration was the added at 0.5 g H_2O_2/g of CN^- to effect cyanide decontamination through oxidation to cyanate. A reaction period of 3 h was allowed to ensure a reasonable level of cyanide oxidation thereafter the oxidized wastewater was then introduced into the aerator for a period of 2 h to increase the dissolved oxygen in the wastewater. After the aeration, wastewater was introduced to a sand filter at a flow rate of 0.6 L/min as recommended for intermediate filters.

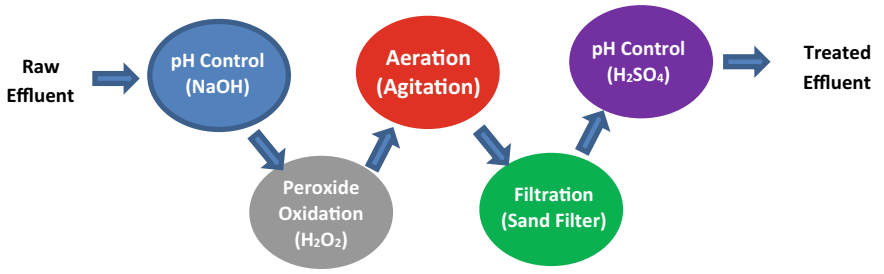

Fig. 21.1 Peroxide-aeration treatment process

Plate 21.1 Collection and Sieving of Soil to Remove Foreign Matter

21.2.3 Collection and Processing of Soil

Samples of soil (sandy loam soil) were taken from the top 12 cm layer at the Southern farm of the Institute of Agricultural Research and Training, Moor Plantation, Ibadan. The soil samples were passed through a 5 mm sieve (to remove plant residues and gravels) then placed in sacks (Plate 21.1) and transferred to the to the screen house where sub-samples were obtained for laboratory analysis to determine of its physico-chemical characteristics. The soil was then put into the buckets before being compacted to a bulk density of 1.39 g/cm^3 which was the value obtained during the initial soil analysis, this was to simulate the bulk density of the soil at source.

21.2.4 Experimental Setup and Soil Treatment

The soil contamination experiment was set up in a randomised block design (RBD) in 6 factors or treatments (0, 25, 50, 75 and 100%) and raw effluent in a screen house as shown in Fig. 21.2. The experiment was set up in four replicates giving a total of 24 experimental units. The control was taken as groundwater obtained from a borehole located around I.A.R.&T, Ibadan. The treatment was applied to each of the 10 kg potted soil samples at the rate of 0.9 L per day for a period of 90 days.

21.2.5 Collection and Pre-treatment of Soil Samples

Triplicate soil samples collected from each of the treatment level experiment as well as control were transported to the laboratory in polyethylene material and kept in the refrigerator until analysed.

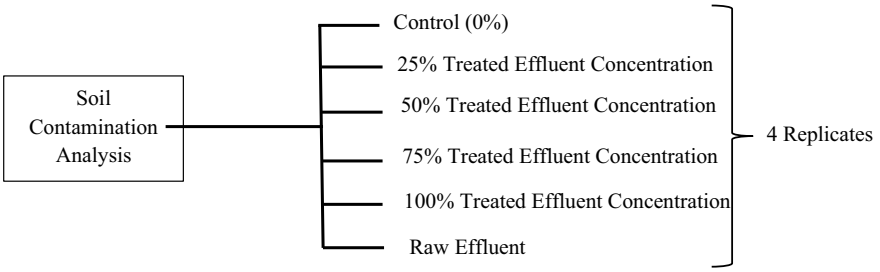

Fig. 21.2 Schematic for treatment of soil

21.2.6 Procedure for Samples Analysis

50 g of each soil sample were ground with an agate mortar, sieved, and oven dried 110 °C until a constant weight was obtained as suggested by Mehmood et al. (2022). A solution consisting of three acids ($HClO_4$, HNO_3, and H_2SO_4) at a ratio of 1:5:10 was prepared. 15 ml of Aqua Regia (HNO_3 and HCL) was added to 0.5 g of each soil sample and left to stand overnight. The following day, the soil samples were placed in a digestion block for complete digestion to take place. The obtained mixture was thereafter heated up to 80 °C for 1 h before increasing the temperature to 160–180 °C until it gave a transparent solution. After this, the solution was cooled and filtered using a 45 μm Whatman paper before being diluted up to 50 ml with distilled water in preparation for the heavy metal analysis (Zhao et al. 2014; Barbieri 2016; Emurotu and Onianwa 2012; Omotosho and Ewemoje 2020; Mehmood et al. 2022; Yasir et al. 2022; Kumari et al. 2016; Silva et al. 2014). The prepared soil samples were then subjected to spectrophotometry using the Atomic Adsorption Spectrophotometer machine (Buck Accusys 211) which was set at the following recommended wavelengths wave lengths (nm): Fe = 248.3, Cr = 357.9, Pb = 283.2, Zn = 213.9, and Ni = 323.0. Blank samples were prepared to ascertain the reliability of the analytical data and a quality control sample measurements done at an interval of seven runs.

21.2.7 Assessment of Heavy Metals Enrichment in Soil

Enrichment Factor. According to Aloud et al. (2022), Enrichment factor (EF) is the ratio of metal in the soil to its average earth crust abundance or unpolluted soil concentration. The E.F was calculated following the relationship stated in equation below;

$$Enrichment\,Factor\,(EF) = \frac{\text{Concentration of heavy metal in the sample } \left(\text{mg kg}^{-1}\ \text{DW}\right)}{\text{Concentration of heavy metal in control} \left(\text{mg kg}^{-1}\ \text{DW}\right)}$$

Contamination Factor (CF). The contamination factor (CF) is a measure of the concentration of metals in a soil sample as against the crustal abundance. The contamination factor for the soil samples was determined with the aid of the equation below,

$$CF = \frac{C_{metal}}{C_{background}}$$

where C_{metal} is concentration of metal in soil sample and $C_{background}$ is the average value of earth crust abundance as given by Wedepohl (1995).

Pollution Load Index (PLI). This provides a simple, comparative means for assessing the level of heavy metal pollution. The PLI was determined as the nth root of the product of the CF for each treatment in this study, this is given as:

$$PLI = (CF_1 \times CF_2 \times Cf_3 \times \cdots \times CF_n)^{1/n}$$

21.2.8 Data Analysis

The data obtained was subjected to one-way analysis of variance (ANOVA) using the Statistical Analysis Systems software (SAS version 9.4) at 5% significance level. All data were presented as mean ± standard deviation.

21.3 Results and Discussion

21.3.1 Physiochemical Characteristics of Soil

Rapid industrialization over the past few decades has increased anthropogenic metalloids and heavy metals contamination in soils thereby causing serious risks to the environment and human health (Cao et al. 2022). Studies have shown that heavy metal concentration in soil mainly depends on factors such as organic matter, moisture, pH, and texture (Han et al. 2022). Detailed information about the average physicochemical condition of soil samples collected for the treatment as shown in Table 21.1 revealed that the pH EC, CEC, organic matter, bulk density and textural class were 6.17 ± 0.01, 98.31 ± 0.41 μS cm^{-1}, 0.84 ± 0.01 Cmol kg^{-1}, 14.3 ± 0.21 g C/kg, 1.16 ± 0.01 mg/m^3 and sandy loam respectively. Similarly, the heavy mental content of the soil were 1.60 ± 0.02, 0.02 ± 0.00, 0.85 ± 0.01, 0.03 ± 0.00 and 100.21 ± 0.55 mg kg^{-1} for Zn, Cr, Pb, Ni and Fe respectively. The storage and residual pores of the soil were also observed to have been 0.198 ± 0.002 and 0.199 ± 0.002 mm^3/mm^3

Table 21.1 Physico-chemical properties of collected soil (0–15 cm depth)

Soil properties	Value
Textural class	Sandy loam
Bulk density (mg/m^3)	1.61 ± 0.01
Soil organic carbon (g C/kg soil)	14.30 ± 0.21
pH (1:1 soil:water suspension)	6.17 ± 0.01
Saturated hydraulic conductivity, K_{sat} (mm/h)	11.11 ± 0.05
Total pores (mm^3/mm^3)	0.478 ± 0.006
Storage pores (mm^3/mm^3)	0.199 ± 0.004
Transmission pores (mm^3/mm^3)	0.081 ± 0.002
Residual pores (mm^3/mm^3)	0.198 ± 0.002
EC (μS cm^{-1})	98.31 ± 0.41
CEC (Cmol kg^{-1})	0.84 ± 0.01
Zn (mg kg^{-1})	1.60 ± 0.02
Cr (mg kg^{-1})	0.02 ± 0.00
Pb (mg kg^{-1})	0.85 ± 0.01
Ni (mg kg^{-1})	0.03 ± 0.00
Fe (mg kg^{-1})	100.21 ± 0.55

respectively out of the total pore size of 0.478 ± 0.006 mm^3/mm^3. This indicates a good water retention capacity which is important for the study.

21.3.2 Effects of Treatment on Soil Heavy Metal Content

Results of average values of Cr, Ni and Fe content in the soil after the treatment as shown in Table 21.2 were observed to have been not significantly ($p > 0.05$) different for control, 25 and 50% treated effluent concentrations. Figure 21.3 also showed that pollution in the soil treated with the treated effluent (100%) was observed to have reduced by 85.00, 86.27, 71.69, 46.45 and 78.47% for Cr, Ni, Fe, Pb and Zn respectively when compared to results obtained from soils treated with raw effluent. The soils collected from the 75% treated effluent concentration gave 85.00, 86.29, 69.58, 57.03 and 88.73% reductions for Cr, Ni, Fe, Pb and Zn respectively. There was however a 100% reduction in heavy metal concentration for soils treated at 25% treated effluent concentration when compared with raw effluent treatment.

Table 21.2 Average concentration level of heavy metals at the end of treatment

Treatment level	Parameter**				
	Cr	Ni (Cmol/kg)	Fe	Pb	Zn
Control	$0.021^{a} \pm 0.001$	$0.031^{a} \pm 0.001$	$108.011^{a} \pm 0.113$	$0.861^{a} \pm 0.043$	$1.627^{a} \pm 0.031$
25%	$0.021^{a} \pm 0.02$	$0.031^{a} \pm 0.002$	$108.008^{a} \pm 0.122$	$0.803^{a} \pm 0.034$	$1.635^{a} \pm 0.042$
50%	$0.021^{a} \pm 0.02$	$0.035^{a} \pm 0.002$	$109.001^{a} \pm 1.111$	$0.921^{b} \pm 0.034$	$1.728^{b} \pm 0.02$
75%	$0.024^{a} \pm 0.02$	$0.038^{b} \pm 0.003$	$122.00^{b} \pm 1.122$	$1.020^{c} \pm 0.032$	$1.739^{b} \pm 0.043$
100%	$0.024^{a} \pm 0.01$	$0.038^{b} \pm 0.002$	$121.031^{b} \pm 1.111$	$1.059^{c} \pm 0.042$	$1.841^{b} \pm 0.052$
Raw effluent	$0.041^{b} \pm 0.01$	$0.082^{c} \pm 0.002$	$154.001^{c} \pm 1.113$	$1.231^{d} \pm 0.035$	$2.621^{c} \pm 0.045$

** Units are in mg/kg except where otherwise stated

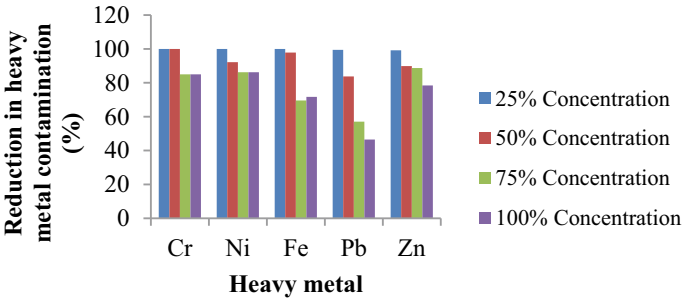

Fig. 21.3 Graph showing reduction level in heavy metal in soil at different treated effluent concentrations

21.3.3 Enrichment Factor (EF)

According to Aloud et al. (2022), one of the most common indices of soil pollution classification is enrichment factors (EF). In this study the parameter was used to differentiate between the heavy metals originating from anthropogenic activities (cassava processing) and those from natural processes this is with a view to assessing the degree of anthropogenic input. Information displayed in Fig. 21.4 reveals the heavy metal enrichment factors of the soil samples. Enrichment factor values between 0.5 and 1.0 reveals that the metal content might be entirely due to natural weathering/leaching processes (Zhang and Liu 2002). The fact that the enrichment factor is near to one (EF = 1) indicates that the element in question came from the soil (Chiarenzelli et al. 2001). The enrichment factor EF > 1.5 implies that non-crustal material or anthropogenic activities provided a considerable part of the metals (Sutherland et al. 2000). The EF of heavy metals ranged from 1.01 to 2.73 showing that the considered heavy mental concentrations in the soil were due to a combination of both the soil and the cassava processing wastewater.

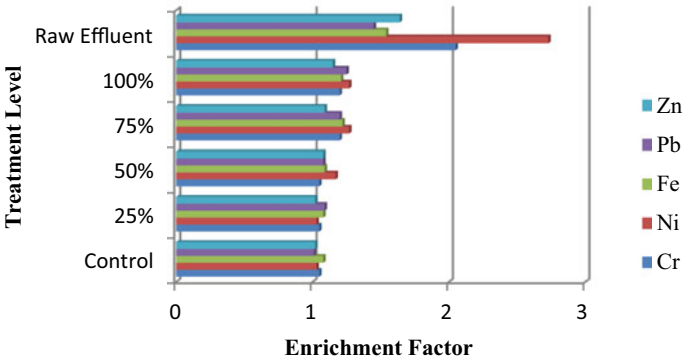

Fig. 21.4 Enrichment factors at the different treatment levels

21.3.4 Contamination Factor (CF) and Pollution Load Index (PLI)

The soil contamination level as indicated by the calculated values for contamination factor of heavy metals in the soil samples collected from each of the treatments as shown in Table 21.3 revealed that the contamination factor recorded for the control and various dilution treatments (25, 50, 75 and 100%) were much lower than what was observed for the raw effluent treatment. Chromium in the control and dilution treatments were observed to have ranged between 2.80E−04 to 3.20E−04 as compared to a value of 5.47E−04 recorded for raw effluent, Ni ranged between 1.67E−03 to 2.04E−03 as against 4.41E−03. Contamination factor for iron was in in soil treated with the fresh water and treated effluent dilution levels were between 5.06E−02 and 3.92E−03 while the soil collected from raw effluent treatment had a factor of 7.24E−02. The result also revealed that the PLI in soil collected from raw effluent treatment increased by 76.15% increment in heavy metal pollution when compared with value obtained for the control there by confirming the heavy mental pollution tendencies of cassava processing effluent as observed in previous research (Iwegbue et al. 2013; Famuyini and Sedara 2022). The increment in PLI values for 25, 50, 75 and 100% treated effluent concentration were 0.14, 5.30, 14.91 and 16.92% respectively; this further confirms that the treatment was effective in reduction of heavy metal pollution.

Table 21.3 Contamination factor (CF) and pollution load indices (PLI) of treatments on soil

	Contamination factor					Pollution index
	Cr	Ni	Fe	Pb	Zn	
Control	2.80E−04	1.67E−03	3.50E−03	5.06E−02	3.13E−02	4.81E−03
25%	2.80E−04	1.67E−03	3.50E−03	5.08E−02	3.14E−02	4.82E−03
50%	2.80E−04	1.88E−03	3.53E−03	5.42E−02	3.32E−02	5.07E−03
75%	3.20E−04	2.04E−03	3.95E−03	6.00E−02	3.34E−02	5.53E−03
100%	3.20E−04	2.04E−03	3.92E−03	6.23E−02	3.54E−02	5.63E−03
Raw effluent	5.47E−04	4.41E−03	4.99E−03	7.24E−02	5.04E−02	8.48E−03

21.4 Conclusion

In conclusion, although effluent produced from peroxide-oxidation peroxide treatment of cassava processing effluent at 25% concentration level gave the best result in terms of attenuation of heavy metal pollution in receiving soil higher concentrations can also be considered where the residual pollution levels is still tolerable. This treatment procedure therefore offers a good prospect in wastewater resource conservation and utilization having in mind the current global erratic rainfall trends especially as it affects cultivation of crops.

Acknowledgements The authors will like to acknowledge support received from management of the Institute of Agricultural Research and Training, Obafemi Awolowo University, Moor Plantation in actualizing this research.

References

Aloud SS, Alotaibi KD, Almutairi KF, Albarakah FN (2022) Assessment of heavy metals accumulation in soil and native plants in an industrial environment, Saudi Arabia. Sustainability 14:5993. https://doi.org/10.3390/su14105993

Barbieri M (2016) The importance of enrichment factor (EF) and geoaccumulation index (Igeo) to evaluate the soil contamination. J Geol Geophys 5:1. https://doi.org/10.4172/2381-8719.1000237

Cao J, Xie C, Hou Z (2022) Ecological evaluation of heavy metal pollution in the soil of Pb-Zn mines. Ecotoxicology 31:259–270

Chiarenzelli JR, Aspler LB, Dunn C, Cousens B, Ozarko DL, Powis KB (2001) Multi element and rare earth element composition of lichens, mosses and vascular plants from the central barren lands, Nunavut, Canada. Appl Geochem 16(2):245–270

Emurotu JE, Onianwa P (2012) Bioaccumulation of heavy metals in soil and selected food crops cultivated in Kogi State, north central Nigeria. Environ Syst Res 6:2. https://doi.org/10.1186/s40068-017-0098-1

Famuyini J, Sedara A (2022) Impact of cassava processing mill effluent on physical and chemical properties of soil in Akure, Ondo State, Nigeria. Turk J Agric Eng Res 3(2):265–276

Han Y, Cheng J, An D, He Y, Tang Z (2022) Occurrence, potential release and health risks of heavy metals in popular take-out food containers from China. Environ Res 206:112265

Iwegbue CMA, Bassey FI, Tesi GO, Nwajei GE, Tsafe AI (2013) Assessment of heavy metal contamination in soils around cassava processing mills in sub-urban areas of Delta State, Southern Nigeria. Nigerian J Basic Appl Sci 21(2):96–104. https://doi.org/10.4314/njbas.v21i2.2

Kumari A, Lal B, Rai UN (2016) Assessment of native plant species for phytoremediation of heavy metals growing in the vicinity of NTPC sites, Kahalgaon, India. Int J Phytoremediation 18:592–597

Mehmood S, Ahmed W, Rizwan M, Ditta A, Irshad S, Chen DY, Bashir S, Mahmood M, Li W, Imtiaz M (2022) Biochar slag and ferrous manganese ore affect Pb, Cd, and antioxidant enzymes in water spinach (*Ipomoea aquatica*) grown in multi-metal contaminated soil. Crop Pasture Sci 74(2). https://doi.org/10.1071/CP21043

Okereke JN, Nduka JN, Adanma UA, Ogidi OI (2020) Heavy metals in cassava (*Manihot esculenta* Crantz) harvested from farmlands along highways in Owerri, Nigeria. Turk J Agric Food Sci Technol 8(4):800–806. https://doi.org/10.24925/turjaf.v8i4.800-806.2737

Omotosho OA, Ewemoje TA (2020) Sequential peroxide-oxidation and adsorption treatment of cassava processing wastewater: prospects and limitations in augmentation of water budgeting practices. Open J Environ Res 1(1):47–58

Osakwe AS (2012) Effect of cassava processing mill effluent on physical and chemical properties of soils in Abraka and Environs, Delta State, Nigeria. Chem Mater Res 2(7):27–39

Da Silva YB, Do Nascimento CA, Biondi CM (2014) Comparison of USEPA digestion methods to heavy metals in soil samples. Environ Monit Assess 186:47–53

Sutherland RA, Tolosa CA, Trck FMG, Verloo MG (2000) Characterization of selected element concentrations and enrichment ratio in background and anthropogenically impacted roadside areas. Arch Environ Contam Toxicol 38(4):428–438

Wedepohl KH (1995) The composition of the continental crust. Geochim Cosmochim Acta 59(7):1217–1232

Yasir TA, Aslam M, Rizwan MS, Wasaya A, Ateeq M, Khan MN, Tanveer SK, Soufan W, Ali B, Ditta A et al (2022) Role of organic amendments to mitigate Cd toxicity and its assimilation in *Triticum aestivum* L. Phyton. Int J Exp Bot 91:2491–2504

Zhang J, Liu CL (2002) Riverine composition and estuarine geochemistry of particulate metals in China weathering features, anthropogenic impact and chemical fluxes. Estuar Coast Shelf Sci 54(6):1050–1070

Zhao Y, Fang X, Mu Y, Cheng Y, Ma Q, Nian H, Yang C (2014) Metal pollution (Cd, Pb, Zn, and As) in agricultural soils and soybean, Glycine max, in southern China. Bull Environ Contam Toxicol 92:427–432

Chapter 22
Feasibility Study on Using Coal Chemical Residue for Cement Road Construction

Yan Zhuang, Zhenhua Rui, Bo Liu, and Tianyu Ding

Abstract The waste residue produced by coal gasification is called coal gasification slag, and there is no effective use of this residue. In order to solve the problems of resource wastage and environmental pollution, we have analyzed the properties of coal gasification slag and found that its main components are similar to silicate cement and hence it can be used as an additive to replace a portion of aggregates and cement. In this paper, we analyzed the properties of coarse and fine slag and evaluated their compatibility with cement paste at different dosages. The main study includes characterization methods such as chemical elemental analysis, thermogravimetric analysis, XRD, stretching and SEM. The results showed that the coarse slag was flaky or granular with a smooth and dense surface, and some of the slag samples were completely melted and agglomerated into spheres, while the fine slag was flocculated with a honeycomb surface. In addition to carbon, the chemical compositions of coarse slag and fine slag are similar, mainly containing SiO_2, silica-aluminate and Fe_2O_3. The mass loss of fine slag is 4.3 mg. Coal gasification fine slag has a high weight loss rate, and it has a certain ability for decomposition and oxidation reactions at high temperatures, but it is less stable. We added different dosages of fine slag to cement paste and evaluated the properties by assessing the expansion, hydration, density and fluidity of the paste.

Keywords Coal gasification slag · Cement · Resource utilization · Solid wasted

Y. Zhuang
Shaanxi Provincial Transport Planning Design and Research Institute Co., Ltd, Xi'an 710060, China

Z. Rui · B. Liu
Shaanxi Road & Bridge Group Co., Ltd, Xi'an 710060, China

T. Ding (✉)
Shaanxi Province Key Laboratory of Environmental Pollution Control and Reservoir Protection Technology of Oilfields, Xi'an Shiyou University, Xi'an 710065, China
e-mail: d199947@163.com

Z. Sun and P. K. Das (eds.), *Proceedings of the 10th International Conference on Energy Engineering and Environmental Engineering*, Environmental Science and Engineering, https://doi.org/10.1007/978-3-031-48204-5_22

22.1 Introduction

With industrialization and growing energy demand, coal plays a pivotal role as an important energy resource. However, the traditional way of coal combustion has serious environmental problems, such as air pollution and greenhouse gas emissions. To solve these problems and promote sustainable development, coal gasification technology has emerged. Coal gasification technology is a process that converts coal into gaseous fuels and valuable products, which not only improves combustion efficiency and reduces pollutant emissions, but also converts organic substances in coal into liquid fuels and chemicals. However, coal gasification slag and crude residue, the waste produced in the coal gasification process, have become an urgent problem (Martins et al. 2021). Coal gasification slag is a kind of waste with high carbon content and fine particles generated in the process of coal gasification, while crude slag is another kind of waste composed of inorganic substances in coal that are difficult to be gasified. These wastes not only pose potential risks to the environment, but also waste valuable resources. Therefore, how to realize the resource utilization of coal gasification slag and slag has become an urgent problem in the field of coal chemical industry. In this paper, we will focus on the resource utilization of coal gasification slag and slag, and explore its potential value and feasibility. By analyzing the physicochemical properties of coal gasification slag and crude residue, and combining the existing resource utilization technologies and practice cases, we will explore how to transform these wastes into valuable products, such as in the fields of building materials, cement manufacturing, fertilizer production, etc. (Liu et al. 2021).

The research in this paper aims to provide new ideas and methods for the treatment and utilization of coal gasification slag and crude residue, to promote the development of clean energy industry, and to promote the coordinated development of industry and environment. By fully exploiting the potential value of coal gasification slag and crude residue, we expect to reduce the emission of waste, lower the consumption of resources and realize the goal of sustainable development. As can be seen in Fig. 22.1, coal gasification slag is converted into gas by oxidizer under certain temperature and pressure in a certain flow way to get crude water gas, which is then used as raw material to make natural gas, methanol and other first-grade products by certain technology. The system takes coal gasification as the core, and the syngas produced in the coal gasifier is widely used in chemical industry, metallurgy, oil refining, electric power and other sectors through the organic coupling and optimal utilization of various production processes. In general, the resource utilization of coal gasification slag and crude residue can not only solve the environmental problems, but also promote the upgrading and transformation of the coal chemical industry. Through the research of this paper, we will provide theoretical support and technical guidance for the practice of resource utilization of coal gasification slag and crude residue, and make positive contributions to the construction of a resource-saving and environment-friendly society (Zhu et al. 2021).

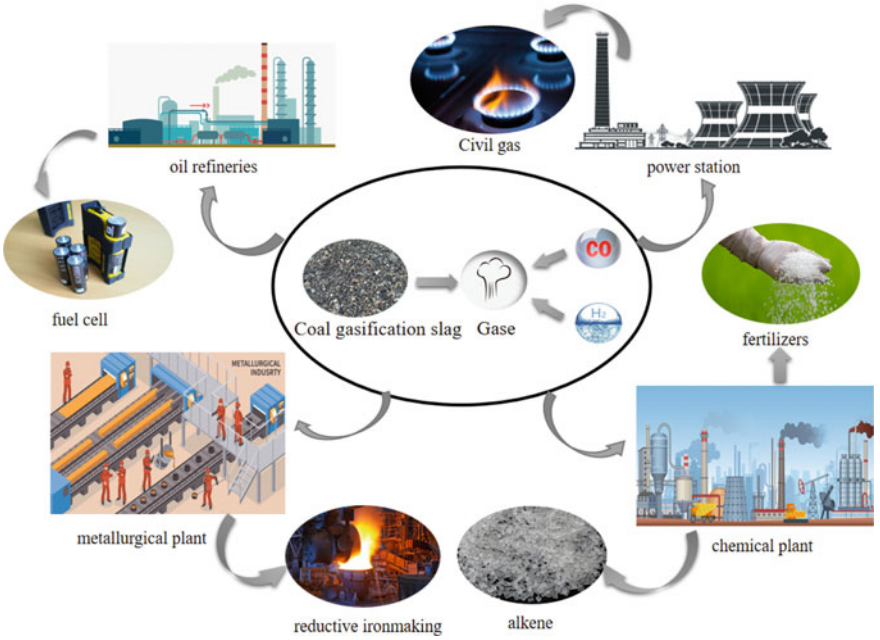

Fig. 22.1 Coal gasification slag resource utilization

22.2 Analysis of Coal Gasification Slag Properties

22.2.1 SEM of Coal Gasification Slag

Scanning electron microscope (SEM) experiments were carried out on the coal gasification coarse slag and fine slag, and the micro-morphological results are shown in Fig. 22.2. From Fig. 22.2, it can be seen that the coarse slag is flaky or granular, with a smooth and dense surface, and part of the slag samples are completely melted and agglomerated into spheres. The residual carbon in the gas slag is mostly in the form of irregular flocculent, and the surface is rough and oxidized, this special form of existence makes the residual carbon particles have a large specific surface area, and will be attached to a large number of fine-grained ash. It can be inferred that the gas coarse residue is more suitable to be used in wet mix road construction materials.

22.2.2 Elemental Analysis of Coal Gasification Slag

Table 22.1 shows the results obtained from the elemental analysis of coal gasification slag, the high content of SiO_2 in coal gasification slag is conducive to improving the

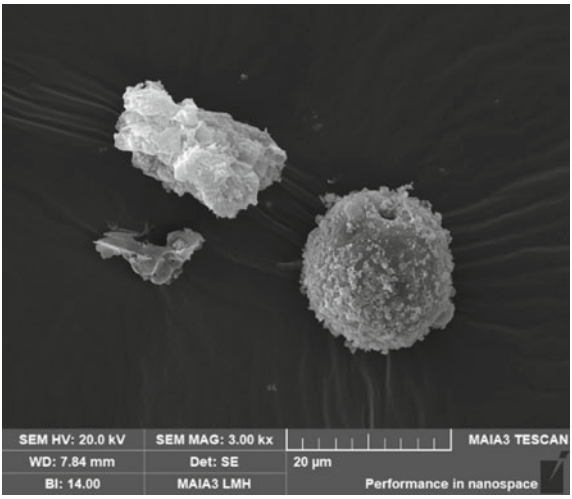

Fig. 22.2 Scanning electron microscope diagram of coal gasification crude slag

Table 22.1 Elemental composition of coal gasification slags

Coal gasification slag	N/%	C/%	H/%	S/%	Si/%	Fe/%
Coal gasification fine slag	0	38.21	8.156	0.306	10.218	8.704
Coal gasification coarse slag	0	17.81	13.125	0.59	12.605	7.387

strength and durability of its cement and concrete; at the same time, the reasonable composition of alumina, iron oxide, etc., coal gasification slag also helps to regulate the hardening time of the cement and to improve the workability of concrete. In addition, coal gasification slag contains some trace elements, such as Cr, Ni, Zn, etc., and the high content of these elements may affect the overall performance of the materials, so they need to be further analyzed to ensure the engineering safety of the materials (Ishikawa 2012).

22.2.3 Thermogravimetric Analysis of Coal Gasification Slag

Thermogravimetric analysis of coarse and fine slag of coal gasification slag was carried out according to the method described, and the experimental results are shown in Fig. 22.3.

As can be seen in Fig. 22.3, there is a mass loss between 0 and 75 °C, which by the model of L. T. Zhuravlev (Liu et al. 2017) can be It is known that this is the disappearance of adsorbed water in physical multilayers on the surface of gasified fine slag. The thermogravimetric curve image shows that there is a significant weight loss between 600 and 1000 °C, which indicates that the carbon in the coal gasification slag is almost completely burned away between 600 and 1000 °C. In addition, the

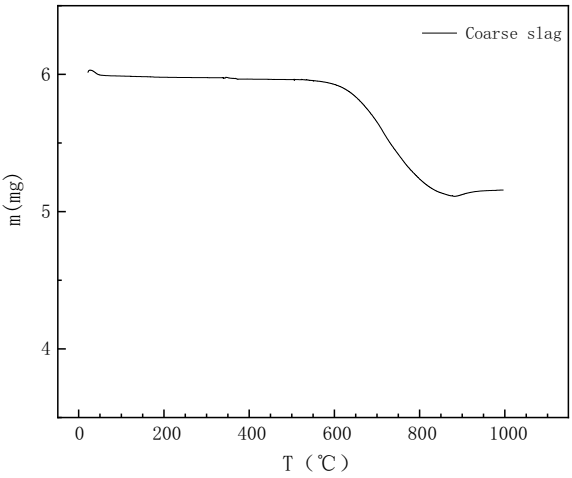

Fig. 22.3
Thermogravimetric curve of coal gasification slag

thermogravimetric curve image shows that the weight loss of coal gasification fine slag between 400 and 600 °C is about 4.3 mg. And the mass loss of coarse slag is mainly concentrated between 600 and 900 °C, and the mass loss of coarse slag is about 0.85 mg. From this analysis, it can be concluded that the coal gasification fine slag has high weight loss, strong decomposition and oxidation reaction ability at high temperature, and poor stability; in contrast, the coal gasification coarse slag has weaker decomposition and oxidation ability at high temperature, and stronger stability, so as to make the specimen formulated with cement more stable in practical application.

22.2.4 XRD Analysis of Coal Gasification Slag

XRD analysis of coal gasification slag was carried out according to the method described (Ishikawa 2012), and the experimental results are shown in Fig. 22.4.

It can be seen from the XRD patterns that the main crystalline phases of the coal gasification coarse slag and fine slag are SiO_2, silica-aluminate, Fe_2O_3, and kaolinite (i.e., silica-aluminate minerals), and so on. The X-ray diffraction patterns of coal gasification slag, fine slag and fly ash have a small number of sharp SiO_2 diffraction peaks and kaolinite diffraction peaks, and the content of SiO_2 and kaolinite in the slag is higher than that in the coal gasification fine slag. The large number of irregular diffraction peaks indicates that the gasification slag contains both crystalline and amorphous mineral phases. Kaolinite and quartz are the residues of the original coal gasification, and the clay minerals in the original coal reacted thermally to form amorphous silica-alumina minerals as well as to generate silica-calcium aluminate minerals, such as calcium feldspar and calcium-alumina pyroxene feldspar, with

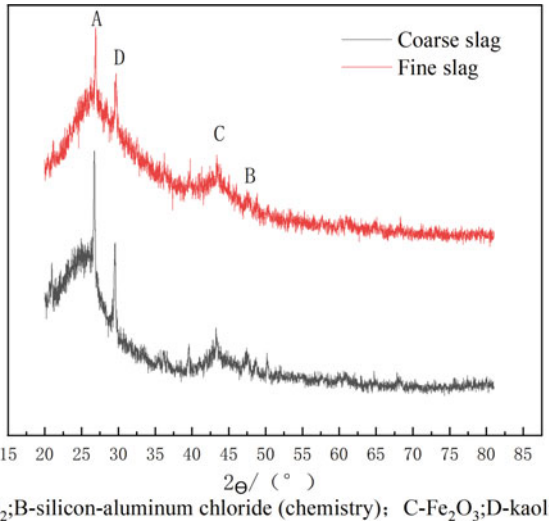

Fig. 22.4 XRD pattern of coal gasification slag

other minerals, which are an important source of the volcanic ash activity of the coarse slag (Yuang et al. 2022).

22.3 Evaluation of the Performance of Slag Formulated Cement

22.3.1 Effect of Gas Slag on the Expansion and Contraction of Cement Paste

Figure 22.5 shows the results of the stretching experiment. As can be seen from the figure, the rate of change of specimen length increases with time, but overall the change in specimen length is not significant. For the specific analysis of the expansion and contraction experiment can be found, the overall expansion and contraction of slag cement is smaller than the expansion and contraction of pure cement, and the rate of change of the length of the specimen tends to stabilize in the parameter of 20–25%. Analyze the reason, after the cement meets water, the components such as tricalcium silicate (Ca_3SiO_5), dicalcium silicate (Ca_2SiO_4) and tricalcium aluminium silicate ($Ca_3Al_2O_6$) will react with water and produce a series of new hydration products, such as calcium silicate hydrate (C-S-H), calcium alumina ($CaSO_4$-$Al_2(SO_4)_3$-nH_2O), calcite ($CaCO_3$) etc., and release a lot of hydration products, such as calcium silicate hydrate (C-S-H), calcium alumina ($CaSO_4$-$Al_2(SO_4)_3$-nH_2O), calcium alumina ($CaCO_3$), and calcite ($CaCO_3$) etc., and release a large amount of slag.), etc., and

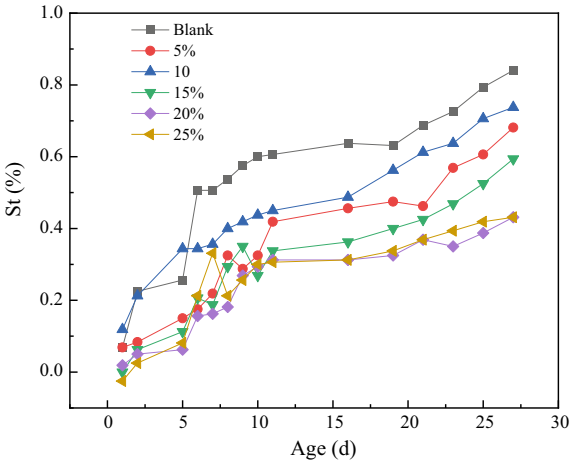

Fig. 22.5 Experimental results of coarse slag expansion rate

releases a large amount of heat. This process is known as the incipient setting reaction of cement, and these hydration products subsequently grow, crystallize and gradually fill the pores in the cement mortar, thus hardening the concrete and making it stronger and stronger. These substances are alkaline in nature, and in reacting with SiO_2, Fe_2O_3, Al_2O_3, etc. in the gasification slag, the mixture of gasification slag and cement mortar becomes more stable, which improves the stability of the specimen in practical applications (Gao et al. 2009).

22.3.2 Effect of Gas Slag on the Degree of Hydration of Cement Paste

The results of experiments to determine the cement loss on ignition (LOI) can reflect the degree of sintering of the cement as well as the degree of adequacy of the firing, which indirectly reflects the degree of hydration of the cement. A low cement loss on ignition may be due to insufficient maturation of the cement or a low sintering temperature, which may result in a reduction of the cement strength.

From the analysis of Fig. 22.6, it can be seen that the reaction between cement and water results in the formation of hydration reaction products such as hardened cement aggregates and gels. With the prolongation of hydration time, the number and types of these hydration reaction products will gradually increase, further promoting the crystallization and hardening of cement. As the hydration reaction proceeds, the colloid in the cement starts to crystallize, which makes the crystallinity of the cement gradually increase. When the crystallinity of the colloid in the cement approaches the limiting value, the amount of loss on burnout reaches a stable value. In cement, various hydration reaction products interact with each other and the lattice structure is constantly rearranged, and this interaction also leads to the gradual stabilization of

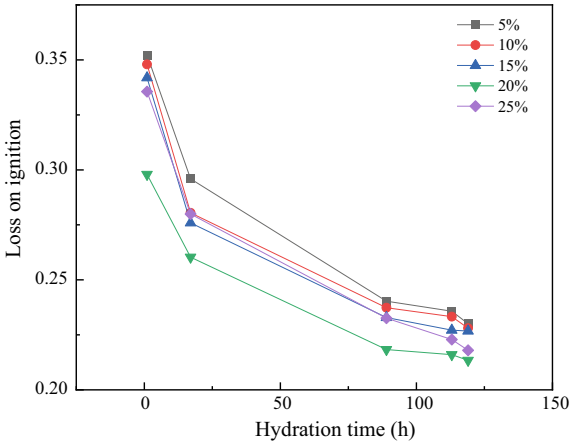

Fig. 22.6 Burning loss of different dosages of crude slag at different hydration times

the physical and chemical properties of cement. Coal gasification slag cement paste in with the increase of hydration time, the lower the water content of the specimen. And the loss on burning decreases with the increase of dosage, and the best degree of hydration is achieved at 20% dosage (Wu 2015).

22.3.3 Effect of Gas Slag on the Density of Cement Paste

As in Table 22.2 Density of gasified slag cement paste with different dosage. This experiment can be seen that the density of gasification slag cement firstly decreases with the increase of dosage, and then increases with the increase of dosage, because its dosage between 20 and 25% of the expansion rate tends to stabilize, and the density shows a rising trend.

Analyze the reason, when adding coal gasification slag, due to the coarse slag particles are large, it will increase the relative viscosity of the slurry, resulting in a decrease in the density of the slurry. In addition, the coal gasification slag contains lumps and air pores, which further reduces the slurry density. However, with the passage of time and the contact of the slurry with the external environment, the adsorption of water on the surface of the slag particles is gradually enhanced, so that the air pores in the gasification slag are gradually filled, and the relative distance between the gasification slag particles is reduced, thus increasing the slurry density. Secondly, another factor that affects the slurry density is that the alumina and calcium

Table 22.2 Density of coal gasification slag cement slurry with different dosages

Slag mixing	5%	10%	15%	20%	25%
Densities	1.877	1.710	1.706	1.720	1.858

Table 22.3 Coarse slag cement fluidity at different dosages

Slag mixing	5%	10%	15%	20%	25%
Flow diameter	10.54	9.43	8.68	7.85	7.71

oxide in the coal gasification slag will have a chemical reaction with water to generate new solid products. This reaction leads to an increase in slurry density, but it also has an impact on aspects such as slurry strength, homogeneity and durability. Finally, while the slurry density changes, the coal gasification slag will also have an effect on the slurry strength. Coal gasification slag contains a large amount of aluminum silicate, alumina and silicon, which play the role of crystal nucleation in the preparation of cement slurry, which is conducive to the improvement of the early strength of cement slurry.

22.3.4 Effect of Gas Slag on the Fluidity of Cement Paste

According to the method, the flowability experiments were carried out on the cement slurry mixed with different dosage of coal gasification slag, and the experimental results are shown in Table 22.3. From Table 22.3, it can be seen that with the increase of the dosage of coal gasification slag, the flowability of cement paste decreases gradually, which indicates that the viscosity of the cement paste is enhanced and its flowability performance decreases after the addition of coal gasification slag. This may be due to the fact that the gasification slag contains a certain amount of fine powder and tiny particles, which makes the particle concentration in the cement paste system increase, and the viscosity increases, which leads to a decrease in the flowability. With the increase of coal gasification slag dosage, the flowability of the cement paste gradually deteriorated.

22.3.5 XRD Analysis of Cementite

XRD analysis of cement paste with different dosage of coal gasification slag was carried out according to the method, and Fig. 22.7 shows the XRD spectra of the cement doped with coal gas crude slag. As can be seen from Fig. 22.7, there is an obvious raised peak-like structure in the diffraction curve at Ca_3SiO_5, indicating that the substance contains more amorphous, and after the hydration reaction with cement, the diffraction peaks of slag and cement hydration products become clear and independent, and the original peak-like structure disappears, and amorphous substances in the slag participate in the hydration reaction more fully. Through the XRD analysis, it can be seen that with the increase of the dosage of coal gasification

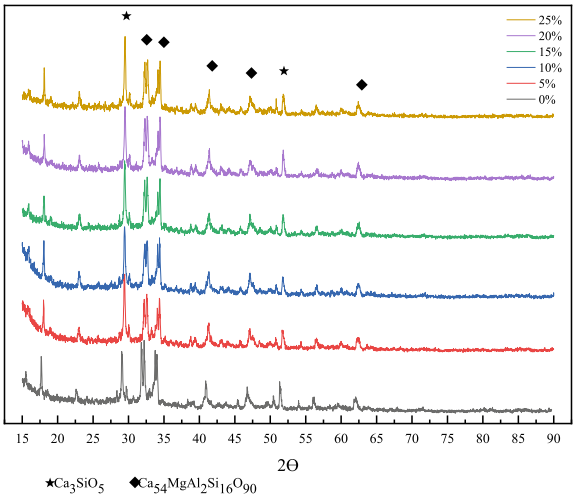

Fig. 22.7 XRD spectra of different dosages of slag cement

slag, the amorphous material in the cement participates in the hydration reaction to form a more stable crystalline material (Yang and Shi 2013).

22.4 Conclusions

In this study, coal gasification slag was used as a raw material and blended in cement paste at a certain ratio, the properties of coal gasification slag were analyzed and the compatibility of coal gasification slag with cement was evaluated. The properties of coal gasification slag cement paste in terms of mixing ratio, shrinkage performance, chemical stability and fluidity were mainly investigated. We conducted a discussion and analysis of the properties of coal gasification slag cement paste. The results showed that during the gradual addition of coal gasification slag to the cement paste, the fluidity of the paste gradually deteriorated when the dosage was gradually increased, while the fluidity of the coarse slag was better. It was analyzed that the coarse slag was flaky or granular with smooth and dense surface. Some of the slag samples were even completely melted and agglomerated into spheres, which led to the difficulty of water and cement entering into the interior of the gasification slag, but adhered to the surface, and thus had better fluidity. It was found by diffraction curve analysis that an obvious raised peak-like structure appeared at $Ca(OH)_2$, indicating that the slag contained more amorphous substances. However, after the hydration reaction with cement, the diffraction peaks of the gasification slag and the hydration products of cement became clear and independent, and the original raised peak-like structure disappeared. This indicates that the amorphous material in the coal gasification slag is more fully involved in the hydration reaction. Comprehensive analysis

can be concluded that coal gasification coarse slag and cement with better chemical stability.

Acknowledgements The work was supported financially by the Shaanxi Key Research and Development Plan (2023-YBGY-052) and the Key Scientific Research Program of Shaanxi Provincial Department of Education (21JY035).

References

Gao X, Guo X, Gong X (2009) Characteristics of air-flow bed coal gasification slag. J East China Univ Sci Technol: Nat Sci Ed 35(9):677–683

Ishikawa Y (2012) Utilization of coal gasification slag collected from IGCC as fine aggregate for concrete. In: Proceedings of the EUROCOALASH 2012 conference. Thessaloniki, Greece

Liu K, Zhao H, Li Z et al (2017) Effect of coal gasification slag on cement concrete properties. J Build Sci Eng 34(5):190–195

Liu X, Jin Z, Jing Y et al (2021) Review of the characteristics and graded utilisation of coal gasification slag. Chin J Chem Eng 35(7):92–106

Martins A, Carvalho J, Costa L et al (2021) Steel slags in cement-based composites: an ultimate review on characterization, applications and performance. Constr Build Mater 291:123–265

Wu Z (2015) Principles of coal gasification and its technology development direction. Pet Refin Chem Ind 46(4):22–28

Yang S, Shi L (2013) Analysis of coal gasification fine residue components and its comprehensive utilization discussion. Coal Chem Ind 38(4):29–31

Yuang A, Yang J, Zhang Q et al (2022) Pathway and development trend of coal gasification fine residue resource utilization. Appl Chem Eng 51(3):891–896

Zhu J, Li J, Yan L et al (2021) Research progress and application prospect of resource utilization of coal gasification residue. Clean Coal Technol 27(6):11–21